


AN ABSTRACT OF THE THESIS OF

SURAJ L. HINDAGOLLA for the degree of DOCTOR OF PHILOSOPHY
in CHEMISTRY presented on OCTOBER 25, 1985

Title : A STUDY OF THE OXIDE/SOLUTION INTERFACE BY CAPACITANCE
MEASUREMENTS OF ELECTROLYTE/OXIDE/SEMICONDUCTOR STRUCTURES
AND POTENTIOMETRIC TITRATIONS OF COLLOIDAL OXIDE SUSPENSIONS

Redacted for Privacy

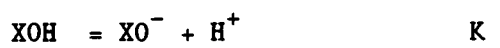
Abstract approved : _____

 Dr. John C. Westall

The oxide/electrolyte solution interface has been studied experimentally by two methods, and a mathematical model for the interface has been developed. The change in interfacial potential with solution composition was determined through the capacitance of electrolyte/oxide/semiconductor (EOS) structures and the charge through potentiometric titrations of colloidal oxide suspensions.

The differential capacitance of the EOS structures was determined as a function of applied voltage for several electrolyte solutions with different compositions (pH, ionic strength). The shifts of the capacitance-voltage curves along the voltage axis with changes in solution composition represent directly the corresponding changes in the potential at the oxide/electrolyte interface, $\Delta\psi_0$. A rigorous mathematical model based on the chemical and electrostatic properties of the oxide/electrolyte interface and the physics of the

metal/oxide/semiconductor structures have been proposed to explain the behavior of the EOS structures. The following surface hydrolysis reactions were used to describe the chemistry at the oxide/electrolyte interface.



An apparent surface ionization constant K_D is defined as

$$K_D = (K_+ K_-)^{1/2}$$

The Gouy-Chapman model has been used to describe the electrostatics of the interface. The mathematical model has been used to derive an equivalent circuit for the oxide/electrolyte interface, which allows the behavior of the interface to be understood at an intuitive level.

The $\Delta\psi_0/\Delta\text{pH}$ values were obtained for the EOS structures with an n-type Si semiconductor and SiO_2 in KNO_3 solutions of pH range 3-7 and ionic strength range 0.01-0.1 M. These $\Delta\psi_0/\Delta\text{pH}$ values have been explained reasonably well by the proposed model, with a K_D value of 0.01 and a surface site density N_s of 8×10^{14} .

The surface excess concentrations of H^+ on TiO_2 suspended in KNO_3 solutions have been determined by potentiometry. From the intersection of surface excess vs. pH curves, the pH of zero charge of anatase in KNO_3 solutions was found to be 6.4. The surface excess concentration of the electrolyte cation K^+ was also determined by potentiometry. Comparison of surface excess concentrations of H^+ and K^+ and the calculated charge in the diffuse layer indicate that K^+ and NO_3^- are specifically adsorbed on the TiO_2 surface.

A STUDY OF THE OXIDE/SOLUTION INTERFACE BY CAPACITANCE
MEASUREMENTS OF ELECTROLYTE/OXIDE/SEMICONDUCTOR STRUCTURES
AND
POTENTIOMETRIC TITRATIONS OF COLLOIDAL OXIDE SUSPENSIONS

by

Suraj L. Hindagolla

A THESIS

submitted to

Oregon State University

in partial fulfillment of
the requirements for the
degree of

Doctor of Philosophy

Completed October 25, 1985

Commencement June 1986

APPROVED:

Redacted for Privacy

U
Professor of Chemistry in charge of major

Redacted for Privacy

Chairman of Department of Chemistry

Redacted for Privacy

Dean of Graduate School

Date thesis is presented October 25, 1985

Typed by Weranjala Hindagolla for Suraj Hindagolla

Dedicated to

My Parents

and

My Wife Weranjala

for their constant support, patience and love

ACKNOWLEDGEMENT

I am indebted to a number of individuals who have helped me to accomplish this work in many ways:

My wife, Weranjala for typing the entire thesis and drawing all the figures, and mostly for her understanding, tolerance and love.

Hector Morales for making his IBM PC available unconditionally, without which writing the thesis would have taken much longer.

My major professor, Dr. John Westall, for his guidance and constructive criticism which greatly helped to improve the quality of this work.

Dr. Mike "never say no" Schuyler for practically donating his computers and electronic equipment for my research.

Sara Church for the excellent suggestions given during the proofreading the manuscript and for her friendship.

Scott Hein and Claudia Seyfert who had helped me in a number of ways, including doing some experiments pertaining to this work.

Paul Collins and Bob Eierman for the friendship, lots of cool frosties and fun which made my school life enjoyable.

Cecilia Yappert and Marcia Ikeda, the last few members from the old crew, for dragging me through the long nights in the laboratory, at least until the Class Reunion closed.

Last, but not least, "the Sri Lankan contingent" in Corvallis which provided an environment for home-style relaxation during the very difficult times of the last stretch, of course, always with a few cups of tea and laughter.

Table of Contents

	Page
1. INTRODUCTION	1
2. OVERVIEW	6
2.1. Studies of colloidal oxide suspensions of oxide particles	6
2.2. Studies with oxide electrodes	10
3. THEORY	14
3.1. Metal/electrolyte interface	15
3.2. Oxide/solution interface	29
3.3. Metal/oxide/electrolyte (MOE) structure	40
3.4. Electrolyte/oxide/semiconductor (EOS) structure	50
Metal/oxide/semiconductor structure	51
Application of MOS theory for EOS structure	68
Determination of flat-band potential	69
Unified view of EOS system	71
3.5. Equivalent circuit for the electrochemical cell	90
4. EXPERIMENTAL	96
4.1. Techniques for capacitance measurements	96
4.2. Capacitance measurements	98
4.3. Titrations of oxide suspensions	105
4.4. Reagents	112
5. RESULTS AND DISCUSSION (STUDIES WITH EOS STRUCTURES)	113
5.1. Performance of instrumentation used in the capacitance measurements	113
5.2. Verification of results from C-V curves of EOS structures by independent methods	133
5.3. Drift in the C-V response	145
5.4. Effect of pH on the C-V curves	148

	Page
6. RESULTS AND DISCUSSION (STUDIES WITH COLLOIDAL OXIDE SUSPENSIONS)	163
6.1. Determination of surface excess of H^+	164
6.2. Determination of surface excess of K^+	185
6.3. Potentiometry in low ionic strength solutions	194
6.4. Surface charge studies of TiO_2	217
7. SUMMARY AND CONCLUSION	233
8. REFERENCES	239
9. APPENDICES	
A. Program to calculate C-V curves for MOS capacitors	245
B. A method for capacitance measurement in electrochemical cells	247
C. Program to acquire data from impedance measurements	264
D. Description of the circuit used in serial data transfer between two AIM 65 computers via 20 mA loop	271
E. Program to compute resistance and capacitance from the in-phase and out-of-phase component of the cell current	273
F. Calculation of titration curves	280
G. Program for subtracting titration curves by cubic spline smoothing method	285
H. Table of symbols	292

List of Figures

Figure		Page
3.1	Schematic representation of an electrochemical cell.	16
3.2	(a) Concentration, (b) charge, and (c) potential profile near the metal electrode	17
3.3	Physical description of the Grahame model for the electrical double layer.	19
3.4	(a) Charge density and (b) potential profile at the interface according to the Grahame model.	20
3.5	Equivalent circuit for Stern model for the double layer	22
3.6	Differential capacitance as a function of applied potential as calculated from Equation 3.14.	28
3.7	A simplified mechanism for the hydration of an oxide	30
3.8	Equivalent circuit for the oxide/electrolyte interface	37
3.9	Charge and potential profiles at the metal/oxide/electrolyte (MOE) interface	42
3.10	Equivalent circuit for the metal/oxide/electrolyte interface	45
3.11	Variation of C_{obs} with applied potential for metal/oxide/electrolyte structure	48
3.12	Schematic diagram of a metal/oxide/semiconductor	56

Figure		Page
3.13	Energy bands and charge distribution in an ideal MOS structure with an n-type semiconductor under different bias condition	57
3.14	Theoretical differential capacitance of semiconductor of an MOS structure as a function of applied potential	66
3.15	Normalized observed capacitance as a function of applied potential for the MOS structure	67
3.16	Schematic diagram of the EOS structure as used in the experiment	72
3.17	Equivalent circuit for the EOS structure	77
3.18	A family of C-V curves calculated for an EOS structure in 1.0×10^{-4} M 1:1 electrolyte	79
3.19	A family of C-V curves calculated for an EOS structure in 1×10^{-2} M 1:1 electrolyte	81
3.20	Calculated C_{rxn} , C_d , ψ_o , and $d\psi_o/d\log H$ as a function of pH ($N_s = 1.0 \times 10^{15}$)	84
3.21	Variation of (a) C_{rxn} and C_d and (b) $d\psi_o/d\log H$ with bulk concentration	86
3.22	The influence of N_s on (a) C_{rxn} and C_d and (b) $d\psi_o/d\log H$	87
3.23	The effect of K_D on (a) C_{rxn} and C_d and (b) $d\psi_o/d\log H$	88

Figure		Page
3.24	Equivalent circuit for the electrochemical cell used in the capacitance measurement	91
3.25	Reduced form of Figure 3.24	94
4.1	Block diagram of the instrumentation used in the capacitance measurement	99
4.2	Electrode holder	103
4.3	Wilhelm-Brucke reference electrode	107
4.4	K^+ Ion-sensitive electrode	108
4.5	A schematic diagram of the automatic titration system	109
5.1	Instrumentation used in the capacitance measurement	115
5.2	Model circuit used in the dummy cell	119
5.3	The frequency dependance of the phase shift	122
5.4	Relative error in resistance as a function of frequency for a totally resistive dummy cell	123
5.5	Phase shift caused by different amplifiers in the potentiostat circuit	125
5.6	Model circuit for the current to voltage converter	127
5.7	Effect of correction for the impedance of the current to voltage converter	128

Figure		Page
5.8	Improvement in the accuracy of determination of (a) resistance and (b) capacitance of a parallel circuit by impedance correction	130
5.9	Improvement in the accuracy of determination of (a) resistance and (b) capacitance determination in a series circuit by impedance correction	131
5.10	Capacitance - Voltage curves obtained for EOS in 0.01 M KNO_3 at pH 3.	136
5.11	C_{\min}/C_{ox} ratio for ideal MOS structures	140
5.12	Mott - Schottky plot for the C-V curve shown in figure 5.10	143
5.13	Schematic diagram of a four point probe	144
5.14	Drift of C-V curves obtained in 0.01 M KNO_3 at pH	147
5.15	A family of C-V curves obtained for the EOS system in the pH range of 3 - 7	149
5.16	C-V curves obtained for the EOS structure in (a) 0.01 M, (b) 0.05 M, (c) 0.1 M KNO_3 solutions	153
5.17	$\Delta\psi_0$ as a function of ΔpH for EOS structures in 0.01, 0.05 and 0.1 M KNO_3 solutions	154
5.18	Calculated $\Delta\psi_0$ as a function of ΔpH for EOS structures in 0.01 M solutions	156

Figure		Page
5.19	Calculated $\Delta\psi_o$ ($K_D=0.01$, $N_S=8\times 10^{14}$) and experimental $\Delta\psi_o$ as functions of ΔpH	158
6.1	Calibration plots: electrode response of the glass electrode vs $\log(a_{H^+})$ in the acid branch	168
6.2	Calibration plots obtained in the base branch	171
6.3	Calculated and experimental curves for titrations of KNO_3 solutions contaminated with strong residual acid vs 0.01 M base	173
6.4	Calculated and experimental titration curves assuming monoprotic impurity.	174
6.5	Calculated and experimental titration curves when the contaminant is a diprotic weak acid	176
6.6	Typical titration curves obtained in the acid region for blank solution and oxide suspension	178
6.7	Polynomial function of the form, $E=a_0+a_1V+a_2V^2+....a_nV^n$, fitted to experimental data by least squares method.	181
6.8	Cubic spline fit for experimental data from the (a) acid branch (b) base branch.	183
6.9	Typical electrode calibration curves for K^+ ISE	187
6.10	Effect of pH on the response of K^+ ISE cell:	191

Figure		Page
6.11	E_H vs $\log(\text{activity of } H^+)$ plots for sample solutions (a) 0.1 M $NaNO_3$, (b) 0.001 M, (c) 0.0001 M KNO_3 in type I cells	199
6.12	Estimated and experimental junction potentials as a function of pH for acid branch titrations in type I cells	202
6.13	Estimated junction potentials for entrapped solution and experimental junction potential vs. pH	204
6.14	Effect of renewal of liquid junction on the response of the cell	206
6.15	Drift of cell responses of glass electrode and K^+ ISE vs reference electrode when the solution junction is not renewed.	208
6.16	Experimental junction potentials (a) with (b) without renewing the junction.	210
6.17	Glass electrode response vs $\log(\text{activity of } H^+)$ for the cell of type II.	214
6.18	Glass electrode response corrected for junction potential vs $\log(\text{activity of } H^+)$.	215
6.19	Surface excess H^+ as a function of pH for TiO_2 .	223
6.20	Loss of K^+ as a function of pH in TiO_2 suspension.	228

Figure		Page
6.21	Surface excess concentrations of (a) H^+ (b) K^+ and calculated charge in the diffused layer in (a) 1×10^{-3} M (b) 5×10^{-4} KNO_3 solutions	231
B.1	(a) Schematic diagram of a potentiostat connected to a three electrode cell.	248
	(b) Equivalent cell for an electrochemical cell.	249
B.2	Instrumentation block diagram.	251
B.3	Actual component circuit diagram for amplitude measurement.	253
B.4	Timing diagram (Wave forms at various points of the circuit.)	254
B.5	Calibration curves (cell current vs capacitance) at 100, 500 and 1000 Hz.	256
B.6	Effect of R_p on the cell current when the applied potential is a triangular waveform.	258
B.7	Effect of R_s on the cell current when the applied potential is a triangular wave.	259
B.8	Double layer capacitance measured at (a) Hanging mercury drop electrode (HMDE), (b) Titanium, and (c) Aluminum electrodes.	262
D.1	Circuit for inter-computer data transfer	272

List of Tables

Table		Page
2.1	Studies of the oxide/electrolyte interface by potentiometric methods.	8
2.2	Studies of oxide/electrolyte interface by semiconductor electrodes.	13
3.1	Relative magnitudes of capacitive elements metal/oxide/solution interface.	47
3.2	Some analogies between semiconductors and electrolyte solutions .	52
3.3	Circuit elements in the equivalent circuit.	92
5.1	Definitions of symbols used for circuit elements pertinent to capacitance measurements	116
5.2	Definitions of R_{exp} , C_{exp} and relative error different circuit models	120
5.3	Comparison of experimental conditions in C-V study in different laboratories.	160
6.1	Slope (s_H) and intercept (b_H) determined in 0.1 M KNO_3 from the acid branch.	170
6.2	Results from K^+ electrode calibration.	188

Table		Page
6.3	Effect of pH on the calibration parameters of the K^+ electrode.	192
6.4	Reported values of pH_{zc} for TiO_2 from surface excess measurements.	225
B.1	The range of R_s in which capacitance can be measured with in 10% error.	261

A STUDY OF THE OXIDE/SOLUTION INTERFACE BY CAPACITANCE
MEASUREMENTS OF ELECTROLYTE/OXIDE/SEMICONDUCTOR STRUCTURES
AND POTENTIOMETRIC TITRATIONS OF COLLOIDAL OXIDE SUSPENSIONS

1. INTRODUCTION

The interface between oxides and aqueous electrolytes is of interest in many different areas of science and technology. As an introduction to this study of fundamental properties of the oxide/electrolyte interface, some applied areas for which the results of this study are important are discussed.

A new class of devices for ion sensing was introduced by Bergveld (1) in the early 1970's. These devices, called Ion-Selective Field Effect Transistors (ISFET's), have essentially the same physical structure as conventional metal-oxide-semiconductor field effect transistors (MOSFET's), except that the metal gate in the MOSFET is replaced by an ion-sensitive layer. During the last decade, a large volume of work has been reported on the fabrication and response characteristics of these ISFET's. Recent developments in the analytical applications of ISFET's have been reviewed by Arnold and Meyerhoff (2).

A MOSFET is a sandwich comprised of a metal gate, an insulating oxide and a semiconductor. In the operation of a MOSFET, a potential is applied to the metal gate, creating an electric field

and affecting the charge distribution in the surface region of the semiconductor known as the channel. The channel conductivity is a function of the charge distribution. Thus, the conductivity of the channel, which can be measured, is a function of the applied gate potential. The ISFET structure is similar to the MOSFET structure, except that the metal gate is replaced by a gate comprised of the interface between the electrolyte solution and an ion-sensitive layer on the FET insulator. The ion sensitive layer on the ISFET is composed of a material similar to those used in conventional ion-selective electrodes. The electric potential generated at this solution/FET interface controls the channel current in the same way as the gate potential of the MOSFET. Thus the current through the channel can be used as an indicator of ionic activity in the solution.

A few of the potential advantages of ISFET's over conventional ion-selective electrodes are noted here. Their small size is favorable for use in biomedical sensors, sensors for miniature flow systems and multi-ion probes. Also, inexpensive on-line mass production of ISFETs is conceivable. However, practical problems such as incorporation of reference electrodes into the ISFET structure, encapsulation of the device, and chemical stability of the gate insulator remain to be resolved before commercial production is realized. The studies on the oxide/aqueous solution interface described in this work will contribute to the understanding of the stability of gate insulators.

Corrosion and passivation of metals is an important problem of technological interest. In most corroding systems, a metal oxide is in contact with aqueous solutions. The properties of the oxide/aqueous electrolyte interface influence the rate of corrosion or passivation in many ways. It has been shown that the formation of surface complexes between the surface oxide and the ligands in the solution influence the dissolution rate of the oxide and thereby the rate of corrosion of the metal.

Oxide surfaces are important in geochemistry in controlling the transport of many trace elements, particularly toxic metals. Oxide surfaces are found in association with suspended particles and sediments in natural waters. Ions from the aqueous phase can be adsorbed onto the suspended and sedimenting particles. By this mechanism, many heavy metals of environmental concern become concentrated in the sediments of rivers and lakes, causing long term harmful effects on benthic organisms. Experimental evidence, reported by many authors (3-8), implies that the adsorption to surfaces is largely responsible for controlling the concentration of many metal ions in fresh water. Inorganic surfaces of suspended material in natural waters consists of clays, oxides of Al, Si, Mn, and Fe. Schindler (8) has correlated the residence time of many metals in fresh water with their affinities to oxide surfaces. Adsorption on the hydrous oxides of Mn and Fe is believed to be a major factor affecting the trace metal ion concentration in fresh water (3). Gibbs (4) and Shuman (5) have shown that metal ions have

greater affinity for hydrous and crystalline oxides of Mn and Fe than for organic particulates in natural water.

An important process by which groundwater can be contaminated is the release and transport of toxic materials from waste dumps, sewage sludge deposits and nuclear waste repositories. The transport of metal ions in soils and aquifers is a phenomenon governed largely by adsorption-desorption processes taking place at the solid/water interface. Again, the properties of the oxides are representative of the properties of aquifer materials. Therefore, it is important from an environmental standpoint to understand the properties of the oxide/aqueous electrolyte interface. Many studies on oxides pertinent to the environmental aspects of metal transport are reported in two recent books (9,10).

In all of the above applications, the adsorption of ions from the aqueous phase on the oxide surface is the primary mechanism which alters the chemical and electrical properties at the interface. Therefore, it is of great interest to understand the adsorption energy and the structure of the electrical double layer at the interface.

The energy of adsorption of an ion at a charged interface can be divided into two principal components: a chemical component associated with the chemisorption of the ion with the uncharged surface and an electrostatic component associated with the coulombic interaction of the ion with the charged surface. Although many studies have been published on the metal oxide/aqueous electrolyte

interface, the contribution of each component to the total energy of adsorption has not yet been identified clearly.

A principal goal of this work is to resolve this ambiguity. For this purpose, variation of surface potential and surface charge of the oxides with solution composition has to be studied. The variation in interfacial potential with the solution composition is obtained from the measurement of capacitance of electrochemical cells of the type

reference electrode/solution/oxide/semiconductor/metal

Surface charge of the oxides is obtained by potentiometric measurements of surface excess concentrations of ions on the colloidal suspensions.

2. OVERVIEW

In recent years, the interfacial potential difference at the oxide/electrolyte interface in two types of environments has been studied:

- (1) colloidal suspensions of oxide particles
- (2) oxide electrodes

The results of these studies have appeared in the literature of two disciplines: the suspension studies in the colloid and surface science literature and the oxide electrode studies in the solid state science literature. However, a significant gap exists between the two types of studies, as work done in one area has not been cited extensively in the literature of the other. A brief overview of literature from both areas is presented here.

2.1 Studies of colloidal suspensions of oxide particles

In colloidal suspensions, the ratio of surface area of the solid phase to volume of the liquid phase is very high. Thus adsorption of species on the surface of the colloid can create a detectable change in its concentration in solution. This concentration change can be detected potentiometrically.

Surface excess concentrations have been obtained directly from potentiometric titrations of colloidal oxides. Bolt (11) and Parks et al. (12) were among the first to employ potentiometric techniques to study the oxide/aqueous solution interface. Their investigations showed the potential determining role of H^+ and OH^- ions. A large volume of work has been done by potentiometric studies of oxide suspensions. This work is summarized in Table 2.1.

In the early studies, the surface charge on oxide surfaces was calculated from the surface excesses as shown in the following equation.

$$\sigma_o = q (\Gamma_{H^+} - \Gamma_{OH^-}) \quad 2.1$$

where σ_o is the surface charge on the oxide and Γ_{H^+} and Γ_{OH^-} are the surface excesses of H^+ and OH^- respectively. All symbols are defined in Appendix H. The surface potential was calculated from the Nernst relationship (32,19,33).

$$\frac{d\psi_o}{d \ln a_{H^+}} = \frac{kT}{q} \quad 2.2$$

where k is the Boltzmann constant, T is the absolute temperature, q is the elementary charge, a_{H^+} is the activity of H^+ ions and ψ_o is the surface potential of the oxide. This approach is similar to that used in the studies of the AgI/solution interface by Lyklema et al. (34). The validity of the Nernst expression for the AgI/solution interface can be recognized by considering the following equation for electrochemical equilibrium at the interface:

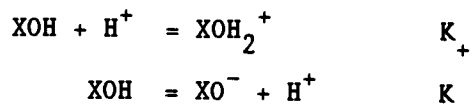
$$\Delta\psi = \mu_{Ag^+(solid)}^o - \mu_{Ag^+(soln)}^o + \frac{kT}{q} \ln \frac{a_{Ag^+}(soln)}{a_{Ag^+}(solid)} \quad 2.3$$

Table 2.1. Studies of the oxide/electrolyte interface
by potentiometric methods.

worker(s)	year	oxide	pH at zero charge	solution	reference
Bolt	1957	SiO ₂	3.5	NaCl	11
Parks and de Bruyn	1962	Fe ₂ O ₃	8.5	KNO ₃	12
Ahmed	1966	ZrO ₂	5.5	KNO ₃	13
		ThO ₂	5.9	KNO ₃	
Li and de Bruyn	1966	SiO ₂	2.0		14
Onoda and de Bruyn	1966	Fe ₂ O ₃	8.3	NaClO ₄	15
Atkinson et al.	1967	Fe ₂ O ₃	9.1	KCl	16
Ahmed and Maskimov	1968	Fe ₂ O ₃	5.3	KNO ₃	17
Tadros and Lyklema	1968	SiO ₂	3.0	KCl	18
Berube and de Bruyn	1968	TiO ₂	6.0	NaClO ₄	19
Ahmed and Maskimov	1969	TiO ₂	5.3	KNO ₃	20
		SnO ₂	5.5	KNO ₃	
Block and de Bruyn	1970	ZnO	8-10	NaNO ₃	21
Breeuvsma and Lyklema	1971	Fe ₂ O ₃			22
Schindler and Gamsjager	1972	TiO ₂	6.4	NaClO ₄	23
Huang and Stumm	1973	Al ₂ O ₃	8.5	NaCl	24
Hohl and Stumm	1976	Al ₂ O ₃			25
Davis and Leckie	1978	FeOOH	7.9	NaNO ₃	26
Yates and Healy	1980	TiO ₂	5.8	KNO ₃	27
James et al.	1981	TiO ₂	5.8	KNO ₃	28
Regazzoni et al.	1983	ZrO ₂	6.4	KNO ₃	29
		Fe ₃ O ₄	6.7	KNO ₃	
Blesa et al.	1984	ZrO ₂	6.4	KNO ₃	30
		Fe ₃ O ₄	6.7	KNO ₃	
Houchin and Warren	1984	SnO ₂	4.3	KNO ₃	31

where μ 's are the chemical potentials of Ag^+ in the phases as indicated. The chemical potential of Ag^+ in the AgI phase is a constant because Ag^+ is a part of the AgI lattice. However, as Hunter and Wright (35,36,37) pointed out, the chemical potential of H^+ is not a constant in the oxide phase, since neither H^+ nor OH^- is a part of the oxide lattice, as Ag^+ is of the AgI lattice. Therefore, equation 2.2 has no direct thermodynamic basis for the oxide surfaces.

In another approach the potential and charge at the oxide/electrolyte interface are explained by a model based on the ionization of surface hydroxyl groups (XOH). Infrared (IR) studies of hydrated oxides have revealed the presence of surface hydroxyl groups at various oxide surfaces (38,39). The following protonation and deprotonation reactions of XOH groups have been postulated.



Equations have been derived by Levine et al. (40,41) showing that the change in oxide/solution interfacial potential per unit change in pH ($d\psi_0/d\ln a_{\text{H}^+}$) is less than kT/q (59 mV at 25°C) by an amount dependent on the surface hydroxyl group density, the intrinsic acidity constants K_+ and K_- , and an electrostatic model of the electric double layer at the interface.

The potential changes at the oxide/solution interface are usually estimated by the shifts of these microscopic acidity constants obtained from the potentiometric titrations of oxide suspensions.

The estimated interfacial potential changes are much less than 59 mV/pH at 25⁰C. Therefore, it has been the consensus among the colloid chemists that the interfacial potential-pH relationship for most oxides is sub-Nernstian. However, this behavior is different from the well known Nernstian behavior of the pH electrodes with oxide (glass) membranes. Also, most interfacial potential determinations with oxide electrodes agree with Nernstian response.

2.2 Studies with oxide electrodes

As described in the previous section, the potential at the oxide/solution interface can be estimated only indirectly through the potentiometric titration of oxide suspensions. The changes in interfacial potential with changes in solution composition can be determined in a more direct manner by oxide electrodes. Since many oxides are either insulators or poor conductors, a direct measurement of the oxide/electrolyte interfacial potential is not possible, because of the unknown potential drop across the oxide. However, the changes in interfacial potential with solution composition can be deduced from a phenomenon that is directly measurable and related to the interfacial potential, such as differential capacitance or conductance.

In this work, a method for interfacial potential difference determination through the use of electrochemical cells of the type reference electrode/electrolyte/oxide/semiconductor/metal will be presented.

The use of semiconductor electrodes for determination of interfacial potential change has been reported by many workers. In some studies, differential capacitance has been used, while in others conductance has been used.

Among the earliest determinations of interfacial potential difference through the use of semiconductors was the work of Brattain and Garrett (42) on the single crystal germanium/electrolyte interface. Boddy and Brattain (43,44) employed a galvanostatic pulse technique for capacitance measurements of the same interface. They reported 59 mV/pH for the change in the interfacial potential.

A change of 59 mV/pH for the 001 face of single crystal TiO_2 has been observed by Watanabe et al. (45) via capacitance measurements.

Schenk (46) has studied the behavior of ISFETs with SiO_2 gates in electrolytes with different concentrations and found a response of 47 mV/pH in 0.01M NaCl and 37 mV/pH in 0.1M NaCl.

Abe et al. (47) studied the properties of chemical vapor deposited oxides on ISFET gates. The SiO_2 gates showed large drifts and response of 20 to 35 mV/pH while Al_2O_3 gates showed excellent stability and nearly Nernstian response.

Capacitance of electrolyte/SiO₂/Si structures were measured by Siu and Cobbold (48) and Barabash and Cobbold (49). The change in interfacial potential of the system was explained through a site-binding model proposed in colloid chemistry literature. A shift of 52 mV/pH was reported by the former workers and a 38 mV/pH shift by the latter.

In a similar experiment with Si/SiO₂/electrolyte system, Bousse et al. (50) reported a 25 mV/pH change in interfacial potential, while a 52 mV/pH was observed in the case of Al₂O₃.

Akiyama et al. (51) have studied the behavior of SiO₂, ZrO₂ and Ta₂O₅ gates in ISFETs, and responses of 43 mV/pH, 50 mV/pH and 56 mV/pH, respectively, have been reported.

Horowitz (52) investigated the behavior of Zr doped α -Fe₂O₃ single crystal electrodes using capacitance-voltage curves, and a shift of 59 mV/pH has been reported.

Recently, Kinoshita and Madou (53) have observed Nernstian behavior of single crystal Pt, Ir and Ti oxides through potential shifts obtained by impedance measurements.

A summary of work carried out on oxide surfaces in solutions using oxide electrode is shown in Table 2.2

Table 2.2 Studies of oxide/electrolyte interface
by oxide electrodes

Investigator	oxide	electrolyte	slope	reference
Watanabe	TiO ₂	0.5 M KCL	59	45
Schenk	SiO ₂	0.1 M NaCl	37	46
		0.01 M NaCl	47	
Abe et al.	SiO ₂	-	20-35	47
Siu & Cobbold	SiO ₂	buffers	52	48
Barabash et al.		buffers	38	49
Bousse et al.	SiO ₂	0.1 M NaNO ₃	25	50
	Al ₂ O ₃		52	
Akiyama et al.	SiO ₂	buffers	43	51
	ZrO ₂		50	
	Ta ₂ O ₅		56	
Horowitz	Fe ₂ O ₃	-	59	52
Kinoshita et al.	TiO ₂	1 M KCl	59	53
	PtO ₂		59	

3. THEORY

Electrolyte/oxide/semiconductor (EOS) structures are used in this work to measure the change in potential difference at the oxide/electrolyte interface with change in solution composition. In this section the choice of the EOS structure for the measurement of interfacial potential change is justified through a theoretical analysis of the EOS structure. Such an analysis is complicated, because it involves the concepts in interfacial solution chemistry, colloid chemistry, and semiconductor physics. To simplify the exposition of the theory, the various interfaces which comprise the EOS structure will be introduced separately; then the complete EOS structure will be discussed. Circuit models necessary to analyze the experimental data will be presented at the end of this section. This section is organized in the following subsections:

- 3.1 metal/solution interface
- 3.2 oxide/solution interface
- 3.3 metal/oxide/solution structure
- 3.4 electrolyte/oxide/semiconductor structure
- 3.5 circuit models to analyze the data

3.1 Metal/Solution Interface

Consider a cell made up of a metal (mercury) electrode and a reversible reference electrode immersed in a solution of electrolyte such as NaF. Figure 3.1 shows a schematic diagram of such a cell. Over a certain limited range, an external potential can be applied across the two electrodes without any charge being transferred across the metal/solution interface, i.e., the mercury electrode is ideally polarized. Since charge is stored on opposite sides of the interface, this interface behaves as a capacitor.

When a negative potential is applied to the metal electrode, positive ions are attracted towards the metal, and their concentration near the surface of the metal is larger than that in the bulk. The concentration, charge and potential profiles in the vicinity of the metal electrode surface are shown in Figure 3.2.

At the metal/solution interface, electronic charge exists on the surface of the metal and the ionic counter charge in the adjacent solution. This charged region is called the electrical double layer (EDL). The capacitance of the EDL can be measured and is of great importance in understanding the properties of the interfacial region.

The capacitance of the EDL is usually discussed with the aid of models. Several theories have been proposed to describe the EDL. Major contributions came from Helmholtz (54), Gouy (55), and Chapman (56). Stern (57) proposed a model for the EDL which is essentially a

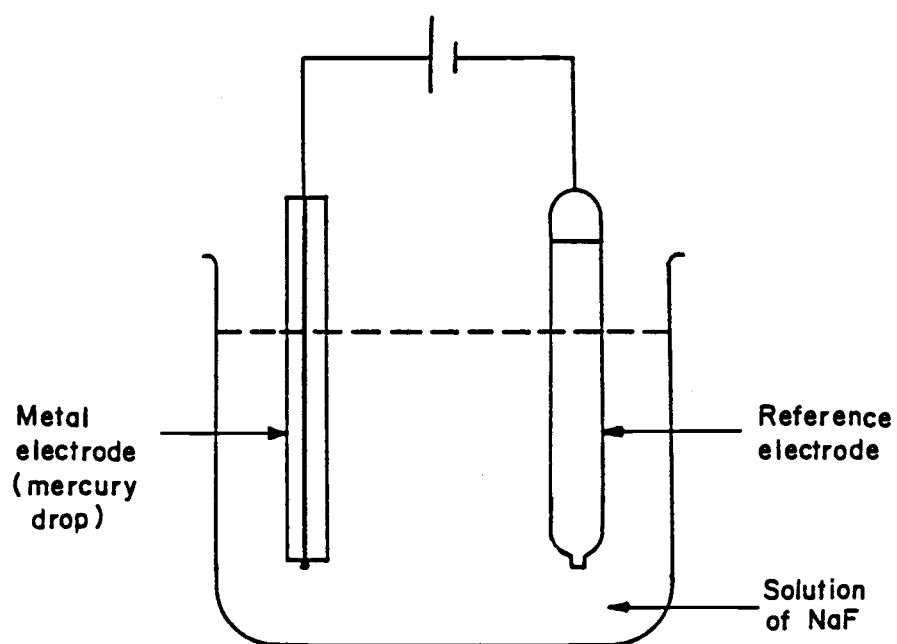


Figure 3.1. Schematic representation of
an Electrochemical Cell

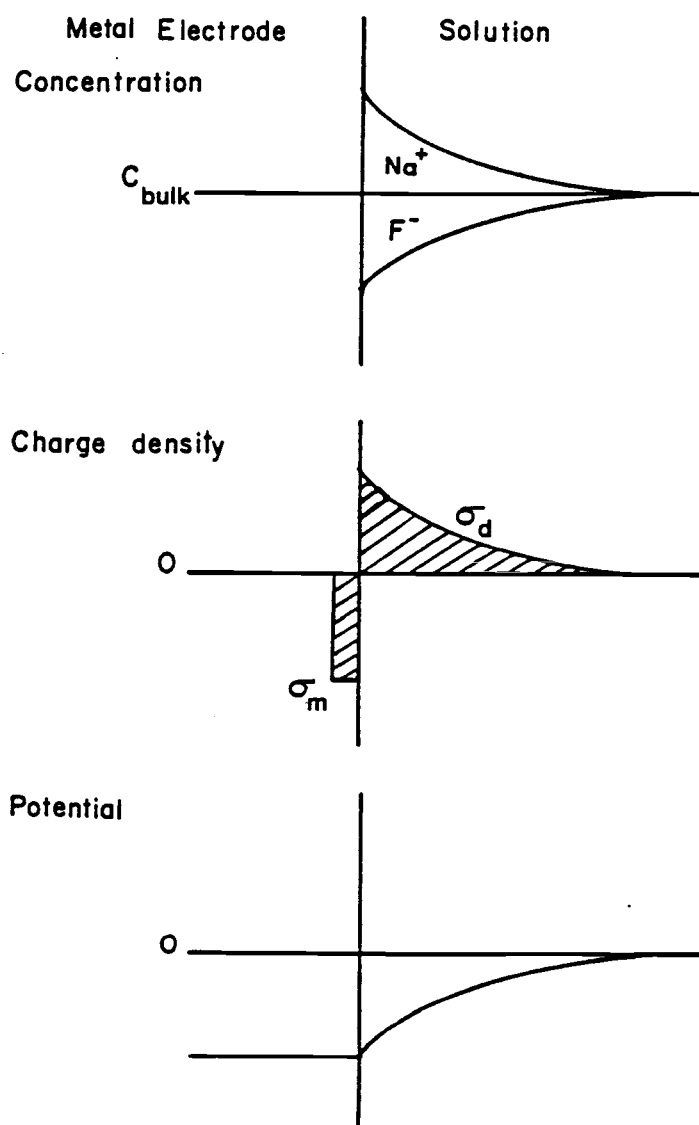


Figure 3.2. (a) Concentration, (b) Charge and (c) Potential profiles near the metal electrode when a negative potential is applied to the metal.

combination of the models proposed by the former. Grahame (58) described the interface in a more descriptive manner.

The physical structure of the metal/solution interface as proposed by Grahame is given in Figure 3.3. The distribution of charge and potential through the interface according to the model is shown in Figure 3.4(a) and 3.4(b). In this model, the solution side of the interface is divided conceptually into three regions. Each of these regions is separated by imaginary planes.

In the first region, solvent molecules in the solution become non-randomly oriented near the surface of the metal. Other ions or molecules in the solution also can be attracted to the surface by chemical or electrostatic forces. These ions and molecules are said to be specifically adsorbed. The locus of the specifically adsorbed ions define a plane known as the inner Helmholtz plane (IHP). The region between the metal surface plane and the IHP is referred to here as the inner Helmholtz layer.

From the distance of their closest approach to the metal surface, solvated ions in the solution interact with the metal surface by long range electrostatic forces. These ions are said to be non-specifically adsorbed and can be considered as loosely bound to the metal. The locus of the centers of these ions is known as the outer Helmholtz plane (OHP). The region between the IHP and OHP is referred to as the outer Helmholtz layer.

The region which extends from the OHP to the bulk of the solution is known as the diffuse layer or the Gouy-Chapman layer. This region contains the non-specifically adsorbed ions, the distribution of which can be described by the Poisson-Boltzmann equation.

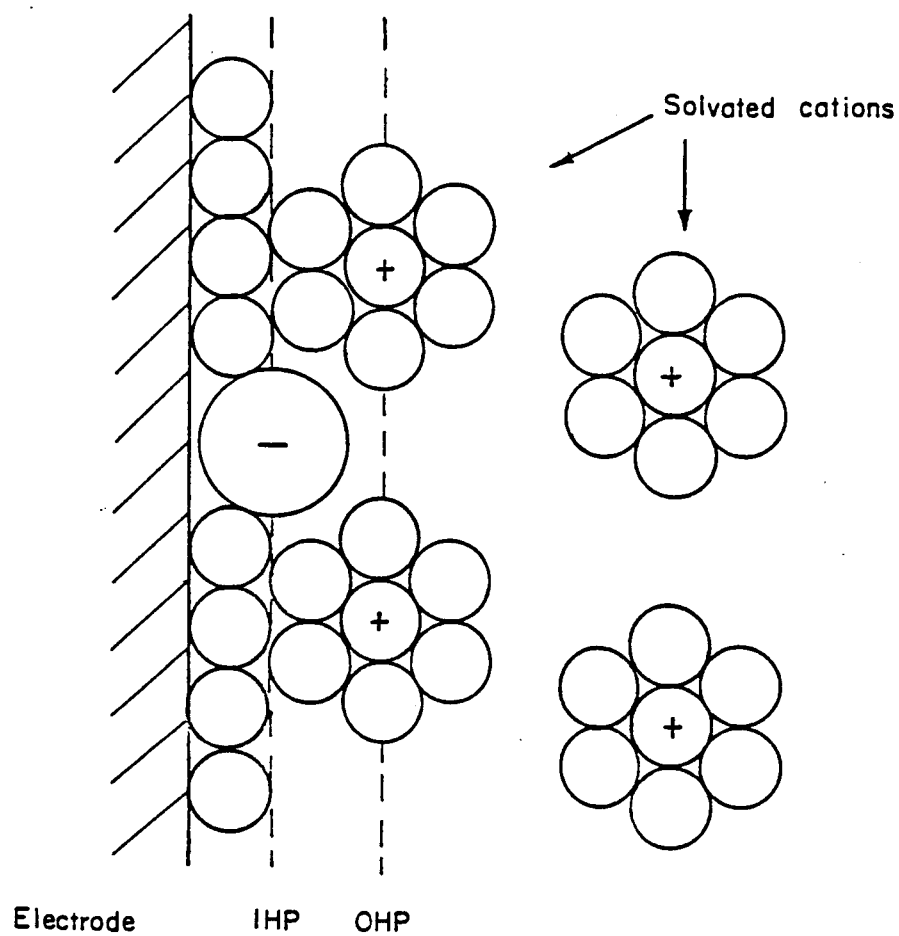


Figure 3.3. Physical description of the Grahame Model
for the Electrical Double Layer
(after reference 59)

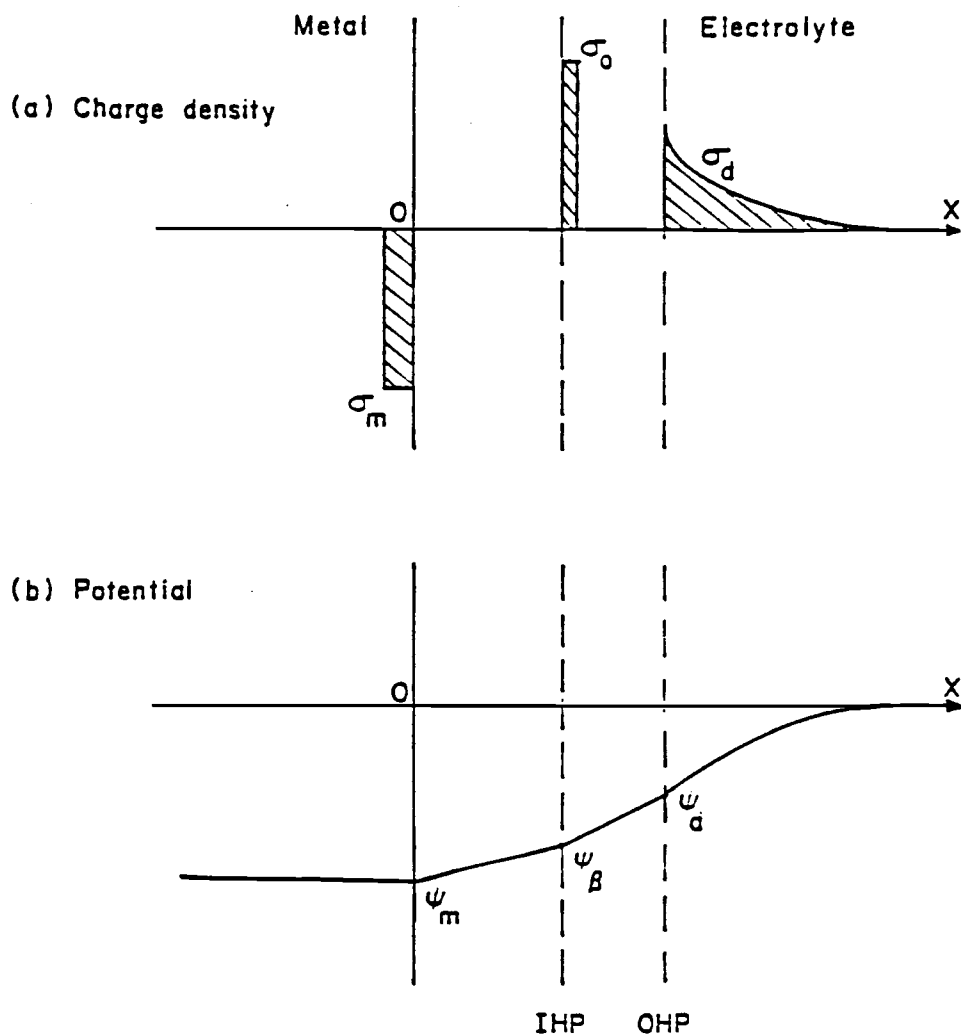


Figure 3.4. (a) Charge density and (b) potential profile
at the interface according to the Grahame model

The inner and the outer Helmholtz layers can be viewed as two parallel plate capacitors whose capacitances are independent of the properties of the bulk solution. Although Stern included these two layers in his model for the EDL, he omitted the outer layer to simplify the calculations. This simplified model will be used to describe the double layer in our discussion. Since the OHP is neglected, the IHP and the inner Helmholtz layer will be referred to simply as the Helmholtz plane and layer, respectively.

The electrical properties of the interfaces can be understood at an intuitive level by using circuit models known as equivalent circuits. An equivalent circuit which represents the metal/solution interface with the above-mentioned simplifications consists of two capacitors in series as shown in Figure 3.5. The capacitances of the Helmholtz layer and the diffuse layer are designated C_H and C_d respectively.

The double layer characteristics at solid electrodes are often studied via capacitance measurements. The experimentally observed differential capacitance of the interface, C_{obs} , can be represented as follows,

$$\frac{1}{C_{obs}} = \frac{1}{C_H} + \frac{1}{C_d} \quad 3.1$$

The properties of C_H and C_d are discussed next.

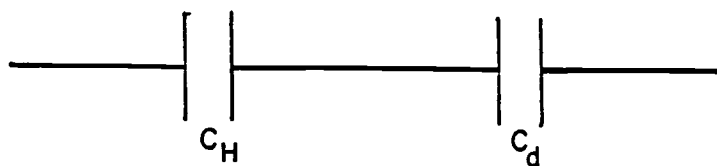


Figure 3.5. Equivalent circuit for Stern model
for the EDL at metal/solution interface
 C_H = Capacitance of the Helmholtz layer
 C_d = Capacitance of the diffuse layer

Helmholtz layer

C_H is given by the simple expression for the parallel plate capacitor,

$$C_H = \frac{\epsilon'_w \epsilon_o}{d} \quad 3.2$$

where d is the distance from the electrode surface to the OHP, ϵ'_w is the dielectric constant inside the Helmholtz layer and ϵ_o is the permittivity of free space. Since the water molecules in the Helmholtz layer are tightly bound to the surface of the metal, the dielectric constant is different from that of the bulk. A value between 6 to 40 is often used (60,61). As shown in Equation 3.2, C_H is independent of the concentration of the electrolyte and the chemical nature of the solute.

Diffuse layer

An expression for the capacitance of the diffuse layer C_d , will be derived through a theoretical description of the diffuse layer. Details may be found in Bard and Faulkner (62).

To avoid mathematical complexity, the discussion is restricted to the following

- (1) Only a 1:1 (symmetrical) electrolyte is considered.
- (2) The coordinate system is defined as x direction perpendicular to the surface of the electrode and y and z directions parallel to the surface. Charge distribution is independent of y and z coordinates, and is considered only in the x direction with $x=d$ at the Helmholtz plane and $x \rightarrow \infty$ in the bulk of solution.

To start with, the fundamental equations necessary to describe the diffuse layer can be summarized as follows.

- (1) The charge density at a distance x, $\rho(x)$, from the Helmholtz plane is given by

$$\rho(x) = \sum z_i q C_i(x) \quad 3.3$$

where $C_i(x)$ is the concentration of ions at x and qz_i is the charge on the ion.

- (2) The concentration distribution is represented by a Boltzmann type equation

$$C_i(x) = C_{\text{bulk}} \exp \left(\frac{-z_i q \psi(x)}{kT} \right) \quad 3.4$$

where C_{bulk} = concentration of ions in the bulk of the solution

$C_1(x)$ = concentration of ions at a distance x from the
Helmholtz plane

k = Boltzmann constant

T = absolute temperature

q = elementary charge

$\psi(x)$ = potential at x with respect to the bulk

Note that the concentrations are expressed in particles/volume.

(3) From electrostatics, the charge density $\rho(x)$ can be related to the potential $\psi(x)$ by the Poisson equation

$$\rho(x) = -\epsilon_w \epsilon_0 \frac{d^2 \psi(x)}{dx^2} \quad 3.5$$

where ϵ_w is the dielectric constant of water.

(4) The charge per unit surface area σ_d , is found from the integral of the charge density.

$$\sigma_d = \int_{-\infty}^x \rho(x) dx \quad 3.6$$

(5) The quantity of interest, the differential capacitance of the diffuse layer, C_d , is given by

$$C_d = - \frac{d\sigma_d}{d\psi_d} \quad 3.7$$

where ψ_d is the potential at the Helmholtz plane. Equations 3.3-3.7, along with the appropriate boundary conditions, completely define the potential-charge relationship for the diffuse layer. It remains to solve for C_d in terms of ψ_d and C_{bulk} .

Integration of Poisson's equation (3.5) with boundary conditions (limit $x \rightarrow \infty$, $d\psi/dx=0$) gives

$$\sigma_d = -\epsilon_w \epsilon_o \left. \frac{d\psi}{dx} \right|_{x_d} \quad 3.8$$

An expression for $\frac{d\psi}{dx}$ as a function of ψ can be obtained as follows. Equations 3.3-3.5 can be combined to yield

$$\frac{d^2\psi(x)}{dx^2} = - \frac{1}{\epsilon_w \epsilon_o} \sum z_i C_i q \exp \left(\frac{-z_i q \psi}{kT} \right) \quad 3.9$$

Integrating Equation 3.9 with boundary conditions (limit $x \rightarrow \infty$, $\psi=0$ and $d\psi/dx = 0$) and rearranging the result gives

$$\frac{d\psi}{dx} = \left(\frac{8 kT C_{bulk}}{\epsilon_w \epsilon_o} \right)^{1/2} \sinh \left(\frac{zq\psi}{2kT} \right) \quad 3.10$$

Equations 3.8 and 3.10 can be combined to yield an expression for charge in the diffuse layer.

$$\sigma_d = - \left(8 \epsilon_w \epsilon_o kT C_{bulk} \right)^{1/2} \sinh \left(\frac{zq\psi}{2kT} \right) \quad 3.11$$

Equation 3.11 can be differentiated with respect to ψ_d , and from Equation 3.7, the differential capacitance C_d can be given by

$$C_d = \left(\frac{2 z^2 q^2 \epsilon_w \epsilon_o C_{bulk}}{kT} \right)^{1/2} \cosh \left(\frac{zq\psi}{2kT} \right) \quad 3.12$$

Thus, C_d is dependent on the concentration of the electrolyte. By expressing concentration of the electrolyte in units of

moles/volume, Equation 3.11 can be rewritten as

$$\sigma_d = - \left(8 \epsilon_w \epsilon_o RT C_{\text{bulk}} \right)^{1/2} \sinh \left(\frac{zF\psi_d}{2RT} \right) \quad 3.13$$

and Equation 3.12 as

$$C_d = \left(\frac{2 z_i^2 F^2 \epsilon_w \epsilon_o C_{\text{bulk}}}{RT} \right)^{1/2} \cosh \left(\frac{zF\psi_d}{2RT} \right) \quad 3.14$$

where R is the gas constant and F is Faraday's constant.

The differential capacitance of the diffuse layer as a function of ψ_d , calculated from Equation 3.14, is shown in Figure 3.6. The minimum of the capacitance curve corresponds to the point at which ψ_d is zero, or net charge on the metal and specifically adsorbed ions is zero.

As shown in Equation 3.1, the observed capacitance depends on both C_d and C_H . At high concentrations and potentials, $C_d \gg C_H$, and the observed capacitance according to Equation 3.1, reduces to

$$C_{\text{obs}} \sim C_H$$

Similarly, at low concentrations and low potentials $C_d \ll C_H$ and hence

$$C_{\text{obs}} \sim C_d$$

In this section, the metal/solution interface has been described. In the next section, the oxide/electrolyte interface will be discussed. The solution side of this interface (i.e., C_H and C_d) is similar to that of the metal/solution interface, but the charging mechanism at the oxide surface is considerably different than that described for the metal surface.

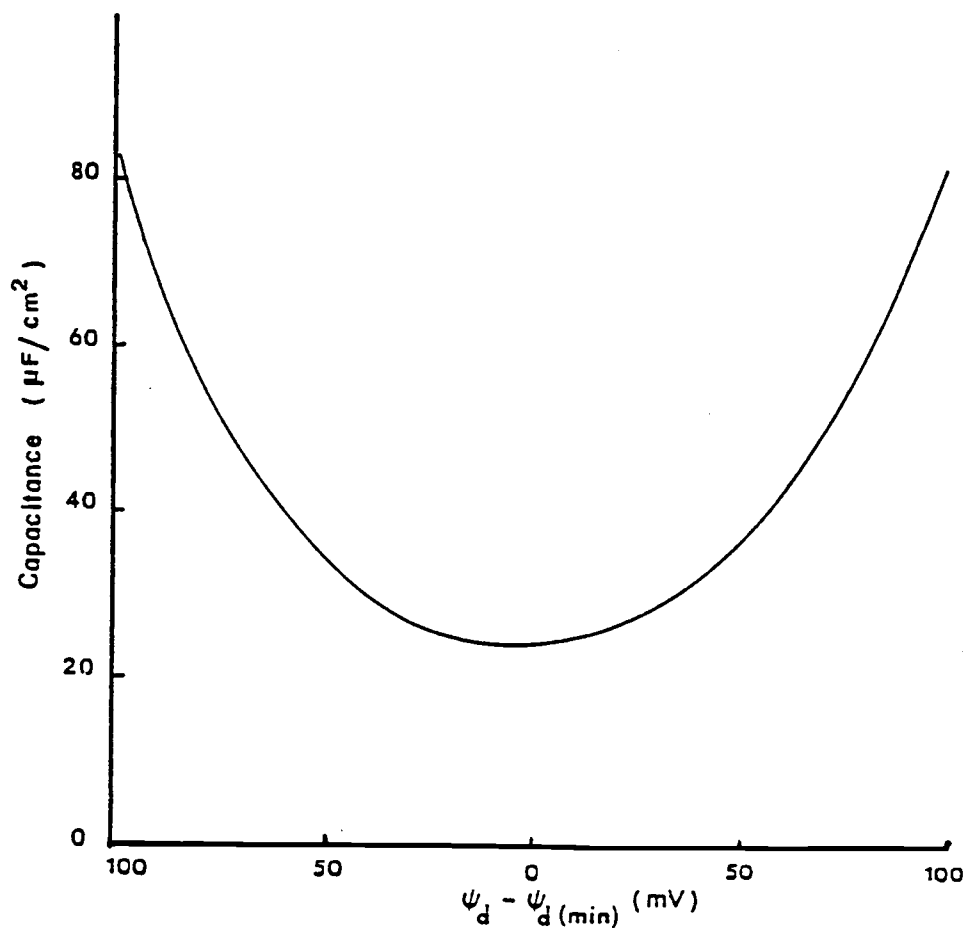


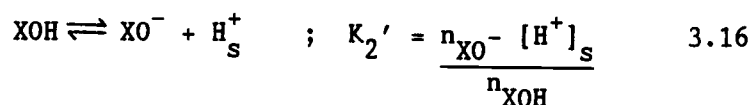
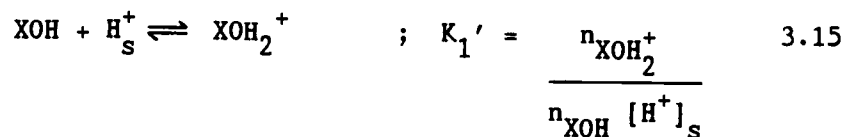
Figure 3.6. Differential capacitance as a function of applied potential as calculated from Equation 3.14.

3.2 Oxide/solution interface

The theories discussed for the electrical double layer at the metal/solution interface can be applied to the analysis of the oxide/electrolyte interface. However, the chemical interaction between the solution and the oxide must be considered in the analysis. In this section, the properties of the oxide/electrolyte interface are discussed by incorporating the chemical properties of the oxide with electrical double layer theory. Expressions for interfacial charge and potential in terms of properties of solution and oxide are derived.

A simple mechanism by which water can react with an oxide is illustrated in Figure 3.7. The water molecules adsorb onto the oxide surface and hydrolyze as indicated to yield surface hydroxyl groups. Thus, the surface of a hydrated oxide can be viewed as containing a large number of surface hydroxyl groups, often denoted by XOH. These hydroxyl groups are known as surface sites.

Equilibrium reactions and microscopic (surface charge dependent) equilibrium constants (K'_1 , K'_2) can be written for the protonation and de-protonation of these groups as follows.



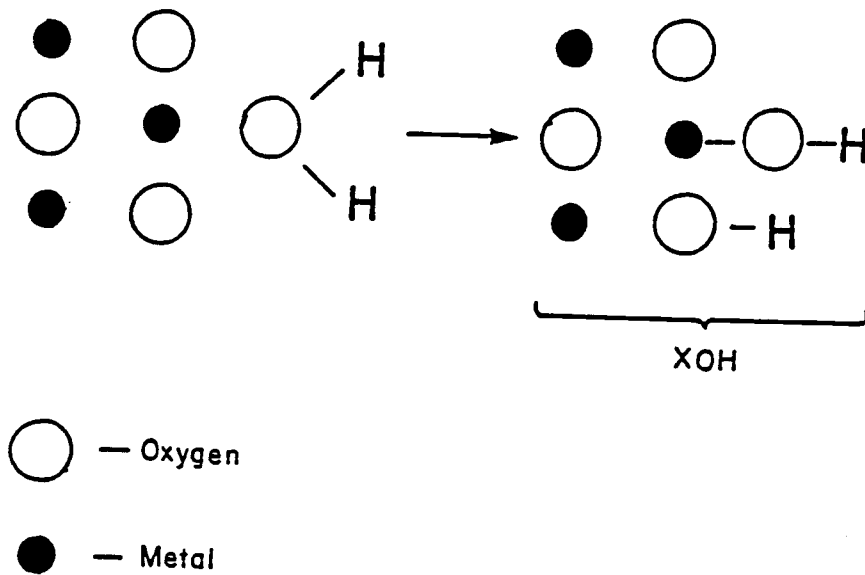


Figure 3.7. A simplified mechanism for the hydration of an oxide

In Equations 3.15 and 3.16, surface concentrations of positively charged, negatively charged, and neutral groups are denoted by $n_{\text{XOH}_2^+}$, n_{XO^-} and n_{XOH} . The subscript s denotes surface. The surface concentration of H^+ is related to the concentration of H^+ in the bulk of the solution by the following equation.

$$[\text{H}^+]_s = [\text{H}^+]_{\text{bulk}} \exp \left(\frac{-q \psi_o}{kT} \right) \quad 3.17$$

ψ_o is the potential of the surface of the oxide with respect to the bulk solution. The equilibrium expressions can then be expressed as

$$n_{\text{XOH}_2^+} = K_+ n_{\text{XOH}} [\text{H}^+] \exp \left(\frac{-q \psi_o}{RT} \right) \quad 3.18$$

$$n_{\text{XO}^-} = K_- n_{\text{XOH}} [\text{H}^+]^{-1} \exp \left(\frac{q \psi_o}{RT} \right) \quad 3.19$$

K_+ and K_- are known as intrinsic equilibrium constants for surface hydroxyl groups. These equations are similar to the mass action equations normally written for a homogeneous system, except for the exponential term included to account for the energy associated with moving an ion from the bulk of solution through an electric field to the surface.

It is believed that H^+ and OH^- ions are primarily responsible for the charge on the oxide surface, and thus for the potential of the oxide/solution interface. Therefore, H^+ and OH^- are generally known as potential determining ions. Cations

and anions from the electrolyte solution can also be adsorbed onto the charged oxide surface. The interactions between these ions and the oxide surface are considered to be weak, and as a first approximation, electrolyte ion adsorption will be disregarded in the following discussion.

In addition to the law of mass action equations given above, equations must be formulated for the conservation of sites (material balance) and charge density on the oxide. The material balance equation is

$$N_s = n_{XOH} + n_{XOH_2^+} + n_{XO^-} \quad 3.20$$

where N_s is the total XOH group density. The surface charge density on the oxide σ_d is given by

$$\sigma_o = q (n_{XOH_2^+} - n_{XO^-}) \quad 3.21$$

The following quantities are defined to facilitate the solution of Equations 3.18-3.21.

(1) The pH value at which the oxide surface is electrically neutral is defined as the pH of zero charge, denoted by pH_{zc} . At pH_{zc} , the concentrations of XOH_2^+ and XO^- are equal. It follows from Equations 3.18 and 3.19 that

$$[H^+]_{zc} = (K_-/K_+)^{1/2} \quad 3.22$$

(2) A surface dissociation constant K_D is defined as

$$K_D = (K_+ K_-)^{1/2} \quad 3.23$$

From Equations 3.18 and 3.19, K_D can also be expressed as

$$K_D = [XOH_2^+][XO^-]/[XOH]^2 \quad 3.24$$

From the definition of K_D and $[H^+]_{zc}$

$$K_+ = K_D/[H^+]_{zc} \quad 3.25$$

$$K_- = K_D [H^+]_{zc} \quad 3.26$$

(3) The function ϕ is defined such that

$$\phi = \frac{\ln [H^+]}{[H^+]_z} - \frac{q \psi_o}{RT} \quad 3.27$$

Solution of Equations 3.18 through 3.27 for σ_o yields

$$\sigma_o = \frac{2 q K_D N_s \sinh \phi}{1 + 2 K_D \cosh \phi} \quad 3.28$$

To complete the mathematical description of the interface, an independent electrostatic model is necessary to relate the surface charge to surface potential. In the previous section, it was indicated that the Helmholtz model is a more appropriate approximation for concentrated solutions, and the Gouy-Chapman model is more appropriate for dilute solutions. These two models are used separately as limiting cases in the following analysis of the oxide/electrolyte interface to illustrate the principles, while

avoiding complicated arithmetic. Regardless of the models used, the charge in the solution side of the interface σ_d can be given by the following general expression.

$$\sigma_d = \sigma_d(\psi_o, C_{\text{bulk}}) \quad 3.29$$

If the Helmholtz model is used, σ_d represents the charge on the Helmholtz plane and Equation 3.22 can be re-expressed as

$$\sigma_d = -C_d \psi_o \quad 3.30(a)$$

If the Gouy-Chapman model is used, σ_d represents the charge in the diffuse layer. To preserve the simplicity of the model, the potential at the inner boundary of the diffuse layer, ψ_d , is set equal to the surface potential ψ_o . Equation 3.22 can then be rewritten as follows.

$$\sigma_d = - \left(8 \epsilon_w \epsilon_o kT C_{\text{bulk}} \right)^{1/2} \sinh \left(\frac{q\psi_o}{2kT} \right) \quad 3.30(b)$$

Finally, electroneutrality through the interface requires

$$T_\sigma = \sigma_o(\psi_o, H^+) + \sigma_d(\psi_o, C_{\text{bulk}}) \quad 3.31$$

Equations 3.18 through 3.31 describe the oxide/solution interface completely. The unknowns in these equations are n_{XOH} , $n_{\text{XOH}_2}^+$, n_{XO^-} , σ_o , σ_d and ψ_o , and a solution of these equations is possible.

The mathematical description of the oxide/electrolyte interface presented above can be summarized as follows.

(1) σ_o has been expressed as an explicit function of H^+ , ψ_o and parameters K_D , N_s , $[H^+]_{zc}$.

(2) σ_d has been expressed as an explicit function of C_{bulk} and ψ_o using the Helmholtz model or the Gouy-Chapman model as the electrostatic model for the electrical double layer.

(3) The interfacial potential ψ_o has been expressed as an implicit function of H^+ , C_{bulk} , N_s , K_D and $[H^+]_{zc}$.

One of the goals of this study is to measure the change in the potential at the oxide/electrolyte interface with changes in the solution composition such as pH, i.e., the quantity of interest is $\partial\psi_o/\partial\ln[H^+]$. An expression for $\partial\psi_o/\partial\ln[H^+]$ can be derived as follows.

From the total differential of T_σ in Equation 3.31 the following equation is obtained.

$$\left(\frac{\partial\sigma_o}{\partial\psi_o}\right)_{\ln H^+} d\psi_o + \left(\frac{\partial\sigma_o}{\partial\ln H^+}\right)_{\psi_o} d\ln H^+ + \left(\frac{\partial\sigma_d}{\partial\psi_o}\right)_{C_{bulk}} d\psi_o + \left(\frac{\partial\sigma_d}{\partial C_{bulk}}\right)_{\psi_o} dC_{bulk} = 0 \quad 3.32$$

Equation 3.32 can be rearranged to yield

$$\left(\frac{\partial\psi_o}{\partial\ln H^+}\right)_{T_\sigma} = \frac{-(\partial\sigma_o/\partial\ln H^+)\psi_o}{(\partial\sigma_o/\partial\psi_o)_{\ln H^+} + (\partial\sigma_d/\partial\psi_o)_{C_{bulk}}} \quad 3.33$$

The derivatives on the right hand side of Equation 3.33 can be evaluated and re-expressed as effective differential capacitances.

The contribution of the surface hydrolysis reactions described in Equations 3.15 and 3.16 to the observed capacitance is denoted by

C_{rxn} and is defined from the derivative of Equation 3.28 by the following equation.

$$C_{\text{rxn}} = - \frac{\partial \sigma_o}{\partial \psi_o} = \frac{q}{kT} \frac{2q K_D N_s (2 K_D + \cosh \phi)}{(1 + 2 K_D \cosh \phi)^2} \quad 3.34$$

The differential capacitance of the solution side of double layer regardless of the model is given by

$$C_d = - \frac{\partial \sigma_d}{\partial \psi_o} \quad 3.35$$

By inspection of Equation 3.27 and 3.28 it can be seen that the derivative in the numerator of Equation 3.33 can be re-expressed as

$$\left(\frac{\partial \sigma_o}{\partial \ln H^+} \right)_{\psi_o} = - \frac{kT}{q} \left(\frac{\partial \sigma_o}{\partial \psi_o} \right)_{\ln H^+} \quad 3.36$$

Equation 3.33 can now be rewritten as follows by combining 3.33–3.36

$$\left(\frac{\partial \psi_o}{\partial \ln H^+} \right)_{T_\sigma} = \frac{kT}{q} \left(\frac{C_{\text{rxn}}}{C_{\text{rxn}} + C_d} \right) \quad 3.37$$

From Equation 3.37, it can be seen that $\left(\frac{\partial \psi_o}{\partial \ln H^+} \right)_{T_\sigma}$ approaches kT/q when $C_{\text{rxn}} \gg C_d$. This condition occurs when

- C_d is small
- K_D is large
- N_s is large

Another important result which emerges from Equation 3.37 is the equivalent circuit for the oxide/electrolyte interface as shown in Figure 3.8. Note that the basis for the equivalent circuit is Equation 3.26 rather than any a priori assumption about the nature of the interface.

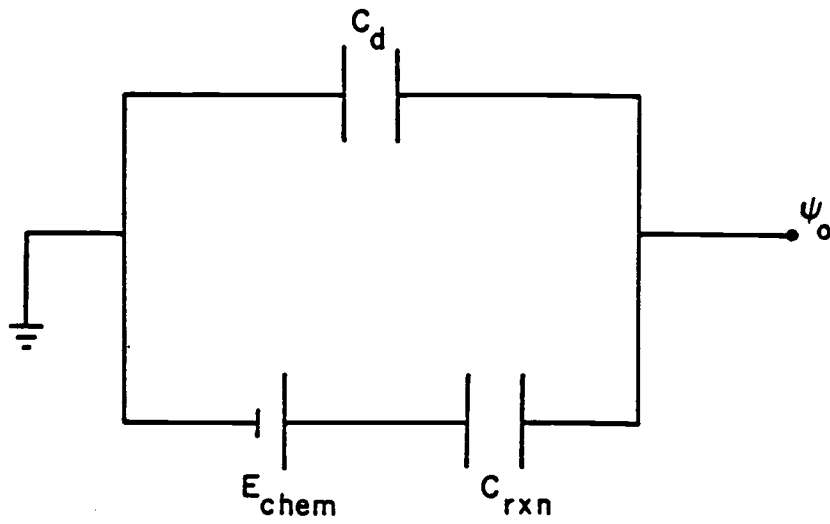


Figure 3.8. Equivalent circuit for oxide/electrolyte interface.

The driving force of the chemical reaction at the oxide/electrolyte interface is represented in the equivalent circuit by an electrostatic potential E_{chem} . E_{chem} is a function of H^+ activity in the solution, and is given by

$$E_{\text{chem}} = kT/q \ln [H^+]/[H^+]_{zc} \quad 3.38$$

How the oxide surface potential responds to this Nernstian driving force may be seen by considering (i) the overall reaction for charging the interface and (ii) the resistance to charging offered by the capacitances C_{rxn} and C_d .

The overall reaction leading to charging of the oxide surface can be divided into two steps.

- (1) transfer of H^+ and OH^- to the oxide surface
- (2) transfer of the counter charge to the solution part of the double layer.

If the primary resistance to charging is offered by the counter charge ($C_d \ll C_{\text{rxn}}$), then the full Nernstian potential is seen at the oxide surface. If the transfer of charge to the oxide surface itself offers a significant resistance ($C_d \sim C_{\text{rxn}}$), then the response is sub-Nernstian.

This interpretation is elucidated by considering an analog of Equation 2.3, valid for oxide surface. The surface potential is approximately Nernstian if the activity of H^+ at the surface is approximately constant. If the primary impedance to charging of the oxide surface is transfer of the counter charge into the diffuse layer, then the activity of H^+ at the surface does remain relatively constant, and Nernstian response is seen.

Equation 3.37 will be used as the working hypothesis for the relationship between the interfacial potential difference and $[H^+]$. To test the hypothesis, one needs to measure the surface potential on the oxide at various solution compositions.

The structures suitable for the measurement of potential changes at the oxide/solution interface will be examined in the next section.

3.3 Metal/oxide/electrolyte (MOE) structure

In the discussion of differential capacitance of the metal/solution interface, it was shown (Figure 3.6) that there is a minimum in the capacitance-applied potential curve. This minimum occurs at the potential at which there is zero charge on the metal (pzc). The pzc depends on the composition of the solution. The shifts of the pzc with solution composition at constant charge on the metal is $\left(\frac{\partial \psi_0}{\partial \ln C} \right)_{\sigma_m}$, the Esin-Markov coefficient.

Consider a metal electrode in a solution poised at the pzc. If a salt containing anions which are specifically adsorbed is added to the solution, the anions will tend to accumulate at the metal surface. To restore the interface to the zero charge condition, a negative electrical potential should be applied to the metal to drive the anions from the surface. Thus the minimum of the capacitance-voltage curve occurs at a more negative applied potential compared to that for the case where there is no specific adsorption. Thus one can observe shifts in the potential of capacitance minimum towards negative potentials when anions are specifically adsorbed on the metal (61,63). Such shifts could also be expected for the capacitance-voltage curves for the oxide/solution interface.

Thus changes in the electrode potential with changes in solution composition, under the condition of constant charge on the metal, can be determined through differential capacitance

measurements. Differential capacitance of metal/oxide/electrolyte (MOE) structures could be used, in principle, to detect the potential changes at the oxide/electrolyte interface. However, it will be shown that the observed capacitance of the MOE structure is not very sensitive to the interfacial potential difference, and that this structure is not suitable in detecting the potential changes at the oxide/electrolyte interface. To demonstrate this fact, an expression for observed differential capacitance of an MOE structure will be derived and discussed.

The charge and potential distribution at the metal/oxide/electrolyte (MOE) structure at $\text{pH} < \text{pH}_{\text{zc}}$ is shown in Figure 3.9. The MOE structure can be viewed as being comprised of two parts; the oxide/electrolyte interface and a metal oxide capacitor. The oxide/electrolyte interface in the MOE structure can be described by the same equations used in Section 3.2 (Equations 3.18-3.27). Two additional equations are necessary to describe the entire MOE structure.

(1) The charge on the metal is related to the oxide capacitance and potential difference by:

$$\sigma_m = C_{\text{ox}} (\psi_m - \psi_o) \quad 3.39$$

Where ψ_m is the potential applied to the metal relative to the bulk of the solution and σ_m is the charge on the metal.

(2) Charge neutrality in the interface is expressed as

$$T_\sigma = \sigma_o (\psi_o, H^+) + \sigma_d (\psi_o, C_{\text{bulk}}) + \sigma_m (\psi_m, \psi_o) \quad 3.40$$

and ψ_o is a function of H^+ , $[H^+]_{\text{zc}}$, K_D , N_s , and C_{bulk} .

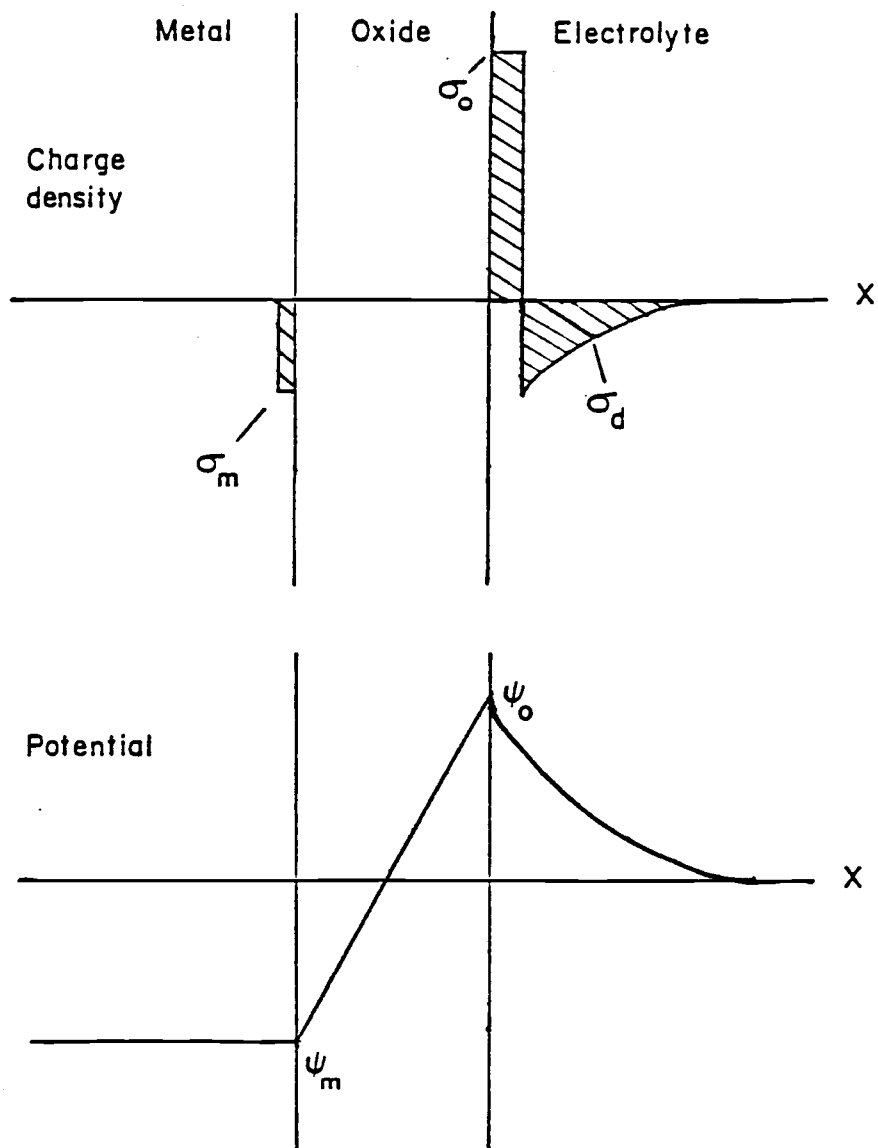


Figure 3.9. Charge and Potential profile at the metal/oxide/electrolyte (MOE) structure at $\text{pH} < \text{pH}_{zc}$.

As in the case of metal/solution interface, it is necessary to find the observed differential capacitance for the MOE structure.

The observed differential capacitance C_{obs} for the MOE structure can be given by

$$C_{\text{obs}} = - \left(\frac{\partial \sigma_m}{\partial \psi_m} \right)_{T_\sigma} \quad 3.41$$

An expression for C_{obs} can be found analytically as follows. From the total differential for

$$d\sigma_m = \left(\frac{\partial \sigma_m}{\partial \psi_m} \right)_{\psi_o} d\psi_m + \left(\frac{\partial \sigma_m}{\partial \psi_o} \right)_{\psi_m} d\psi_o \quad 3.42$$

an expression for the derivative equal to C_{obs} can be derived:

$$\left(\frac{\partial \sigma_m}{\partial \psi_m} \right)_{T_\sigma} = \left(\frac{\partial \sigma_m}{\partial \psi_m} \right)_{\psi_o} + \left(\frac{\partial \sigma_m}{\partial \psi_o} \right)_{\psi_m} \left(\frac{\partial \psi_o}{\partial \psi_m} \right)_{T_\sigma} \quad 3.43$$

An expression for $\left(\frac{\partial \psi_o}{\partial \psi_m} \right)_{T_\sigma}$ can be found from the total differential for T_σ in Equation 3.40. ^{σ}

$$\left(\frac{\partial \psi_o}{\partial \psi_m} \right)_{T_\sigma} = \frac{-(\partial \sigma_m / \partial \psi_m)_{\psi_o}}{\left(\frac{\partial \sigma_m}{\partial \psi_o} \right)_{\psi_m} + \left(\frac{\partial \sigma_o}{\partial \psi_o} \right)_{H^+} + \left(\frac{\partial \sigma_d}{\partial \psi_o} \right)_{C_{\text{bulk}}}} \quad 3.44$$

The derivatives of the right hand side of Equation 3.44 can be re-expressed as effective differential capacitances as before.

By differentiating σ_m in Equation 3.39 with respect to ψ_m or ψ_o , one obtains

$$\left(\frac{\partial \sigma_m}{\partial \psi_m} \right)_{\psi_o} = - \left(\frac{\partial \sigma_m}{\partial \psi_o} \right)_{\psi_m} = C_{\text{ox}} \quad 3.45$$

Equation 3.41 - 3.45 can be combined, and the definitions for C_{rxn} (Equation 3.34) and C_d (Equation 3.35) can be used to obtain the following expression for C_{obs} .

$$C_{\text{obs}} = \frac{C_{\text{ox}} (C_{\text{rxn}} + C_d)}{C_{\text{ox}} + C_{\text{rxn}} + C_d} \quad 3.46$$

From Equation 3.46 an equivalent circuit can be deduced as given in the Figure 3.10. Comparison of the equivalent circuits for the oxide/solution interface and the metal/oxide/electrolyte structure (Figures 3.8 and 3.10) show that the only difference between them is the presence of an additional oxide capacitance in the circuit for the metal/oxide/electrolyte structure. This difference is consistent with the difference in physical structure of the two cases.

The observed capacitance depends on the relative magnitude of the terms in Equation 3.33. When the oxide thickness is large, C_{ox} is very small in comparison to $(C_{\text{rxn}} + C_d)$, and this equation reduces to

$$C_{\text{obs}} \approx C_{\text{ox}}$$

and when C_{ox} is large in comparison to $(C_{\text{rxn}} + C_d)$, it reduces to

$$C_{\text{obs}} \approx C_{\text{rxn}} + C_d$$

C_{ox} can be calculated for oxides using the following relationship

$$C_{\text{ox}} = \frac{\epsilon_o \epsilon_{\text{ox}}}{d_{\text{ox}}} \quad 3.47$$

where ϵ_{ox} is the dielectric constant of the oxide and d_{ox} is the thickness of the oxide.

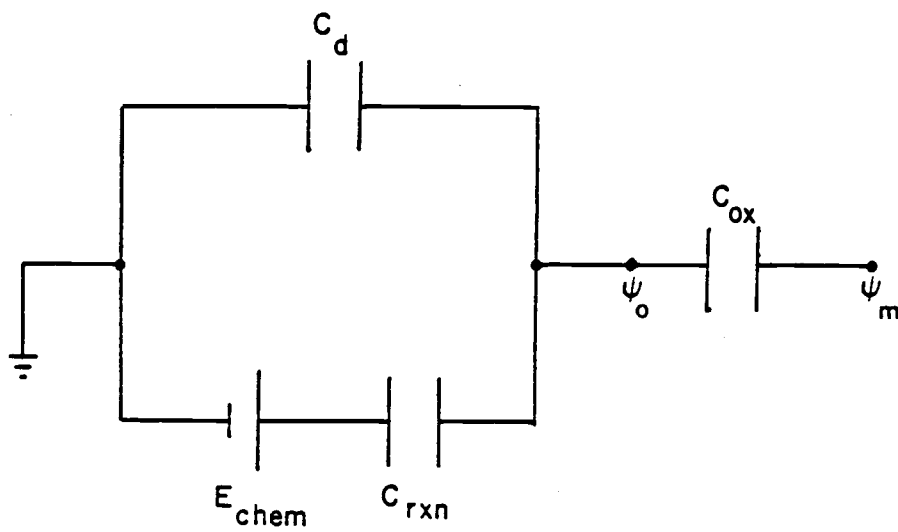


Figure 3.10. Equivalent circuit for the metal/oxide/electrolyte structure.

An estimate for the capacitance of the diffuse layer can be obtained from Equation 3.14. Table 3.1 shows the relative magnitude of C_{ox} , C_d and C_{obs} expected for the metal/oxide/electrolyte structures in solutions of different concentrations. The reaction capacitance C_{rxn} is not included in the comparison since it depends on the chemical properties of the oxide. However, it can be seen that the exclusion of C_{rxn} would have had no effect on the end result that C_{obs} is almost equal to C_{ox} in all cases shown in the table. This result is a consequence of the very small oxide capacitance. Oxide thicknesses would have to be impractically small to make the value of C_{ox} to be approximately the same magnitude as the value of C_d .

The calculated change in C_{obs} of a metal/oxide/solution structure with applied potential is shown in Figure 3.11 for typical values of C_d , C_{rxn} and C_{ox} . Thus, it is impossible to detect the changes in the potential of the metal/oxide/electrolyte structure via differential capacitance measurements.

As shown here, the observed capacitance of the metal/oxide/solution structure is dominated by the small capacitance of the oxide, and the potential dependent capacitance of the double layer cannot be detected. In order to detect changes in interfacial potential by changes in differential capacitance, another capacitor with potential dependent capacitance of magnitude similar to that of the oxide would have to be incorporated in the structure next to the oxide.

Table 3.1 Relative magnitudes of capacitive elements
metal/oxide/solution interface ($\epsilon_{\text{ox}}=3.9$)

d_{ox} (nm)	C_{ox} (F/m ²)	C_{bulk} (M)	C_d (F/m ²)	C_{obs} (F/m ²)
20	0.0017	0.1	0.72	0.0017
		0.01	0.23	
		0.001	0.072	
50	0.0007	0.1	0.72	0.0007
		0.01	0.23	
		0.001	0.072	

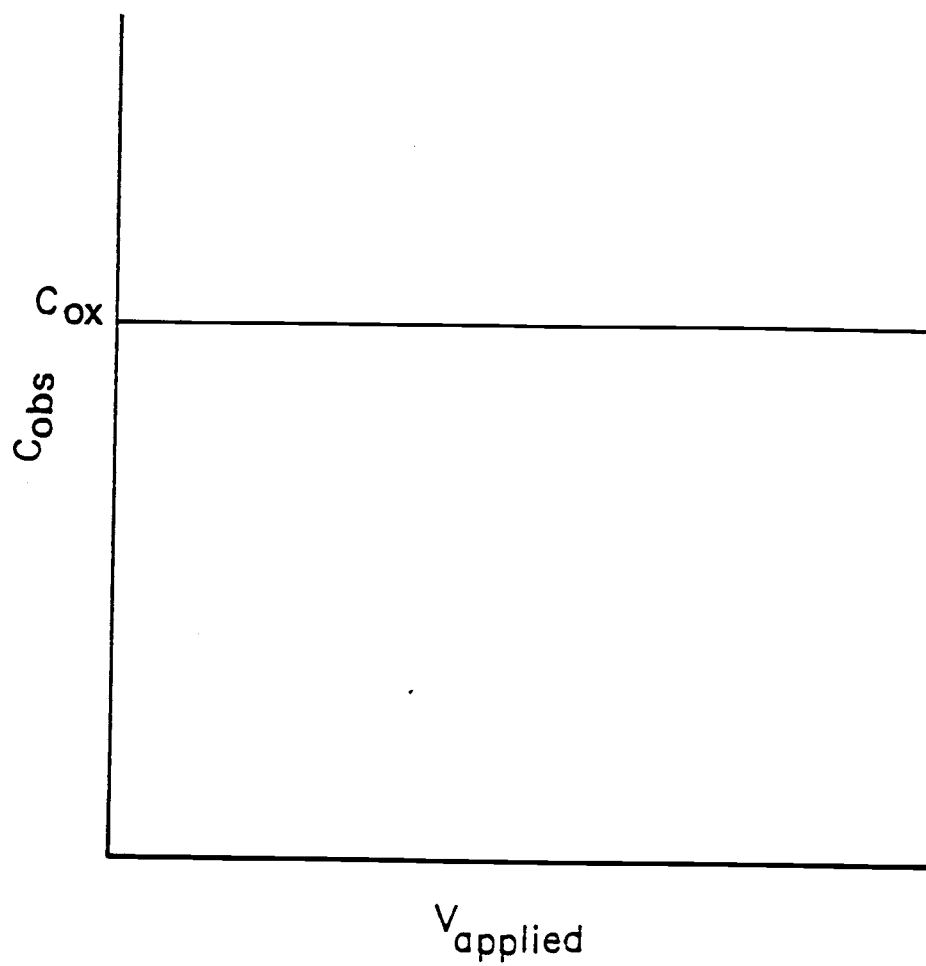


Figure 3.11. Variation of C_{obs} with applied potential
for metal/oxide/electrolyte structure
($d_{ox} = 50$ nm, $\epsilon_{ox} = 3.9$, $C_{bulk} = 0.1$)

A semiconductor can be prepared for this purpose and used in an electrolyte/oxide/semiconductor/metal (EOS) structure to detect the changes in the surface potential of the oxide.

3.4 Electrolyte/oxide/semiconductor (EOS) structure

It was shown in the previous section that the capacitance of the metal/oxide/electrolyte structure is dominated by the small capacitance of the oxide. The insertion of a semiconductor between the oxide and the metal makes the total capacitance of this structure dependent on the potential at oxide/electrolyte interface. The goal, measurement of the change in interfacial potential with change in solution composition, can be achieved by detecting the shift of capacitance-voltage (C-V) curves obtained for the EOS structure. Alternatively, the shift of a characteristic reference point, the flat-band potential of the EOS structure, can be used to detect such potential changes.

To illustrate the use of the EOS structures in capacitance measurements, it is convenient to exclude the electrolyte solution from the initial discussion. If the complexity of the electrolyte solution is replaced by the relative simplicity of a metal, a metal/oxide/semiconductor (MOS) structure can be considered instead of an EOS structure. The semiconductor side of the EOS structure would behave, in principle, in the same way as an MOS structure. A brief discussion of the properties of MOS structures is presented as an introduction to EOS structures. A detailed account on this subject can be found in excellent books by Grove (64) and Sze (65).

Metal/Oxide/Semiconductor (MOS) structure

Capacitance-voltage (C-V) characteristics of EOS structures are expected to be similar to those of the metal/oxide/semiconductor structures. In this section, an introduction to the fundamentals of MOS structures followed by a theoretical analysis of C-V characteristics of MOS structure is presented.

Semiconductors are classified according to the type of the majority charge carriers they possess. In n-type semiconductors the majority carriers are electrons, and in p-type positively charged holes. Some of the basic concepts in semiconductor physics are analogous to those in solution chemistry (66). This analogy is illustrated in Table 3.2.

Some important concepts from semiconductor physics which are necessary for the understanding of the C-V characteristics of the MOS structure are presented here. A metal/SiO₂/Si structure will be considered in this discussion.

Work function of materials

The electronic work function of a material is defined as the energy required to remove an electron from the material at the Fermi level to vacuum (64). The Fermi level is the electrochemical potential of electrons in the material relative to the energy of an isolated electron in a vacuum.

Table 3.2. Some analogies between semiconductors and electrolyte solutions (after reference 66)

phenomenon	in aqueous solution	in semiconductor
dissociation	$H_2O = H^+ + OH^-$	lattice = $e^- + h^+$
	$k_W = [H^+] + [OH^-]$	$K_{sc} = np$
	$n_{H^+} \sim n_{OH^-} \sim 10^{-14}$	$n=p \sim 10^{10} - 10^{12}$
acid addition	$HX = H^+ + X^-$ (proton donor)	$D = D^+ + e^-$ (electron donor)
	adding acid to water increases H^+ concentration	adding electron donor to intrinsic semiconductor increases e^- concentration

Surface states

Surface states are considered as electronic energy levels of a solid which are located at the surface. The sources of these energy levels are the imperfections of crystal structure normally found at the surfaces. Clean surfaces of covalent solids can have surface states due to "dangling bonds." These states are known as Schokley states. Ionic solids have surface energy levels due to unsymmetrical ionic distribution at the surface. These levels are called Tamm states. Both Tamm and Schokley states are known as intrinsic surface states. Surface states also arise due to adsorption of ions or molecules from another phase. In the MOS structure, surface states can be present at the oxide/semiconductor interface and the oxide/metal interface. These states contribute to the capacitance of the MOS structure.

Charge in the oxide

Three types of charges are associated with oxide layers obtained by thermal oxidation of silicon.

- (1) Surface state charge
- (2) Fixed charge
- (3) Mobile ionic charge

The surface state charge in the oxide is associated with defects at the oxide surface, as discussed above. These defects can be present either at the oxide/semiconductor interface or at the oxide/metal interface.

A layer of non-stoichiometric silicon oxide SiO_x exists at the surface of silicon due to incomplete oxidation of silicon. It has been suggested that excess silicon near the Si/SiO_2 interface is the origin of fixed oxide charge (65).

Mobile ionic charges are found in the oxide as a result of the diffusion of impurities such as Na^+ or K^+ ions into the oxide. The diffusion of these ions in the oxide causes instabilities in the characteristics of MOS structures.

As a practical matter, all forms of charge associated with the interior of the oxide and the oxide/semiconductor interface are lumped together as an equivalent fixed charge at the oxide/semiconductor interface as follows.

$$\sigma_{\text{ox}} = \sigma_{\text{ss}} + \sigma_{\text{f}} \quad 3.48$$

where σ_{ss} is the charge of the surface states and σ_{f} is the fixed charge in the oxide. Mobile ionic charge and potential dependent surface states are obviously poorly approximated by this representation.

Effect of applied potential on charge distribution

The effect of the an applied potential on the charge distribution in a MOS structure is discussed in a qualitative manner. All potentials are expressed relative to the bulk of the semiconductor. Consider the schematic diagram of an MOS structure shown in Figure 3.12. The potential at the semiconductor/oxide interface is designated by ϕ_s , and it can be changed by varying the potential applied to the metal field plate (V_{appl}).

The semiconductor is said to be under positive or negative bias depending on the sign of ϕ_s . Energy bands and charge distribution in an ideal MOS structure, with an n-type semiconductor, under different bias conditions are shown in Figure 3.13. When $\phi_s > 0$, the concentration of electrons, in this case the majority carriers, is increased near the semiconductor surface. This condition of increased concentration of majority carriers is called "accumulation" and is shown in Figure 3.13(a). If a small negative potential is applied such that $\phi_s < 0$, majority carriers are depleted from the surface, leaving a "depletion region" containing of uncompensated donor ions as shown in Figure 3.13(b). When the applied potential is made more negative i.e, $\phi_s \ll 0$, more and more electrons are depleted from the semiconductor surface increasing the

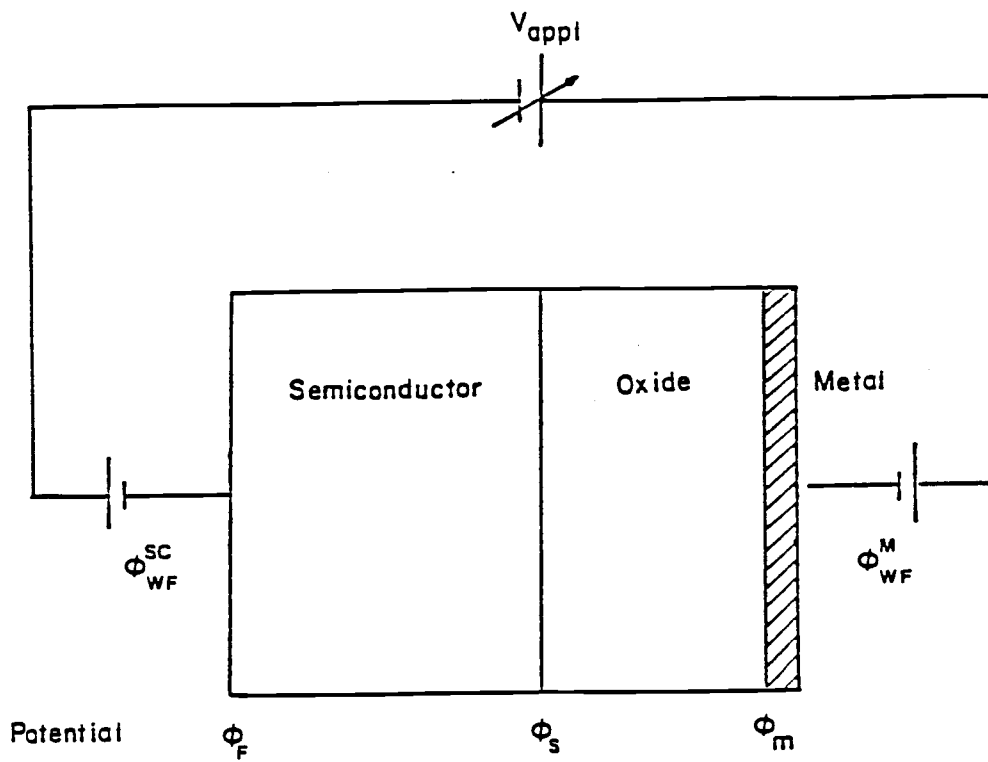


Figure 3.12. Schematic diagram of a metal/oxide/semiconductor

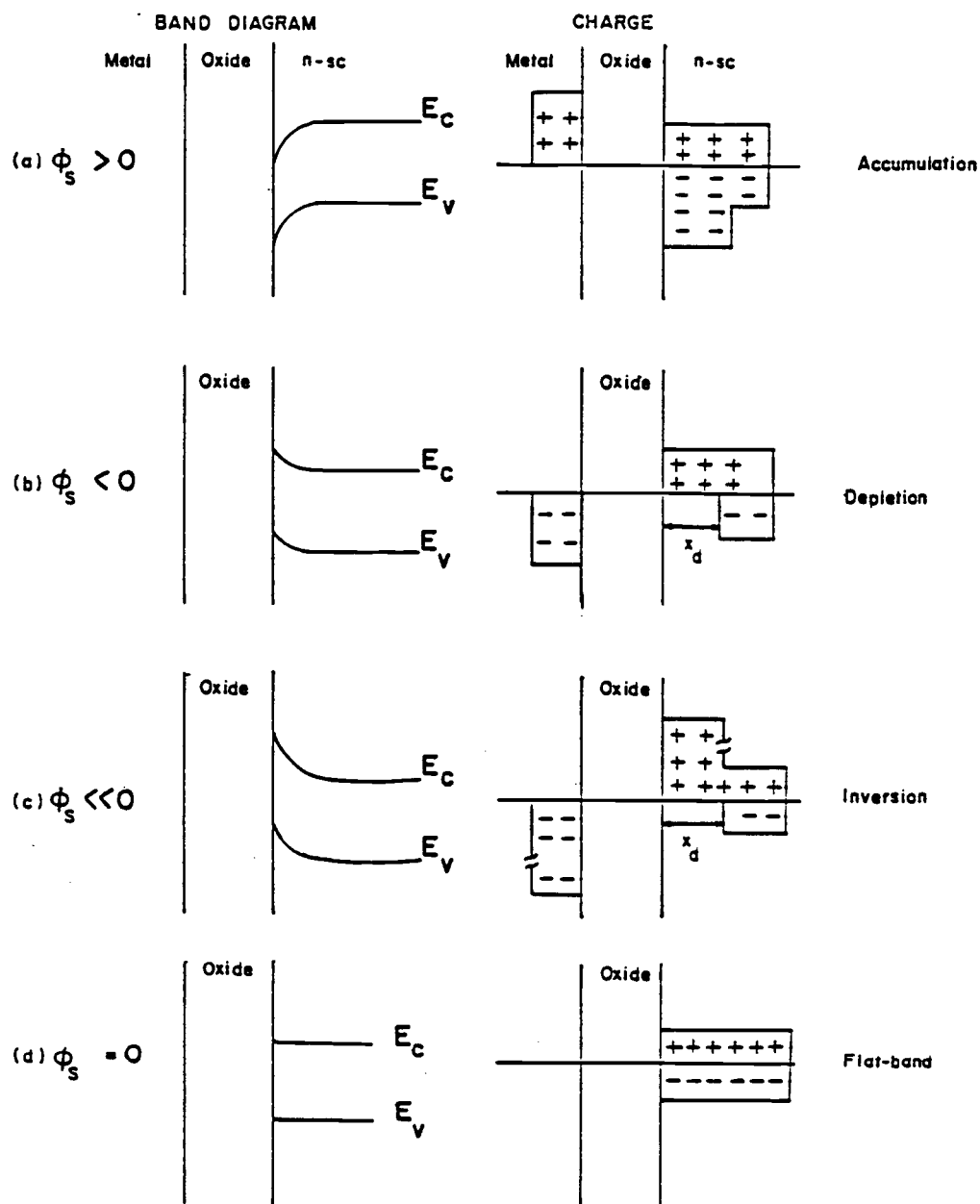


Figure 3.13. Energy bands and charge distribution in an ideal MOS structure with an n-type semiconductor, under different bias conditions.

width of the depletion region x_d . Eventually, when the applied potential is negative and large, Si atoms in the lattice begin to ionize, and a sharp rise in the hole concentration occurs near the surface. This condition is known as "inversion" and is shown in Figure 3.13(c). When ϕ_s is zero (Figure 3.13(d)), there is no potential drop across the MOS structure, and the charge in the semiconductor is zero. Since energy bands are not bent at this bias condition, it is called the "flat-band" condition. The potential that should be applied to reach this condition is called the flat-band potential of the MOS structure.

Capacitance-Voltage relationship for an ideal MOS structure

It was shown in the preceding discussion that the charge distribution in the semiconductor of an MOS structure depends on the applied potential. Information on the relationship between charge and potential can be gained from study of the capacitance-voltage (C-V) characteristics of MOS structures. C-V studies are used often in the semiconductor industry as a diagnostic tool. Zaininger et al. (67) discuss the great deal of information that can be extracted from the C-V curves. The principles used in the derivation of the C-V relationship for an MOS structure are almost the same as those used previously for the electrical double layer, and they are briefly described here. Determination of the flat-band potential from the C-V data will be discussed at the end of the description.

The goal of the following discussion is to express the differential capacitance of the semiconductor C_{sc} , as a function of the applied potential V_{appl} . For the purpose of simplification we restrict this discussion to the following

(1) An ideal MOS structure with an n-type semiconductor is considered.

(2) The coordinate system is defined with x direction perpendicular to the semiconductor surface and y and z directions parallel to the surface. Charge distribution is independent of y and z coordinates and is considered only in the x-dimension with $x=0$ at the surface and $x \rightarrow \infty$ in the bulk of the semiconductor.

To start out with, the fundamental equations which describe the space charge layer are presented.

(1) The charge in the semiconductor is due to ionized donors and acceptors, electrons and holes. The charge density $\rho(x)$ is given by

$$\rho(x) = q (N_D - N_A + p(x) - n(x)) \quad 3.49$$

The concentrations of ionized donors, ionized acceptors, electrons, and holes are given as N_D , N_A , n , and p respectively.

(2) The distributions of electrons and holes as functions of potential are given by

$$n(x) = n_0 \exp (q\phi(x)/kT) \quad 3.50$$

$$p(x) = p_0 \exp -(q\phi(x)/kT) \quad 3.51$$

where $\phi(x)$ is the potential relative to the bulk of the semiconductor. n_0 and p_0 are the equilibrium densities of electrons and holes in the bulk of the semiconductor. The

concentrations N_A and N_D are assumed to be independent of potential. A more complete expression for the components of $\rho(x)$ is given in Section 3.4.

(3) The charge density $\rho(x)$ is related to the potential by Poisson's equation.

$$\rho(x) = -\epsilon_s \epsilon_0 \frac{d^2 \phi(x)}{dx^2} \quad 3.52$$

where ϵ_s is the dielectric constant of the semiconductor.

(4) The charge per unit surface area ϕ_{sc} is expressed as

$$\sigma_{sc} = \int_0^\infty \rho(x) dx \quad 3.53$$

(5) The differential capacitance of the semiconductor C_{sc} , is given by

$$C_{sc} = - \frac{d\sigma_{sc}}{d\phi_s} \quad 3.54$$

where ϕ_s is the surface potential of the semiconductor.

Equations 3.48 through 3.54 with the appropriate boundary conditions define the potential-charge relationship for the semiconductor in terms of the the surface potential ϕ_s . It remains to solve for C_{sc} in terms of the applied potential V_{appl} . First, C_{sc} will be expressed as a function of ϕ_s by manipulating the above equations. Then from the relationship between ϕ_s and V_{appl} , the dependence of C_{sc} on V_{appl} will be shown.

Integration of Poisson's equation (3.52) with boundary condition ($\lim x \rightarrow \infty, \phi = 0$) yields

$$\sigma_{sc} = -\epsilon_s \epsilon_0 \left. \frac{d\phi}{dx} \right|_{x=0} \quad 3.55$$

An expression for $\frac{d\phi}{dx}$ can be obtained as follows. Consider the charge neutrality in the bulk of the semiconductor. From Equation 3.49, zero charge density in the bulk of the semiconductor can be expressed as

$$N_D - n_o + p_o - N_A = 0 \quad 3.56$$

Equations 3.49-3.51 and 3.56 can be combined to give

$$\rho(\phi) = q \left\{ n_o \left[1 - \exp \left(\frac{q\phi}{kT} \right) \right] + p_o \left[\exp \left(\frac{-q\phi}{kT} \right) - 1 \right] \right\} \quad 3.57$$

Combination of Equation 3.52 with 3.57 yields

$$\frac{d^2\phi}{dx^2} = \frac{-q}{\epsilon_s \epsilon_o} \left\{ n_o \left[1 - \exp \left(\frac{q\phi}{kT} \right) \right] + p_o \left[\exp \left(\frac{-q\phi}{kT} \right) - 1 \right] \right\} \quad 3.58$$

Integration of Equation 3.58 in the limits $x = \infty$ (bulk where $\phi=0$) and $x = 0$ (surface where $\phi = \phi_s$)

$$\begin{aligned} & \left(\frac{d\phi}{dx} \right)^2 \Big|_{n=0} \\ &= \left(\frac{2kT}{q} \right)^2 \left(\frac{q^2 n_o}{2\epsilon_s \epsilon_o kT} \right) \left[\left(e^{q\phi_s/kT} - \frac{q\phi_s}{kT} - 1 \right) + \frac{p_o}{n_o} \left(e^{-q\phi_s/kT} + \frac{q\phi_s}{kT} - 1 \right) \right] \end{aligned} \quad 3.59$$

To simplify the notation, we define the Debye length of the semiconductor L_D as

$$L_D = \left(\frac{q^2 n_o}{2\epsilon_s \epsilon_o kT} \right)^{1/2} \quad 3.60$$

and

$$F(\phi, p_o, n_o) = \left[\left(e^{q\phi_s/kT} - \frac{q\phi_s}{kt} - 1 \right) + \frac{p_o}{n_o} \left(e^{-q\phi_s/kT} + \frac{q\phi_s}{kT} - 1 \right) \right]^{1/2} \quad 3.61$$

Then Equation 3.59 can be rearranged to a simpler form as follows

$$\frac{d\phi_s}{dx} = \pm \sqrt{2} \frac{kT}{L_D q} F(\phi_s, p_o, n_o) \quad 3.62$$

Equations 3.62 can be substituted into Equation 3.55 to yield the following expression for σ_{sc}

$$\sigma_{sc} = \pm \sqrt{2} \frac{\epsilon_s \epsilon_o kT}{q L_D} F(\phi_s, p_o, n_o) \quad 3.63$$

In Equation 3.63, σ_{sc} is an explicit function of ϕ_s . Therefore, it can be differentiated with respect to ϕ_s to obtain the following expression for differential capacitance.

$$C_{sc} = \sqrt{2} \frac{\epsilon_s \epsilon_o kT}{q L_D} F'(\phi_s, p_o, n_o) \quad 3.64$$

Equation 3.63 is not practically significant since ϕ_s cannot be measured. An expression relating C_{sc} and the applied potential V_{appl} would be more useful than Equation 3.63. However, such an expression cannot be obtained until a relationship between V_{appl} and ϕ_s is found.

The relationship between V_{appl} and ϕ_s can be found by considering the voltage drops around the circuit in Figure 3.12.

$$V_{appl} = \phi_{WF}^M + (\phi_m - \phi_s) + (\phi_s - \phi_F) - \phi_{WF}^{sc} \quad 3.65$$

Where ϕ_{WF}^M and ϕ_{WF}^{sc} are work functions of metal and semiconductor respectively. The difference between the work functions of the metal and the semiconductor can be represented by

$$\Delta\phi_{MS} = \phi_{WF}^M - \phi_{WF}^{sc} \quad 3.66$$

The voltage drop across the oxide is related to the charge in the semiconductor, and the equivalent fixed charge at the semiconductor/oxide interface by

$$\phi_m - \phi_s = - \frac{(\sigma_{sc} + \sigma_{ox})}{C_{ox}} \quad 3.67$$

where σ_{sc} is given by Equation 3.63. The voltage drop across the semiconductor can be expressed as

$$\phi_s - \phi_F = \phi_s \quad 3.68$$

since the potential at the surface of the semiconductor is defined with respect to the bulk of the semiconductor. A combination of Equations 3.65-3.68 yield a single equation relating V_{appl} to ϕ_s :

$$V_{appl} = \Delta\phi_{MS} - \frac{\sigma_{ox}}{C_{ox}} - \frac{\sigma_{sc}}{C_{ox}} + \phi_s \quad 3.69$$

The applied voltage when $\sigma_{sc} = \phi_s = 0$ is referred to as the flat-band voltage, V_{FB} . From Equation 3.69, the following expression for V_{FB} can be obtained.

$$V_{FB} = \Delta\phi_{MS} - \frac{\sigma_{ox}}{C_{ox}} \quad 3.70$$

For an ideal semiconductor, V_{FB} is zero. Then if V_{appl} is referenced to V_{FB} ,

$$V_{appl} - V_{FB} = - \frac{\sigma_{sc}}{C_{ox}} + \phi_s \quad 3.71$$

Equation 3.71 can be solved numerically for ϕ_s , and the value obtained for ϕ_s can be used in Equation 3.64 to find C_{sc} as a

function of V_{appl} . The computer program PSI2, given in Appendix A, was used in the calculations.

The principles and mathematical procedure involved in the computation of the differential capacitance of the semiconductor as a function of applied voltage can be summarized as follows.

- (1) The fundamental equations necessary to describe the charge distribution of a semiconductor are given.
 - (a) charge density at a given point of the semiconductor (Equation 3.49)
 - (b) distribution of electrons, and holes in the semiconductor as a function of potential (Equations 3.50, 3.51)
 - (c) relationship of charge density to potential (Equation 3.52)
 - (d) charge per unit area (Equation 3.53)
- (2) The differential capacitance of the space charge layer C_{sc} is defined as $\frac{d\sigma_{\text{sc}}}{d\phi_s}$ (Equation 3.54).
- (3) Expression for σ_{sc} is obtained as explicit functions of ϕ_s . (Equations 3.55-3.63)
- (4) An expression for C_{sc} is obtained by differentiation of the expression for σ_{sc} (Equation 3.64).
- (5) ϕ_s can be related to V_{appl} by considering the potential drop across the MOS structure (Equations 3.65-3.69).
- (6) Using the ϕ_s value from step 5, C_{sc} is computed from Equation 3.64 at a given V_{appl} .

Figure 3.14 shows a theoretical C-V curve calculated for an MOS structure with an n-type Si semiconductor ($N_D = 5 \times 10^{15}$ and $d_{ox} = 500 \text{ \AA}$, $C_{ox} = 69 \text{ nF/cm}^2$). It can be seen from this figure that C_{sc} is very large when the applied potential is large. The total capacitance of the system is represented by a series combination of the oxide capacitance and the semiconductor capacitance.

$$C_{obs} = \frac{C_{ox} C_{sc}}{C_{ox} + C_{sc}} \quad 3.72$$

When the applied potential is such that the semiconductor is either in accumulation or the inversion region (i.e., $V_{appl} \gg 0$), C_{sc} is much larger than C_{ox} ; hence

$$C_{obs} \sim C_{ox}$$

The normalized observed differential capacitance C_{obs}/C_{ox} for the above MOS structure as a function of applied voltage is shown in Figure 3.15. This figure shows that the potential dependence of C_{sc} can be observed only in the depletion region and in the weak inversion region.

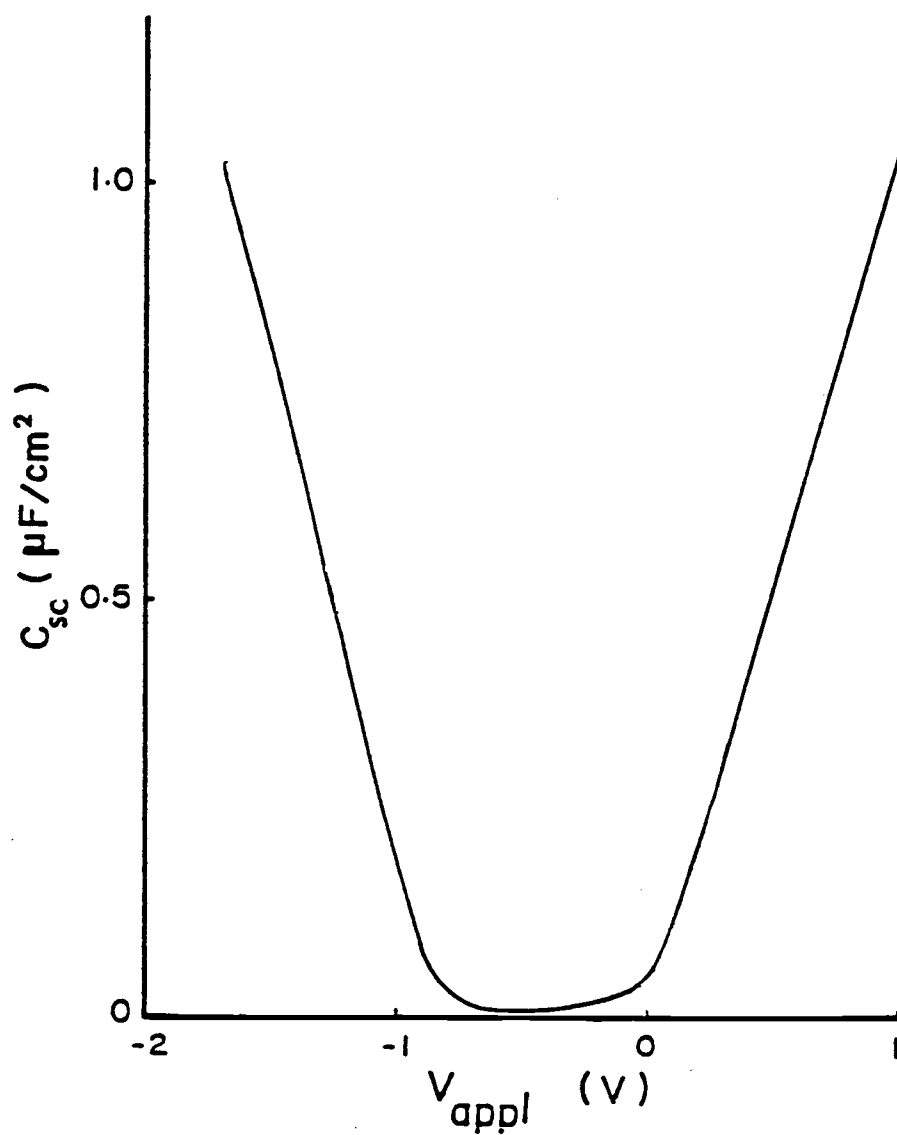


Figure 3.14. Theoretical differential capacitance of the semiconductor of an MOS structure as a function of applied potential
(n-type Si, $N_D = 1 \times 10^{15}$ and $d_{ox} = 550$ Å)

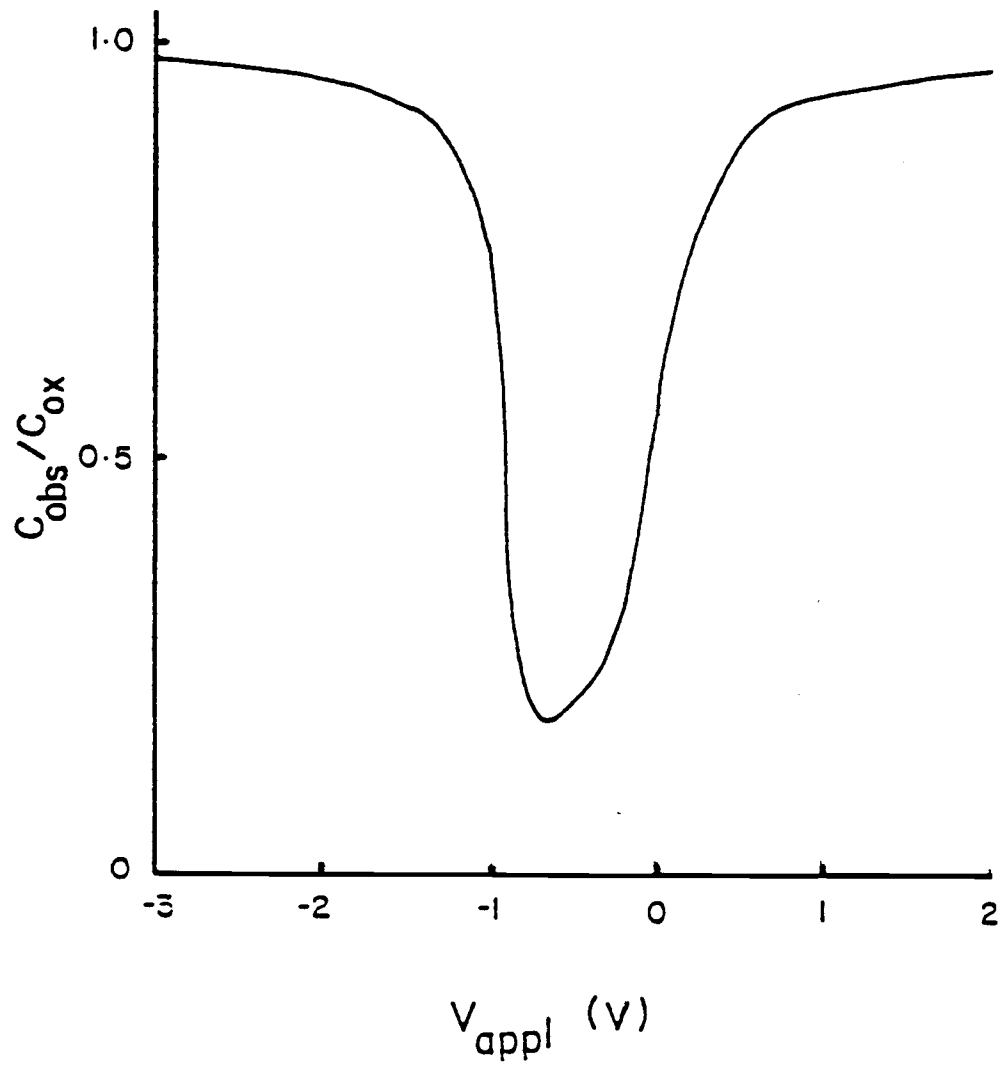


Figure 3.15. Normalized observed capacitance as a function of applied potential for the same MOS structure as in Figure 3.14.

Application of MOS theory for EOS structures

The observed capacitance of an MOS structure was shown to be dependent on the potential applied to the metal gate. In the EOS structure to be used in the determination of potential changes at the oxide/electrolyte interface, the metal of the MOS structure is replaced conceptually by an electrolyte. Therefore, C-V curves similar to those obtained for the MOS structures can be expected for the EOS structures upon application of potential to the electrolyte gate. In Section 3.2, it was shown that the electrolyte ions (primarily H^+) can change the surface potential of the oxide. Based on this principle, the observed capacitance for the EOS structures can be expected to change with the solution composition, at a given applied potential. Therefore, the C-V curves can be expected to shift along the voltage axis as the solution composition changes. The magnitude of the shift along the voltage axis is equal to the magnitude of the change in potential at the oxide surface. The magnitude of the shift, hence the potential change at the oxide/electrolyte interface, can be measured graphically or numerically. The shift between two C-V curves can be determined numerically by finding the offset that should be added to the voltage axis data of one curve to superimpose it on another.

An alternative method of detecting of the potential changes at the oxide/electrolyte interface from C-V curves is through the determination of flat-band potential shifts. This method will be discussed next.

Determination of flat-band potential

As mentioned in the beginning of Section 3.4, the flat-band potential of the EOS structure can be taken as a reference point from which the changes in potential at the oxide/electrolyte interface are measured. It will be shown that the change in the flat-band potential with solution composition can be translated to potential change at the oxide/solution interface. A method involving a further simplification of the equations to determine flat-band potential is presented in the following discussion.

When the bias potential of the semiconductor is such that the majority carriers are depleted from the semiconductor surface, the charge in the depletion region is due to uncompensated donor ions. Therefore, the charge density $\rho(x)$ can be approximated by,

$$\rho(x) = q N_D \quad 3.73$$

Compare Equation 3.73 with Equation 3.49 where $\rho(x)$ is expressed in terms of all charged species in the semiconductor. The charge distribution is approximated, in this case, by a region of fixed width x_d of total depletion, bordered by neutral bulk of the semiconductor, instead of the continuous charge distribution as used earlier. The variability in total charge is then expressed simply by the width of the depletion region.

The surface charge on the semiconductor σ_{sc} is expressed as

$$\sigma_{sc} = x_d \int_0^0 \rho(x) dx = q N_D x_d \quad 3.74$$

Integration of the Poisson equation (3.52) twice yields

$$\phi_s = - \frac{q N_D x_d^2}{2 \epsilon_s \epsilon_o} \quad 3.75$$

Equations 3.74 and 3.75 can be combined with Equations 3.63, 3.64, 3.71 and 3.72 to obtain the following equation.

$$\left(\frac{C_{obs}}{C_{ox}} \right)^{-2} = 1 - \frac{2 C_{ox}^2}{\epsilon_s \epsilon_o q N_D} (V_{appl} - V_{FB}) \quad 3.76$$

The above expression is known as the Mott-Schottky relationship.

The slope of a plot between $(C_{obs}/C_{ox})^{-2}$ vs V_{appl} yields the dopant density and the x-intercept of this plot with $y=1$ yields the flat-band potential.

The potential at the oxide/electrolyte interface is dependent on the activity of H^+ solution. Therefore, for an EOS structure, the applied potential necessary to make the charge in the semiconductor zero, i.e, flat-band potential V_{FB} , changes with the pH of the solution. The shift of V_{FB} can be determined by the method outlined above.

The determination of V_{FB} via the Mott-Schottky method is tedious. One of the strong points of this method is that it is possible to determine V_{FB} and the dopant density from the same experiment. Dopant density of the semiconductor used in the EOS system is usually known before the experiment. Determination of dopant density from C-V curves is not essential, but would be useful in verification of the C-V data. In cases where determination of dopant density is not necessary, the much simpler method of curve superposition can be used. Both methods yield the same shift for two given curves.

Unified view of EOS structures

It was shown that the change in potential at the oxide electrolyte interface could be indicated by the shift of C-V curves. In the discussion which led to the above conclusion, it was tacitly assumed that neither the applied potential nor the charge on the semiconductor influenced the potential difference at the oxide/electrolyte interface. A more complete theoretical analysis of the entire EOS structure is required, not only to check the validity of the assumption, but also to provide a firm basis for the interpretation of the experimental data. The principles involved in this analysis are outlined in this section.

A schematic diagram of the EOS structure is given in Figure 3.16. A reference electrode immersed in the solution must be used to complete the electrochemical cell, and it is included in the diagram as E_{ref} . All potentials ψ shown in the figure are expressed relative to the bulk of the solution, which is represented as ground.

The sum of voltage drops around the circuit is

$$E_{\text{Ref}} + V_{\text{Appl}} - \Delta\phi_{\text{MS}} + (\psi_{\text{S}} - \psi_{\text{F}}) + (\psi_{\text{O}} - \psi_{\text{S}}) - \psi_{\text{O}} = 0 \quad 2.77$$

where the difference between the work functions of the semiconductor

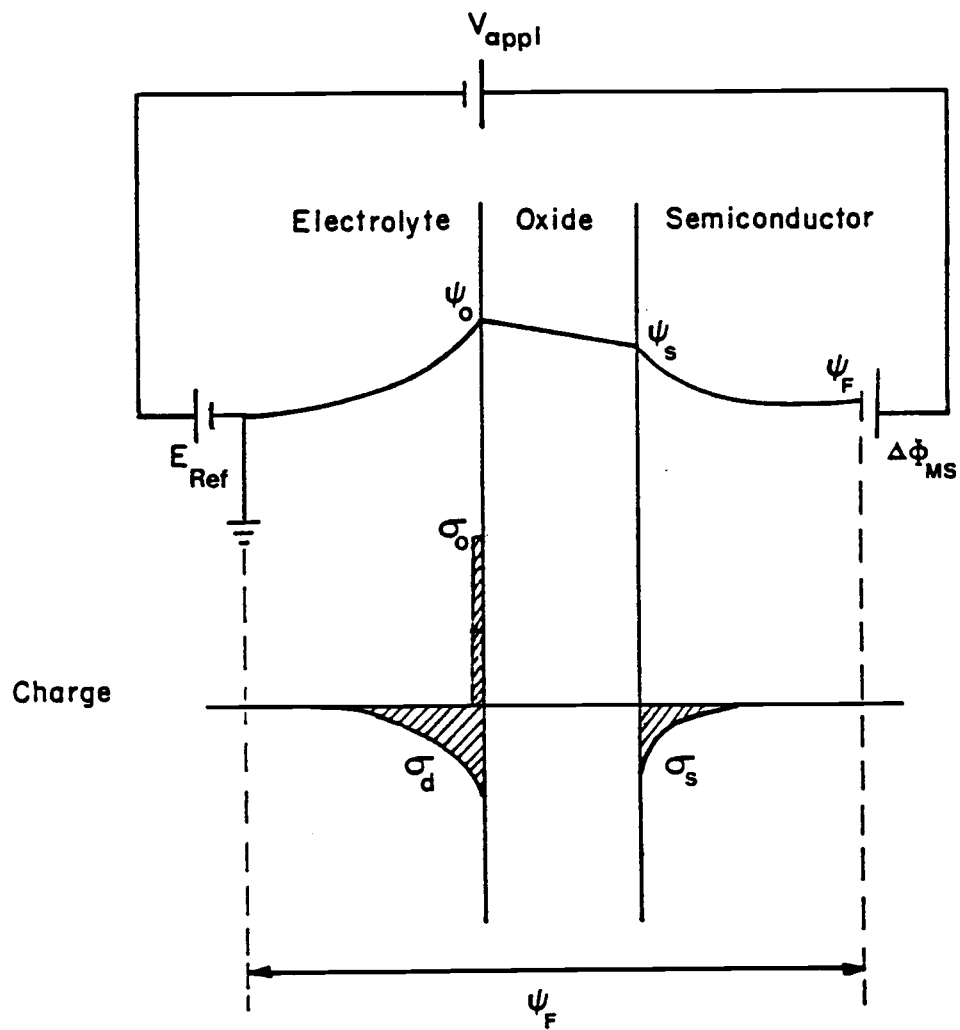


Figure 3.16. Schematic diagram of the electrochemical cell consisting of the EOS structure

and the metal of the reference electrode is represented by $\Delta\phi_{MS}$.

Equation 3.77 can be reduced to

$$\psi_F = V_{\text{appl}} + E_{\text{Ref}} - \Delta\phi_{MS} \quad 3.78$$

where ψ_F is the potential of the Fermi level of the semiconductor with respect to the bulk of solution.

The oxide/electrolyte interface of the EOS structure can be described by the same set of equations used in Section 3.2 (3.18 to 3.21). The semiconductor/oxide interface was examined under the discussion of the MOS structure. The principles used to analyze the semiconductor/oxide part of the EOS structure are essentially the same. In the analysis of the MOS structure the assumption was made that the density of ionized donors and acceptors was independent of potential, merely to simplify the mathematics. This assumption is not made in the following theoretical treatment of the EOS structures. The charge density in the semiconductor is now expressed as

$$\rho(x) = q [D^+(x) - n(x) + p(x) - A^-(x)] \quad 3.79$$

A general expression for density of charged species X_i is given by

$$x_i = \frac{N_i}{1 + g_i \exp [q (E - E_F) / kT]} \quad 3.80$$

where E_F is the Fermi level of the semiconductor, and g_i is the ground state degeneracy of states. The g_i value for donor levels, electrons, and holes is 2, and is 4 for acceptor levels.

The following set of equations give the charge density of each species.

electron density $n(x)$:

$$n(x) = \frac{N_C}{1 + g_n \exp \{q [E_C - (E(x) + E_F)] / kT\}} \quad 3.81$$

hole density $p(x)$:

$$p(x) = \frac{N_V}{1 + g_p \exp \{-q [E_V - (E(x) + E_F)] / kT\}} \quad 3.82$$

ionized donor density $D^+(x)$:

$$D^+(x) = \frac{N_D}{1 + g_D \exp \{-q [E_D - (E(x) + E_F)] / kT\}} \quad 3.83$$

ionized acceptor density $A^-(x)$:

$$A^-(x) = \frac{N_A}{1 + g_A \exp \{q [E_A - (E(x) + E_F)] / kT\}} \quad 3.84$$

where E_V , E_C , E_D and E_A are energies of valence band, conduction band, donor levels and acceptor levels respectively. $E(x)$ is the applied potential expressed relative to the Fermi level. N_V , N_C , N_D and N_A are density of states of holes, electrons, donors and acceptors respectively.

For a given semiconductor, E_V , E_C , E_A , E_D , N_C , N_V , N_D and N_A are known, and the Fermi potential E_F can be found numerically (101a).

Semiconductor space charge σ_{sc} is given by Equation 3.53. In the EOS structure, σ_{sc} can also be related to the potential across the oxide by

$$\sigma_{sc} = C_{ox} (\psi_s - \psi_o) \quad 3.85$$

The following equation can be written considering the electrical neutrality of through the entire EOS structure, .

$$T_\sigma = \sigma_o (\psi_o, H^+) + \sigma(\psi_o, C_{bulk}) + \sigma_{sc}(\psi_o, \psi_s) \quad 3.86$$

Equations 3.18-3.21, 3.79-3.86, and 3.53 describe the EOS system completely. The unknowns in these equations are n_{XOH2^+} , n_{XO^-} , n_{XOH} , σ_o , σ_d , ψ_o , ψ_s , $\rho(x)$, $n(x)$, $p(x)$, $D^+(x)$, $A^-(x)$ and there are 13 equations. These equation can be solved using a computer program developed by Westall EOS (68). A thorough analysis of the operation of the EOS structure is possible through the solution of these equations.

An equivalent circuit for the EOS structure is helpful in understanding the properties of the structure at an intuitive level. Equivalent circuits have been derived mathematically for the oxide/electrolyte interface (Figure 3.8) and for the metal/oxide/electrolyte (MOE) structure (Figure 3.10). It was also shown that the circuit deduced for the oxide/electrolyte interface could be extended to postulate an equivalent circuit for the

metal/oxide/electrolyte structure, based on the structural difference between the two structures. In a similar way, by noting the structural differences between the oxide/electrolyte interface, the MOE structure and the EOS structure, and by recognizing that the semiconductor has a finite capacitance, an equivalent circuit can be proposed for the EOS structure as shown in Figure 3.17. It should be noted that this circuit can also be derived just the same way the equivalent circuits were derived for oxide/electrolyte and the MOE structures.

Two capacitance terms are introduced in this figure to simplify the notation, and they are defined as follows.

$$C_{elec} = (C_{ox} C_{sc}) / (C_{ox} + C_{sc}) \quad 3.87$$

$$C_{sol} = C_{rxn} + C_d \quad 3.88$$

The validity of the assumption that the applied potential has no significant effect on the potential at the oxide/electrolyte interface of the EOS structures can be examined by evaluating the quantity $d\psi_o/dV_{appl}$. This quantity was evaluated using the computer program EOS and was found to be extremely small ($\ll 1 \times 10^{-5}$).

The isolation of ψ_o from V_{appl} can be explained by considering the equivalent circuit shown in Figure 3.17. The oxide capacitance C_{ox} is a constant for a given EOS structure, and the semiconductor capacitance C_{sc} is potential dependent. By inspection of Equation 3.87, it can be seen that the value of C_{elec} can never be greater than the value of C_{ox} .

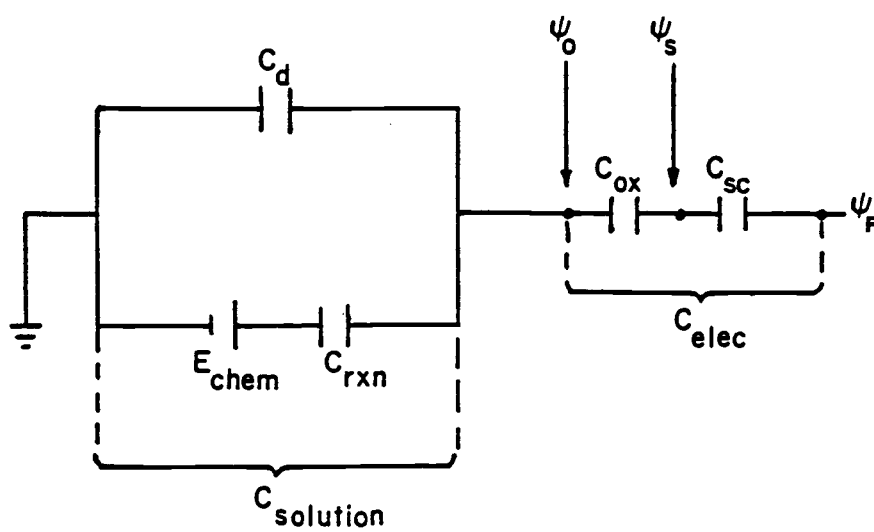


Figure 3.17. Equivalent circuit for the EOS structure.

In Section 3.3, it has been shown that C_d is larger than C_{ox} by several orders of magnitude (Table 3.1). Therefore, $C_{electrode}$ is small compared to C_{sol} . Charge neutrality across the interface can be expressed as follows.

$$(\psi_F - \psi_o) C_{elec} - \psi_o C_{sol} = 0 \quad 3.89$$

Differentiation of equation 3.89 with respect to ψ_F yields

$$\frac{d\psi_o}{d\psi_F} = \frac{C_{elec}}{C_{elec} + C_{sol}} \quad 3.90$$

From equation 3.78,

$$d\psi_F = dV_{appl} \quad 3.91$$

Since $C_{sol} \gg C_{elec}$, Equation 3.86 can then be reduced to

$$\frac{d\psi_o}{d\psi_F} = \frac{d\psi_o}{dV_{appl}} \approx \frac{C_{elec}}{C_{sol}} \quad 3.92$$

The conclusion from this analysis is that the effect of V_{appl} on ψ_o is negligible.

Response of EOS structure to pH changes

Figure 3.18 shows a family of C-V curves constructed from theoretical calculations, for an EOS structure ($K_D=0.001$, $N_s=1 \times 10^{15}$, $C_{bulk}=1 \times 10^{-4}$ M 1:1 electrolyte) at different pH values. The translation of C-V curves along the voltage axis is a direct consequence of the changes in ψ_o with pH, as was explained before.

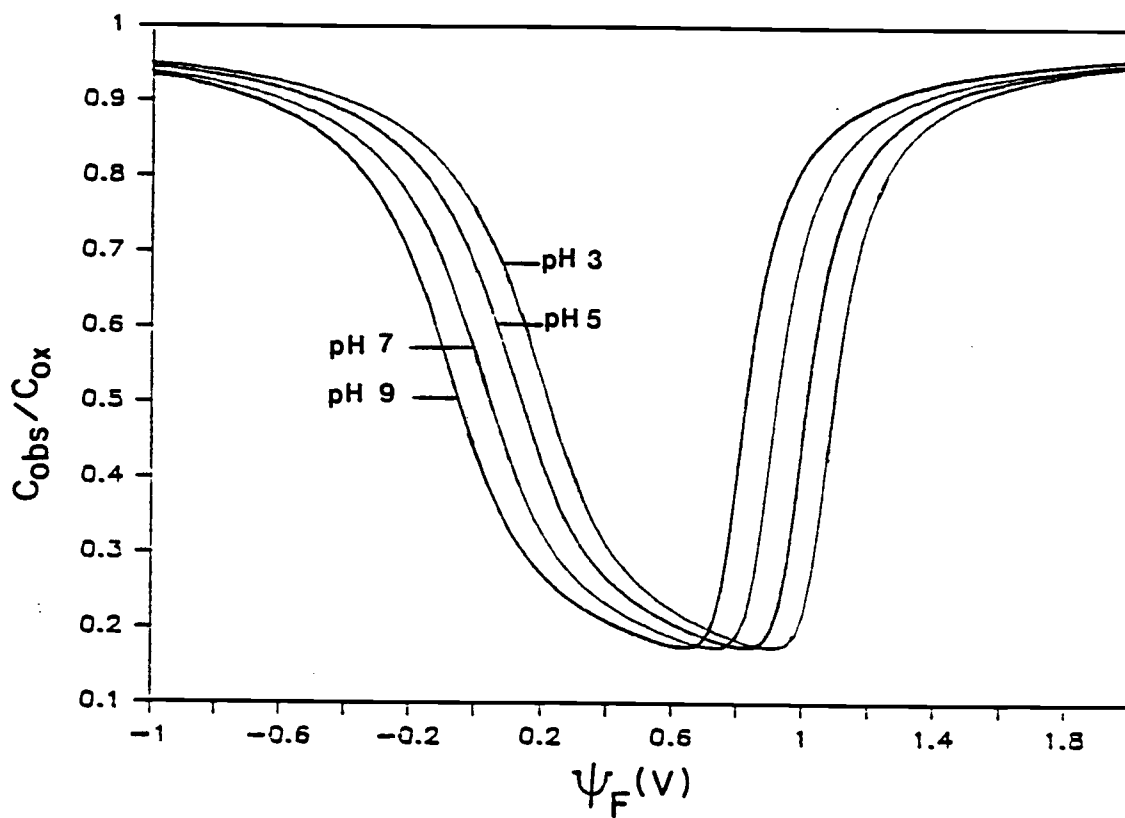


Figure 3.18. A family of C-V curves constructed for an EOS structure with ($K_D=0.001$, $N_S=1 \times 10^{15}$ and $C_{bulk}=1 \times 10^{-4}$.)

The shift of curves with pH appears to be uniform in the pH range $(\text{pH}_{\text{zc}} - 2)$ to $(\text{pH}_{\text{zc}} + 2)$. Another family of C-V curves, constructed for the same structure in a 0.01 M solution EOS is shown in Figure 3.19. The shift of curves, in this case, is not uniform in the given pH range. More information on how ψ_0 changes under different conditions is required to obtain a clear picture.

It is not only more elegant, but also more convenient to approach the above problem analytically by examining the quantity $\partial\psi_0/\partial\log H$ as a function of pH, K_D , N_s and C_{bulk} .

Mathematical expression for $\partial\psi_0/\partial\log H$ can be obtained as follows. The total charge T_σ across the EOS structure is zero as shown in Equation 3.86. The total differential of T_σ can be set equal to zero, and the resulting expression can be rearranged to yield

$$\left(\frac{\partial\psi_0}{\partial\ln H^+} \right)_{T_\sigma} = \frac{-(\partial\sigma_0/\partial\ln H^+)\psi_0}{\left(\frac{\partial\sigma_0}{\partial\psi_0} \right) + \left(\frac{\partial\sigma_d}{\partial\psi_0} \right) + \left(\frac{\partial\sigma_{sc}}{\partial\psi_s} \right) \left(\frac{\partial\psi_s}{\partial\psi_0} \right)} \quad 3.93$$

The numerator in Equation 3.93 can be obtained from Equation 3.36, and then Equation 3.93 can be rewritten as follows.

$$\left(\frac{\partial\psi_0}{\partial\ln H^+} \right)_{T_\sigma} = \frac{kT}{q} \frac{-(\partial\sigma_0/\partial\psi_0)}{\left(\frac{\partial\sigma_0}{\partial\psi_0} \right) + \left(\frac{\partial\sigma_d}{\partial\psi_0} \right) + \left(\frac{\partial\sigma_{sc}}{\partial\psi_s} \right) \left(\frac{\partial\psi_s}{\partial\psi_0} \right)} \quad 3.94$$

It is appropriate to express the terms on the right hand side of Equation 3.91 in quantities that are easily identifiable in a physical model. The terms $\frac{\partial\sigma_0}{\partial\psi_0}$, $\frac{\partial\sigma_d}{\partial\psi_0}$ and $\frac{\partial\sigma_{sc}}{\partial\psi_s}$ in Equation 3.94

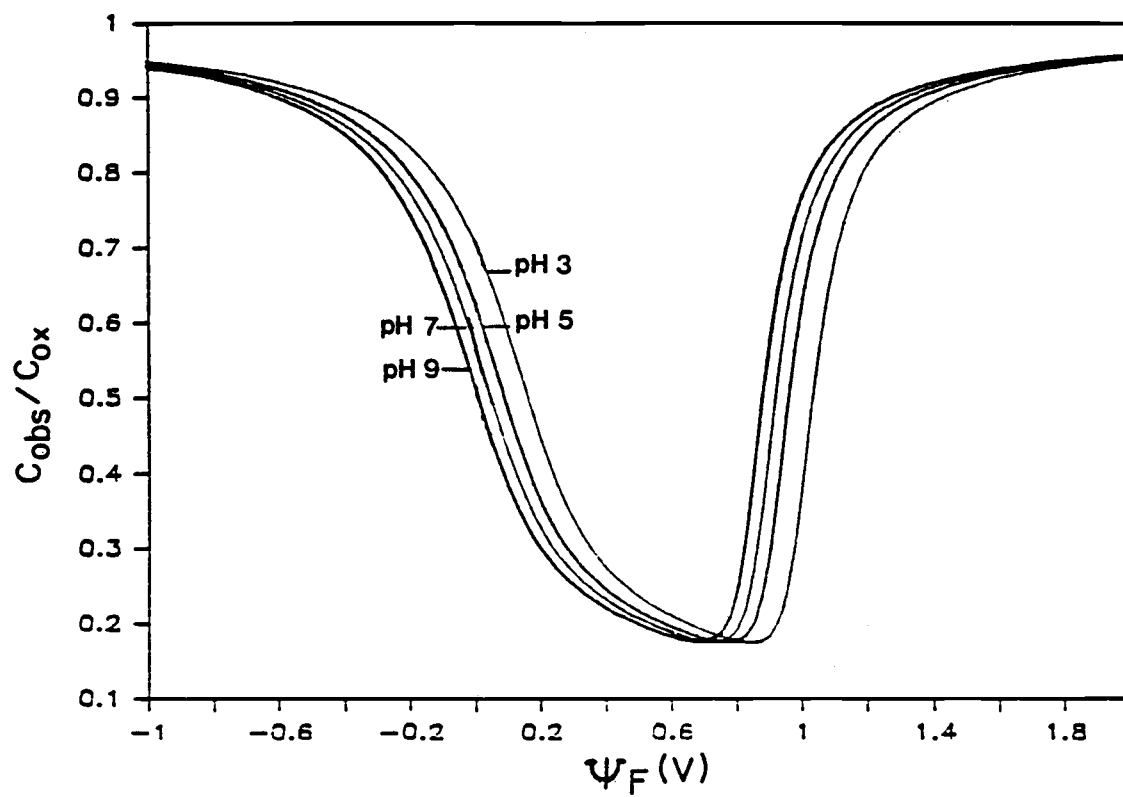


Figure 3.19. A family of C-V curves constructed for an EOS structure with the same properties as in Figure 3.18, except $C_{bulk}=1 \times 10^{-2}$ M.

have already been defined as C_{rxn} , C_d and C_{sc} in Equations 3.34, 3.35 and 3.54 respectively. The following expression for $\frac{\partial \psi_s}{\partial \psi_o}$ can be obtained by differentiating Equation 3.85 with respect to ψ_s and rearranging the result.

$$\frac{\partial \psi_s}{\partial \psi_o} = \frac{C_{\text{ox}}}{C_{\text{ox}} + C_{\text{sc}}} \quad 3.95$$

Therefore,

$$\left(\frac{\partial \sigma_s}{\partial \psi_s} \right) \left(\frac{\partial \psi_s}{\partial \psi_o} \right) = \frac{C_{\text{sc}} C_{\text{ox}}}{C_{\text{ox}} + C_{\text{sc}}} = C_{\text{elec}} \quad 3.96$$

Then Equation 3.94 can be re-expressed as

$$\left(\frac{\partial \psi_o}{\partial \ln H^+} \right)_{T_\sigma} = \frac{kT}{q} \left(\frac{C_{\text{rxn}}}{C_{\text{rxn}} + C_d + C_{\text{elec}}} \right) \quad 3.97$$

It has been shown that C_{elec} in Equation 3.97 is several orders of magnitude smaller than C_{rxn} and C_d . Therefore, the limiting value of $\left(\frac{\partial \psi_o}{\partial \ln H^+} \right)_{T_\sigma}$ is determined by the relative magnitudes of C_{rxn} and C_d . This is the same result obtained in the discussion of oxide/electrolyte interface in Section 3.2 (page 36). It is an important observation since one can conclude that the pH response of the EOS structure is influenced only by the oxide/electrolyte interface and not by the semiconductor.

Equation 3.97 is the basis for investigation of $\frac{\partial \psi_o}{\partial \ln H}$ as a function of the properties of the EOS structure. Variations in C_d and C_{rxn} will be shown from which $\frac{\partial \psi_o}{\partial \ln H^+}$ and ψ_o vs. $\log H^+$ will be calculated.

A study of the following four cases provides adequate information to understand the response of the EOS structure to pH.

- (1) $\frac{\partial \psi_o}{\partial \log H}$ vs pH
- (2) $\frac{\partial \psi_o}{\partial \log H}$ vs $\log C_{\text{bulk}}$
- (3) $\frac{\partial \psi_o}{\partial \log H}$ vs $\log K_D$
- (4) $\frac{\partial \psi_o}{\partial \log H}$ vs $\log N_s$

The computer program EOS can be used to calculate these quantities for a given set of EOS properties.

Figure 3.20 shows the quantities C_{rxn} , C_d , ψ_o and $\frac{\partial \psi_o}{\partial \log H}$ as a function of pH. The left hand side of Figure 3.20 shows these quantities for $K_D=0.1$ and the right hand side shows the same for $K_D=0.001$. All the quantities are calculated for 1×10^{-2} M solution.

The magnitudes of C_{rxn} and C_d for a given set of conditions can be compared in Figures 3.20 (a) and (b). When C_{rxn} is much larger than C_d a Nernstian response is expected, and when C_{rxn} is about the same as C_d , a sub-Nernstian response is expected. These expectations are borne out in Figures 3.20 (c) and (d) where ψ_o is shown as a function of pH, and in Figures 3.20 (e) and (f) where $\frac{\partial \psi_o}{\partial \log H}$ as a function of pH is shown. It is seen that high values of ionic strength favor a sub-Nernstian response. An interesting feature seen in Figure 3.20 (e) and (f) is that the curve has a maximum at pH_{zc} when K_D is 0.1, but a minimum when K_D is 0.001.

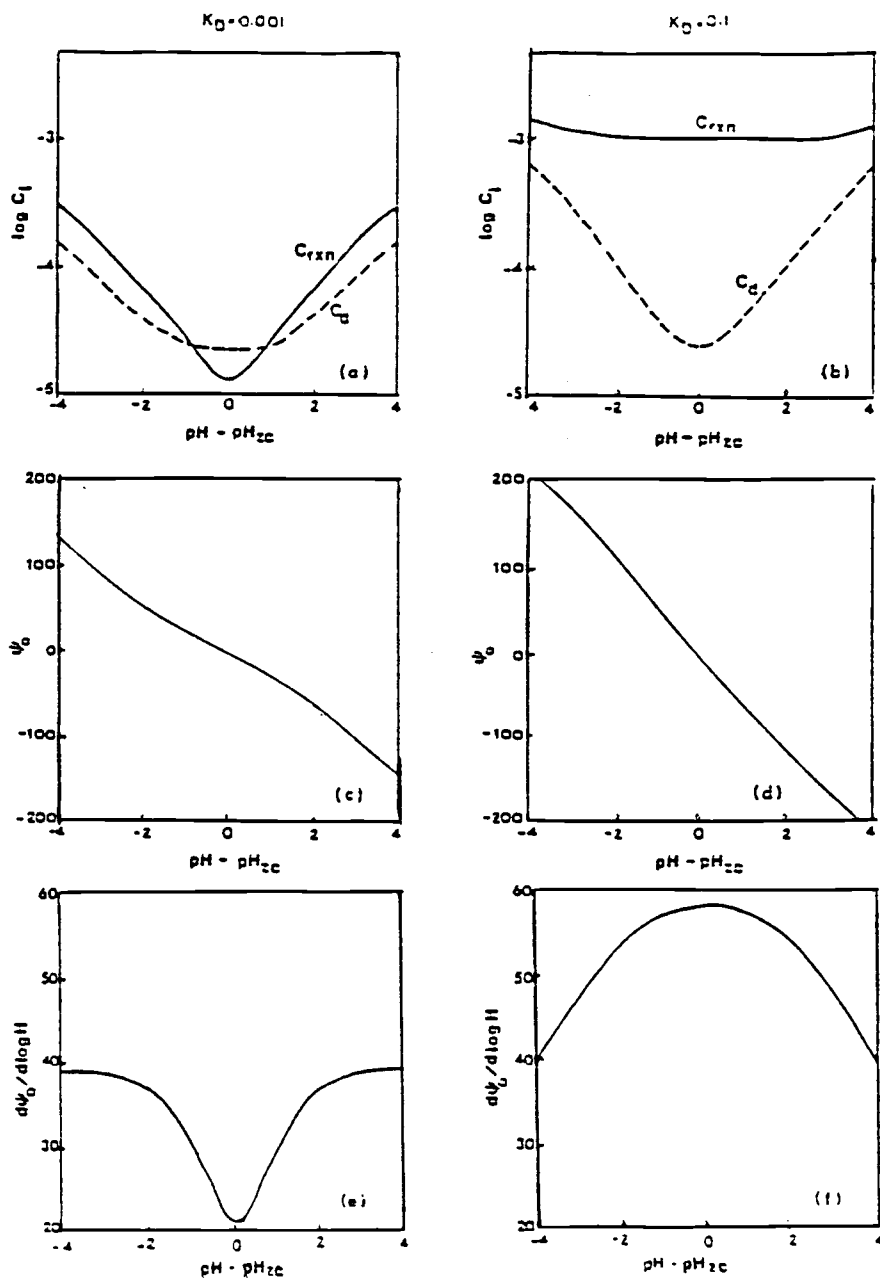


Figure 3.20. Calculated C_{rxn} , C_d , ψ_0 and $d\psi_0/d\log H$ as a function of ΔpH : ($N_s = 1.0 \times 10^{15}$)

- (a), (b) C_{rxn} and C_d with $K_D = 0.1$ and 0.001
 (c), (d) ψ_0 with $K_D = 0.1$ and $K_D = 0.001$
 (e), (f) $d\psi_0/d\log H$ with $K_D = 0.1$ and $K_D = 0.001$

C_{rxn} and C_d defined in Equations 3.34 and 3.12.

The reason for this behavior can be traced back to the derivatives given in Equations 3.34 and 3.12, but will not be discussed further here.

In Figure 3.21 (a), the variation of C_{rxn} and C_d as a function of concentration of the electrolyte is shown. C_{rxn} is much greater than C_d when the bulk concentration of electrolyte is low. Therefore, it is expected that $\frac{\partial \psi_o}{\partial \log H}$ approaches 59 mV in dilute solutions. Figure 3.21 (b) shows the dependence of $\frac{\partial \psi_o}{\partial \log H}$ on $\log C_{\text{bulk}}$. As expected, $\frac{\partial \psi_o}{\partial \log H}$ approaches 59 mV as C_{bulk} decreases.

The influence of N_s on C_{rxn} and C_d is shown in Figure 3.22 (a). C_{rxn} is directly proportional to N_s . Again, at high N_s values, C_{rxn} dominates; therefore, $\frac{\partial \psi_o}{\partial \log H}$ should approach 59 mV. Figure 3.22 (b) shows a plot of $\frac{\partial \psi_o}{\partial \log H}$ vs $\log N_s$, and it shows agreement with the expected result.

Effect of K_d on C_{rxn} and C_d is illustrated in Figure 3.23 (a). Figure 3.23 (b) shows its influence on $\frac{\partial \psi_o}{\partial \log H}$. Both figures can be considered together, and it can be shown that $\frac{\partial \psi_o}{\partial \log H}$ asymptotically approaches 59 mV under the conditions which C_{rxn} becomes large relative to C_d .

From the theoretical development of the response of an EOS structure to pH, it can be concluded that $\frac{\partial \psi_o}{\partial \log H}$ increases and approaches 59 mV when

- (1) N_s increases
- (2) K_d increases
- (3) C_{bulk} decreases

$K_D = 0.01$
 $N_s = 10^{15}$
 $pH = pH_{zc}$

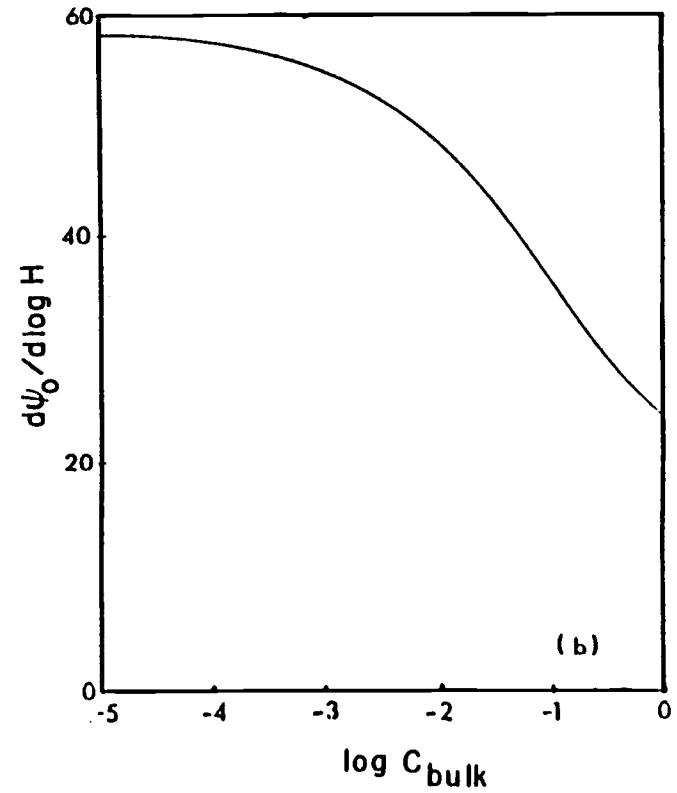
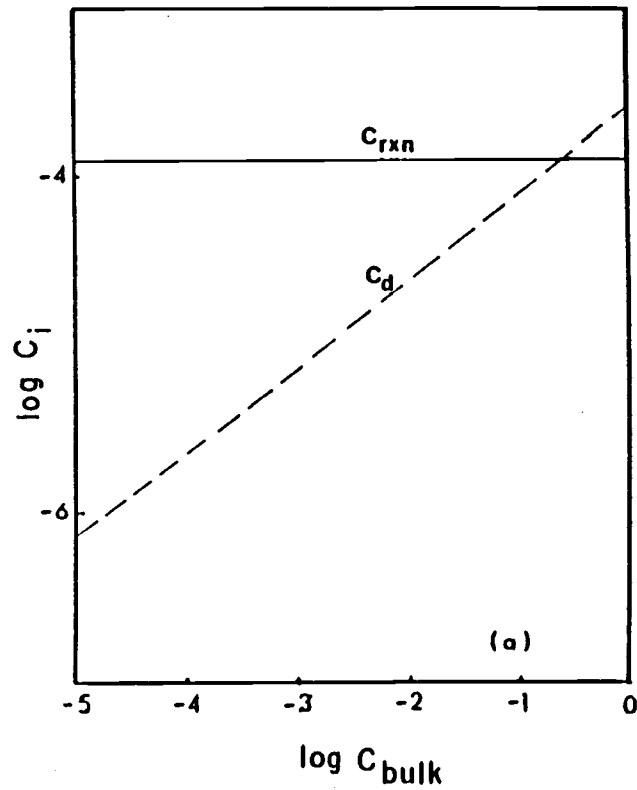


Figure 3.21. Variation of (a) C_{rxn} and C_d
 (b) $\partial\psi_0/\partial\log H$ with concentration.

$K_D = 0.01$
 $C_{\text{bulk}} = 0.01$
 $\text{pH} = \text{pH}_{\text{zc}}$

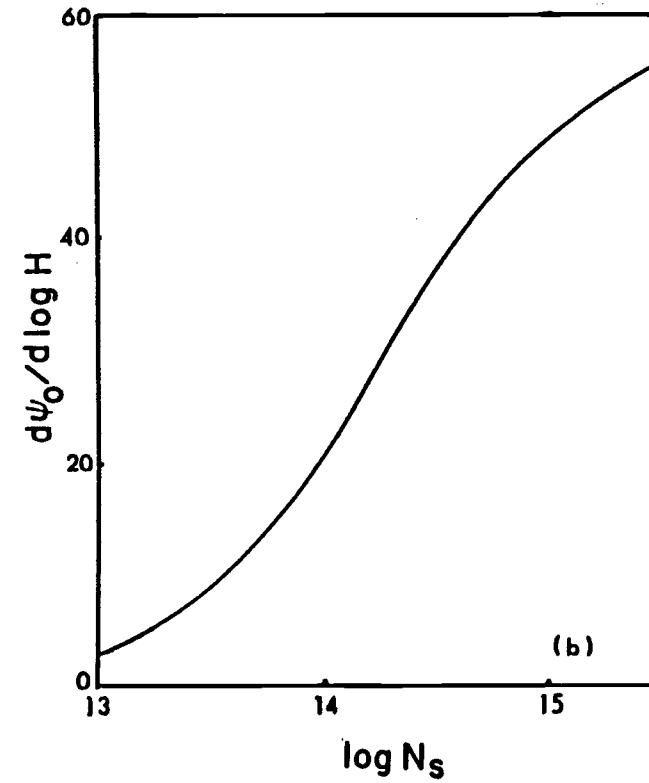
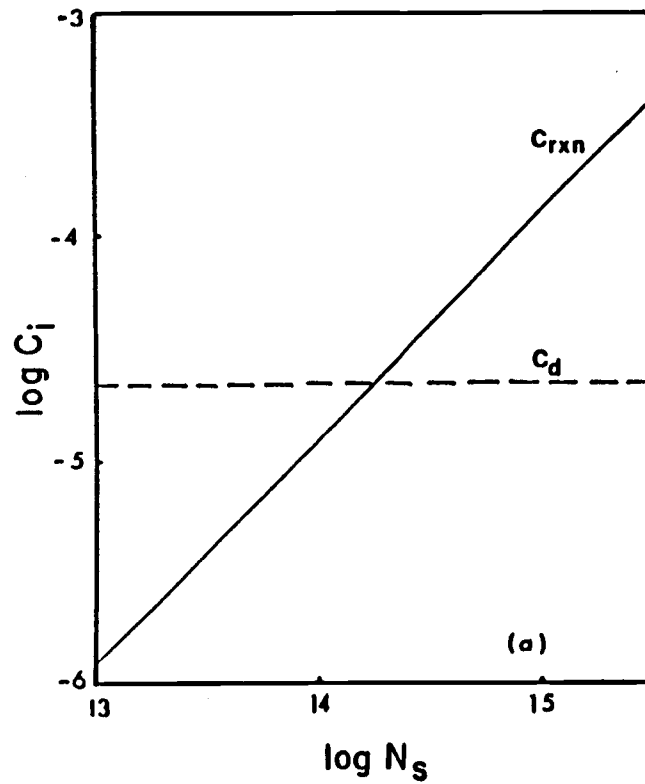


Figure 3.22. The influence of N_s on (a) C_{rxn} and C_d (b) $\partial\psi_0/\partial \log H$.

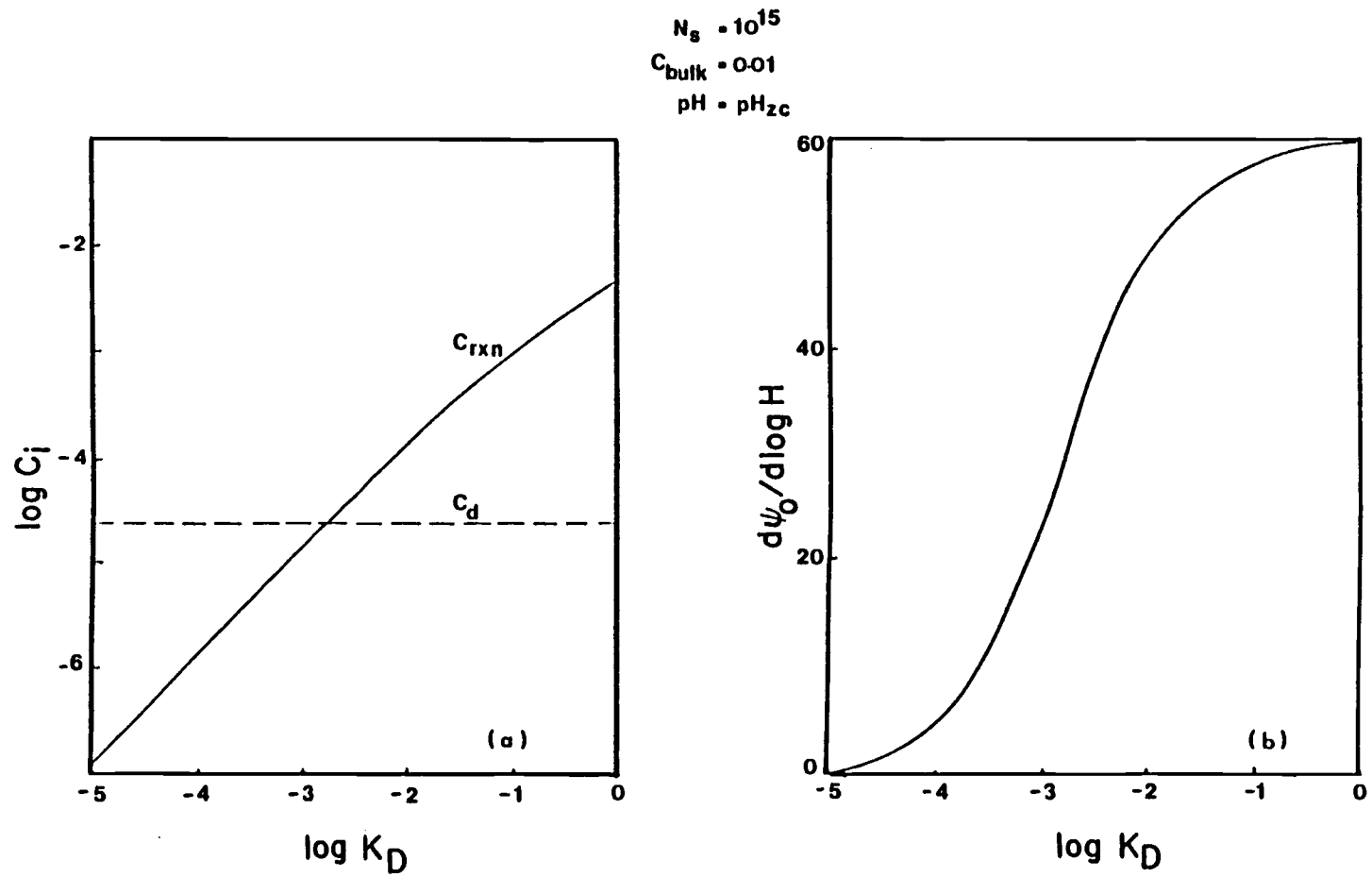


Figure 3.23. The effect of K_D on (a) C_{rxn} and C_d
 (b) $\partial\psi_o/\partial\log H$.

Also, $\frac{\partial \psi_0}{\partial \log H}$ reaches a maximum at pH_{zc} at larger K_D values but is a minimum for smaller K_D values (< 0.01). In every case, the value of $\frac{\partial \psi_0}{\partial \log H}$ is dictated by the relative values of C_{rxn} and C_d .

3.5. Equivalent circuit for the electrochemical cell

Analysis of the current response of a network of impedances is possible through the use of a suitable equivalent circuit. In this section the electrochemical cell used in the C-V measurements is represented by a complex equivalent circuit, which is then reduced to a simpler one so that results can be interpreted at an intuitive level.

Figure 3.24 shows an equivalent circuit for the electrochemical cell used in the capacitance measurement. Each symbol in the circuit is defined in Table 3.3.

The electrical potential and capacitance associated with the chemical reaction which charges the oxide surface is represented by E_{chem} (Equation 3.38) and C_{rxn} (Equation 3.34) respectively. Surface states are also included in the circuit model.

The counter electrode area is generally large compared to the area of the other electrodes in the cell as it is often made of a platinum mesh. The capacitance C_{ctr} is therefore very high and R_{ctr} is very small, providing a low impedance for the current flow from or to counter electrode from point P of the circuit in Figure 3.24.

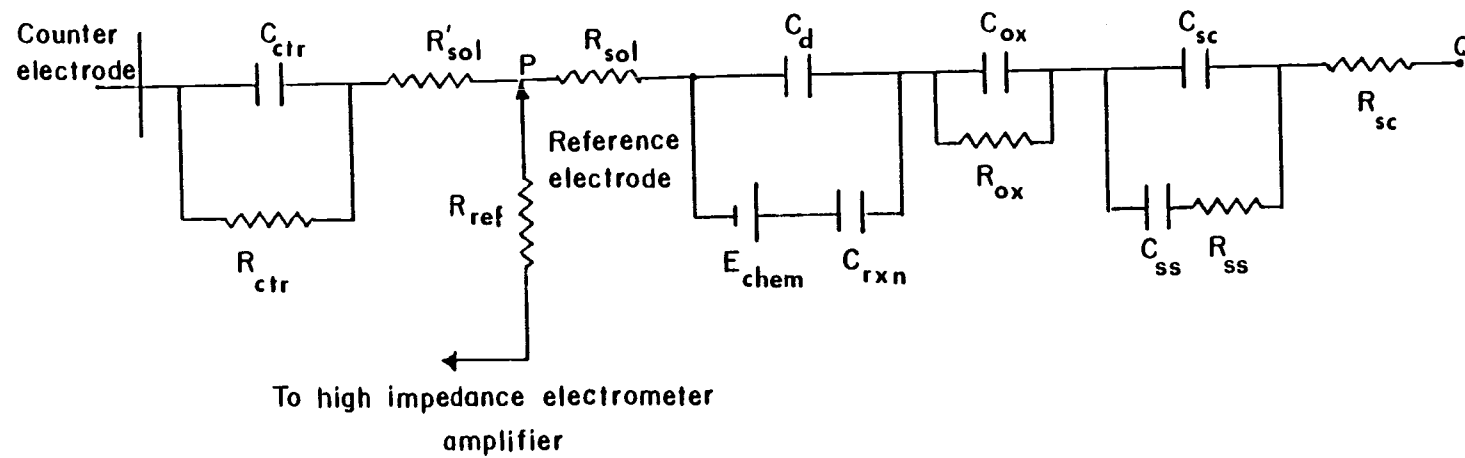


Figure 3.24. Equivalent circuit for the electrochemical cell used in capacitance measurements.

Table 3.3. Circuit elements in the equivalent circuit

C_{ctr}	counter electrode capacitance
C_d	electrical double layer capacitance
C_{rxn}	capacitance associated with the charging process of the oxide
C_{ox}	oxide capacitance
C_{sc}	semiconductor capacitance
C_{ss}	surface state capacitance
R_{ctr}	counter electrode resistance
R_{ox}	resistance of the oxide
R_{ref}	resistance associated with the reference electrode
R_{sol}	resistance of the solution between the counter and reference electrodes
R'_{sol}	resistance of the solution between the reference working electrode
R_{sc}	resistance of the semiconductor
R_{ss}	resistance representing the surface states
E_{chem}	electrochemical potential of charging the oxide surface

The input impedance of the electrometer amplifier is extremely high ($10^{13} \Omega$) and virtually no current is drawn through the reference electrode. From the principles of operation of the potentiostat, the voltage at point P is equal to the applied voltage.

The actual circuit analysis, it is sufficient to consider the elements between point P and the working electrode contact. The time constant of the surface states, $R_{ss}C_{ss}$, indicate whether the surface states are charged fast or slowly. The surface states at the semiconductor/oxide interface are considered to be fast states (67,69). Therefore, R_{ss} is small and can be ignored. The capacitances C_{rxn} and C_d can be represented by C_{sol} , (Equation 3.84). It has been shown that C_{sol} is much larger compared to C_{ox} and C_{sc} . Therefore, C_{sol} is negligible in series with these two capacitors. Silicon dioxide is a good insulator. Therefore R_{ox} is very high. Then the circuit in Figure 3.24 can be reduced to the circuit shown in Figure 3.25. The impedance of this circuit can be expressed as

$$Z_{total} = (R_{sol} + R_{sc}) - j \frac{1}{\omega} \left[\frac{1}{C_{ox}} + \frac{1}{(C_{ss} + C_{sc})} \right] \quad 3.98$$

Equation 3.98 is of the form

$$Z_{total} = R_T - j \frac{1}{\omega C_T} \quad 3.99$$

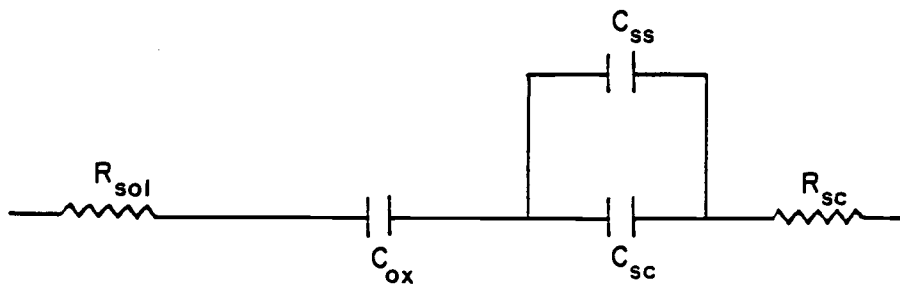


Figure 3.25. Reduced form of the equivalent circuit in
Figure 3.24.

Therefore, it is justifiable to analyze the experimental data using a series circuit model for the electrochemical cell.

$$R_T = R_{sol} + R_{sc} \quad 3.100$$

$$\frac{1}{C_T} = \frac{1}{C_{ox}} + \frac{1}{C_{ss} + C_{ox}} \quad 3.101$$

and in the absence of surface states

$$\frac{1}{C_T} = \frac{1}{C_{ox}} + \frac{1}{C_{sc}} \quad 3.102$$

4. EXPERIMENTAL

4.1 Techniques for interfacial capacitance measurements

The interfacial capacitance at metal/aqueous solution interfaces has been measured and studied by many workers.

The ac impedance bridge method used by Graham (70,71) is among the most accurate methods for double layer capacitance measurement, and has been widely used for Hg/aqueous solution interfaces. The longer time required for balancing the bridge makes the bridge method less preferred for solid electrodes, because the surfaces of the solid electrodes are not reproducible and may change considerably during an experiment.

Mc Mullen and Hackerman (71) applied a square wave current through an electrochemical cell with a solid electrode, and measured the potential across the cell. For a totally capacitive interface (ideally polarizable interface with negligible solution resistance) the potential across the cell appears as a triangular wave, the slope of which is related to the capacitance.

Ramaley and Enke (73) have improved the square wave technique mentioned above by using better instrumentation. In the same publication, they have reported another method for capacitance measurements in which a sinusoidal voltage is imposed on an electrochemical cell and the amplitude and the phase difference of

the cell have been measured. They used an oscilloscope or an ac voltmeter for the amplitude measurement, and a phase angle meter or an oscilloscope to determine the phase angle.

Babai et al.(74) employed a conventional potentiostat and applied a triangular potential wave form to perturb the electrochemical cell. Their method of capacitance determination is based on the fundamental property of electrical capacitance that the current i is given by

$$i = C (dV/dt) \quad 4.1$$

where V is the potential across the capacitance C . It follows from the above relationship that the cell current is a square wave form if the potential applied to the cell is a triangular wave. The amplitude of the square wave current is directly proportional to the capacitance. The instrument used by Babai et al. was capable of measuring the amplitude of the square wave rapidly and output a voltage proportional to the capacitance.

Power & Caldwell (75) designed a similar instrument, with simpler but improved electronic circuitry to measure capacitance. The circuit proposed by them was modified in this work and adapted to use in conjunction with the commercial instruments available in the laboratory. A description of the circuit and its performance is discussed in Appendix B. The lowest capacitance that could be measured satisfactorily by this method was about 20 nF. The capacitance of the EOS structures reported in this work varied in the range 5-20 nF. Therefore this method was not pursued further.

Bousse (76) and De Rooij (77) have employed a quasi-static technique, as described by Kuhn (69), to measure the capacitance of

EOS structures. In this method, a voltage ramp $V(t)$ is applied to across a cell, and the current $i(t)$ is measured. The current is given by

$$i(t) = C(V(t)) \, dV(t)/dt \quad 4.2$$

where $C(V(t))$ is the capacitance of the cell. Since $V(t)$ is a linear ramp $dV(t)/dt$ is a constant, and $i(t)$ is directly proportional to the capacitance. A simultaneous display of $V(t)$ and $i(t)$ can be obtained.

The method which measures the phase and amplitude of the current response of an electrochemical cell to an applied sinusoidal voltage as suggested by Ramaley and Enke is used currently, but with sophisticated phase and current detecting instruments which were not available then. In this work, a lock-in-amplifier is used for phase and current detection.

4.2 Capacitance measurement

The capacitance determination was accomplished by AC impedance measurement of an electrochemical cell consisting of the oxide electrode, a reference electrode and a counter electrode. Figure 4.1 shows the block diagram of the instrumentation used in the measurement.

A small sinusoidal signal (~ 10 mV) was obtained from the internal oscillator of the Princeton Applied Research (PAR) 5301 lock-in-analyser unit and was fed to one of the summing inputs (external inputs) of the PAR 173 potentiostat. The DC bias applied

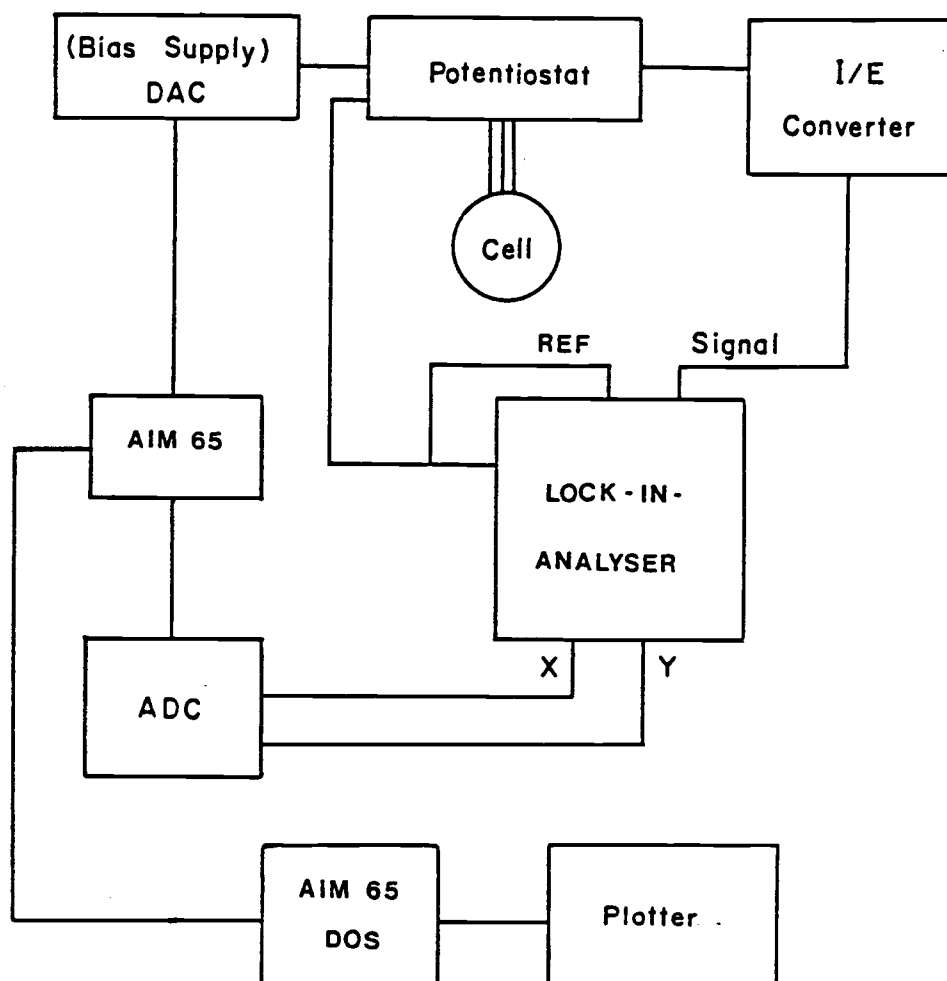


Figure 4.1. Block diagram of the instrumentation used
in the capacitance measurement

to the electrochemical cell was supplied to the summing input by a digital to analog converter (DAC) controlled by an AIM 65 micro computer. The sinusoidal current $i(t)$, through the electrochemical cell, was converted to a voltage proportional to it by the PAR 179 coulometer/current to voltage converter. The output of the PAR 179 was compared with the oscillator output signal using the lock-in-analyser. The magnitudes of the in-phase component and the out-of-phase component can be read directly in the two digital displays of the lock-in-analyser. Voltages proportional to the displayed values are available at two analog output ports of the lock-in-analyser. The proportionality constant can be changed according to the needs of the user by selecting an appropriate sensitivity.

In this experiment, the analog voltages at these outputs were digitized by a multi-channel analog to digital converter (ADC) controlled by the AIM 65 micro computer. The operation and circuit description of the ADC and the DAC used in this experiment are discussed elsewhere (78).

The sensitivity of the response to the applied bias varies for a semiconductor electrode depending on the relative displacement of the potential from the flat band condition of the semiconductor. Therefore, a quick bias potential scan was performed manually to identify the regions of different sensitivities, and suitable magnitudes of potential steps were initialized for different regions. The potential was stepped in 30 second intervals. After

each step, the X and Y output ports of the lock-in-analyser were read many times in 1 ms intervals, until the relative standard deviation over the last ten data points was below 1%.

The basic language program and the assembly language programs which accomplish the data acquisition and the experiment control are listed in Appendix C.

Once the potential had been stepped over the desired range, data was transmitted to another AIM 65 computer equipped with a disk operating system. This allowed permanent storage of the data and hence the convenience of using various data analysis techniques. Serial data transfer was chosen to avoid possible communication errors since the computers were located more than ten feet apart. AIM 65 computers do not support hardware or software for standard RS 232 communication. Therefore, the data were transferred via the 20 milliamperes current loop available for the serial communication with peripherals.

The circuit necessary for data transmission is shown, and its operation is explained in Appendix D.

After each scan, the pH of the solution was changed by adding 1M KOH or 1M HNO₃ in the pH dependence studies. In the ionic strength dependence studies the entire solution was replaced by a solution of different ionic strength.

In place of the actual electrochemical cell, dummy cells with passive electrical components were used to calibrate the instrumental response. Low inductance metal film resistors were used as resistance standards and polystyrene capacitors were used as capacitance standards. The resistances and capacitances used as

standards were measured independently by a HP 4260 bridge. At frequencies below 1000 Hz, the impedances calculated from the instruments used in this work agreed with those obtained from the bridge. All the experiments reported here were conducted at 500 Hz.

Electrodes used in the capacitance measurements

The electrode at which the interfacial capacitance is studied is the main part of the electrochemical cell. In this case, the electrode was a Si wafer with a thin layer ($\sim 500 \text{ \AA}$) of SiO_2 grown on it. The devices were fabricated at the Corvallis division of Hewlett-Packard company by thermally oxidizing phosphorous doped n-type silicon wafers at 1200°C in dry oxygen atmosphere. The resistivity of the silicon wafers were $7 \text{ } \Omega \text{ cm}$ as measured by the four point probe technique. The oxide thickness was measured for each batch of wafers by the reflectance technique.

The wafers were scribed into $1 \text{ cm} \times 1 \text{ cm}$ squares. An ohmic contact to the silicon surface was made by plating Cu onto silicon from a $1:1 \text{ CuSO}_4 / \text{HF}$ buffer solution. To prevent the plating solution from wetting the oxide side of the wafer, a hydrophobic barrier was drawn around the edges of the silicon side of the wafer using a permanent marking pen.

These squares were then mounted in a Delrin holder as shown in Figure 4.2. Two Viton 'O' rings prevent the aqueous solution from leaking into the device. The compressed inner 'O' ring defines the

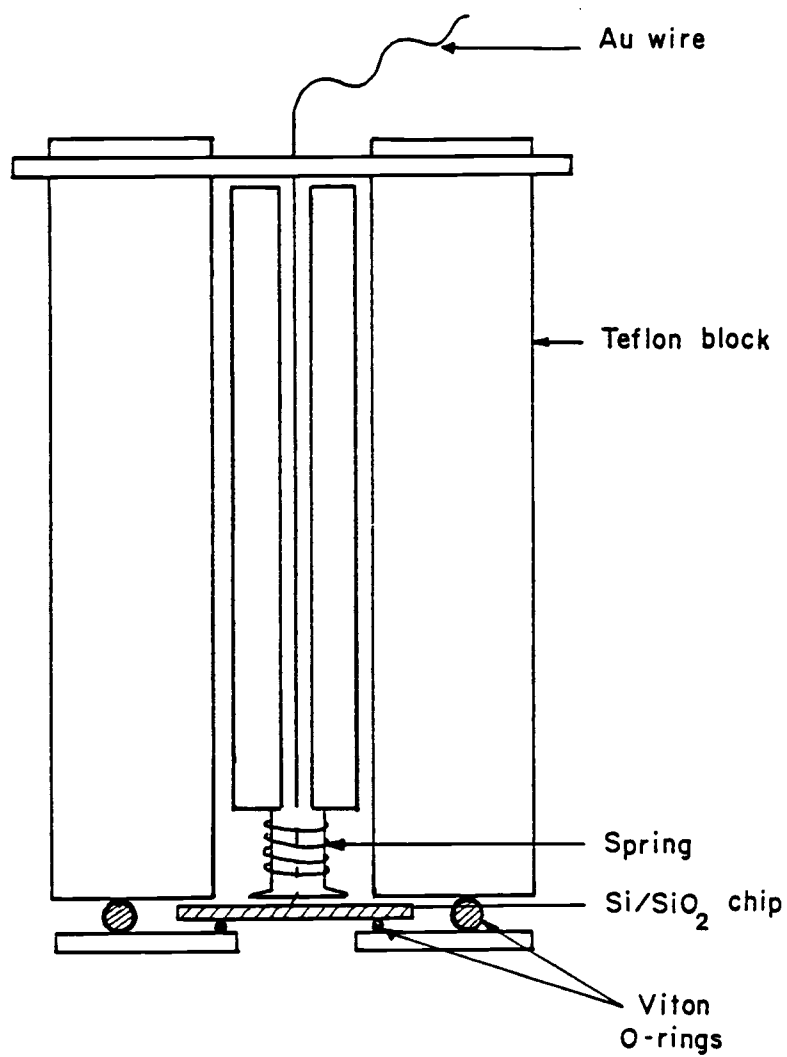


Figure 4.2. Electrode holder

area of the exposed wafer. Electrical contact to the plated Cu was made by a gold wire pressed against the wafer by the spring loaded Delrin rod.

Due to the hydrophobicity of Delrin, an air bubble often became trapped in the electrode cavity when the electrode was immersed in the solution. These bubbles were removed by a Teflon capillary, and the absence of bubbles was assured by visual inspection.

The reference electrode used was a saturated calomel electrode (SCE) manufactured by Broadly-James corporation. A platinum gauze counter electrode was used.

For pH measurements, an electrode couple consisting of the above mentioned reference electrode and an Ingold model 5055-07 pH electrode was employed. The electrodes were calibrated at pH 4, 7 and 10 using pHDrion buffer solutions. For all pH measurements, an Orion 701 pH-mV meter analyser was used.

4.3. Titration of oxide suspensions

Preparation of the oxide suspensions

Titanium dioxide powder (Degussa P-25) (~30g) was suspended in 200 ml Millipore water purged of oxygen by nitrogen. The suspension was centrifuged at 19000 rpm using a high speed centrifuge manufactured by IEC-Daemon corporation (IEC-B20A).

The centrifugate was re-suspended in 200 ML oxygen free Millipore water using a Branson (model 200) Sonifier. The temperature of the suspension was maintained at $25 \pm 2^{\circ}\text{C}$.

The supernatant solution was analysed potentiometrically for Cl^- ions by an electrode couple consisting of an Orion double junction reference electrode (model 90-01) and a GamRad ultra-sensitive Cl^- ion selective electrode.

Centrifugation, re-suspension and the analytical procedure for the supernatant were repeated until the Cl^- level of the washings was reduced to less than 1×10^{-5} M. In most cases, six washings were required to achieve this. After the final centrifugation step, the solid was re-suspended in oxygen free deionized water. The amount of water used was dependent on the efficiency of recovery of the solid and the desired density of the suspension. Usually, about 30% of the solid is lost during the lengthy washing procedure.

The titanium oxide suspensions (50 g/L) so prepared were stored in plastic bottles, and they showed excellent stability over a long

period of time. The stability was checked by pipetting a known volume of suspension into a beaker and weighing it. Also, an aliquot was freeze-dried and weighed to check the reproducibility in solid content.

Electrode used in the titration experiment

Figure 4.3 shows the Wilhelm-Brucke reference electrode used in all the titration experiments. There are two liquid junctions J_1 and J_2 , across which a diffusion potential can exist. The liquid junction J_1 can be renewed by draining solution 1 through valves B and C to waste and then solution 2 through the valves A and C to waste. Junction J_2 is renewed by draining solution 1 through valves A and D to waste. The Ag/AgCl electrode was shielded from light, since the silver halides are known to be photosensitive.

The Orion model 93-19 K^+ ion selective electrode was used for K^+ sensing. Figure 4.4 shows a diagram of the K_+ electrode. A Metrohm model 20-91-090-9 glass electrode used for H^+ measurement.

Titration system

The automatic titration system developed in this laboratory by Seyfert et.al (79) was used in all titrations. A schematic diagram of this system is shown in Figure 4.5. The computer system used in this experiment is an AIM 65 microcomputer (Rockwell International).

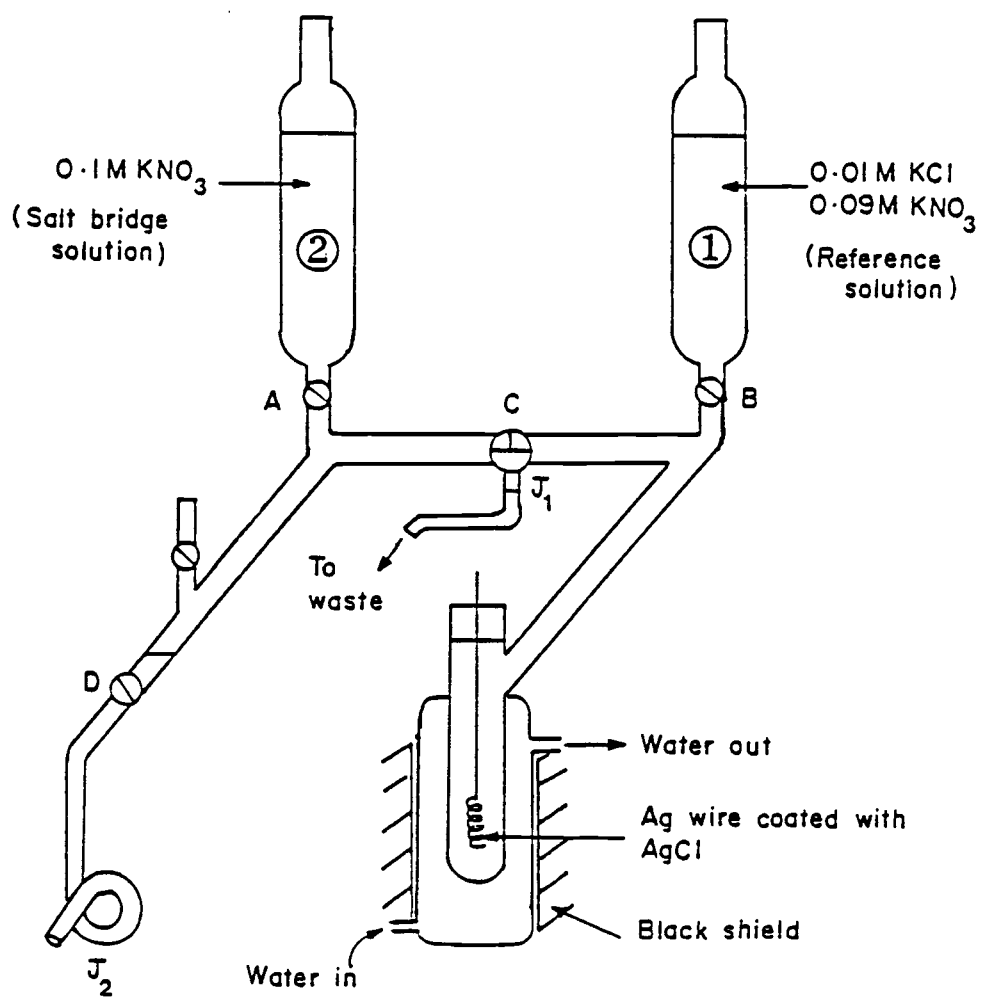


Figure 4.3. Wilhelm-Brucke reference electrode

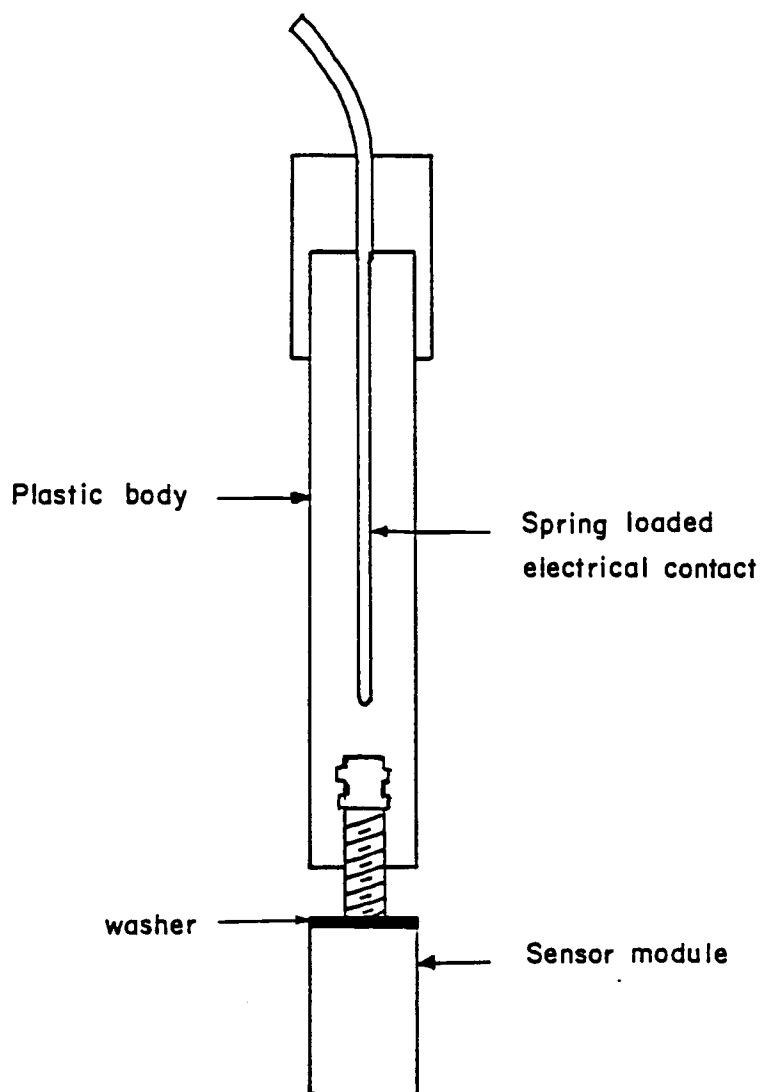


Figure 4.4. K⁺ Ion-Sensitive Electrode

Orion research model 93-19

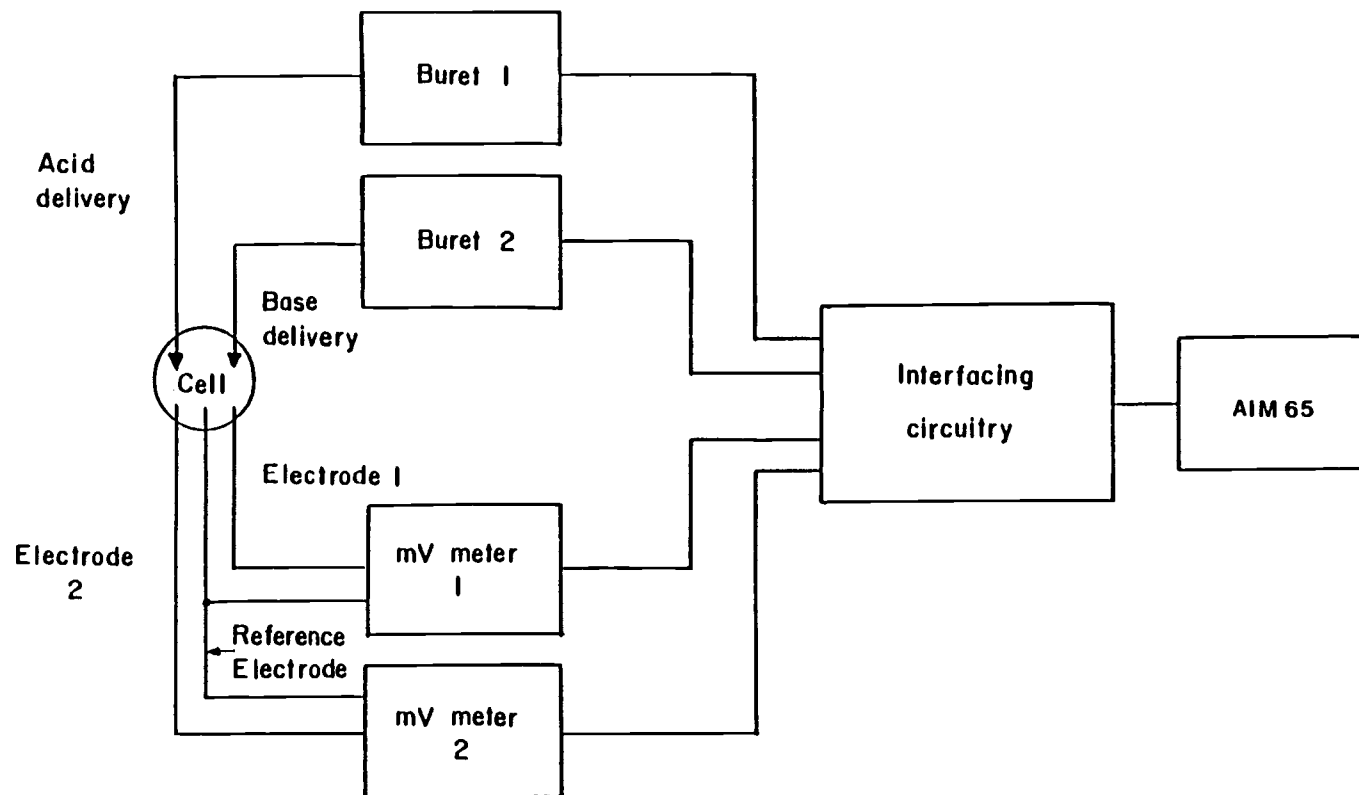


Figure 4.5. A schematic diagram of the automatic titration system used in the experiment

Metrohm 655 Dosimat burettes are used to deliver the titrants, and the electrode response is monitored by Orion 701 pH-mV meters. Burette control and reading of the pH meters are accomplished by several Versatile Interface Adapters (VIA-6522) on the computer system. The digital output of meter A, which is the response of the glass electrode - reference electrode couple in this case, is continually monitored at a sampling rate specified by the user.

Before the addition of the titrant, the time dependence of the electrode response is analysed to determine whether the electrode has reached equilibrium. The operational criterion for "equilibrium" is that the rate of change of electrode potential is less than a user specified threshold value 0.001 mV/s in this case. Once the equilibrium condition is established the mV meters are read and the time, the volume of the titrant and the responses of the electrodes are stored for future use.

Two modes of operations are available in the titration system; fixed ΔV mode and fixed ΔE mode. In fixed ΔV mode, a fixed volume of titrant is added in each step. In fixed ΔE mode, the volume of the titrant that should be added to change the electrode response by a fixed voltage is computed using a quadratic equation fitted to three previous data points. The fixed ΔE mode was used in all the titrations in this work.

Titration procedure

The titration vessel was a Metrohm cell with a water jacket. Before every titration, all the liquid junctions of the reference electrode were renewed, and the cell and the electrodes were rinsed several times with deionized water. For blank titrations, 25.0 ml of the blank was pipetted into the titration vessel. In the case of oxide suspensions, 20.0 ml of the blank was pipetted in, followed by 5.0 ml of the suspension.

The liquid inside the cell was allowed to reach a constant temperature for twenty minutes, during which time N_2 was bubbled through the solution to purge CO_2 and O_2 . During the titration the solution was stirred at a constant rate and N_2 was passed over the surface of the solution. At the conclusion of each analysis, the solution in the cell was removed by suction, and the electrodes and the cell were rinsed several times by Millipore water. The experimental data were then transmitted to the AIM 65/DOS computer as mentioned in section 4.2.

4.4 Reagents

The standard solutions of 0.01 M KOH and 0.01 M HNO_3 were prepared by diluting the standard concentration manufactured by Baker Co. (DILUT-IT). All the other solutions were prepared from corresponding reagent grade chemicals.

5. RESULTS AND DISCUSSION: STUDIES WITH EOS STRUCTURES

5.1 Performance of instrumentation used in capacitance measurements

The performance of instrumentation used in an experiment should be evaluated before proceeding with the actual experiment. In this section, the evaluation of the performance of instrumentation used for capacitance determination of the EOS structures are discussed.

First, a general and brief description of the experimental technique used for capacitance determination is presented. In this experiment, a sinusoidal voltage is applied to an electrochemical cell, and a voltage proportional to the cell current is obtained by means of a current-to-voltage (I/E) converter. Using the applied voltage as the reference, the amplitudes of the in-phase component (X) and the out-of-phase component (Y) of the I/E converter output are measured. The electrochemical cell is represented by a purely electronic circuit model based on the physical description of the cell, and values for the circuit elements in the model are calculated from the measured quantities.

To evaluate the performance of the instrumentation, X and Y values for a dummy cell with electrical components of known impedances were measured over a range of frequencies. The impedance values calculated from the measured response were compared with the known values. It

will be shown that discrepancies between the experimental and known values result at relatively low frequencies, unless special considerations are taken in interpretation of the data. An approach to reduce these discrepancies will be presented in this discussion.

Determination of impedance from experimental data

In the calculation of impedance of elements in the model circuit from experimental data, complex variables must be used. An explanation of the notation used in this discussion is in order. Complex variables will be shown in the bold print. A complex variable Q is represented as

$$Q = \text{Re}(Q) + j \text{Im}(Q) \quad 5.1$$

where $\text{Re}(Q)$ and $\text{Im}(Q)$ are the magnitudes of the real and imaginary parts of the variable, respectively.

Figure 5.1 illustrates the instrumentation used in the capacitance measurement. The symbols in Figure 5.1, and other symbols which describe the quantities pertinent to the calculation of impedance are defined in Table 5.1.

The output of the I/E converter is represented as a vector sum of the amplitudes of in-phase and out-of-phase components as follows.

$$E_{\text{out}} = X + j Y \quad 5.1$$

The phase angle δ is defined by

$$\delta = \tan^{-1} (Y/X) \quad 5.2$$

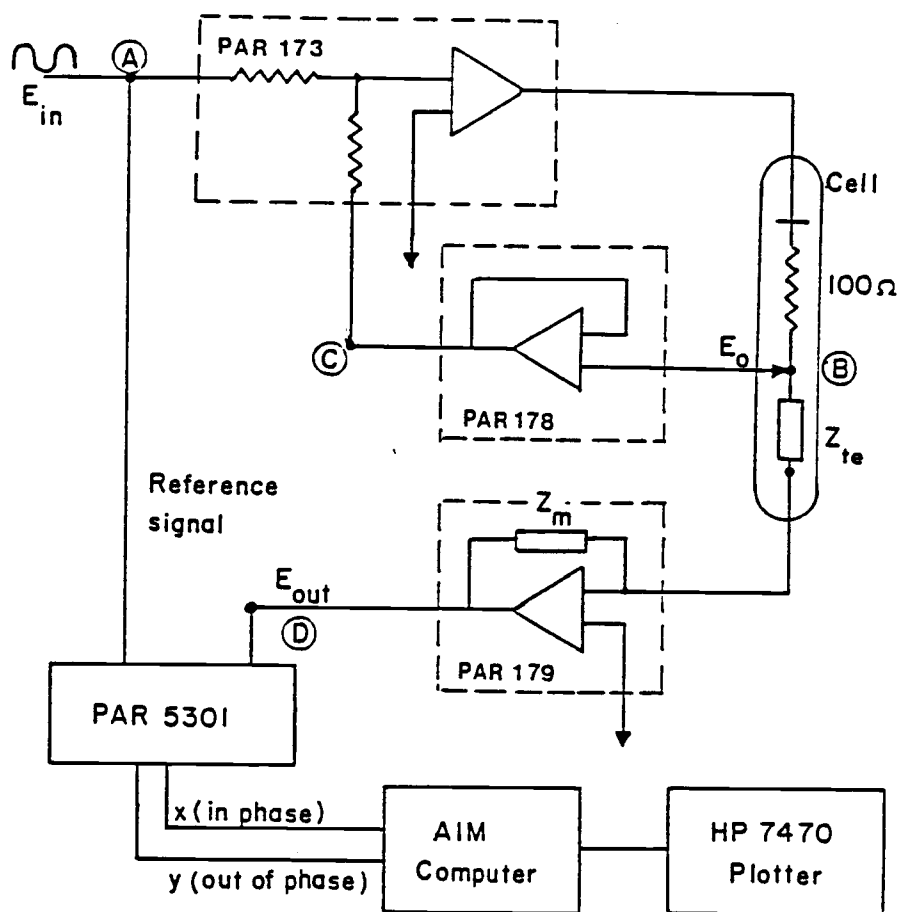


Figure 5.1. Instrumentation used in capacitance measurement;
an illustration of the experimental method

Table 5.1. Definitions of symbols used for circuit elements and other quantities pertinent to capacitance determination

Z_{te}	impedance of the test cell
Z_m	impedance of the feed back loop of the I/E converter
R_{te}	resistance of the test cell
C_{te}	capacitance of the test cell
E_{in}	voltage applied to the cell. (Note that E_{in} is not represented as a complex number since it was taken as the reference signal to which phase angle is related)
E_0	input to the electrometer amplifier
E_{out}	output of the I/E converter
X	amplitude of the in-phase component of E_{out} $\text{Re}(E_{out})$
Y	amplitude of the out-of-phase component of E_{out} $\text{Im}(E_{out})$

From the analysis of the potentiostat circuit in Figure 5.1,

E_{out} can be expressed as

$$E_{out} = - E_0 Z_m / Z_{te} \quad 5.4$$

Also, from the operation of the potentiostat circuit,

$$E_0 = -E_{in} \quad 5.5$$

Since the feedback loop of the I/E converter contains only resistors, the impedance Z_m can be expressed as

$$Z_m = \text{Re}(Z_m) = R_m \quad 5.6$$

Note : It will be shown later that the behavior of the I/E converter is such that there is also a capacitive element in the feed back loop. However, initially, we will not consider such a capacitance. Therefore, Equation 5.6 will be used to represent Z_m , unless otherwise stated.

By combining Equations 5.4 and 5.5

$$Z_{te} = E_{in} Z_m / E_{out} \quad 5.7$$

Equations 5.2-5.7 completely describe the experimental technique mathematically.

In the evaluation of the performance of the instrumentation, three types of circuit models were used; dummy cells with

- (1) resistor only
- (2) series combination of a resistor and a capacitor
- (3) parallel combination of a resistor and a capacitor

These types of cells are shown in Figure 5.2. R_{te} and C_{te} are the values of resistance and the capacitance used in the dummy cell, respectively. The impedance for each cell is defined given as follows.

$$(1) \quad Z_{te} = R_{te} \quad 5.8$$

$$(2) \quad Z_{te} = R_{te} - j/\omega C_{te} \quad 5.9$$

$$(3) \quad Z_{te} = 1/(1/R_{te} + j\omega C_{te}) \quad 5.10$$

where ω is related to the frequency by

$$\omega = 2 \pi f \quad 5.11$$

From the measurement of X and Y the impedance of the cell Z_{te} can be calculated from Equation 5.7, since E_{in} , Z_m and E_{out} are known. Calculated impedance of the cell is denoted by Z_{exp} . Z_{exp} can then be interpreted according to the appropriate equation describing the circuit model to obtain experimental values for resistance (R_{exp}) and capacitance (C_{exp}). These values can be compared with the actual values of R_{te} and C_{te} to evaluate the performance of the instrumentation. To facilitate the comparison, a quantity relative error, is defined as follows.

$$\text{relative error} = \frac{(\text{experimental value} - \text{actual value}) \times 100}{\text{actual value}}$$

Table 5.2 shows the mathematical form of the above definition for each case considered.

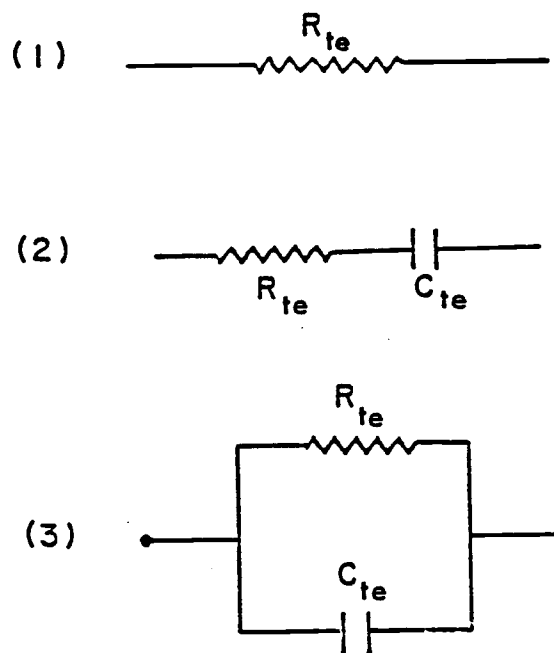


Figure 5.2. Model circuits used in the dummy cell.

Table 5.2. Definitions of, R_{exp} , C_{exp} , and relative error for different circuit models considered in the evaluation of the performance of the instrumentation

	type (1) resistor only	type (2) series circuit	type (3) parallel circuit
R_{exp}	$\text{Re}(Z_{\text{exp}})$	$\text{Re}(Z_{\text{exp}})$	$\frac{1}{\text{Re}(1/Z_{\text{exp}})}$
C_{exp}	-	$\frac{-1}{\text{Im}(Z_{\text{exp}})}$	$\text{Im}(1/Z_{\text{exp}})$
Relative error in resistance	$\frac{(R_{\text{exp}} - R_{\text{te}})}{R_{\text{te}}}$	$\frac{(R_{\text{exp}} - R_{\text{te}})}{R_{\text{te}}}$	$\frac{(R_{\text{exp}} - R_{\text{te}})}{R_{\text{te}}}$
Relative error in capacitance	$\frac{(C_{\text{exp}} - C_{\text{te}})}{C_{\text{te}}}$	$\frac{(C_{\text{exp}} - C_{\text{te}})}{C_{\text{te}}}$	$\frac{(C_{\text{exp}} - C_{\text{te}})}{C_{\text{te}}}$

Results from the dummy cells with resistance only

The X and Y values of the I/E converter output for a dummy cell with only a low inductance metal film resistor was measured. The experiment was conducted for the following four cases.

$$(1) R_{te} = 2 \text{ k}\Omega ; R_m = 10 \text{ k}\Omega.$$

$$(2) R_{te} = 5 \text{ k}\Omega ; R_m = 10 \text{ k}\Omega.$$

$$(3) R_{te} = 2 \text{ k}\Omega ; R_m = 1 \text{ k}\Omega.$$

$$(4) R_{te} = 5 \text{ k}\Omega ; R_m = 1 \text{ k}\Omega.$$

The results expected from the experiment can be predicted by considering the equations relevant for the type of cell used here. From Equation 5.6 and 5.8, it can be seen that neither Z_{te} nor Z_m has an imaginary component. Thus, from Equation 5.4, E_{out} must not have an imaginary component, i.e., Y is expected to be zero. Therefore, the phase shift expected in this experiment is zero.

However, phase shifts calculated from Equation 5.3 using observed X and Y values at different frequencies showed increasing negative phase shift with increasing frequency. The experimental phase shifts as a function of frequency is shown in Figure 5.3 for cells with 2 k Ω and 5 k Ω resistors. Similar results have been observed by Mansfield et al. (80,81).

Relative error in resistance was calculated according to the definition given in the first column of Table 5.2, and is shown as a function of frequency in Figure 5.4.

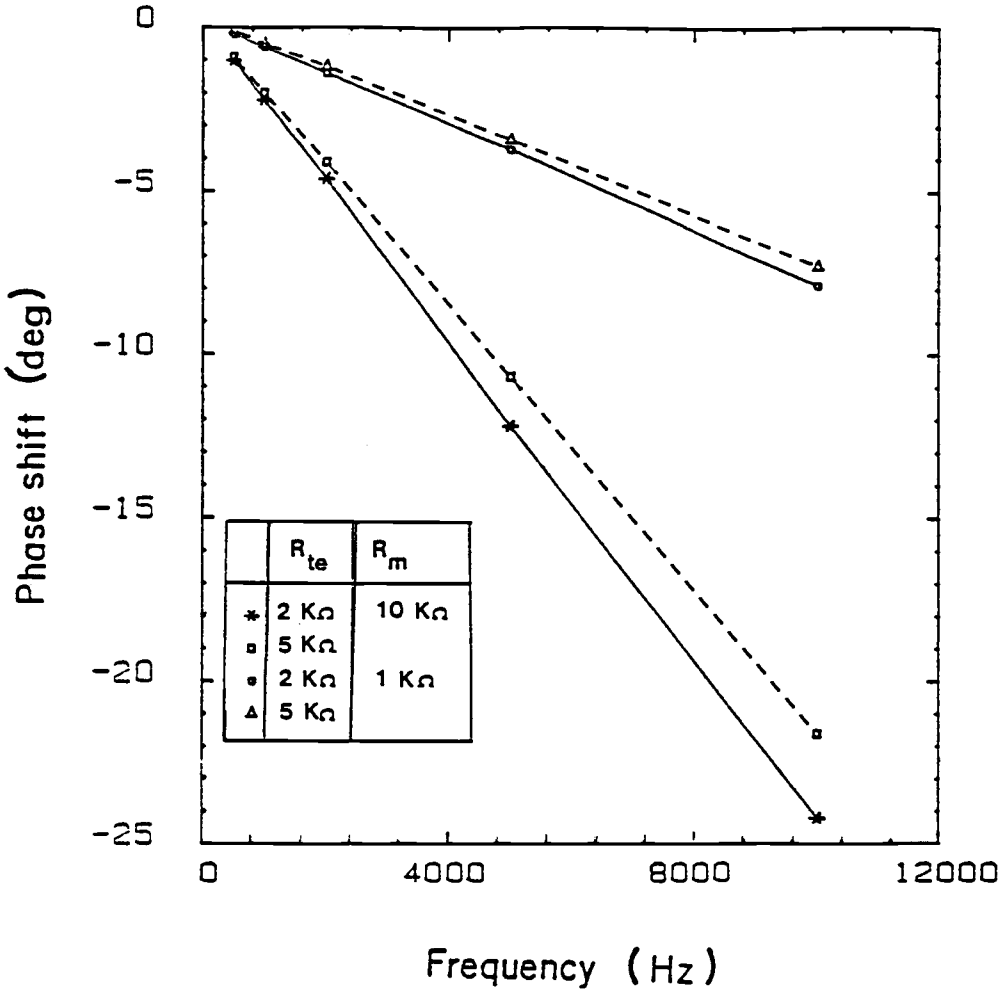


Figure 5.3. The frequency dependence of the phase shift

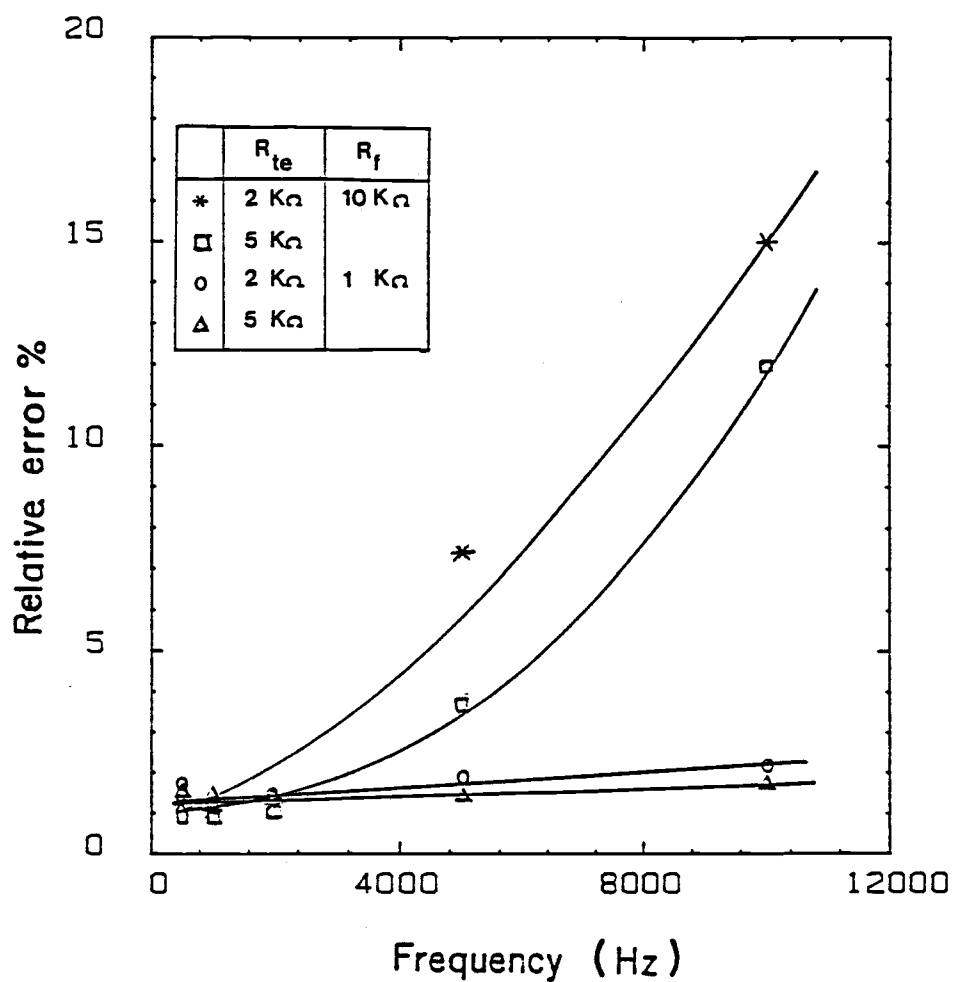


Figure 5.4. Relative error in resistance as a function of frequency for dummy cells with resistors only

Figures 5.3 and 5.4 show that the relative error becomes smaller and the phase shift becomes less negative when a less sensitive range, i.e, smaller R_m is used in the current to voltage conversion step. However, conducting measurements at a less sensitive range may be limited, at times, since the current observed in many experimental systems can be too small to be measured at small applied modulation voltages such as 10 mV p-p. Thus there is an incentive to examine the reasons for the phase shift mentioned above.

Relative contributions to the phase shift from amplifiers

An experiment was carried out to trace the origin of the negative phase shift observed for the totally resistive dummy cells, with expectations to correct the overall response for the phase shift. All three operational amplifiers in the potentiostat circuit shown in Figure 5.1 can cause phase shifts. Relative magnitudes of the phase shift caused by each amplifier was examined separately by comparing the input and output of the individual amplifiers. The frequency dependence of phase shift at each amplifier is shown in Figure 5.5. The points A, B, C and D in Figure 5.5 are indicated the circuit diagram in Figure 5.1. Figure 5.5 shows that the current to voltage conversion step is the most responsible for the observed phase shift.

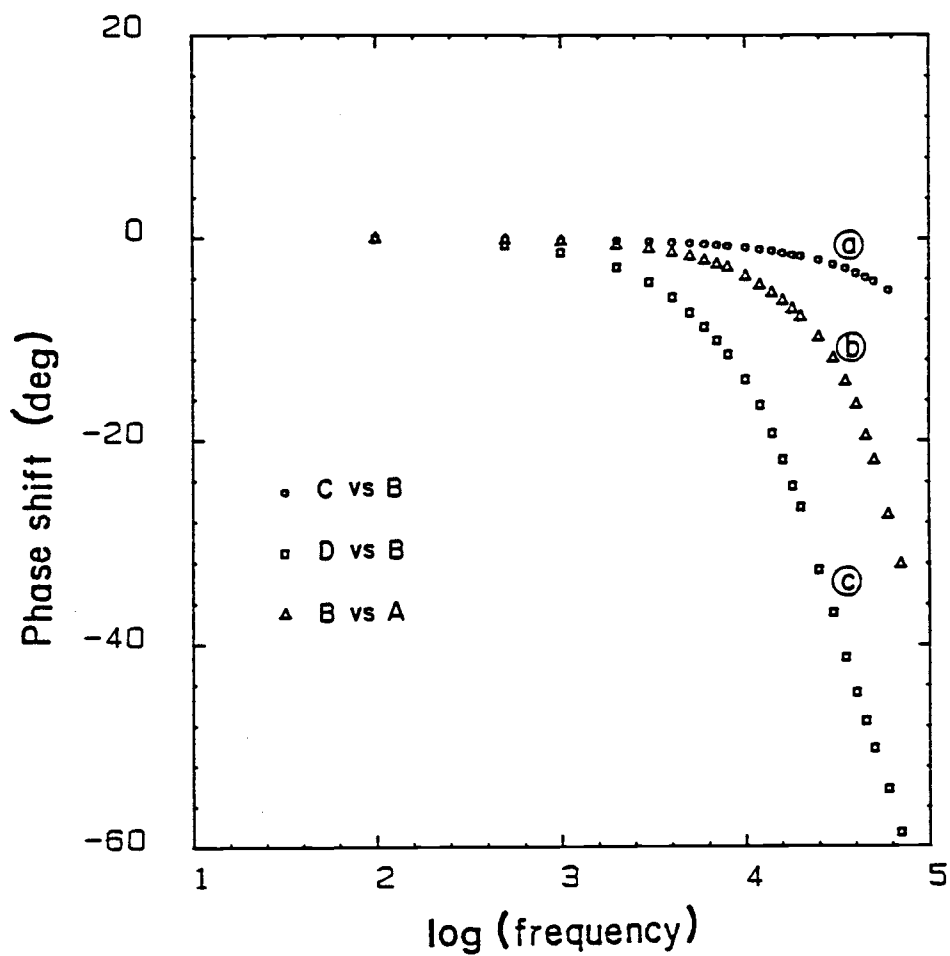


Figure 5.5. The phase shift caused by different amplifiers in the potentiostat circuit. (a) electrometer amp. (b) control amp. (c) current-to-voltage converter amp. $R_{te} = 10 \text{ k}\Omega$, $R_m = 10 \text{ k}\Omega$.

An approach to correct for the phase shift

An approach to correct for the phase shift caused by the current to voltage converter is presented here. This approach is non-instrumental and therefore allows to expand somewhat the useful frequency range of the existing instrumentation.

Although the impedance of the feed back loop of the current to voltage converter consists of only a resistor according to the actual circuit, the amplifier appears to behave as if there were also a capacitive element.

In the proposed correction method, the presence of a capacitor C_m in the feedback loop of the I/E converter is considered, as is shown in Figure 5.6. The impedance of the feed back loop of the I/E converter can now be expressed as

$$Z_m = 1/(1/R_m + j \omega C_m) \quad 5.12$$

From the measured X and Y, Z_{exp} was calculated from Equation 5.7, but this time Equation 5.12 was used to obtain Z_m instead of Equation 5.6. A value for C_m was chosen, by trial and error, such that the relative error in resistance determination remained minimal over a wide range of frequencies and resistances. From the experimental data, this capacitance value was found to be 0.3 nF. The improvement in the accuracy of resistance determination by this correction is illustrated in Figure 5.7. With the correction, the resistance can be determined within 1% accuracy up to 10 kHz, whereas without it, the accuracy drops drastically above 2 kHz.

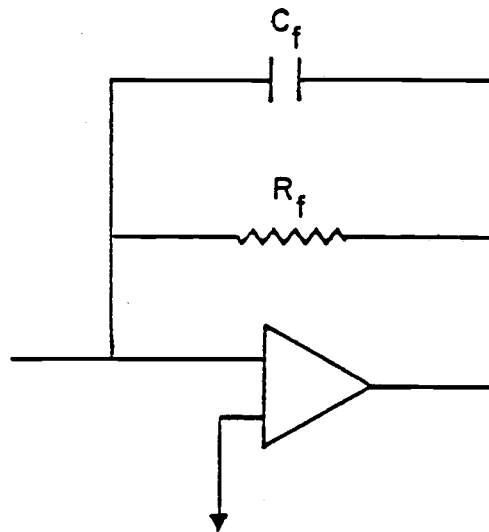


Figure 5.6. Model circuit for the current to voltage converter

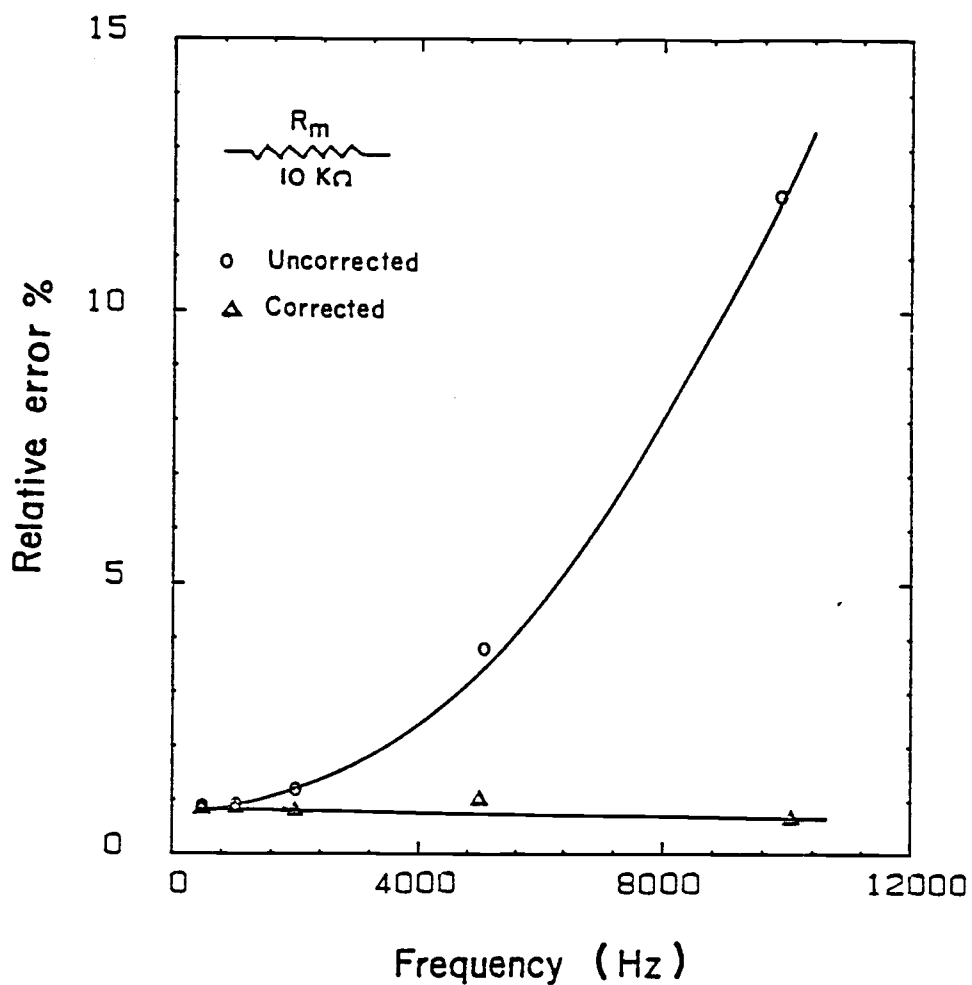


Figure 5.7. The effect of correction for impedance of current voltage converter on the relative error in cell resistance

Results from other dummy cells

The usefulness of the aforementioned impedance correction was further tested for dummy cells with parallel and series RC circuits, as represented in Figure 5.2. Z_{exp} was obtained in a way similar to the one described for the cells with resistance only. R_{exp} and C_{exp} for series and parallel circuits, and the respective errors, were calculated from Z_{exp} data using the appropriate expressions shown in Table 5.2.

Figures 5.8 (a) and (b) show the effect of the impedance correction on the relative error in the resistance and capacitance of the parallel circuit, as a function of frequency. the same information is presented in Figures 5.9 (a) and (b) for the series circuit.

In both types of circuits, it is evident that the correction of impedance of the current-to-voltage converter improves the accuracy of the capacitance and resistance determination.

By examination of relative errors of resistance and capacitance for all three types of cells fig 5.7, 5.8, and 5.9; it can be concluded that the measurements above 1000 Hz would result in significant errors in the determination of impedance.

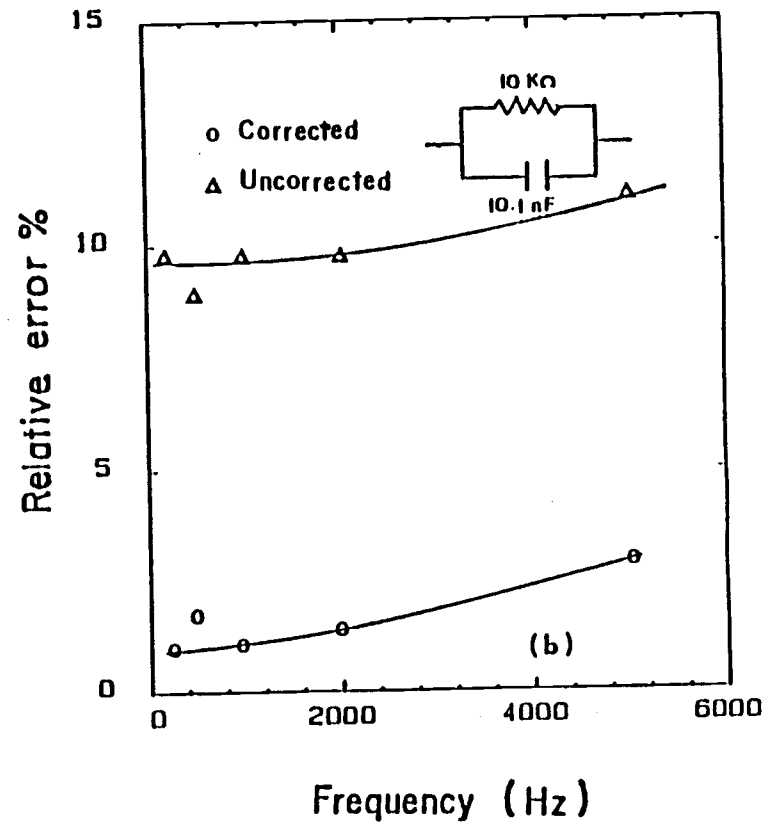
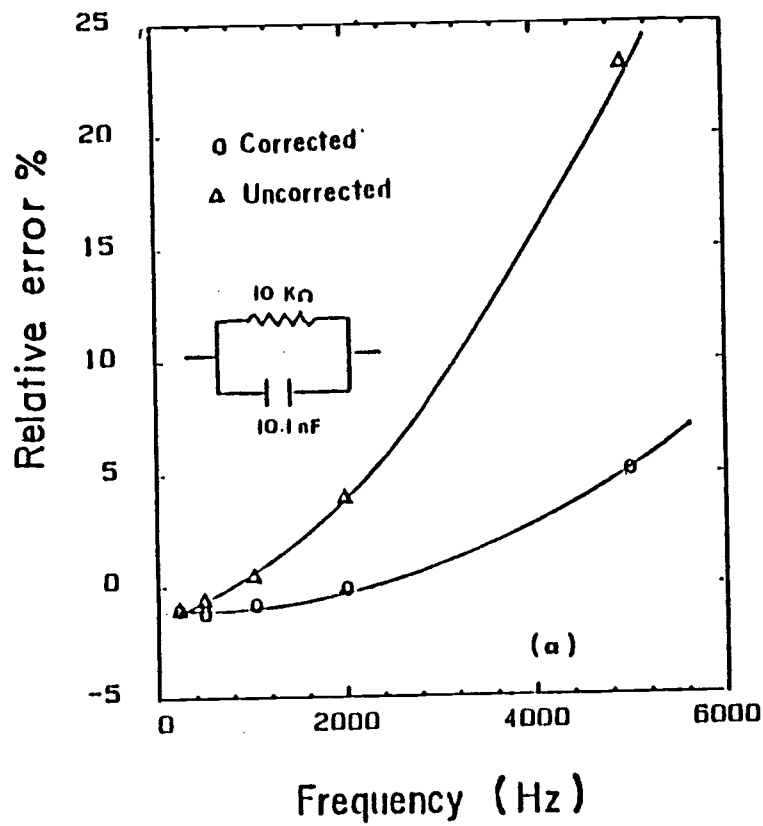


Figure 5.8. Improvement in accuracy of (a) resistance (b) capacitance determination in parallel circuits by correcting for impedance in current to voltage converter

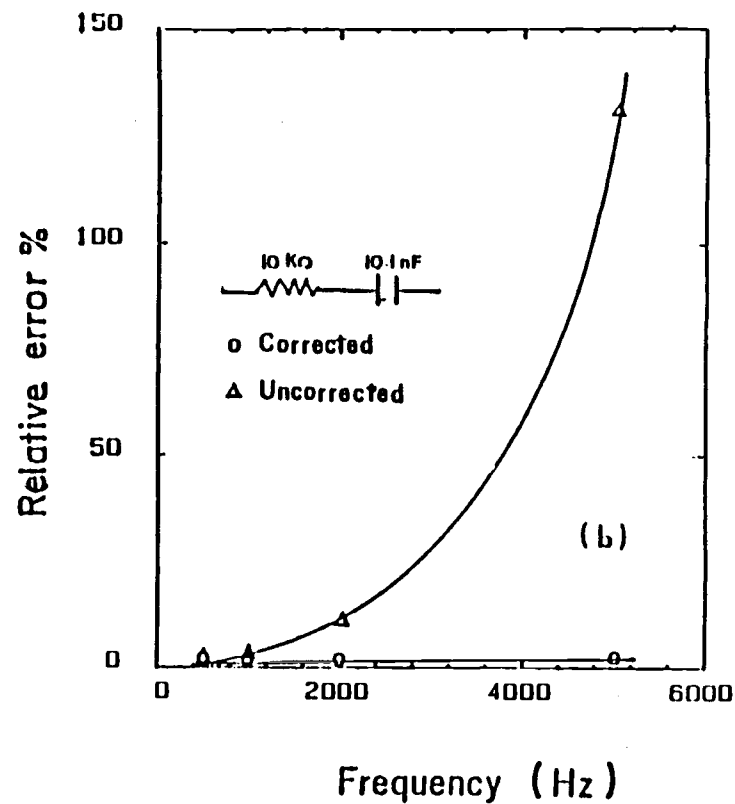
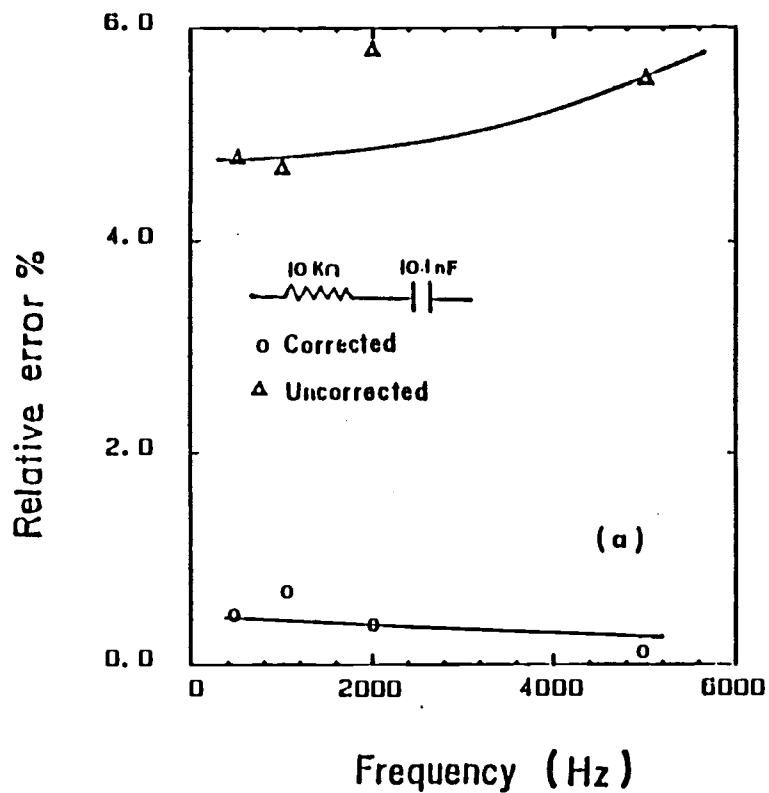


Figure 5.9. Improvement in accuracy of (a) resistance (b) capacitance determination in series circuits by correcting for impedance in current to voltage converter

Summary

Negative phase shifts were observed for the I/E output measured for the dummy cells consisting of resistance. Cell impedance calculated from experimental data without correcting for these phase shifts yielded a systematic error, which limited the frequency range of the potentiostat. The I/E converter in the potentiostat was found to be responsible for most of the phase shift. By accounting for the effect of a 0.3 nF capacitor in parallel with the 10 k Ω resistor in the feedback loop of the I/E converter, it was possible to expand somewhat the useful frequency range.

The upper limit of frequency for the PAR 179 current-to-voltage converter was found to be 1000 Hz. Measurements taken above this frequency should be corrected for phase shifts induced by the current-to-voltage converter.

5.2 Verification of results from the C-V curves of EOS structures by other methods

Capacitance measurements performed for EOS structures are presented in this section. Experimental capacitance-voltage curves are compared to the theoretical ones calculated in Section 3.4.

It was shown in the theory section that the properties of the MOS structures which depend on the fabrication of the device (such as oxide capacitance and dopant density) can be obtained from the C-V curves. These properties can also be measured by other independent methods to be described later in this section. The values obtained from the C-V curves are compared with those from the other methods to support the validity of the theory and the experimental method used here.

The upper frequency limit for the experimental method of capacitance determination was found to be 1000 Hz as shown in the previous section. All capacitance measurements described here were made at 500 Hz.

In this experiment, the dc bias voltage applied to the electrochemical cell containing the Si/SiO₂ electrode was varied. At each applied voltage, the amplitude of the in-phase and out-of-phase component of the I/E converter output were measured.

Capacitance of the EOS structure was calculated with a series circuit model assumed to represent the electrochemical cell. The justification for using a series circuit in the data analysis can be found in Section 3.5. A computer program SILICA developed in this work, was used in the calculations. The program and the numerical method on which it is based is shown in Appendix E. C-V curves were obtained by plotting capacitance against the applied voltage.

The C-V curve obtained for Si/SiO₂/electrolyte structure in 0.01 M KNO₃ solution at pH 3 (near the pH_{zc} of SiO₂) is shown in Figure 5.10 (curve A). The Si/SiO₂ electrode was prepared as described in Section 4.1.

In order to compare the experimental data to theory, it is necessary to recognize the fundamental difference between the theoretical C-V curves calculated in Section 3.4 and the experimental ones. In the experiment, the voltage applied to the cell was measured relative to an SCE reference electrode, and the voltage axis of the C-V curves represents the applied voltage V_{appl} . However, in the theoretical C-V curves, capacitance was calculated as a function of the voltage across the EOS structure ψ_F . The relationship between V_{appl} and ψ_F is given by Equation 3.78 in Section 3.4. It remains to relate the the potential in metals, which is expressed relative to vacuum scale, to the potential of reversible reference electrode (such as NHE). Theoretically, this is impossible because electrode potential is based on a thermodynamic reference state whereas the reference state

in the vacuum scale is a quantum level. As suggested by Bousse (76), an operational relationship of NHE to vacuum scale can be used to bring E_{Ref} and $\Delta\phi_{\text{MS}}$ to the same scale. Bousse represents the potential of the NHE as 4.76 V in the vacuum scale. Using this value, $\Delta\phi_{\text{MS}}$ for the experimental EOS structure can be translated to NHE scale as 0.29 V vs. NHE. The reference electrode used in these experiments is an SCE, and E_{ref} is 0.242 V vs NHE. Thus, the offset between the theoretical and experimental curves, $(V_{\text{appl}} - \psi_F)$, is expected to be 0.532 V.

A theoretical C-V curve was calculated for an EOS structure ($d_{\text{ox}} = 550 \text{ \AA}$, $N_D = 1.3 \times 10^{15}$, $N_S = 10^{15}$, $K_D = 0.01$ and $\text{pH} = \text{pH}_{\text{zc}}$) and the voltage axis was translated to V_{appl} by adding the theoretical offset 0.532 V. This curve is shown in Figure 5.10 (curve B) along with the experimental curve for the purpose of comparison.

Three important differences between the two curves can be observed immediately from Figure 5.10.

- (1) Minima of capacitance of the two curves occur about 0.7 V apart.
- (2) Capacitance in the accumulation region (oxide capacitance) for the experimental curve is lower than that of the theoretical one.
- (3) The dip of the experimental curve is much shallower. (i.e. $C_{\text{min}}/C_{\text{ox}}$ ratio is larger).

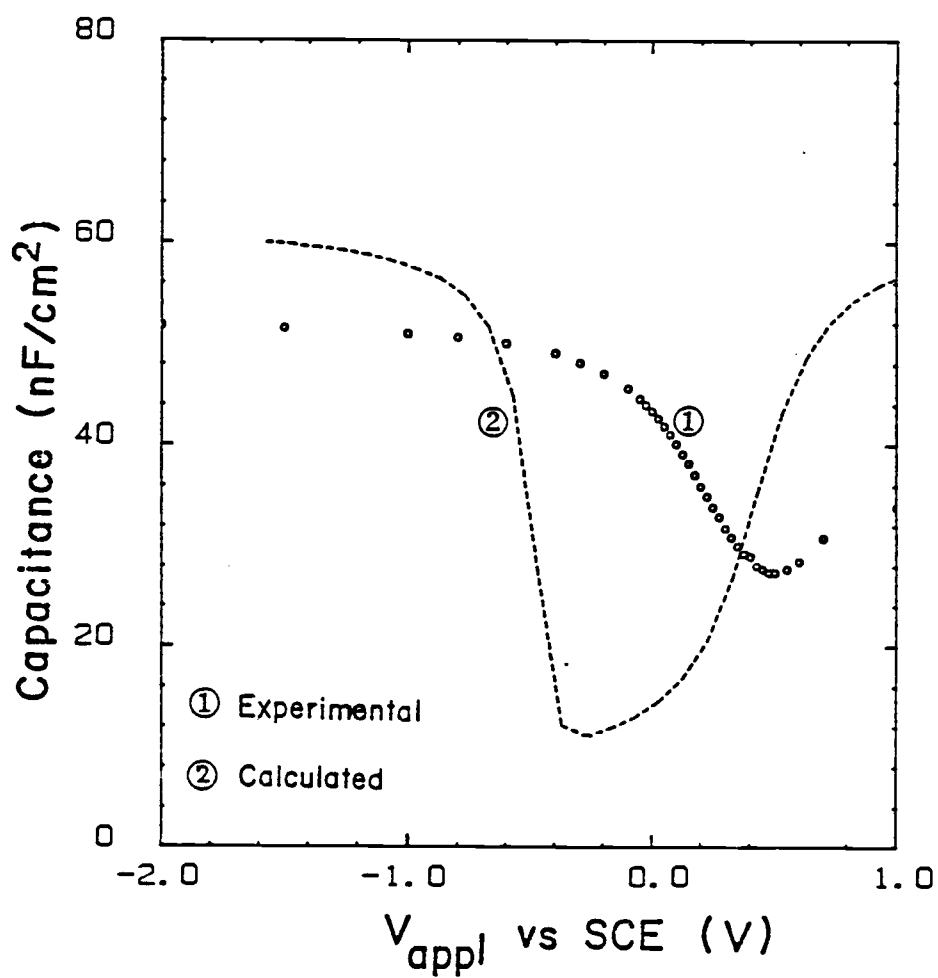


Figure 5.10. Capacitance-Voltage curves obtained at pH 3 for Si/SiO₂/electrolyte system in 0.01 M KNO₃

Minima of capacitance

The difference between the capacitance minima of the experimental and the theoretical curve can be attributed to

(1) the uncertainty in the absolute voltage represented in the vacuum scale. (Several authors (82-84) have reported values for the potential of the NHE relative to the vacuum scale. These values vary in the range 4.31 V to 4.81 V)

(2) the other potential differences, unaccounted in the theoretical calculations. As discussed by Bousse (76), these potentials include dipole potentials existing at Si/SiO₂ and SiO₂/solution interface.

Oxide capacitance

The observed capacitance in the accumulation region of the C-V curve should be equal to the capacitance of the oxide, according to the theory of MOS capacitors. The capacitance of the oxide can also be obtained from its thickness from Equation 5.13.

$$C_{ox} = \frac{\epsilon_o \epsilon_{ox}}{d_{ox}} \quad 5.13$$

The thickness of the oxide was measured by reflectance spectroscopy. Results from both methods, in principle, should yield the same oxide capacitance.

The thickness of the oxide measured by reflectance spectroscopy is $550 \pm 48 \text{ \AA}$, and the capacitance of the oxide as calculated from Equation 5.5 is $62.8 \pm 5.5 \text{ nF/cm}^2$ with ϵ_{ox} taken as 3.9.

The capacitance in the accumulation region of the C-V curve in Figure 5.11 is found to be $52 \pm 3 \text{ nF/cm}^2$, based on the measured capacitance of 18.2 nF and the exposed electrode area of 0.35 ± 0.04 . The lower capacitance obtained from C-V measurements may be explained as follows.

(1) The dielectric constant of SiO_2 is dependent on the method and the conditions of oxide growth. It may be possible that the dielectric constant used to calculate the oxide capacitance was lower than the actual value for the oxide used in the experiment.

(2) An adsorption process may be taking place at the surface of the oxide which may contribute as another capacitance term in series with that of the oxide.

$C_{\text{min}}/C_{\text{ox}}$ ratio

The ratio ($C_{\text{min}}/C_{\text{ox}}$) is characteristic of a given semiconductor/oxide system. This ratio changes with the semiconductor dopant density and the oxide thickness. Theoretical plots of these ratios for ideal MOS structures as functions of oxide

thickness or dopant densities are available in many references (65,67). Figure 5.11 shows such a family of curves. (C_{\min}/C_{ox}) ratio for an ideal MOS structure with the same N_D and C_{ox} as in the experimental system was found to be 0.3, from Figure 5.11. Experimentally, (C_{\min}/C_{ox}) falls between 0.55 and 0.6.

The larger observed (C_{\min}/C_{ox}) ratio can be explained by considering the surface states at the Si/SiO₂ interface. If there are surface states at the Si/SiO₂ interface which can follow the ac signal, then the observed capacitance for an EOS structure can be given by Equation 5.14.

$$\frac{1}{C_{\text{obs}}} = \frac{1}{C_{\text{ox}}} + \frac{1}{C_{\text{ss}} + C_{\text{sc}}} \quad 5.14$$

(This equation is derived in Section 3.5). The capacitances of the surface states and semiconductor are represented by C_{ss} and C_{sc} respectively. When the surface state density is high, C_{ss} is large, and the observed capacitance is closer to that of the oxide capacitance. In other words, if the surface state density is high, the dip in the C-V curve is shallower compared to the curves for ideal MOS structures. The extent of the deviation of (C_{\min}/C_{ox}) ratio from the corresponding ideal value can be used to obtain the

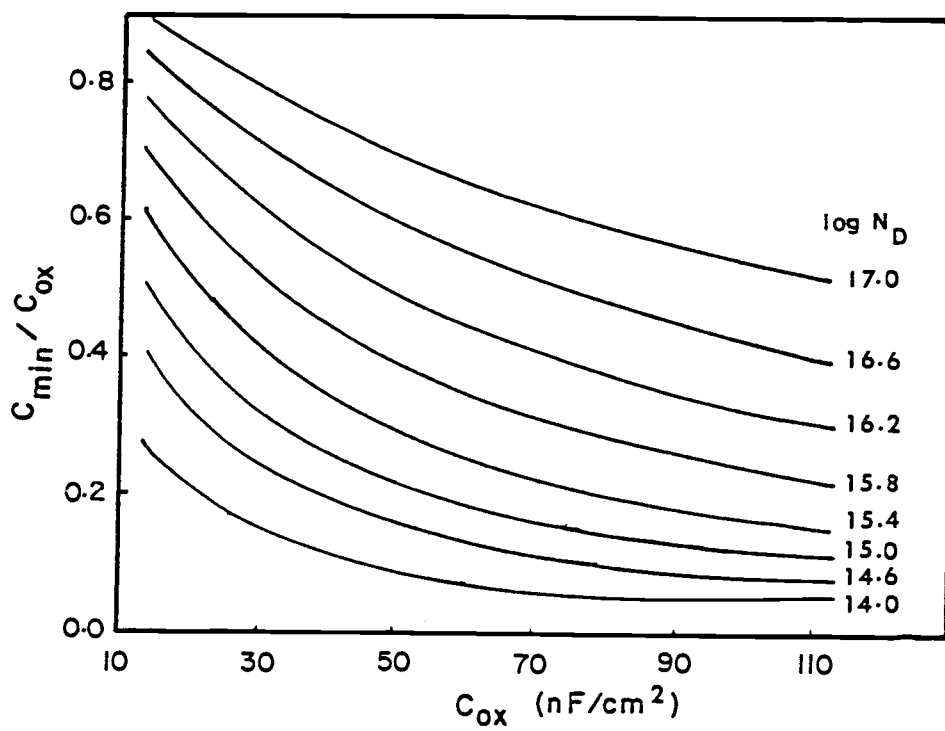


Figure 5.11. C_{\min}/C_{ox} ratio for ideal MOS structures

surface state density. This procedure is outlined as follows.

Equation 5.14 can be rearranged as

$$C_{ss} = C_{ox} \left[\frac{(C_{obs} / C_{ox})}{1 - (C_{obs} / C_{ox})} - \left(\frac{C_{sc}}{C_{ox}} \right) \right] \quad 5.15$$

Also, the surface state capacitance (C_{ss}) is related to the surface state density (N_{ss}) by Equation 5.16.

$$C_{ss} = N_{ss} q \quad 5.16$$

where N_{ss} is given in $\text{cm}^{-2} \text{ eV}^{-1}$. Equations 5.15 and 5.16 can be combined and rearranged to yield the following expression at capacitance minimum

$$N_{ss} = \frac{C_{ox}}{q} \left[\frac{(C_{obs} / C_{ox})_{min}}{1 - (C_{obs} / C_{ox})_{min}} - \left(\frac{C_{sc}}{C_{ox}} \right)_{min} \right] \quad 5.17$$

where $(C_{sc}/C_{ox})_{min}$ is The theoretical value obtained for MOS structure with the same properties as the EOS structure used.

The surface state density N_{ss} in the mid-gap calculated from Equation 5.9 is $4 \times 10^{11} \text{ cm}^{-2}$. The surface state density reported by the manufacturer for the Si/SiO₂ devices varies in a range of 10^{10} to 10^{12} cm^{-2} .

Dopant density

The doping density N_D can be obtained from the Mott-Schottky plots as shown by Equation 3.57 in Section 3.4. A Mott-Schottky plot for the data in the Figure 5.10 is shown in Figure 5.12. The dopant density calculated from the slope of the linear part of the plot is $5 \times 10^{15} \text{ cm}^{-3}$.

The doping density was also obtained from the four point probe method. This method is the most common one used for measuring the resistivity of the semiconductors. Figure 5.13 shows a schematic diagram of a four point probe. A small constant current (I) is passed through the two outer probes and the voltage drop across the inner probes (V) is measured. The resistivity α is calculated from the following equation (65).

$$\alpha = (\xi V W)/I \quad 5.18$$

where W is the thickness of the Si wafer and ξ is a conversion factor which depends on the ratio of the distance between the each probe (S) to the width or the diameter of the wafer (a or d). If the ratio is very small, a limiting value 4.532 is used for ξ . The dopant density is obtained from the resistivity via the following relationship.

$$N_D = \frac{1}{q \mu_n \alpha} \quad 5.19$$

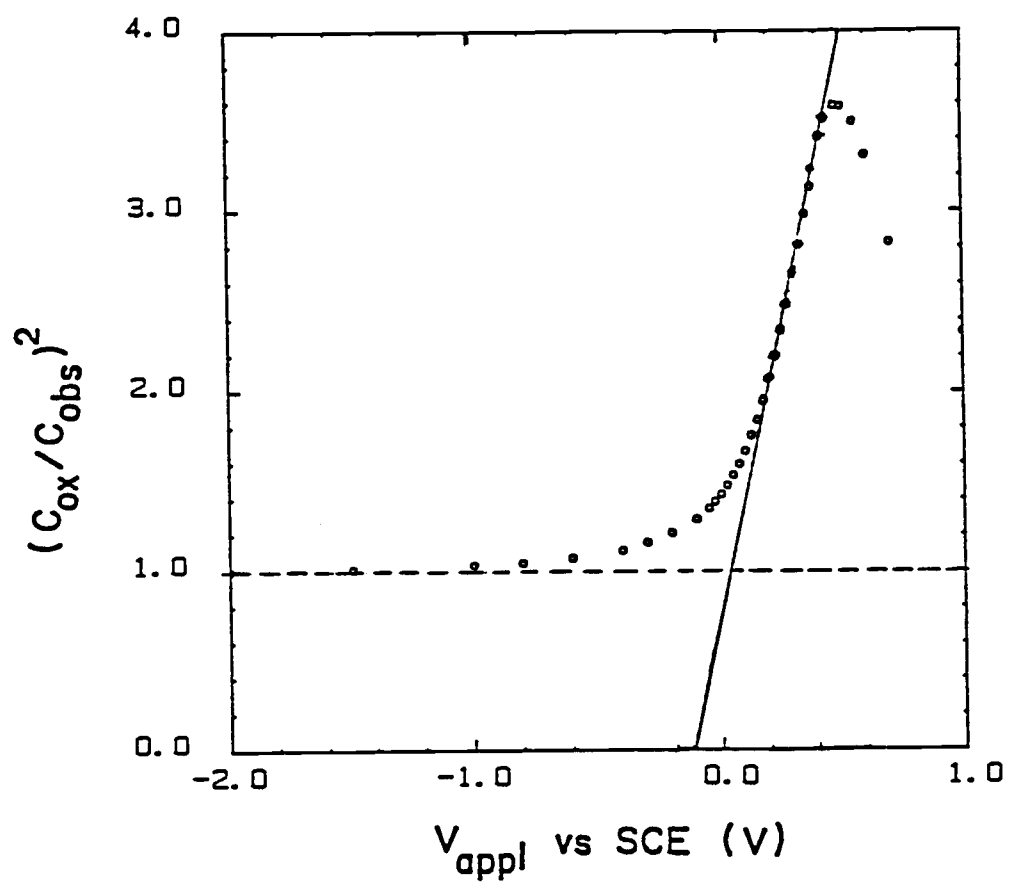


Figure 5.12. Mott-Schottky plot for the C-V curve shown in Figure 5.10

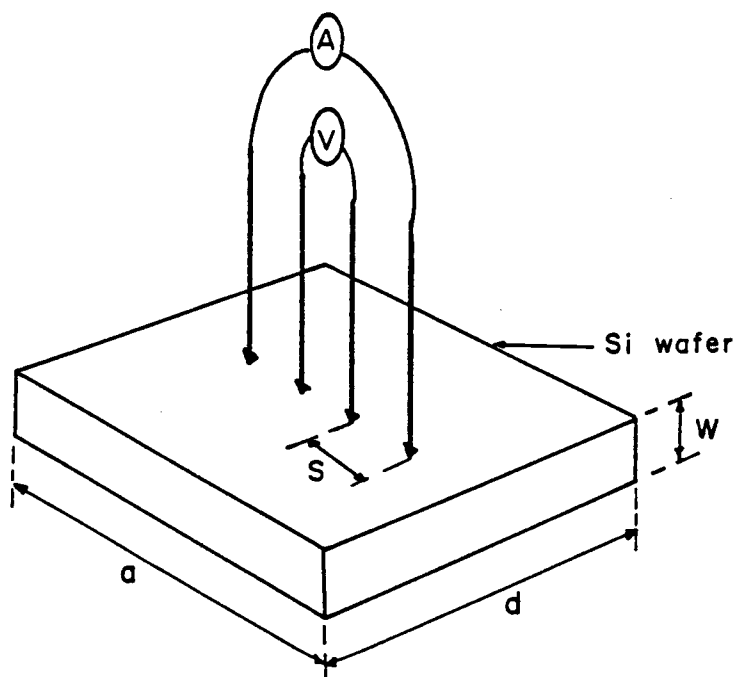


Figure 5.13. Schematic diagram of a four point probe

where N_D = dopant density

μ_n = mobility of electrons in Si ($1500 \text{ V}^{-1} \text{ cm}^{-2} \text{ s}^{-1}$)

q = elementary charge

(See standard text books (64,65) in semiconductor physics for further details).

The dopant density obtained from this technique ($1.3 \times 10^{15} \text{ cm}^{-3}$) agrees well with the value obtained from the Mott-Schottky plots.

Summary

The values obtained from the experimental C-V curves for the doping density, oxide capacitance and the surface state density of the EOS structure agree reasonably well with the values obtained from the independent methods. Based on these results, it can be concluded that the experimental method used here is reliable and suitable for the further studies on the EOS structure.

5.3 Drift in the C-V response

The shift of the C-V curves of the EOS structures are to be measured with changes of solution pH and ionic strength. If the capacitance of the EOS structure is time dependent, it will be difficult to distinguish the effect of solution properties from the effect of time on the C-V curves. The drift of C-V curves was estimated in the experiment described here.

The Si/SiO₂ wafers mounted in the electrode holder were placed in a solution of pH = 3, and AC impedance was measured over several hours. The drift in the C-V curves is shown in Figure 5.14. A noticeable lowering of capacitance with time is observed in the accumulation region. This phenomenon can be attributed to a decrease in the oxide capacitance with time. Adsorption of some species from the solution, as mentioned earlier, may be a reasonable explanation for the drift towards a lower capacitance.

The capacitance minima of the C-V curves did not change substantially over the period of the experiment. The change in oxide capacitance does not influence the observed capacitance near the minimum since it is dominated by the smaller semiconductor capacitance. The C-V curves have not shifted along the voltage axis, indicating that the drift of the flat band potential of the EOS structure is insignificant over a period of 3 days.

The rate of capacitance decay decreases with time after two or three days. The rate of change is slow enough that an experiment to investigate the effect of pH or ionic strength can be done without being affected by the drift. (One scan through the entire potential range takes approximately 20-30 minutes).

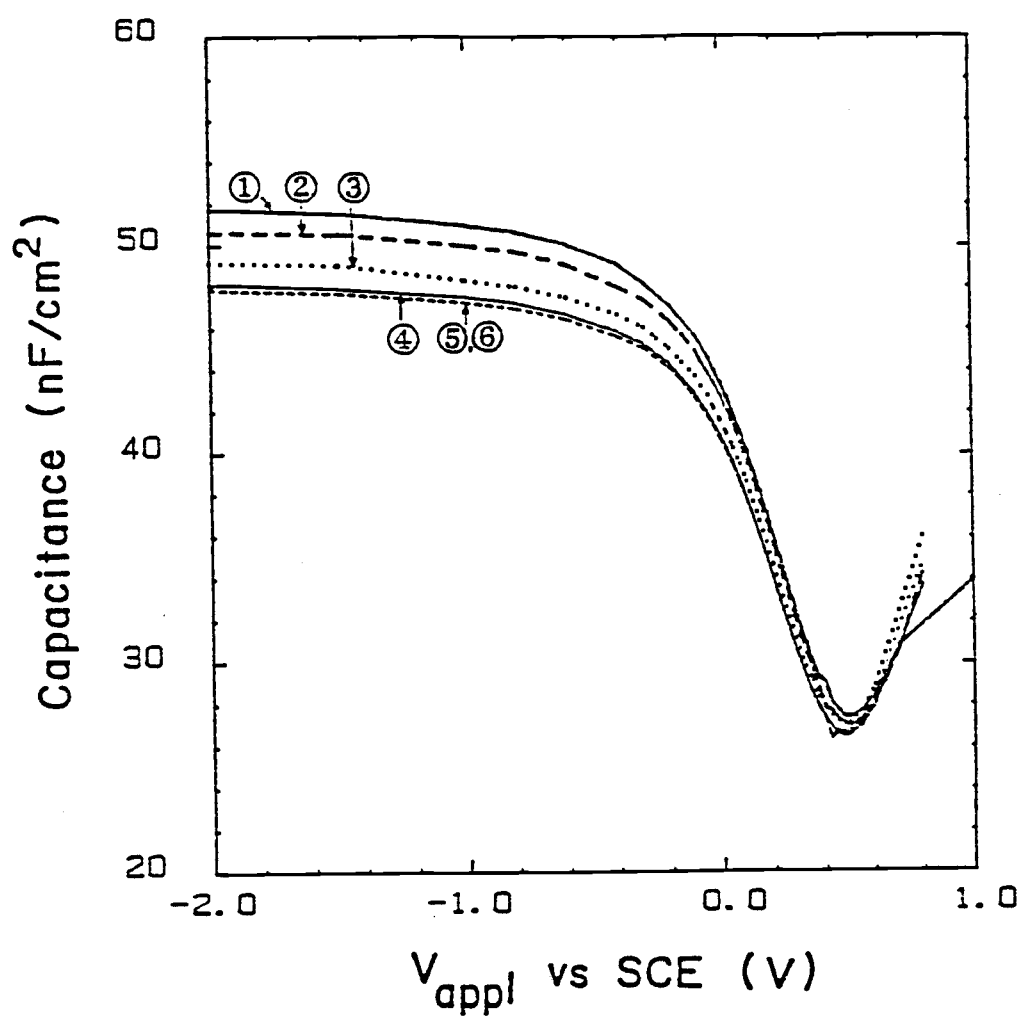


Figure 5.14. Drift of C-V curves obtained in 0.01 M KNO_3 at pH 3.

- | | |
|------------------|------------------|
| (1) after 2 hrs. | (2) after 6 hrs. |
| (3) 23 hrs. | (4) 52 hrs. |
| (5) 67 hrs. | (6) 72 hrs. |

5.4. Effect of pH on the C-V curves

The Si/SiO₂ wafers, mounted on the electrode holder, were immersed in the electrolyte solution for three days before capacitance measurements were made. Figure 5.15 shows a family of C-V curves obtained in the pH range of 3 to 7. These curves resemble with the theoretical C-V curves for a similar EOS structure shown in Figure 3.19. Details of the results are discussed here in conjunction with the model developed in the theory section.

Primary Mechanisms responsible for the shift of curves

The translation of C-V curves along the voltage axis with changes in pH is very pronounced, and this shift clearly represents an effect of the solution on the oxide. In addition to the theory already presented in detail to explain this effect, there is another theory based on a diffusion mechanism.

According to some researchers (77,85), it is the diffusion of ions from the electrolyte through the oxide to the Si/SiO₂ interface that is the primary mechanism whereby the electrolyte ions affect the charge in the semiconductor.

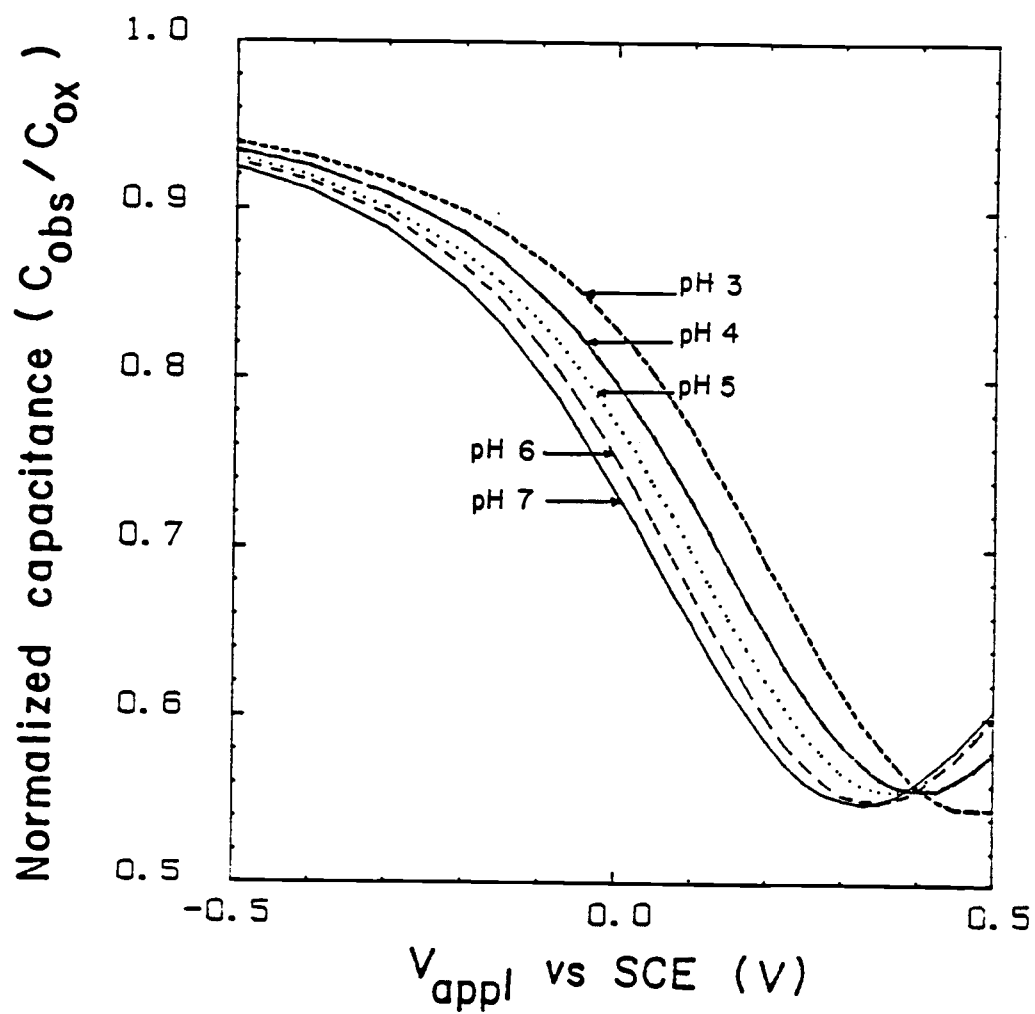


Figure 5.15. A family of C-V curves obtained for the EOS system in the pH range 3-7. ($C_{bulk}=0.01$)

The proponents of the diffusion mechanism argue that the surface state density at the Si/SiO₂ interface is changed by the transport of H⁺ or hydrogen-bearing species across the oxide. According to this theory, the hydrogen-bearing species diffuse to the Si surface, form Si-H bonds and reduce the interface state density. The change in interface state density shifts the C-V curves along the voltage axis and capacitance axis.

In explaining the reversibility of response of EOS structures to pH changes, they claim that the reduction in pH in the solution creates a "hydrogen pressure gradient" sufficient to cause dissociation of Si-H bond and the outdiffusion of hydrogen to the solution (86).

Diffusion of ions through the oxide layer may occur in the EOS systems. However, this process cannot be considered as the primary mechanism by which the electrolyte can affect the semiconductor, as shown by the following experimental evidence reported here and observed by others (87).

(1) The EOS structures studied here responded to pH changes within minutes. Diffusion of Na⁺ or other ions through the oxide is slow at room temperature, so that it may take several hours for the ions to diffuse across a 500 Å⁰ oxide layer.

(2) Deal et al. (88) have shown that Si₃N₄ is an effective barrier against the hydrogen diffusion, compared to SiO₂. However, a comparison of ion-selective field effect transistors (ISFETS) fabricated using SiO₂ and Si₃N₄ gates revealed that the ISFETS with Si₃N₄ are more sensitive to pH than the other (87).

The observations mentioned above do not support the view that the diffusion of ions is the primary mechanism affecting the response. The view that the electrical potential developed at the oxide/solution interface due to electrochemical equilibrium between the oxide and the solution is primarily responsible for the shift of C-V curves was discussed in the theory section. The experimental results will be interpreted in terms of that theory.

Dependence of ψ_0 on pH

It was explained that the applied potential has to be changed in order to maintain the same capacitance when the pH is changed. In other words, a change in the applied potential is necessary to compensate for the changes in ψ_0 at the oxide surface with solution composition (pH). Therefore, $\frac{\Delta\psi_0}{\Delta\text{pH}}$ can be obtained directly from the shift of C-V curves.

According to the theory developed for the EOS system, the magnitude of the shift of C-V curves, $\frac{\Delta\psi_0}{\Delta\text{pH}}$, varies with the surface site density (N_s), dissociation constant of the oxide (K_D), pH of the solution and the concentration of the electrolyte. Surface site density and the dissociation constant are parameters which cannot be controlled in the experiment. They are characteristic properties of the EOS structure under study.

The results of $\frac{\Delta\psi_o}{\Delta pH}$ are presented for EOS structures studied in

(1) 0.01 M

(2) 0.05 M

(3) 0.10 M

KNO_3 solutions in the pH range of 3-7. Figures 5.16 (a), (b) and (c) show families of C-V curves obtained for the same EOS structure in 0.01, 0.05 and 0.1 M KNO_3 solutions. All three families of curves indicate shifts in the same direction for a given pH change. An average shift of C-V curves over the range of pH 3-7 for each solution can be obtained directly from the corresponding figures. Average shifts of 38.5, 34.5 and 26.7 mV/pH were obtained for 0.01, 0.05 and 0.1 M KNO_3 solutions, respectively.

The information that can be obtained from the C-V curves in Figures 5.16 (a), (b), and (c) can be presented in the following way. The shift of C-V curves are measured relative to the position of the C-V curves at pH 3 ($\Delta\psi_o$), and the change in pH is expressed relative to pH 3 (ΔpH). The curve at pH 3 was selected because the zero charge reported for SiO_2 is near pH 3. $\frac{\Delta\psi_o}{\Delta pH}$ can be plotted against ΔpH at each ionic strength, as in Figure 5.17 to give an overall view of the experimental results.

From Figure 5.17, the following observations can be made.

- (1) $\frac{\Delta\psi_o}{\Delta pH}$ less than the Nernst slope of 59 mV/pH.
- (2) $\frac{\Delta\psi_o}{\Delta pH}$ decreases with increasing electrolyte concentration.

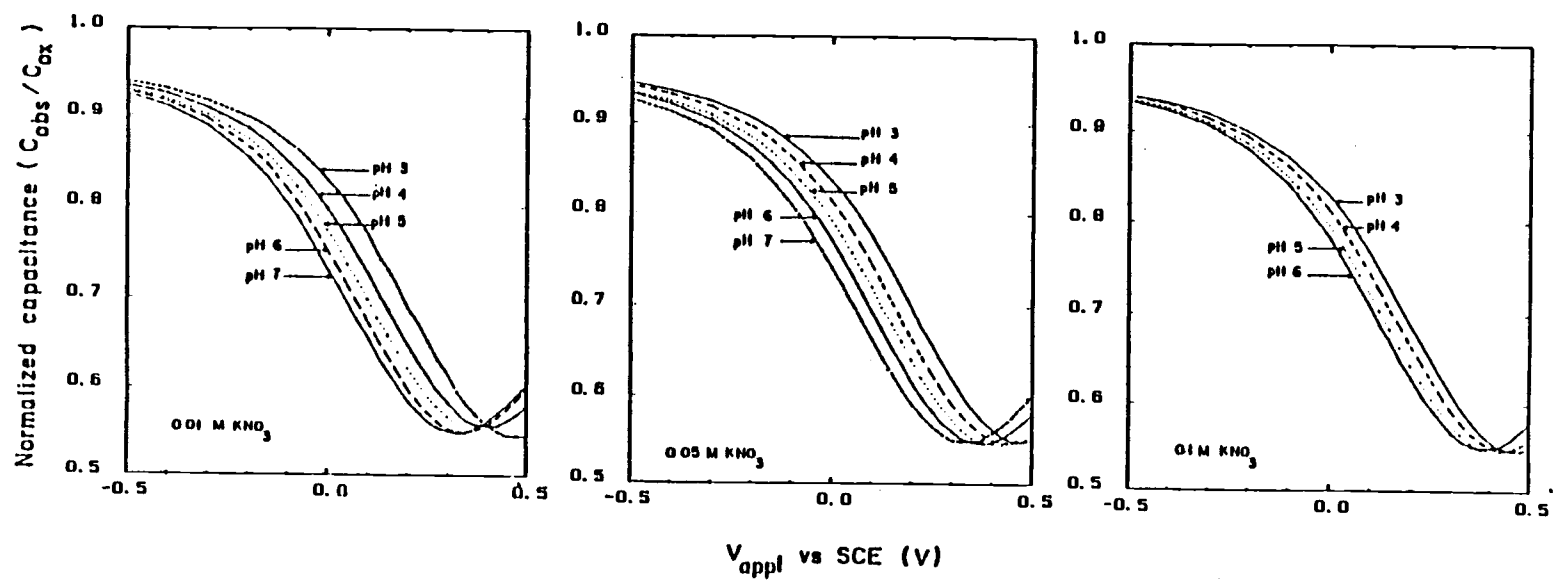


Figure 5.16. C-V curves obtained for EOS structures
in (a) 0.01 M (b) 0.05 M (c) 0.1 M
 KNO_3 solutions.

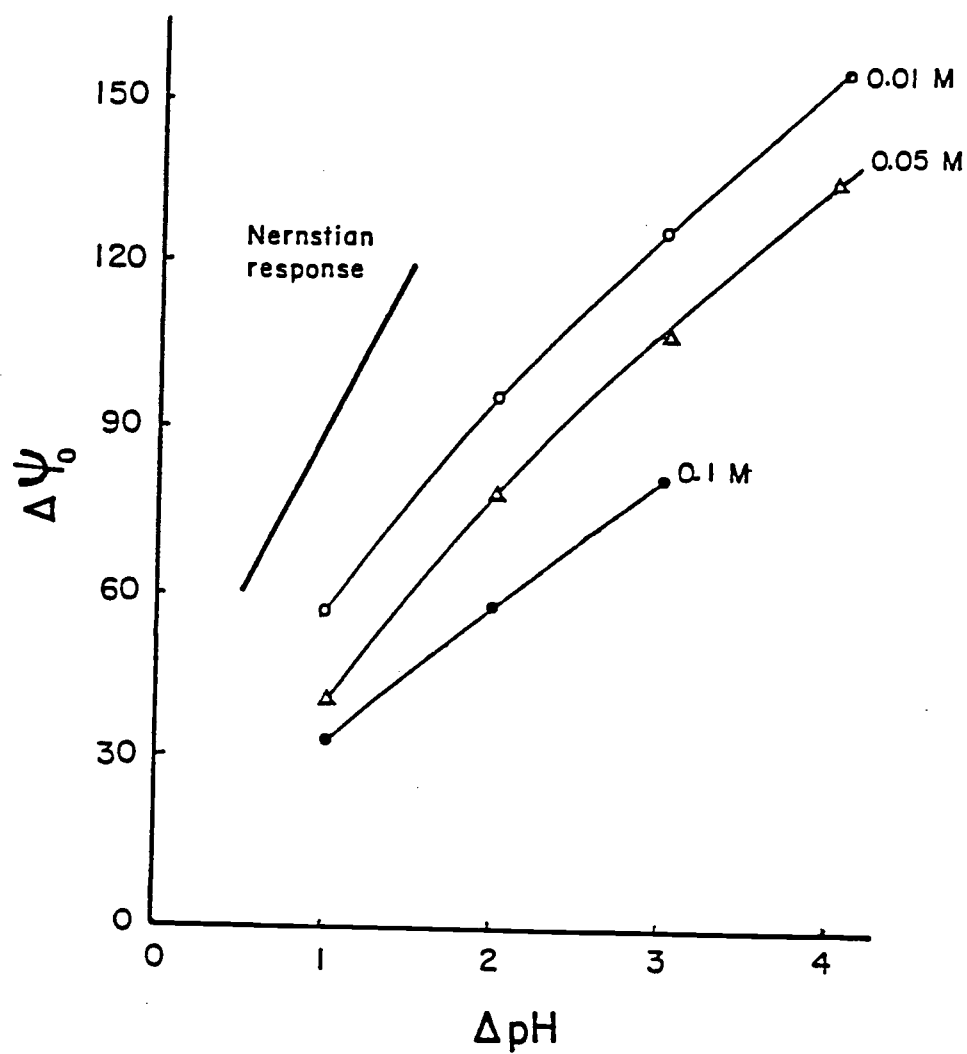


Figure 5.17. $\Delta\psi_0$ as a function of ΔpH in 0.01, 0.05, and 0.1 M KNO_3 solutions

- (3) $\frac{\Delta\psi_o}{\Delta pH}$ is closer to Nernstian behavior near the pH_{zc} , but becomes sub-Nernstian away from it.

Many workers have reported sub-Nernstian response from the experiments with SiO_2 /electrolyte interface. These results can be found in Table 2.2.

Schenk (76) has reported that the sensitivity $\frac{\Delta\psi_o}{\Delta pH}$ of ion-selective field effect transistors with SiO_2 gates decreased as the solution concentration was increased. The second observation in this experiment, as mentioned above, agrees with Schenk's results as well as with the predicted trend in the theory section.

In the theory section, it was shown that the $\frac{\Delta\psi_o}{\Delta pH}$ is a maximum at pH_{zc} , if the surface dissociation constant (K_D) of an oxide is large. It is a minimum, if K_D is small. The experimental results show that $\frac{\Delta\psi_o}{\Delta pH}$ decreases when the pH is increased away from the pH_{zc} , indicating a relatively large K_D value for SiO_2 .

The characteristics of the oxide such as K_D and N_s can be estimated by comparing the experimental $\frac{\Delta\psi_o}{\Delta pH}$ curves with those calculated from theory. Figure 5.18 shows the variation of calculated $\Delta\psi_o$ as a function of pH at different N_s and K_D values. All curves in Figure 5.18 were calculated for an EOS structure in 0.01 M electrolyte solution. By comparing the experimental results in Figure 5.17 with the calculated curves in Figure 5.18, a K_D value of 0.01 and N_s value of 8×10^{14} can be selected as the best values to describe the experimental data.

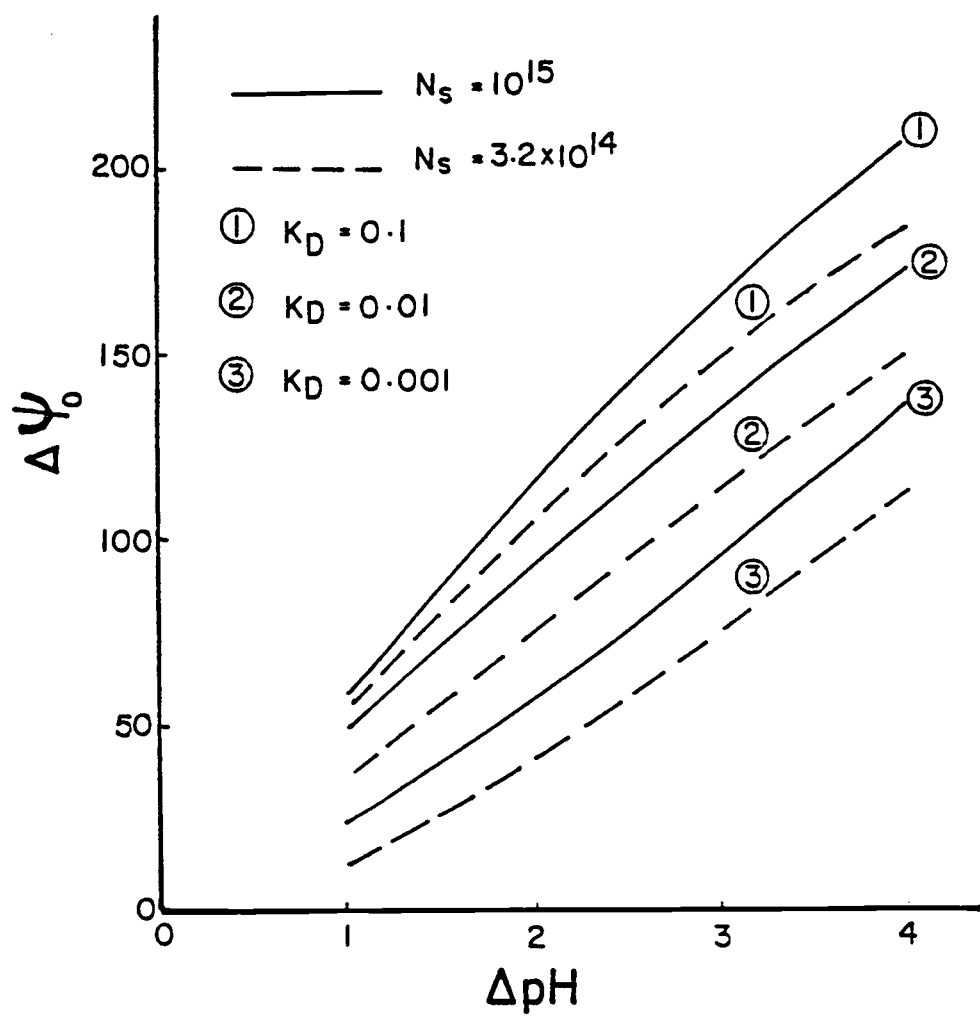


Figure 5.18. Calculated $\Delta\psi_0$ as a function of ΔpH for EOS structures in 0.01 M electrolyte concentration.

In Figure 5.19, the experimental $\Delta\psi_0$ values obtained in 0.01, 0.05, and 0.1 M KNO_3 solutions are plotted against pH along with the calculated values using $K_D = 0.01$ and $N_s = 8 \times 10^{14}$. From this Figure, it can be seen that the experimental data from 0.01 M solution agrees reasonably well with the calculated one. However, for solutions of 0.05 M and 0.1 M, the experimental curves deviate from the calculated ones. The deviation may be explained by considering the following.

(1) For experimental results, ΔpH was obtained by assuming pH_{zc} of SiO_2 to be at pH 3. The reported pH_{zc} values for SiO_2 vary in the range of pH 2 to 3. The actual pH_{zc} of SiO_2 used in this experiment may not be 3.

(2) In the development of the theory of operation of the EOS structure, we have assumed the diffuse layer model for the electrical double layer. The diffuse layer model describes the double layer reasonably well in dilute solutions (≤ 0.01 M) and at low potentials. Away from the pH_{zc} , the potentials are large and the diffuse layer model becomes less useful in describing the double layer. For solutions of intermediate concentrations (0.01 - 1 M), and for the experimental conditions away from the pH_{zc} , the model proposed by Stern (57) is more appropriate.

(3) Electrolyte ions can be adsorbed on the surface of the SiO_2 at pH values away from the pH_{zc} . In the theoretical development, electrolyte ion adsorption has been ignored to simplify the calculations.

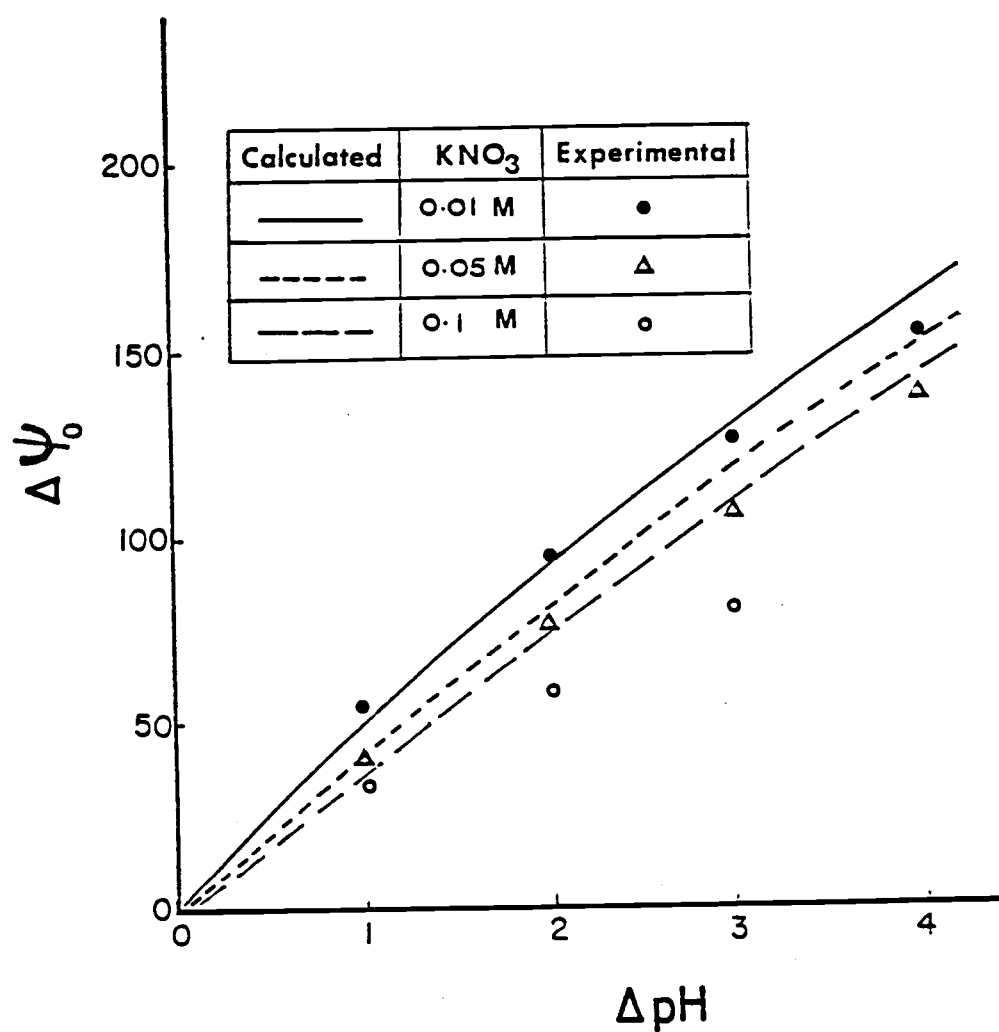


Figure 5.19. Calculated $\Delta\psi_0$ ($K_D=0.01$, $N_s=8 \times 10^{14}$) and experimental $\Delta\psi_0$ as functions of ΔpH .

(All calculated curves are shown by a solid or broken line and the experimental results by a symbol.)

It appears that the results from the C-V measurements cannot be interpreted entirely unless the calculation are made with more complete models.

Effect of electrolyte solution on C_{\min}/C_{ox} ratio

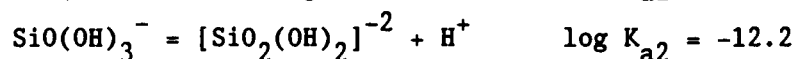
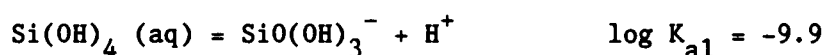
De Rooij and Bergveld (77) had observed a decrease in the value of C_{\min} when the pH was decreased. Siu and Cobbold (48) had observed the opposite effect. Experimental C-V curves obtained in this work did not show a noticeable change in the value of C_{\min} along the capacitance axis with changes in pH of the solution. All C-V curves shown thus far have higher (C_{\min}/C_{ox}) ratios than those expected from theory (cf. Figure 3.19. The reason for these shallow experimental curves was explained earlier by considering surface states at Si/SiO₂ interface.

Bergveld and de Rooij (77,85) proposed that the diffusion of ions through the oxide can cause a change in the surface state density at the Si/SiO₂ interface, thereby changing the (C_{\min}/C_{ox}) ratio. The rate of diffusion of species through the oxide depend on the nature of the oxide and the diffusing species itself. Therefore, the difference in behavior of (C_{\min}/C_{ox}) ratio observed in different laboratories may be explained by comparing experimental conditions of each study. Such a comparison is shown in Table 5.3.

Table 5.3. Comparison of experimental conditions
in C-V study in different laboratories

	de Rooij & Bergveld	Siu & Cobbold	This study
SEMICONDUCTOR			
type	P	P	P
orientation	111	100	100
resistivity (Ωcm)	10	4-10	4-7
OXIDE			
thickness (\AA)	500	800	550
growth temperature	1200	1100	1200
growth procedure	dry O_2	dry O_2	dry O_2
EXPERIMENTAL			
electrolyte	--	buffers	KNO_3
pH range	1-13	1-10	3-7
temperature	--	room temp	25 C

One important difference in experimental conditions used in this work and the others is the pH range in which the experiments have been carried out. Above pH 8 SiO_2 dissolves and forms silicates as shown by the following equilibria of SiO_2 in solutions.



Polymerized forms of silicates are also possible depending on the pH (89). In the experiments reported here, the pH did not exceed 7, to prevent such dissolution from taking place. In the experiment reported by the other workers, the SiO_2 layer might have been dissolved to an extent where diffusion of ions through the oxide occurred during the time frame of the experiment.

Summary

The C-V curves obtained for the EOS structures studied in this experiment showed shifts of 38.5, 34.5, and 26.7 mV/pH in KNO_3 solutions of 0.01, 0.05, and 0.1 M respectively. These results agree with the trends reported values in the literature and those predicted by theory. The experimental $\frac{\Delta\psi_o}{\Delta\text{pH}}$ values can be described theoretically using $N_s = 8 \times 10^{14}$ and $K_D = 0.01$ for the oxide. However, the results in 0.1 M solutions and those obtained farther away from the pH_{zc} do not appear to obey the theory. An accurate estimate of pH_{zc} and more complete models including electrolyte ion adsorption may be necessary to explain the data in the entire range of pH and ionic strength.

6. RESULTS AND DISCUSSION: STUDIES WITH COLLOIDAL SUSPENSIONS

Interfacial chemistry can be characterized in terms of potential and surface excess concentrations. It has been shown that the EOS structures can be used to detect changes in the surface potential of oxides with changes in solution composition. Surface excess concentration at oxide surfaces in equilibrium with solutions can be found from the difference between the total analytical concentration and the measured solution concentration of ions. This difference can be measured if a significant fraction of the ions are adsorbed on the surface of the oxide. Therefore, oxides with a high area-to-volume ratio are suitable for these measurements.

Owing to the low area-to-volume ratio in the EOS structures, they are not used in surface excess measurements. Suspensions of oxides have a high area-to-volume ratio and can be used in these studies. Surface excess concentrations of H^+ or OH^- can be measured in electrolyte solutions in a wide concentration range. However, surface excess of electrolyte ions can be measured only in the solutions of low ionic strength.

In the experiments described here, surface excess concentration of H^+ was measured as a function of pH in 10^{-1} , 10^{-2} , 10^{-3} , and 5×10^{-4} M KNO_3 solutions. Surface excess concentrations of K^+ were measured only in 10^{-3} M and 5×10^{-4} M solutions. The pH of the oxide suspension was adjusted by addition of HNO_3 or KOH. The concentration of H^+ was monitored by a glass electrode

and K^+ concentration by a K^+ ISE. Titanium dioxide was chosen in the initial study of surface excess concentrations for the following reasons.

(1) TiO_2 is insoluble over a wide range of solution pH, which simplifies the interpretation of experimental data.

(2) TiO_2 has been studied extensively in the colloid chemistry literature.

(3) The physical properties of TiO_2 make it suitable gate material for ISFETs.

Potentiometry in colloidal suspensions requires close attention to experimental procedure. A systematic investigation of procedures is presented in this chapter. The discussion is divided into three parts.

(1) Determination of surface excess of H^+ by potentiometry with a glass electrode.

(2) Determination of surface excess of K^+ by potentiometry with a K^+ electrode

(3) Potentiometry in solutions of low ionic strength.

6.1 Determination of surface excess of H^+

The operational definition of surface excess is simply the difference between the "added" concentration and "measured" concentration of H^+ ions.

$$(\Gamma_{H^+} - \Gamma_{OH^-}) = (T_A - T_B + [OH^-] - [H^+]) / A \quad 6.1$$

where $[H^+]$ and $[OH^-]$ are concentrations of H^+ and OH^- respectively. A is the surface area of the suspension per unit

volume of solution (m^2/L). T_A and T_B are total (volumetric) concentration of H^+ and OH^- . They can be calculated from the following general expression.

$$T_i = C_i \cdot V_i / V_T \quad 6.2$$

where T_i = total concentration

C_i = concentration of the titrant

V_i = volume of the titrant

V_T = cumulative total volume of the solution

$(\Gamma_{\text{H}^+} - \Gamma_{\text{OH}^-})$ is positive when excess H^+ is on the surface and negative when excess OH^- is on the surface.

In a typical experiment, an oxide suspension is titrated with acid or base. Two approaches can be used for determination of surface excess concentrations over the course of the titration.

(1) From the response of a glass electrode the concentrations of H^+ and OH^- in solution can be determined and the surface excess is obtained from Equations 6.1 and 6.2. This method is referred to here as the analytical approach.

(2) Titrations can be carried out once for a blank and once for the oxide suspension. For any pH value, the surface excess concentration can be obtained by subtracting the amount of acid or base added to the blank from the amount added to the oxide suspension, when both solutions are at the same pH value. The surface excess concentration for any pH is expressed

$$(\Gamma_{\text{H}^+} - \Gamma_{\text{OH}^-}) = (T_A^{\text{susp}} - T_B^{\text{susp}})_{\text{pH}} - (T_A^{\text{blank}} - T_B^{\text{blank}})_{\text{pH}} \quad 6.3$$

Subscripts "susp" and "blank" are self-explanatory. This method of surface excess determination will be referred to here as the empirical approach.

Both methods were examined for possible use in this experiment.

Analytical approach

The response of an electrochemical cell consisting of a glass electrode and reference electrode can be described by the following equation.

$$E_H = b_H + s_H \log a_{H^+} \quad 6.4$$

where E_H = response of the glass electrode vs. reference electrode

b_H = constant specific to the cell

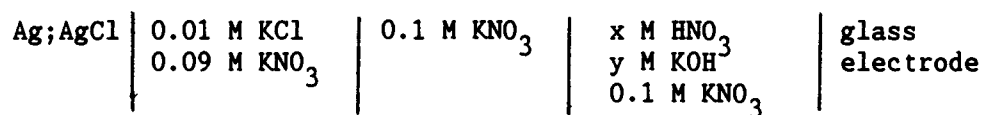
s_H = electrode response slope, approximately equal to

$$2.303 RT/F$$

The calibration procedure discussed here is appropriate for studies in 0.1 M KNO_3 electrolyte solutions. For the studies in other electrolyte solutions, it will be shown that appropriate changes of solutions in the reference electrode and the salt bridge must be made.

Calibration of the cell response

The electrochemical cell represented by



was calibrated by adding HNO_3 or KOH to 0.1 M KNO_3 solutions. This type of experiment will be referred to as a titration, although literally nothing is titrated. The concentration of electrolyte was chosen such that the complications due to liquid junction potentials are minimal. The subject of junction potentials will be discussed in detail in section 6.3.

The activity coefficient for H^+ ions at each titration point was calculated from the Debye-Huckel relationship given in Equation 6.5.

$$\text{Log } \gamma_i = \frac{-A' z_i \mu^{1/2}}{1 + B' a \mu^{1/2}} \quad 6.5$$

where γ_i = activity coefficient of the ion i

$A' = 0.5111$ at 25 C

$B' = 0.3291$ at 25 C

Z_i = ionic charge

μ = ionic strength of the solution

a = size factor

In the acid branch (when adding acid), the H^+ concentration was calculated directly from Equation 6.2. In the base branch, the concentration of H^+ was calculated from Equations 6.3 and 6.6.

$$K_w = \gamma_{\text{H}^+} [\text{H}^+] \gamma_{\text{OH}^-} [\text{OH}^-] \quad 6.6$$

where K_w is the ionic product of water.

The concentration of H^+ was converted to its activity by multiplying it by the activity coefficient. The cell response was plotted against $\log a_{\text{H}^+}$. The plots of this type for several titrations with 0.01 M HNO_3 acid are shown in Figure 6.1.

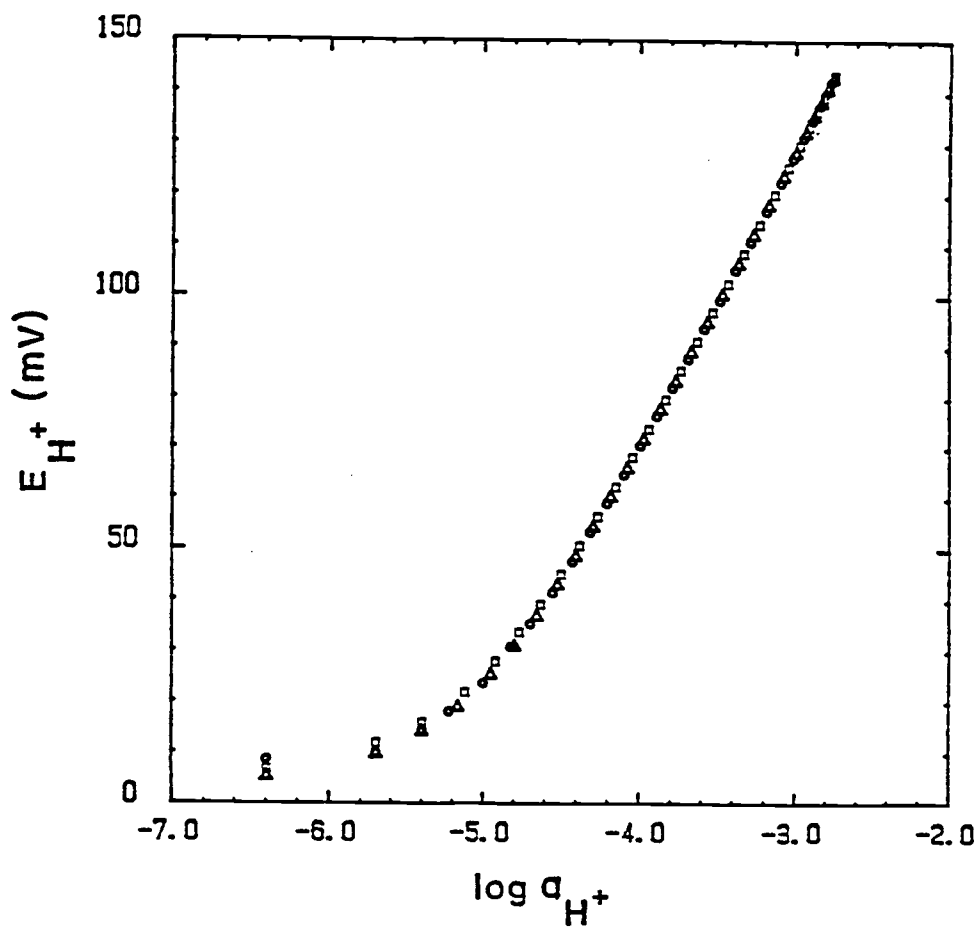


Figure 6.1. Calibration plots : electrode response of the glass electrode vs. $\log (a_{H^+})$ in the acid branch

Excellent linearity was found in the pH region from 2.5 to 4.2.

Table 6.1 summarizes the values obtained for s_H and b_H by a least square fit for the acid branch. These values show excellent reproducibility.

The calibration plots, i.e. cell response vs. $\log a_{H^+}$ plots, obtained for the titrations carried out with 0.01 M NaOH are shown in Figure 6.2. Excellent reproducibility is observed in these titrations as displayed in this figure. However, the values for s_H (67 mV/pH) and b_H (390 mV) calculated from data in the linear part of the curves, in the pH range of 9.5 - 11, differ grossly from those obtained from those obtained from the acid branch; this abnormal slope and intercept still reflect the influence of the curvature below pH 9.5. This disagreement is totally unacceptable and an explanation for the observed fact is necessary before proceeding any further.

The shape of the curves in Figure 6.2 suggests the possibility of a protolytic contaminant in KNO_3 solutions or in the base used in the titration. The possibility of contamination of the base by CO_2 was examined, and found that it was not the cause for the disagreement. KNO_3 was purified by recrystallization, but results from the electrode calibrations with the purified salt were the same.

Corrections for the impurity can be made if the contaminant is identified properly, and its concentration is estimated. Titration curves in the base branch can be calculated assuming the presence of

Table 6.1. Slope (s_H) and intercept (b_H) of the glass electrode response determined in 0.1 M KNO_3 from the acid branch

Date	s_H (mV/pH)	b_H (mV)
11/01	58.24	302.6
	58.32	303.1
	58.22	302.7
11/03	58.08	302.4
11/05	58.81	302.6
	58.52	302.0
11/06	58.40	301.4
	58.64	301.5
11/11	58.31	300.4
11/12	58.48	300.8
11/27	58.67	301.6
	58.26	300.5
	58.51	301.4
Average	58.42	301.8
Standard deviation	0.21	0.9

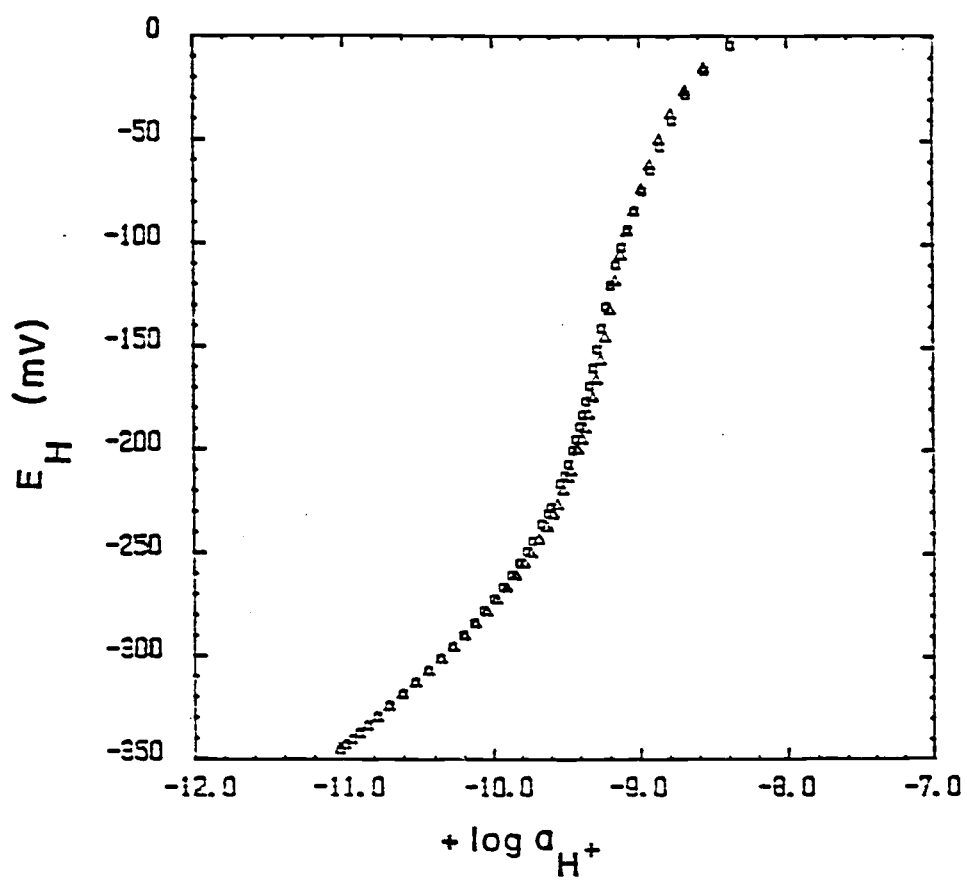


Figure 6.2. Calibration plots obtained in the base branch

a protolytic impurity and can be compared with the experimental ones. This type of comparison can be used to identify the contaminant and estimate its concentration.

Titration curves were calculated in the base branch assuming the protolytic impurity to be a

(1) Strong acid of concentration C_0

(2) Monoprotic weak acid with dissociation constant

K_1 and concentration C_0

(3) Diprotic weak acid with dissociation constants

K_1 and K_2 and concentration C_0 .

The calculation procedure, in brief, can be described as follows. The concentration of H^+ in Cases (1), (2) and (3) were calculated for different volumes of added base. The concentration of H^+ was converted to cell potential through Equation 6.4, with values of s_H and b_H taken from the acid branch, where the cell response is relatively immune to interferences from small amounts of protolytic impurities. Details of the calculations of the titration curves are found in Appendix F.

Figure 6.3 shows the calculated curves for Case (1) along with the experimental data. The experimental data do not exhibit a sharp change in response near the end point, and it can be concluded that the protolytic impurity is not a strong acid.

Figures 6.4 (a) and 6.4 (b) show respectively the effect of dissociation constant and concentration of a monoprotic weak acid on

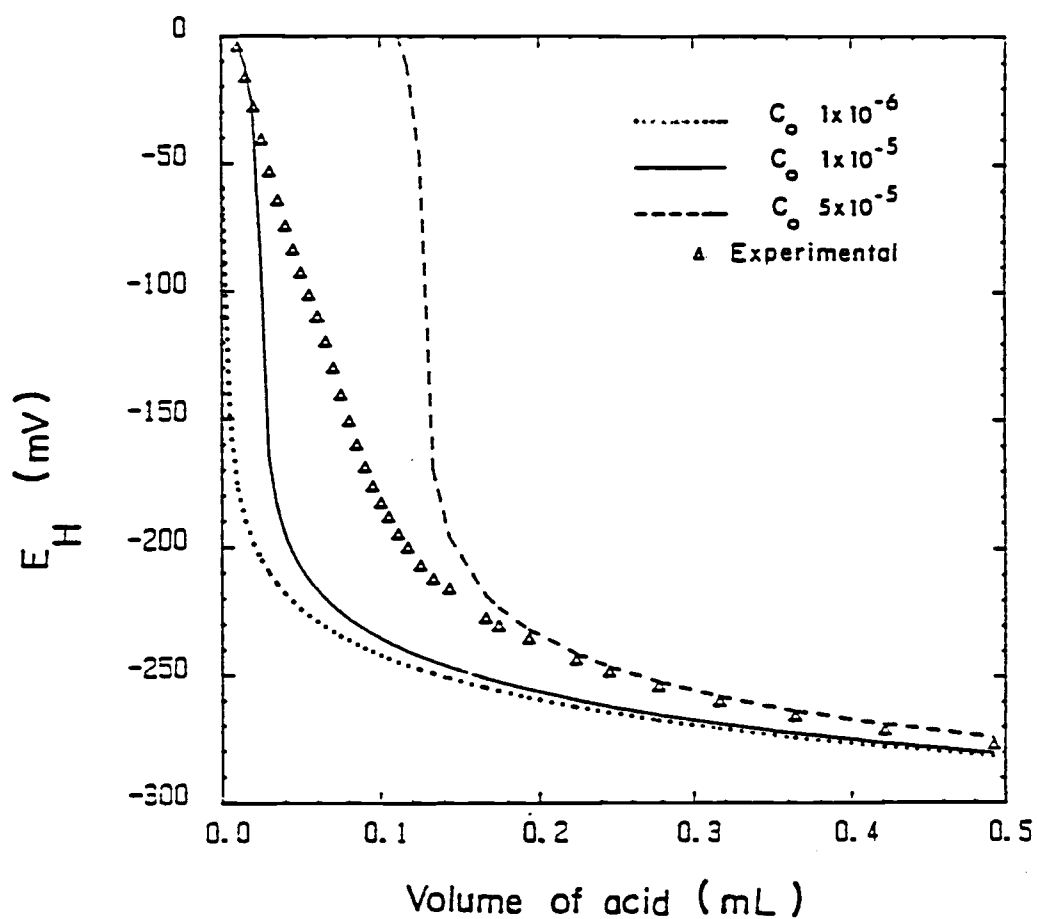


Figure 6.3. Calculated and experimental curves for titrations of KNO_3 solutions contaminated with strong residual acid vs. 0.01 M base. (volume of solution 25.0 mL)

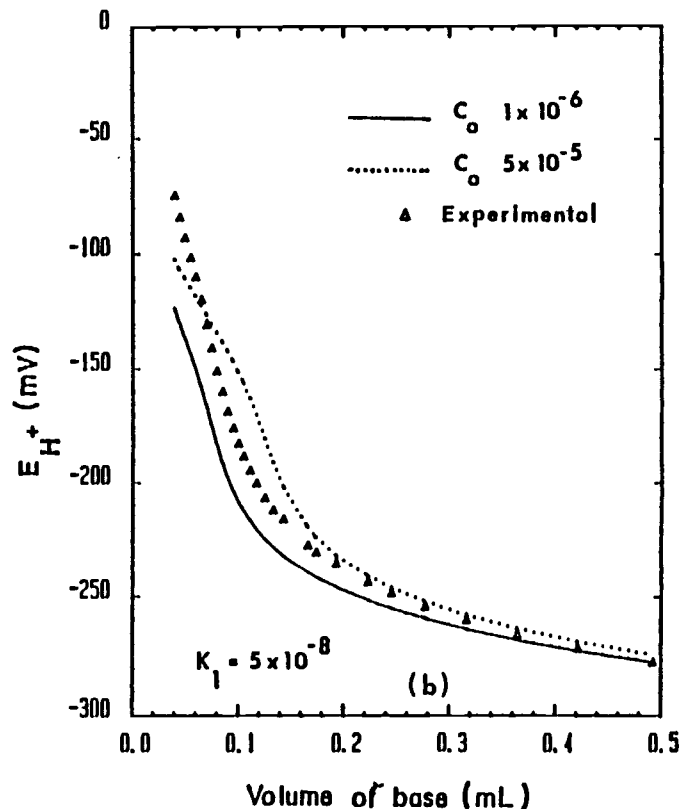
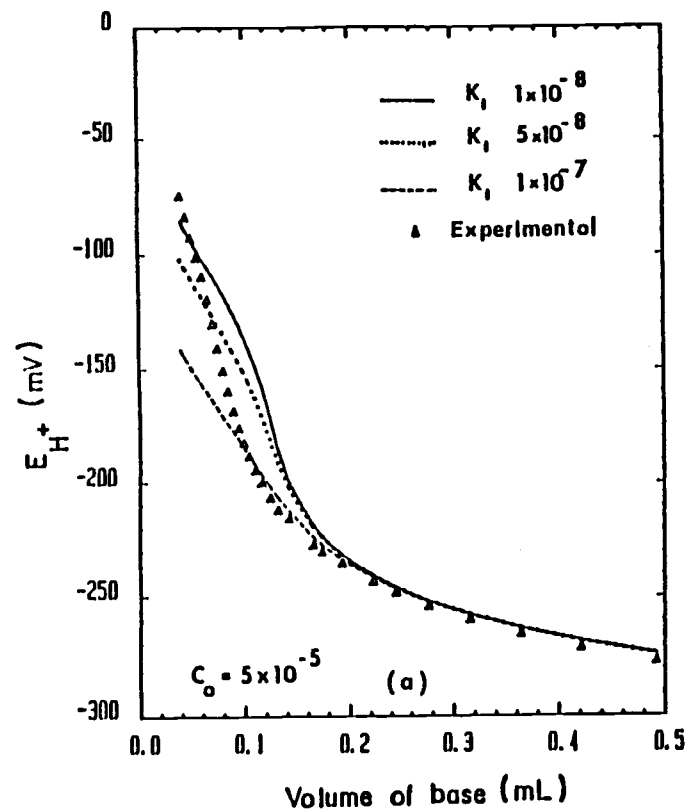


Figure 6.4. (a) Effect of dissociation constant (b) effect of concentration of the residual acid in the simulated for titration curves of KNO_3 solutions contaminated with a mono-protic weak acid vs. 0.01 M base. (volume of solution 25.0 mL)

the shape of the titration curve. The experimental data resemble the calculated response reasonably well for the case in which $C_0 = 5 \times 10^{-5}$ and $K_1 = 5 \times 10^{-8}$.

Similar titration curves were calculated for Case (c). It can be illustrated, from Figure 6.5, that the shape of the experimental titration curve is approximated well by the calculated curve, more closely when the contaminant is assumed to be a diprotic weak acid with $C_0 = 3 \times 10^{-5}$, $K_1 = 6.3 \times 10^{-7}$ and $K_2 = 9.2 \times 10^{-10}$.

From this analysis, one can conclude that there is a small amount of protolytic impurity, which behaves like a diprotic weak acid in KNO_3 solutions. If the analytical approach is to be used in the surface excess determination, this impurity should be identified both qualitatively and quantitatively, and the proper correction should be made. T_A and T_B cannot be calculated simply by Equations 6.2 when such an impurity is present.

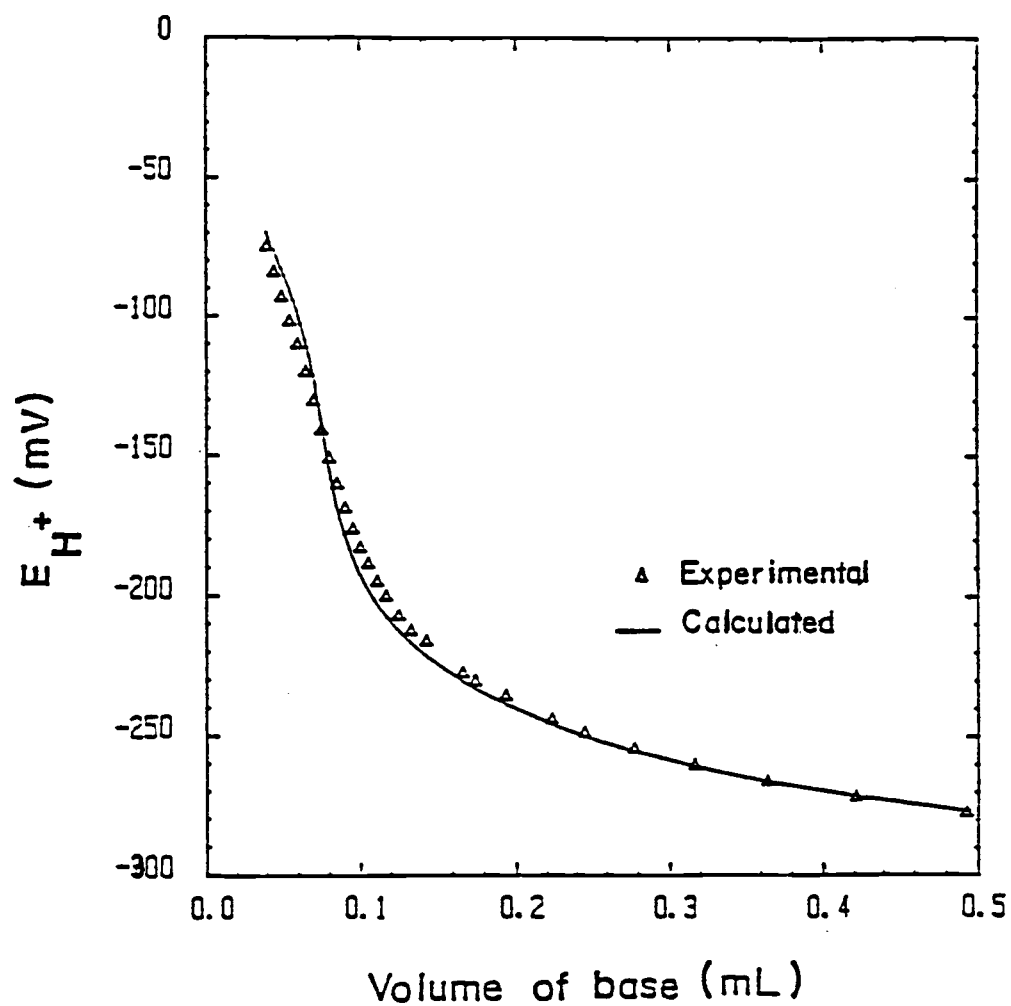


Figure 6.5. Calculated of titration curves when the contaminant is a diprotic weak acid.

Empirical method

The analytical approach of determination of surface excess concentrations of H^+ is complicated by the presence of a protolytic impurity in KNO_3 . Therefore, the possibility of using the empirical approach was examined.

In this method, the titration curves obtained for a blank is subtracted from that obtained for the oxide suspension to yield the surface excess. Figure 6.6 illustrates this method.

Typical titration curves obtained in the acid region for a blank solution and an oxide suspension are shown in Figure 6.6. Because of the adsorption of H^+ ions by the oxide, the volume of acid that must be added to bring the solution to a certain pH value is more for the suspension than for the blank. The difference between the volumes is given by ΔV_i in the figure. For a given electrode potential E' , the corresponding ΔV_i can be found by subtracting the two curves at E' . The surface excess concentration ($\Gamma_{H^+} - \Gamma_{OH^-}$) can be computed from V_i .

$$(\Gamma_{H^+} - \Gamma_{OH^-}) = \frac{C_i \Delta V_i}{V_T} \frac{1}{A} \quad 6.7$$

where C_i is the concentration of the titrant, V_T is the cumulative total volume of the solution.

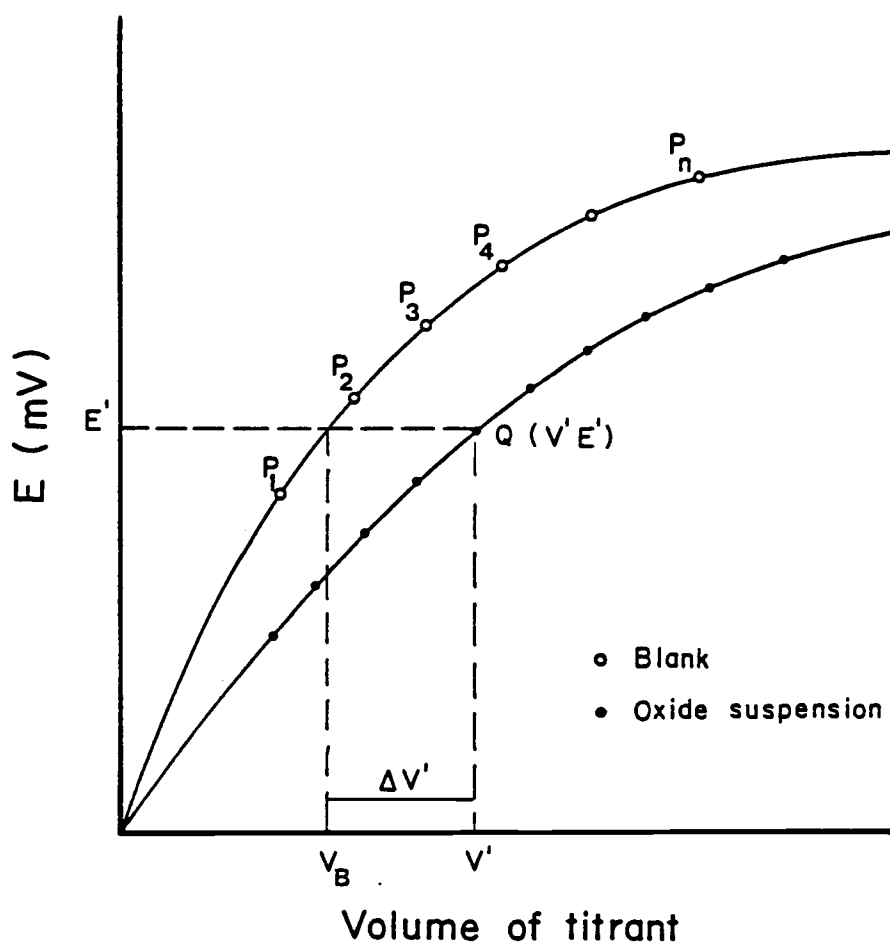


Figure 6.6. Typical titration curves obtained in the acid region for blank solution and oxide suspension

The degree and the type of contamination in the KNO_3 solutions or titrants can be assumed to be the same in both titrations. Therefore, the conversion of ΔV into surface excess concentrations without correcting for blank contamination is acceptable; the only uncertainty is the possible adsorption of the impurity which would alter the acidity of the impurity or the oxide surface or both. But concentration of this impurity is small enough that such an effect can be ignored.

The curve subtraction can be done in two ways. The most obvious is the tedious graphical measurement method. Mathematical subtraction of these curves can be accomplished as follows.

The electrode response vs volume data for both curves can be fitted to a suitable mathematical function. There are several ways in which the data can be fitted. The following methods were tried in fitting the data

(1) Least squares fit to a polynomial.

(2) Cubic interpolating splines.

Method of least squares

A computer program adapted from reference (116) was used to fit a polynomial of the form

$$E = a_0 + a_1V + a_2V^2 + \dots a_nV^n \quad 6.8$$

to the experimental data obtained for addition of 0.01 M HNO_3 to 0.1 M KNO_3 solution.

Polynomials of orders 3, 4 and 6 were fit to the data and plotted in Figure 6.7. This figure shows that none of the fitted curves truly describe the trend of the experimental data. Therefore, this method was not used.

Cubic interpolating spline

If a french curve or a draftsmen's spline is used in drawing a curve through the experimental data points, the curve is generally a smooth one. This curve approximates the behavior of the data points within the range of the data points included in the curve.

Mathematically, a smooth curve can be fitted through the data points by fitting a set of cubics through the points, using a new cubic in each data interval. Each of these cubics are subjected to the following conditions.

(1) A cubic in a given interval should pass through the two data points defining the interval.

(2) The slope and the curvature (1^{st} and 2^{nd} derivatives) of two connecting cubics should be the same at the data point of connection.

The two cubics for the first and the last intervals can not satisfy the second condition at the first and the last data points because there are no two connecting cubics at either end.

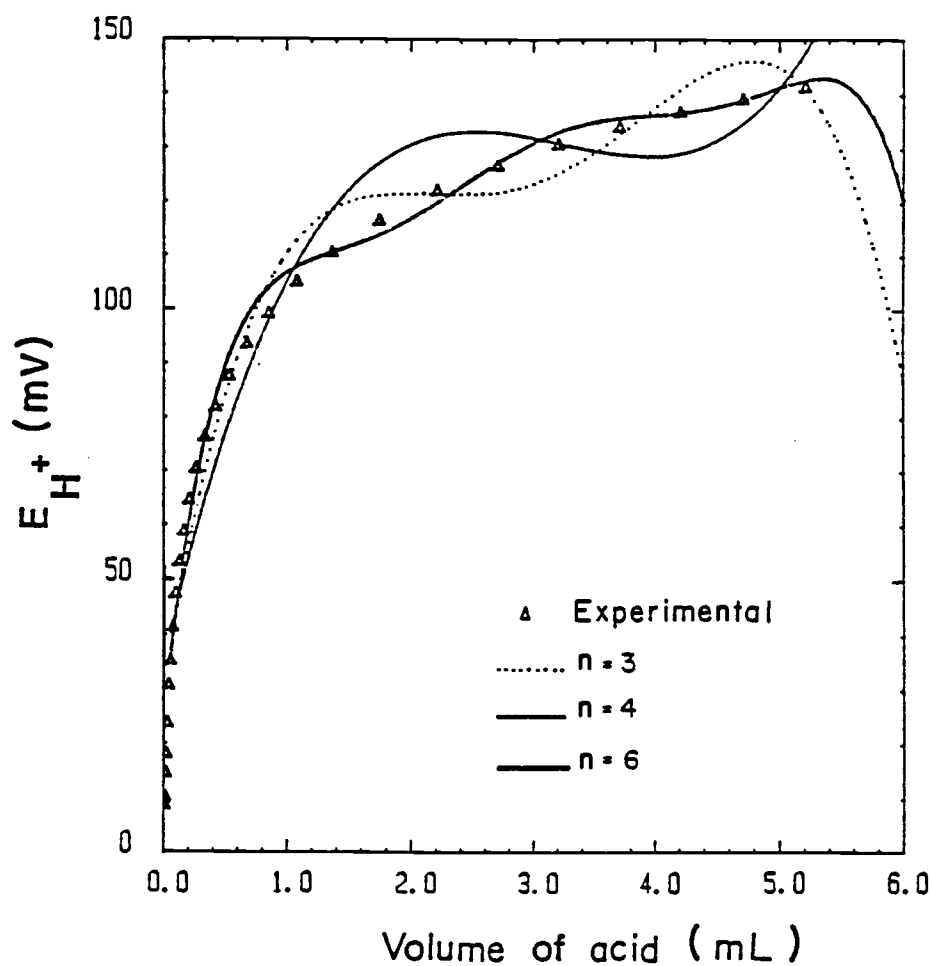


Figure 6.7. Polynomial functions of the form

$$E = a_0 + a_1V + a_2V^2 + \dots + a_nV^n$$

fitted to experimental data by least squares method.

Therefore, the shape of the two ends has to be defined by examining the trends of the data. The trend of the titration data is such that the ends are linear. A more complete description of the cubic splines, including mathematical procedures involved in calculating these cubics can be found in many books (90).

The cubics chosen in the analysis described in here have the form

$$E = aV^3 + bV^2 + cV + d \quad 6.9$$

The behavior of the function in an interval is evaluated using the coefficients a, b, c , and d . Two typical experimental data sets obtained from titration in the acid branch and base branch were used to examine the ability of splines to represent the data.

Experimental data and evaluated cubic splines are displayed in Figure 6.8(a) and 6.8(b) for both acid branch and base branch. These figures show that each of the cubics follow the trend of the data very smoothly. The requirement for such a smooth fit that the data points are close enough together is met in this experiment.

The computer program used to calculate V by this method is given in Appendix G.

Figure 6.6 illustrates the use of cubic splines in the surface excess determination. $P_1, P_2, P_3, \dots, P_n$ represent data points obtained for the blank. Cubic splines can be computed for each data interval $(P_1, P_2), (P_2, P_3), \dots, (P_{n-1}, P_n)$. Consider the data point $Q(V', E')$ obtained for the

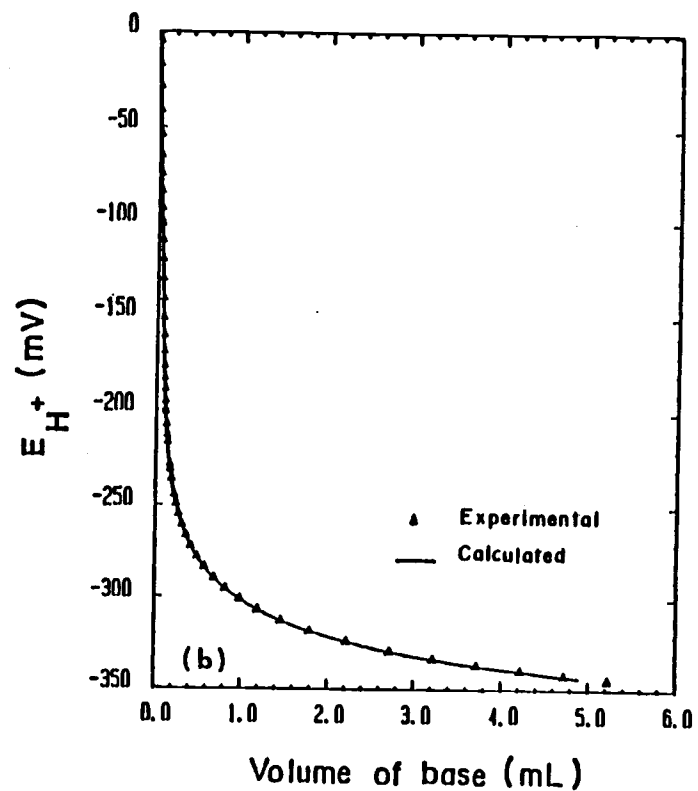
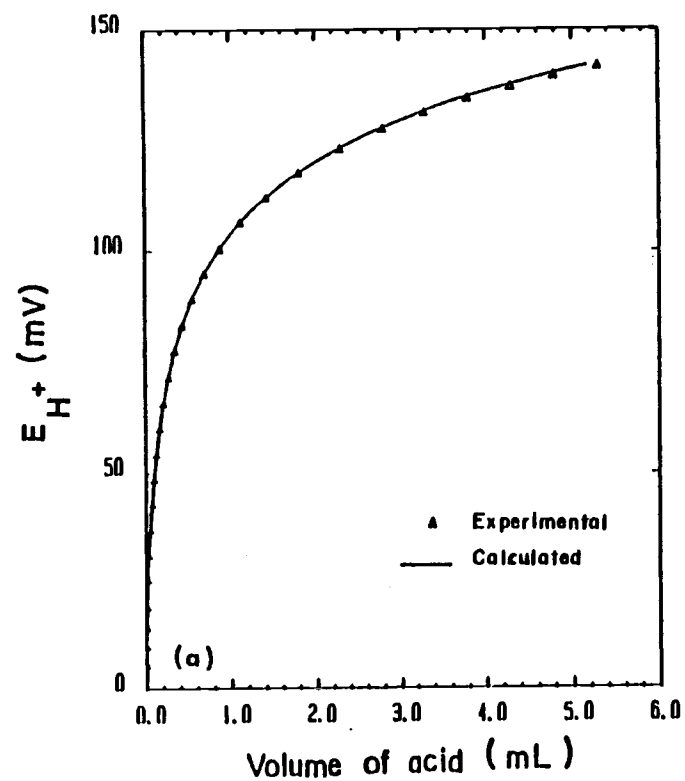


Figure 6.8. Cubic spline fit for experimental data
from the (a) acid branch (b) base branch.

case of oxide suspension. The volume of the titrant necessary in the blank to give the same electrode response E' is shown as V_B . Since the point (V_B, E') lies in the data interval (P_1, P_2) , V_B can be found by solving the cubic spline Equation for data interval (P_1, P_2) . Thus ΔV_i can be found

$$\Delta V_i = V' - V_B \quad 6.10$$

and surface excess concentration can be obtained from Equation 6.7

Summary

Calibration of the glass electrode in KNO_3 solutions gave excellent, reproducible results in the acid branch. However, similar calibrations in the base branch showed large disagreement with the values obtained from the acid branch. The possibility of contamination of the base by CO_2 was examined, and found that it was not the cause for the disagreement. Analysis of the titration curves showed the presence of a protolytic impurity resembling a dibasic weak acid. Recrystallization was the only purification method tried to remove the impurity, but it failed. Although, in principle, the salt could be purified, an empirical approach to obtain the surface excess from titration curves was developed. In this approach, the titration curve for the blank is mathematically subtracted from that for the oxide suspension using an adapted cubic spline fitting method.

6.2. Determination of surface excess of K^+

The surface excess of K^+ , Γ_{K^+} is given by the following equation.

$$\Gamma_{K^+} = T_{K^+} - [K^+] \quad 6.11$$

where T_{K^+} and $[K^+]$ are the total and measured concentrations of K^+ . T_{K^+} is calculated from volumetric information as follows.

$$T_{K^+} = \frac{C_K^O V_O + C_i^K V_i}{V_O + V_i} \quad 6.12$$

C_K^O = Concentration of K^+ in the electrolyte solution

V_O = Volume of the electrolyte solution

C_i^K = Concentration of K^+ in the added titrant

V_i = volume of the titrant

$[K^+]$ was measured from the response of a cell consisting of a liquid membrane type K^+ ion-sensitive electrode (Orion model 93-19) and a reference electrode. The cell response E_{K^+} is given by

$$E_K = b_K + s_K \log a_{K^+} \quad 6.13$$

where b_K is a thermodynamic constant specific to the cell and s_K is the slope of the electrode.

This electrode was tested thoroughly before application. The following characteristics of the electrode were investigated.

(1) Variation of electrode calibration parameters

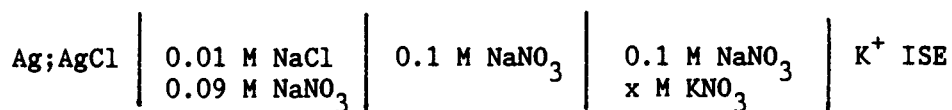
slope (s_K) and b_K with time

(2) Effect of pH on the electrode response

(3) Effect of coating of colloidal oxide films on the membrane

Variation of s_K and b_K with time

The following cell was used in the calibration experiment.



Aliquots of 0.1 M and 1 M KNO_3 solutions were spiked into 0.1 M NaNO_3 solution, and the electrochemical cell response was measured.

Figure 6.9 shows a calibration plot (electrode response E_K vs. $\log a_{K^+}$) for the cell. The response is linear in the concentration range from 1×10^{-4} to 2×10^{-2} M K^+ . The slope s_K and the intercept b_K were obtained by a linear least squares fit, and the results from a number of calibrations are presented in Table 6.2. Comparison of the average values of slope and intercept in Table 6.2 with those in Table 6.1 shows that the standard deviation of intercept term for the K^+ ISE is much larger than that for the glass electrode.

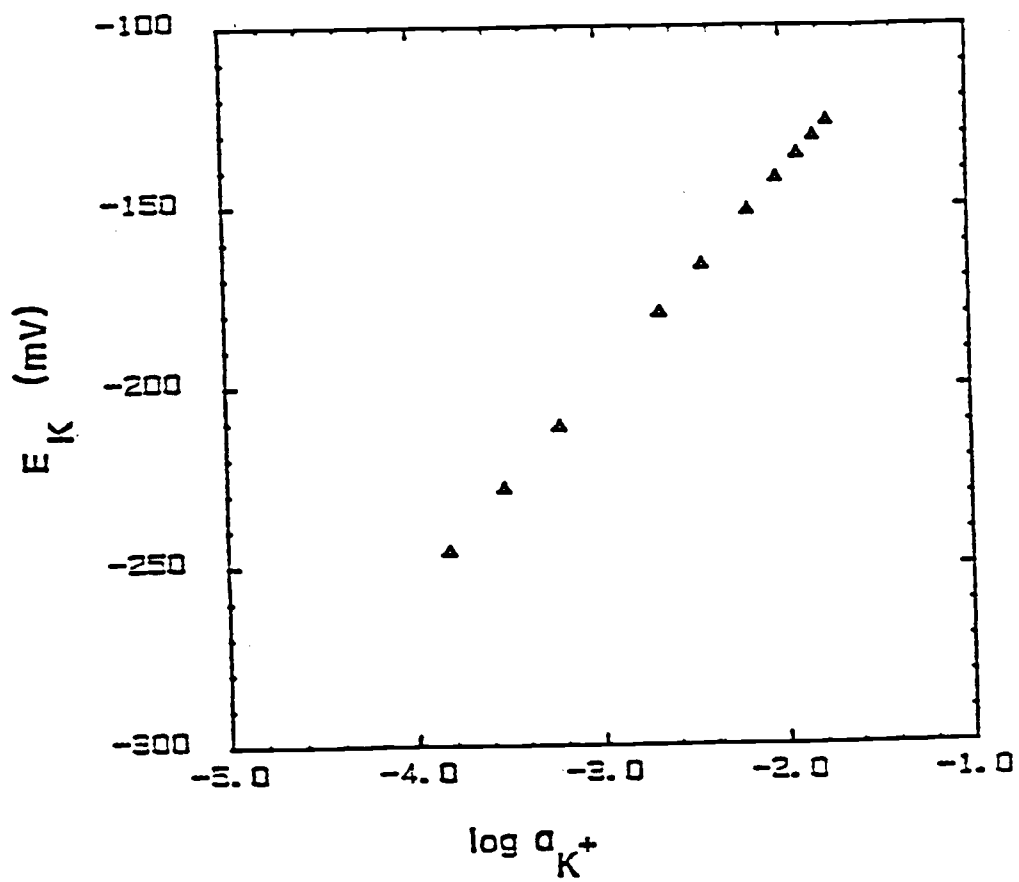


Figure 6.9. Typical electrode calibration curves
for K^+ ISE

Table 6.2. Slope (s_K) and intercept (b_K) of K^+ electrode response with cell II.

Date	s_K	b_K
01/02	57.3	-35.3
	57.6	-34.8
01/03	57.8	-32.8
01/04	57.6	-33.4
01/15	57.4	-70.8
01/21	58.4	-82.7
	58.5	-82.7
01/22	58.5	-85.6
	58.1	-90.4
05/12	57.5	-34.6
05/13	57.4	-30.4
	57.6	-28.7
	57.6	-26.8
05/15	57.7	-25.1
	57.6	-24.9
05/16	57.7	-23.1
average	57.8	-46.4
standard deviation	0.4	25.6

The slope of the electrode remains statistically the same, but the b_K value drifts slowly. Therefore it is necessary to calibrate the K^+ electrode frequently.

Occasionally, the electrode response changed abruptly. This is evident from the sudden changes in b_K , as shown in Table 6.2. The exact reason for this behavior is not known. The possibility of solution leakage through the seal between the sensor module and the electrode was suspected. Teflon tape was wrapped around the seal to minimize solution leakage, but it did not solve the problem completely. The abrupt changes in electrode response were very noticeable. When such a problem was recognized, the electrode was dismantled and reassembled after the electrical contacts had been cleaned. Before it was used again, the electrode was stored in deionized water for three hours, and then in 0.01 M KNO_3 for more than 12 hours. After this "conditioning", the slopes found from electrode calibrations remained somewhat the same, but b_K values were not.

The gradual change in b_K may be characteristic of the long term drift generally observed for membrane electrodes. The drift of the electrode was estimated to be 0.5-1.0 mV/hr over a period of 6 hours.

Effect of pH on the electrode response

The K^+ ISE was intended for use over a wide range of solution pH. Therefore, the effect of pH on the electrode response was examined. Electrode calibration, as described previously, was carried out in 0.1M $NaNO_3$ solutions of different pH. The pH was changed by adding NaOH or HNO_3 .

Calibration plots obtained at different pH values are shown in Figure 6.10. Table 6.3 summarizes the slopes and E^0 values obtained from the same data. The electrode slope or E^0 did not change significantly when the pH of the solution was changed. Therefore, it can be concluded that the effect of pH is negligible in the pH range 3-11.

Effect of coating of oxide film on the electrode membrane

The K^+ electrode was calibrated before and after immersing it in an oxide suspension. A film of colloidal oxide was clearly visible on the electrode, but there was no detectable difference between the calibration parameters of the electrode.

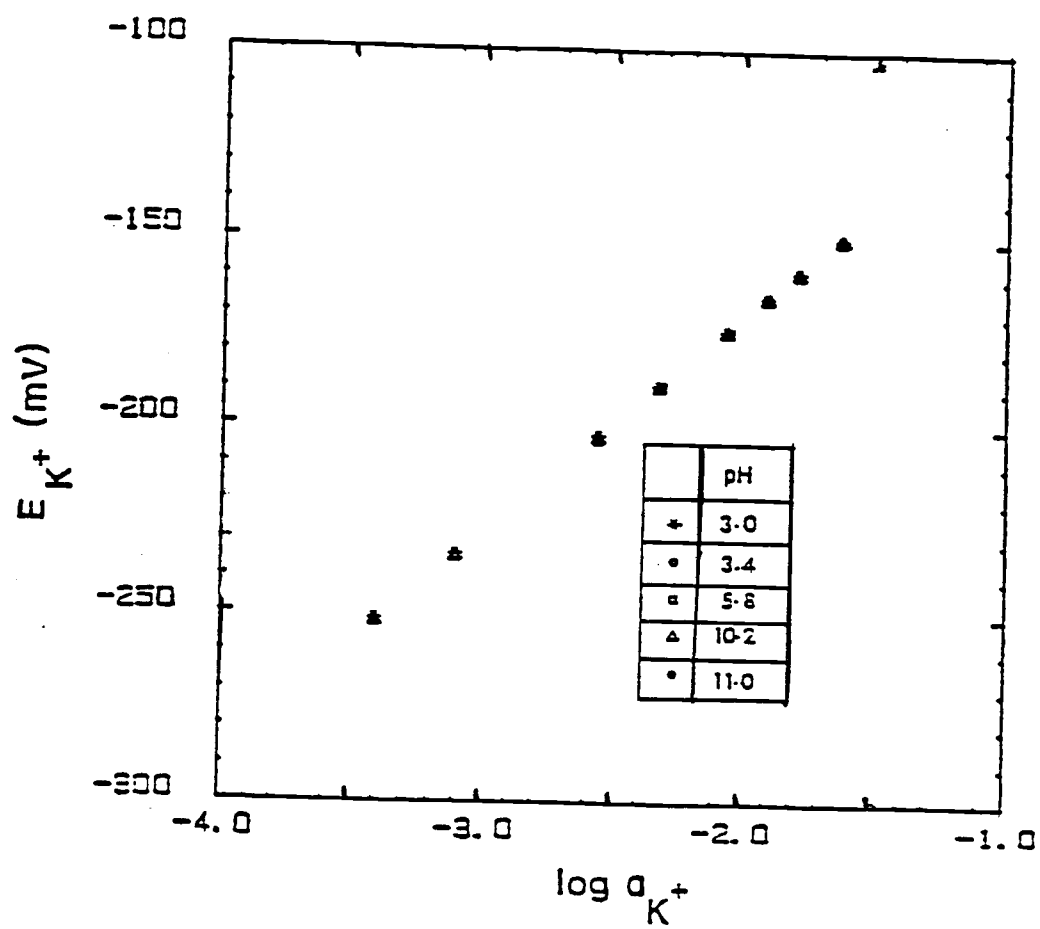


Figure 6.10. Effect of pH on the response of K^+ ISE

Table 6.3. Effect of pH on the calibration parameters of the K^+ electrode

pH	s_K mV/log $[K^+]$	b_K (mV)
3.0	57.5	-55.0
3.4	57.5	-54.8
5.8	57.6	-55.0
10.2	57.3	-54.8
11.0	57.4	-56.0
Average	57.5	-55.1
Standard deviation	0.1	0.5

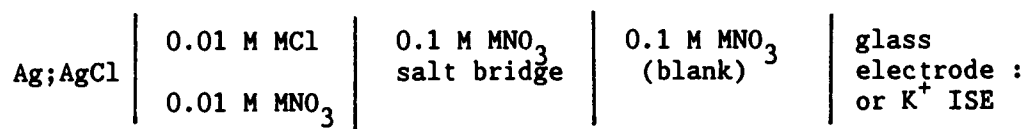
Summary

The K^+ electrode response is linear from 1×10^{-4} M K^+ to 0.02 M K^+ range. The response is not affected by pH in the pH range 3-11. Long term drift of the electrode is approximately 0.5-1.0 mV/hr over a period of 6 hrs. The response of the electrode is not significantly affected by the formation of a colloidal oxide film on the membrane. Thus, it can be concluded that the K^+ ISE is suitable for determination of surface excess of K^+ . It is also recommended that the electrodes be calibrated before and after each titration.

6.3. Electrode measurements in low ionic strength solutions

In the previous sections, it was shown that the calibrations of the K^+ ISE and the glass electrode gave reproducible results.

These electrode calibrations were performed using cells of the type



$M = K^+$ for glass electrode calibrations

$M = Na^+$ for K^+ ISE calibration

Since the pH and concentration of K^+ ions are to be measured in low ionic strength solutions as well, it is necessary to demonstrate reproducible results from electrode calibrations in these solutions.

The potentiometric cell used in the experiment was selected with the following features in mind.

(1) There should be no leakage of ions from the reference solution into the sample cell. This possibility is eliminated with the use of a salt bridge.

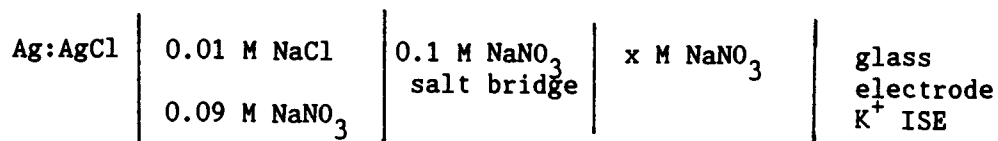
(2) The solution for the salt bridge should satisfy the requirements that the potential between the sample solution and the salt bridge solution is small and remain practically constant during the experiment.

Guggenheim (91,92) showed that this potential can be minimized or kept constant by using a concentrated equitransferent electrolyte such as KCl, KNO_3 or NaNO_3 at the solution junction.

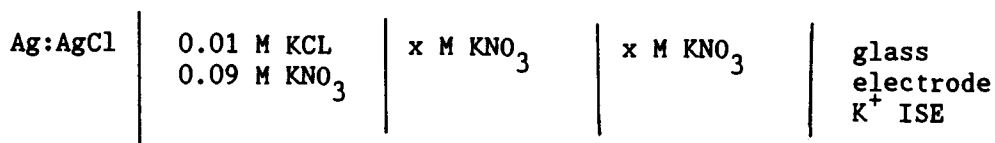
(3) Calibration of the K^+ ISE and the glass electrode should be possible in the same cell. (Frequent electrode calibrations are necessary for reliable measurements. Therefore it becomes very inconvenient if the cell configuration or the solutions in the cell have to be changed very often).

Two types of cells can be used in the determination of surface excess concentrations.

Type I:



Type II:



The cell of Type I appears to be the configuration most appropriate to the conditions mentioned previously. However, the experiments carried out with this type of cell showed severe problems with low ionic strength samples. These experiments, problems, and possible solutions will be discussed in this section.

Cells of Type II satisfies only the condition (1) described previously. One of the disadvantages in these cells is that they are not suitable for the calibration of the K^+ ISE. However, some

of the problems encountered with cell of Type I were not found to be severe in the cells of Type II.

In both types of cells, the liquid junction potential between the salt bridge and the sample solution complicate the interpretation of experimental data. First, we will discuss the liquid junction potential in potentiometric cells in general, and then discuss the experiments with the cells of each type.

Liquid junction potential

Consider the following general representation of a potentiometric cell.

Ag;AgCl	Reference solution	salt bridge solution	sample solution	sensing electrode
1	2	3	4	5

The measured response of the cell E_i is a sum of the potential differences at each interface.

$$E_i = \phi_5 - \phi_1 \quad 6.14$$

$$= (\phi_5 - \phi_4) + (\phi_4 + \phi_3) + (\phi_3 - \phi_2) + (\phi_2 - \phi_1) \quad 6.15$$

where ϕ_r denotes the potential of the phase r . The potential difference across the membrane of the sensor electrode, $(\phi_5 - \phi_4)$, is a function of the analyte ion in the sample, as given by a Nernst-type expression.

$$(\phi_5 - \phi_4) = b' + s_i \log a_i \quad 6.16$$

where s_i is the electrode slope, b' is a constant and a_i is the activity of ion i .

If the other potential differences remain constant during the course of the experiment, then the measured E_i can be expressed as

$$E_i = b_i + s_i \log a_i \quad 6.17$$

which is of the same form as Equations 6.4 and 6.13.

The potential differences $(\phi_3 - \phi_2)$ and $(\phi_2 - \phi_1)$ can be assumed to remain constant during the changes in composition of the sample solution. However, the potential difference across the liquid junction between the sample solution and 0.1 M NaNO_3 , $(\phi_4 - \phi_3)$, is susceptible to changes in the composition of the sample solution. This liquid junction potential is due to unequal mobilities of ions diffusing between the two liquid phases forming the junction.

The equation for response of the potentiometric cell can be rewritten as

$$E_i = b^0 + s_i \log a_i + E_j \quad 6.18$$

where E_j is the liquid junction potential $(\phi_4 - \phi_3)$ and b^0 is an algebraic sum of the constant interfacial potential terms in Equation 6.15 and b' in Equation 6.16.

The magnitude of the liquid junction potential can be estimated from the Henderson equation (62) as shown here.

$$E_j = \frac{\sum z_i / |z_i| u_i [C_i(4) - C_i(3)]}{\sum z_i u_i [C_i(4) - C_i(3)]} \frac{RT}{F} \ln \frac{\sum z_i u_i C_i(3)}{\sum z_i u_i C_i(4)} \quad 6.19$$

where u_i = mobility of ion i

$C_i(3/4)$ = concentration of ion i in phase 4 or 3

z_i = ionic charge

Cells of Type I

Use of the cells of Type I in the measurement of surface excess in low ionic strength solutions is examined in this section.

The initial step is the calibration of the electrodes in low ionic strength solutions. A solution of 0.01 M HNO_3 was added from a burette to three different solutions in the sample cell.

- (1) 1×10^{-3} M KNO_3
- (2) 1×10^{-4} M KNO_3
- (3) 0.1 M NaNO_3

The response of the cell with the glass electrode was monitored after addition of the acid. The solution (3) was used for comparison purposes. These experiments were repeated several times for solution of each ionic strength.

The response of the cell with the glass electrode can be given by Equation 6.18. If E_j is constant, Equation 6.18 can be expressed in the same form as Equation 6.4. Thus plots of E_H vs $\log a_{H^+}$ (calibration plots) for three different solutions should yield three straight lines with the same slope. Figure 6.11 shows E_H vs $\log a_{H^+}$ plots for the three solutions mentioned above. The thickness of the curves indicate variability of response for the solution of the same concentration. From this figure, two observations can be made.

(1) the slope of the calibration plot is much lower than expected for lower ionic strength solutions.

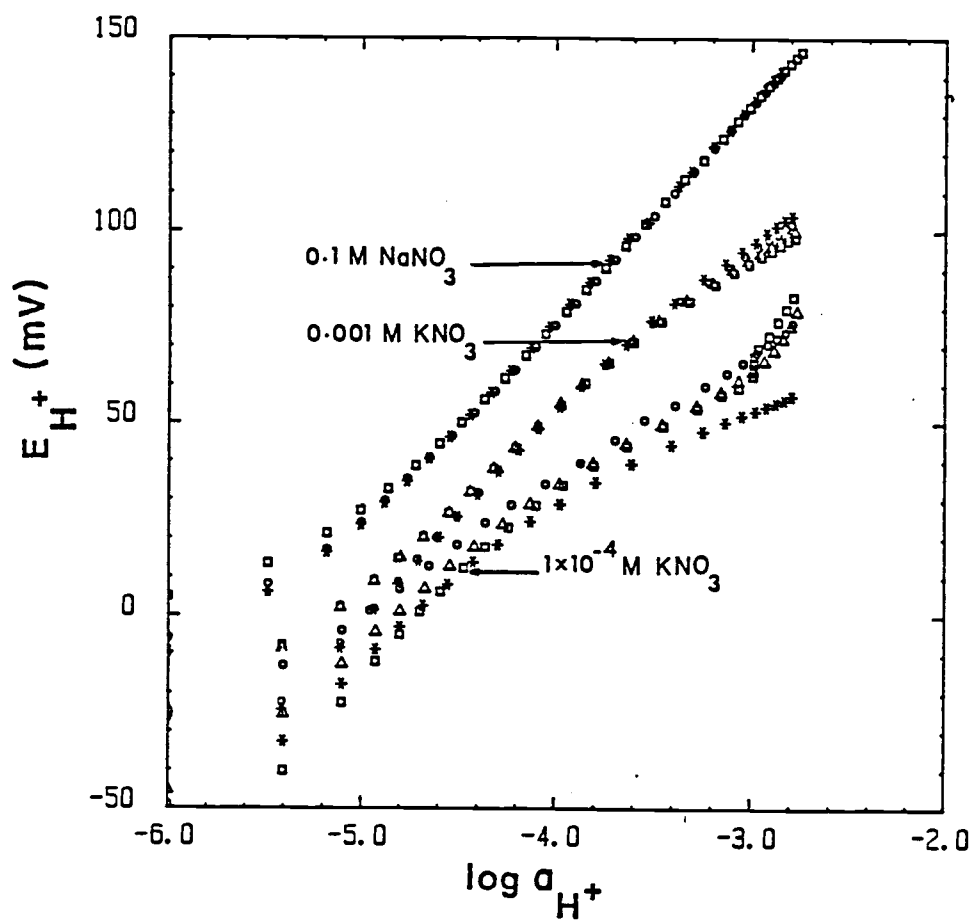


Figure 6.11. E_{H^+} vs. \log (activity of H^+) plots for sample solutions (a) 0.1 M NaNO_3 (b) 0.001 M (c) 0.0001 M KNO_3 in type I cells

(2) The response in dilute solutions is more irreproducible than that in concentrated solutions.

The variation in liquid junction potential between the salt bridge solutions and the sample solutions may be responsible for these observations, and the liquid junction potential in cells of Type I will be examined next.

Liquid junction in Type I cells

To examine whether or not the junction potential is responsible for the large deviations observed for electrode calibration parameters in dilute solutions, the liquid junction potential estimated from the measurement is compared with that calculated from the Henderson Equation. The procedure for comparison is as follows.

(1) Calculate the concentration of all species in solution at each titration point.

(2) Calculate the activity of the H^+ ion at each point from the concentration of H^+ and the Debye-Huckel Equation (Equation 6.5).

(3) Calculate the electrode response from

$$E_H(\text{calc}) = b_H + s_H \log a_{H^+}$$

b_H and s_H are the calibration parameters obtained in 0.1 M $NaNO_3$ solutions where there is only a small junction potential.

(4) Define an experimental junction potential $E_j(\text{exp})$ such that

$$E_j(\text{exp}) = E_H(\text{obs}) - E_H(\text{calc})$$

where $E_H(\text{obs})$ is the observed response of the cell.

(5) Estimate the junction potential $E_j(\text{Henderson})$ at each data point from the Henderson Equation 6.19 using concentration of all species in solution. We denote this junction potential is denoted by $E_j(\text{Henderson})$.

(6) Compare $E_j(\text{Henderson})$ and $E_j(\text{exp})$

If the junction potential is totally responsible for the observed behavior $E_j(\text{Henderson})$ and $E_j(\text{exp})$ should agree closely with each other. Figure 6.12 shows $E_j(\text{Henderson})$ and $E_j(\text{exp})$ as a function of pH, for the experimental data from 1.0×10^{-3} M and 1×10^{-4} M solutions.

In both cases, $E_j(\text{exp}) \gg E_j(\text{Henderson})$. Also, the direction of change of $E_j(\text{Henderson})$ with decreasing pH is opposite from that of $E_j(\text{exp})$.

Brezinski (93) has interpreted the slow drift in potentiometric response and the large errors in potentiometric determinations by considering entrapment of a layer of sample solution between the salt bridge solution and the sample solution. The results from the previous experiment are explained using this concept.

Consider the potentiometric cell used in the calibration of glass electrode in dilute solutions. After the reference electrode and glass electrode couple were placed in the vessel containing the

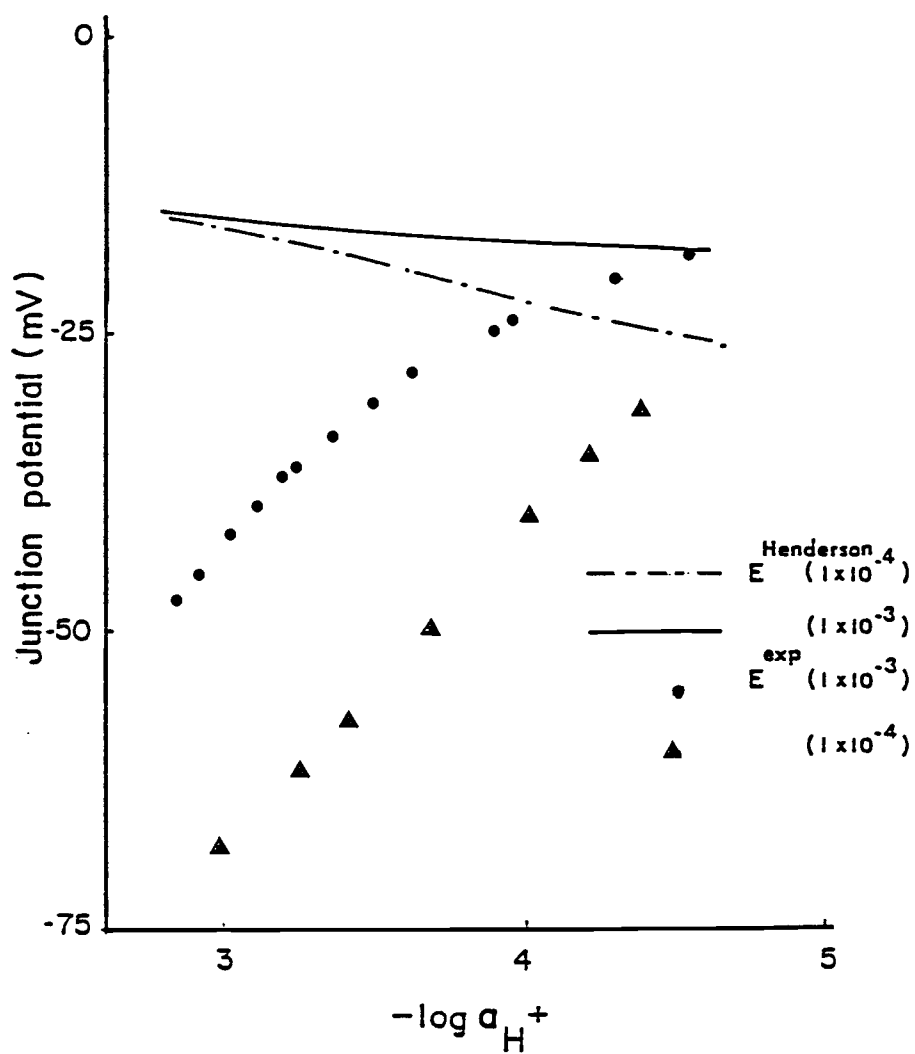
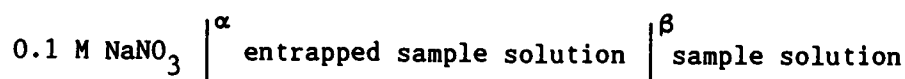


Figure 6.12. Junction potentials estimated from Henderson's Equation ($E_j(\text{Henderson})$) and observed experimentally ($E_j(\text{exp})$) as a function of pH for acid branch titrations in type I cells.

sample, the sample was purged with N_2 to remove CO_2 . During this time, the outer region of the salt bridge solution is diluted by the sample solution.

In effect, now there is a layer of the original sample solution entrapped in the salt bridge. The salt bridge solution-sample solution junction just before the experiment starts can be pictured as follows.



As the titration proceeds, the composition of the sample solution changes. While the junction potential at α in the diagram above remains relatively small and constant, the junction potential at β is subject to large variations, since the junction is between two dilute non-equitransferent solutions. The junction potential at β can be estimated from the Henderson equation, by assuming that the composition of the entrapped layer is the same as that of the original sample solution. We denote this junction potential by E_j (Henderson-entrapped).

Figure 6.13 shows E_j (Henderson-entrapped) and the estimated experimental junction potential $E_j(\text{exp})$ as a function of pH for 1×10^{-3} and 1×10^{-4} M KNO_3 sample solutions.

From this figure it can be seen that the experimental junction potential $E_j(\text{exp})$ agrees more closely with the value estimated for entrapped layer/sample solution junction E_j (Henderson-entrapped).

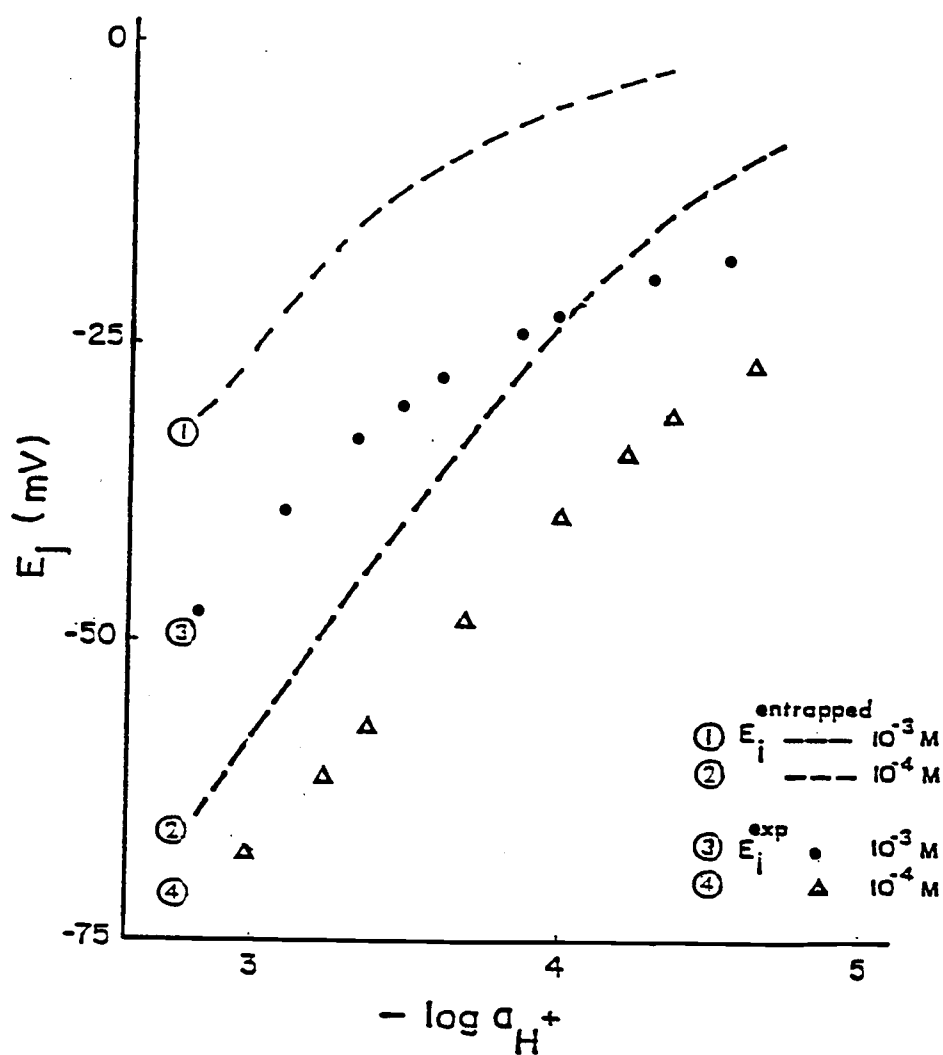
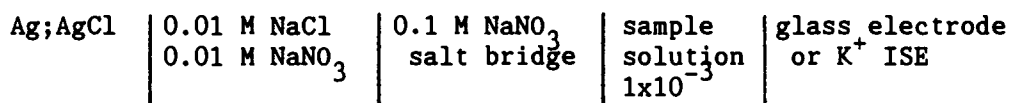


Figure 6.13. E_j estimated from the Henderson equation assuming an entrapped layer (E_j -entrapped) and experimental E_j (E_j^{exp}) as a function of pH.

Confirmation of the presence of an entrapped layer

Two experiments were carried out to confirm the presence of such a "sandwiched" layer of sample solution and to understand the behavior of the junction in dilute solutions.

In these experiments, the reference electrode and sensor electrodes (K^+ ISE and glass electrode) were placed in 25.0 mL of 1×10^{-3} M KNO_3 solution. The potentiometric cell used here was



The sample solution was allowed to reach constant temperature for twenty minutes during which time the solution was purged of CO_2 by bubbling N_2 . As in the previous experiment, aliquots of 0.01 M HNO_3 were added from a burette until the H^+ concentration in the sample solution reached approximately 2×10^{-3} M.

Experiment (1): Immediately following the acid addition, the 0.1 M $NaNO_3$ /sample solution junction was renewed by allowing a very small amount of 0.1 M $NaNO_3$ solution to flow into the sample cell. The response of both sensing electrodes with respect to the same reference electrode were monitored before and after renewing the junction. The results from this experiment are shown in Figure 6.14.

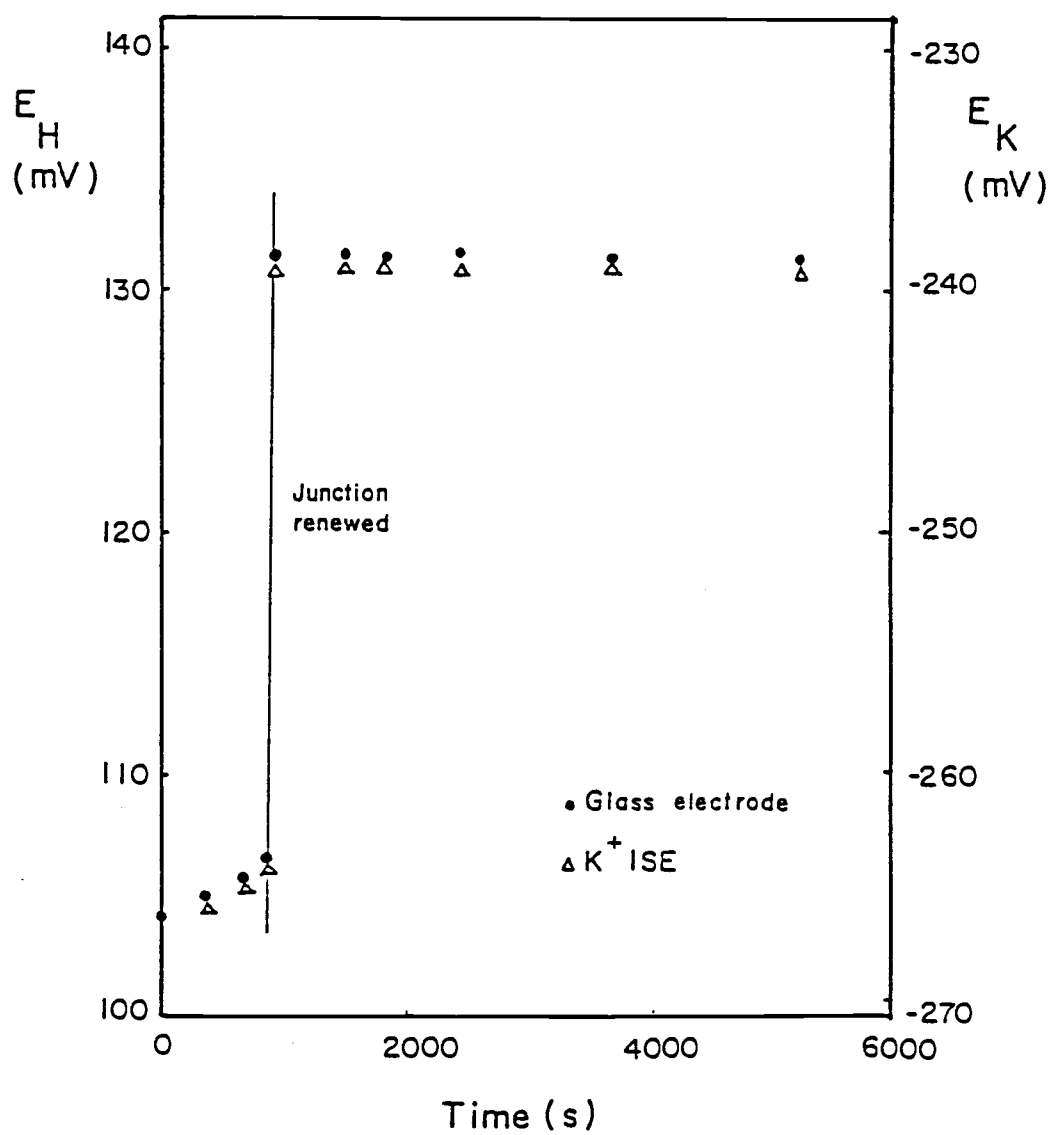


Figure 6.14. The effect of renewal of the liquid junction on the response of the cell

Experiment (2): Following the addition of acid, the drift in response for glass electrode and K^+ ISE was monitored without renewing the junction. Figure 6.15 shows the electrode response of the K^+ ISE and the glass electrode as a function of elapsed time after the addition of acid.

In experiment (1), an abrupt change in electrode response towards a more positive potential was observed immediately after the renewal of the liquid junction (Figure 6.14). This phenomenon can be explained by considering the presence of an entrapped layer of sample solution within the $0.1\text{ M NaNO}_3/\text{sample solution}$ junction. When the junction is renewed this layer of solution is pushed out from the reference junction, creating a fresh $0.1\text{ M NaNO}_3/\text{sample solution}$ junction. In Figures 6.12 and 6.13, it can be seen that the estimated potential at low pH values for the $0.1\text{ M NaNO}_3/\text{sample solution}$ junction $E_j(\text{Henderson})$ is more positive than that for the entrapped sample solution/sample solution $E_j(\text{Henderson-entrapped})$. Since the cell response E_i is given by

$$E_i = b^0 + s \log a_i + E_j,$$

renewal of junction causes a sudden increase in the observed cell response E_i , due to the increase in E_j .

In experiment (2), the change in the response of the glass electrode with time was found to be nearly identical to that of the K^+ ISE (Figure 6.15). Since the response of both electrodes were measured against the same reference electrode, it is reasonable to believe that the drift is associated with the reference electrode.

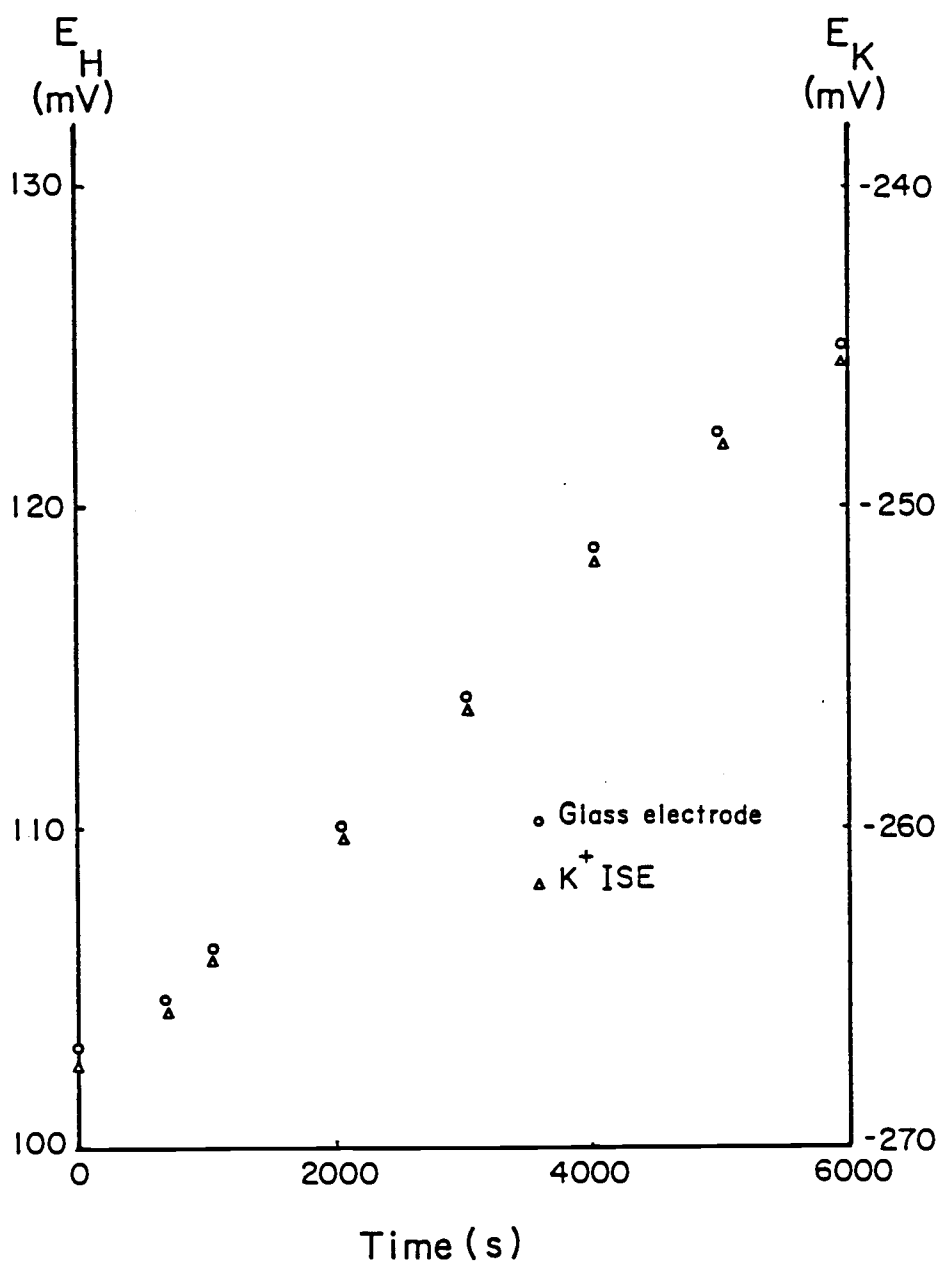


Figure 6.15. The drift of the responses of glass electrode and K^+ ISE vs reference electrode when the solution junction is not renewed.

The data obtained from the two experiments just described can be presented in a different way to obtain a clear picture of the behavior of the liquid junction. Only the glass electrode response is considered here. The experimental junction potential $E_j(\text{exp})$ for the final sample solution

($E_j(\text{exp}) = E_H(\text{obs}) - E_H(\text{calc})$) for both experiments (1) and (2) were obtained. The junction potential for the final sample solution/0.1 NaNO_3 was estimated from the Henderson Equation. In Figure 6.16, all three quantities are plotted as a function of elapsed time from the last addition of acid. The estimated junction potential $E_j(\text{Henderson})$ is independent of time, and is shown by the horizontal line in the figure. The $E_j(\text{exp})$ for experiment (1) becomes nearly the same as $E_j(\text{Henderson})$ immediately after the renewal of the junction. $E_j(\text{exp})$ for experiment 2 slowly drifts towards $E_j(\text{Henderson})$ with time.

The scenario at the salt bridge solution/sample solution junction when the sample solution is dilute can be described as follows, based on the results from the above experiments. Before the addition of acid, the initial sample solution diffuses into the salt bridge and forms an entrapped layer, whose chemical composition is close to that of the initial sample solution. As the titration proceeds, the composition of the sample solution changes. The diffusion from the current sample solution in the cell into the entrapped layer takes place continually. If the addition of the titrant is relatively fast, the change in composition of the sample solution keeps ahead of the change in composition of the entrapped

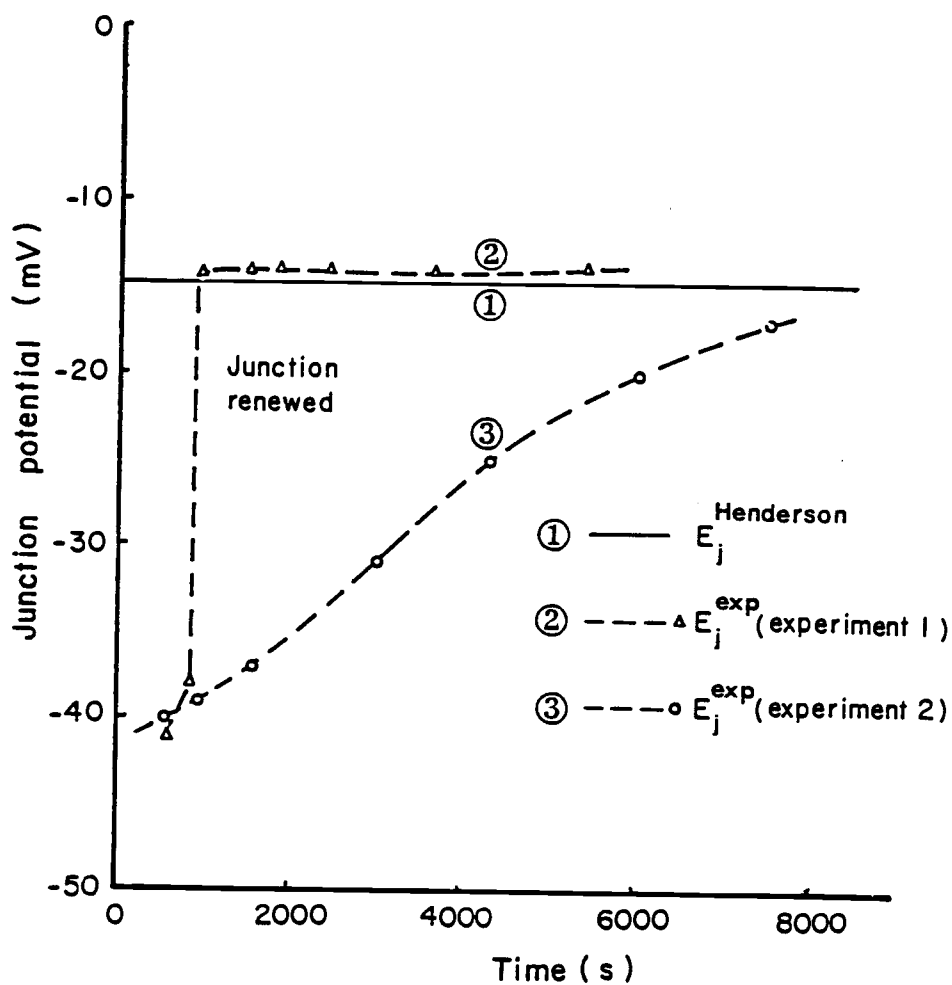
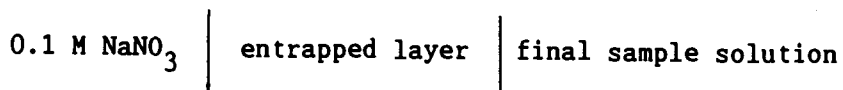
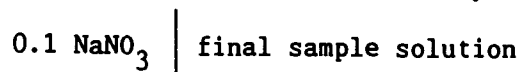


Figure 6.16. Experimental junction potentials $E_j(\text{exp})$
 (a) with (b) without renewing the junction.

layer. At the end of the titration, the junction region can be pictured as follows.



The composition of entrapped layer resembles that of the initial sample solution or the final sample solution depending on the rate of titrant addition. If the junction is renewed after the titration, the junction region immediately assumes the structure:



If the junction is not renewed, the final sample solution diffuses slowly into the entrapped layer, gradually making the entire junction essentially like the junction after renewal.

The composition of the entrapped layer may depend on several factors such as stirring rate, stirrer position, nitrogen bubbling rate, time allowed to reach constant temperature and the titration rate. Thus the titrations in low ionic strength solutions using cells of Type I can be highly irreproducible, as observed in the experiments reported in this work. As these titrations are to be carried out in oxide suspensions in low ionic strength solution, the complications may become even worse due to the presence of the colloidal oxide particles.

The problem with the entrapped layer can easily be eliminated by designing an electrode which has a higher leakage rate for salt bridge solution. In such a design the trapped sample solution will be flushed out making a fresh salt bridge solution/sample solution junction throughout the experiment. However, in the experiments in which low ionic strength sample solutions are used, high leakage of

concentrated salt bridge solution cannot be tolerated because it alters the ionic strength of the solution significantly. An alternative is to use the supporting electrolyte in the salt bridge, i.e., cells of the Type II. The experiments with the cells of Type II will be described next.

Cells of Type II

Many workers have carried out the titrations of colloidal oxide suspension using cells of type. There has been no mention about an entrapped layer as described, or irreproducibility in titrations as was observed for Type I cells. There is no knowledge as to whether the reference electrodes used by previous workers had large leakage rates.

Entrapment of initial sample solution in the liquid junction is possible in these cells as well. Since the initial sample solution is the same as the solution in the salt bridge, there would not be any distinct layer in the junction before the titration starts. As the titration proceeds, the composition of the sample solution changes and a liquid junction potential is expected to develop between the sample and the salt bridge. Large junction potentials can be expected in dilute solutions at extreme pH values owing to the high mobilities of H^+ and OH^- . The following experiments

and their results illustrate the applicability and limitations in the titrations to be carried out for oxide suspensions with Type II cells.

The glass electrode was calibrated in the cells of Type II with KNO_3 solutions of different concentrations (5×10^{-4} , 1×10^{-3} and 1×10^{-2} M) in the sample cell.

Figure 6.17 shows electrode response vs $\log a_{\text{H}^+}$ curves for these titrations. A comparison of these calibration curves with those obtained for a cell with 0.1 M NaNO_3 in the salt bridge (Figure 6.11) shows a higher degree of reproducibility in these curves.

The curve for 0.1 M KNO_3 becomes non linear at hydrogen ion activities less than 10^{-5} M, as indicated by bending of the straight line plot. This non-linearity is observed because of the presence of a residual acid in KNO_3 . The bending of the curves is much less prominent for lower ionic strength solutions, as can be seen from the Figure.

The curves for lower ionic strengths become non-linear and deviate negatively at higher H^+ activities. The reasons for this non-linearity is the increased negative junction potential at higher H^+ activities owing to high ionic mobilities of H^+ . Figure 6.18 shows the electrode response corrected for junction potential as a function of $\log a_{\text{H}^+}$ for the same set of data as shown in Figure 6.17. (The junction potential was estimated by the Henderson Equation 6.13.)

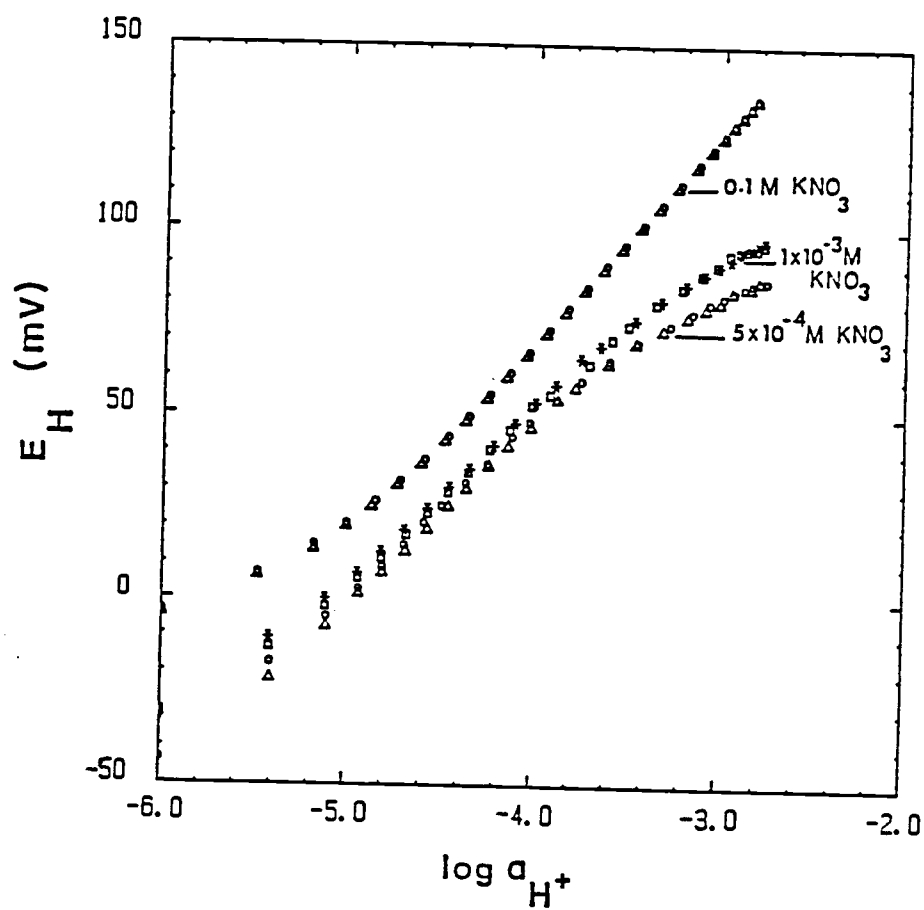


Figure 6.17. The glass electrode response as a function of \log (activity of H^+) for the cells of type II

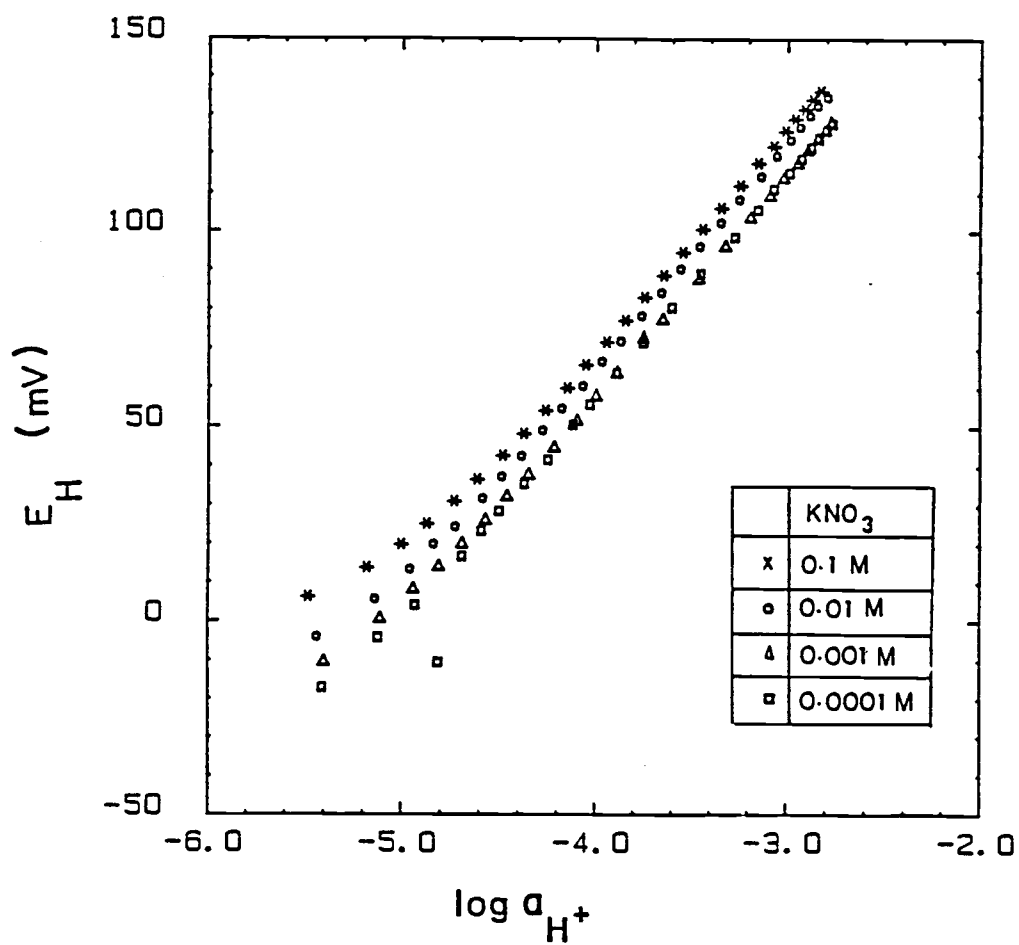


Figure 6.18. The glass electrode response corrected for junction potential as a function of \log (activity of H^+).

The slopes of the four curves are nearly the same, but b^0 values differ by a significant amount. It should be pointed out that the b^0 value includes the potential difference between the salt bridge solution and the reference solution. Since the salt bridge solution was changed with the supporting electrolyte solution, a change in junction potential at the salt bridge solution/reference solution is expected. Therefore, different b^0 values are obtained at different ionic strengths.

Summary

The experiments conducted to calibrate a potentiometric cell consisting of a glass electrode and a Wilhelm-bridge reference electrode in solutions of low ionic strength gave highly irreproducible and unacceptable results, when concentrated electrolyte solutions were used in the salt bridge. It was shown that a layer of sample solution can become entrapped in the liquid junction, and that this layer is responsible for the poor results obtained in the calibration experiment. The problem of irreversibility could be somewhat resolved by using the sample solution in the salt bridge. However, in the titrations with the cells having low ionic strength solutions in the salt bridge, large junction potentials develop at extreme pH values due to high mobilities of H^+ and OH^- , making the data interpretation inaccurate. It is recommended that the titrations be carried out in the pH range of 4-10 where junction potentials are quite small.

6.4 Surface charge studies of TiO_2

Charge distribution at the oxide/electrolyte interface

The charge at the oxide/electrolyte interface can be separated into three components.

- (1) charge due to specific adsorption of ions at the oxide surface (σ_o).
- (2) charge due to the specific adsorption of ions at the inner Helmholtz plane (IHP) (σ_{IHP})
- (3) counter charge in the diffuse layer (σ_d)

In this discussion, the subscripts or superscript "o", "IHP" and "d" will be used to denote the surface, IHP and diffuse layer respectively.

The surface charge is determined from surface excess concentrations. A general expression for the surface excess Γ_i of an ion i can be given as

$$\Gamma_i = \Gamma_i^o + \Gamma_i^{\text{IHP}} + \Gamma_i^d \quad 6.20$$

The three components of the interfacial charge can be expressed in terms of surface excess concentrations.

$$\sigma_o = q \sum z_i \Gamma_i^o \quad 6.21$$

$$\sigma_{\text{IHP}} = q \sum z_i \Gamma_i^{\text{IHP}} \quad 6.22$$

$$\sigma_d = q \sum z_i \Gamma_i^d \quad 6.23$$

for all ions i . Since there is a global charge neutrality through the interface, the total charge is equal to zero:

$$T_{\sigma} = \sigma_o + \sigma_{IHP} + \sigma_d = 0 \quad 6.24$$

Equations 6.20 through 6.24 describe the charge distribution in a simple but reasonably complete manner. We make the following simplifications in our discussion.

(1) It is difficult to separate charge specifically adsorbed at the IHP from that at the oxide surface. For the purpose of this discussion, it is sufficient to consider all specifically adsorbed charge to be located at the oxide surface. Thus Equation 6.24 for charge neutrality can be re-expressed as

$$\sigma_o + \sigma_d = 0 \quad 6.25$$

(2) The concentrations of H^+ and OH^- in the interfacial region are much greater on the oxide surface than in the diffuse layer. Thus the surface excess concentrations of H^+ and OH^- can be represented as

$$\Gamma_{H^+} = \Gamma_{H^+}^o \quad 6.26$$

$$\Gamma_{OH^-} = \Gamma_{OH^-}^o \quad 6.27$$

(3) Significant concentrations of electrolyte ions may be found in the diffuse layer and electrolyte ions can be specifically adsorbed at the interface. Thus, the surface excess concentrations

of electrolyte ions can be expressed as

$$\Gamma_M = \Gamma_M^o + \Gamma_M^d \quad 6.28$$

$$\Gamma_X = \Gamma_X^o + \Gamma_X^d \quad 6.29$$

where M and X denotes electrolyte cation and anion respectively.

The surface excesses in Equations 6.26-6.29, which are measurable quantities, can be represented in the form of charges as follows.

$$\sigma_H = q (\Gamma_{H^+} - \Gamma_{OH^-}) \quad 6.30$$

$$\sigma_M = q \Gamma_M \quad 6.31$$

$$\sigma_X = -q \Gamma_X \quad 6.32$$

In view of the approximations made in Equations 6.25-6.29, the expressions for the interfacial charges σ_o and σ_d may be rewritten as

$$\sigma_o = q (\Gamma_{H^+} - \Gamma_{OH^-}) + q (\Gamma_M^o - \Gamma_X^o) \quad 6.33$$

and

$$\sigma_d = q (\Gamma_M^d - \Gamma_X^d) \quad 6.34$$

The pH at which σ_H is equal to zero is referred to as pH_{ZH} . The pH at which σ_d is equal to zero is referred to as pH_{zc} .

Since specific adsorption of H^+ and OH^- is characteristic of all oxide/solution interfaces, the term specific adsorption will be used in reference to the specific adsorption of electrolyte ions. In the absence of specific adsorption, Equation 6.33 reduces to

$$\sigma_o = q (\Gamma_{H^+} - \Gamma_{OH^-}) \quad 6.35$$

then $\sigma_H = \sigma_o = -\sigma_d$, and $pH_{ZH} = pH_{zc}$. In the case of specific

adsorption, σ_H is generally no longer equal to σ_o (unless $\Gamma_M^o = \Gamma_X^o$), and pH_{zH} is generally not equal to pH_{zc} .

The approximations and the terms introduced in this section is summarized as follows.

(1) Charge at the oxide/electrolyte interface exists on the oxide surface (σ_o) and in the diffuse layer (σ_d). The condition of electrical neutrality requires

$$\sigma_o + \sigma_d = 0$$

(2) The charge on the oxide is due to specifically adsorbed H^+ , OH^- and electrolyte ions.

$$\sigma_o = q (\Gamma_{H^+} - \Gamma_{OH^-}) + q (\Gamma_M^o - \Gamma_X^o)$$

(3) Charge in the diffuse layer consists only of electrolyte ions.

$$\sigma_d = q (\Gamma_M^d - \Gamma_X^d)$$

(4) In the absence of specific adsorption or when both anion and cation of the electrolyte adsorb on the surface equally,

$$\sigma_H = \sigma_o$$

Since pH_{zc} is independent of C_{bulk} when σ_d is zero (Equation 3.13), it can be seen that pH_{zH} is also independent of C_{bulk} , if there is no specific adsorption or equal adsorption of electrolyte anion and cation. Therefore, surface excess concentration of H^+ vs. pH curves obtained for solutions of different ionic strength must exhibit a common point of intersection at zero surface excess of H^+ , if the above-mentioned condition regarding specific adsorption is satisfied.

In the experiments described here, surface excess of H^+ were measured as a function of pH, in solutions of different ionic strength. Surface excess concentration of electrolyte cation was also measured, and results from both measurements will be interpreted using the equations already presented.

Surface excess concentration of H^+

In the experiment described here, surface excess concentrations of H^+ on suspended TiO_2 were determined by potentiometry. The preparation of the oxide suspension and other experimental details are described in Section 4.3. The potentiometric cell of Type II was used in the surface excess determination, since this type of cell was found to be suitable for potentiometric titrations in low ionic strength solutions.

Acid-base potentiometric titrations of oxide suspensions in (a) 0.1, (b) 0.01, (c) 0.001, and (d) 0.0005 M KNO_3 solutions were conducted. A blank titration was carried out before titration of each suspension. The response of the glass electrode and the K^+ ISE were measured during the course of the titration. Surface excess concentrations were calculated as a function of pH from Equation 6.7. ΔV_1 in Equation 6.7 was obtained by subtracting the titration curve of the blank from that of the oxide using a method adapted from the cubic spline curve smoothing technique, as described in Section 6.1.

The surface area of the oxide was not measured in this work. Schindler (59) and Boehm (94) have reported that the specific area of the TiO_2 (Degussa P-25) used in this experiment was $56 \text{ m}^2/\text{g}$, which agrees with the value specified by the manufacturer ($50 \pm 15 \text{ m}^2/\text{g}$). The value reported by the manufacturer was used in the calculations.

The surface excess concentrations of H^+ , converted to units of $\mu\text{C}/\text{cm}^2$ are shown as a function of pH in Figure 6.19. All four $\Delta\psi_0$ vs pH curves intersect at one point at pH 6.4. In the absence of specific adsorption of electrolyte ions, this common point of intersection should correspond to the point of zero surface excess of H^+ and OH^- . Many workers have observed this correspondence for TiO_2 in KNO_3 solutions (43, 64). However, in this experiment the common point of intersection did not coincide with the apparent zero surface excess concentration of H^+ .

There can be several reasons for this occurrence.

(1) The actual zero surface excess and the apparent zero surface excess of H^+ may not be the same due to a systematic error in the determination of $\Gamma_{\text{H}^+} - \Gamma_{\text{OH}^-}$. Presence of residual acid in TiO_2 is a possible source of systematic error.

(2) Specific adsorption of anions or cations other than H^+ and OH^- .

(3) Adsorption of aquo-complexes formed during slow equilibration of the oxide with solution

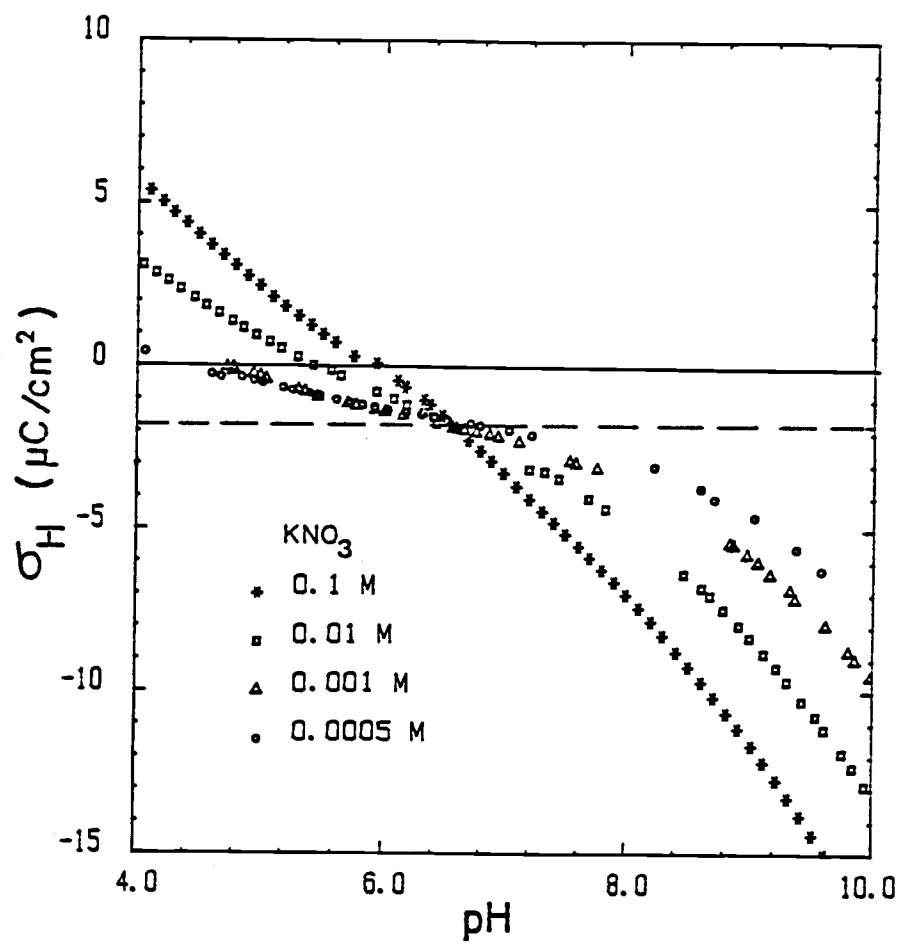


Figure 6.19. Surface excess of H^+ converted to C/cm^2 units as a function of pH for TiO_2 (Degussa P-25). TiO_2 suspension (10 g/L) in 25.0 mL KNO_3 solutions.

In the following section it will be shown that it is very likely that the surface excess concentrations calculated in this experiment have a negative deviation due to residual acid in the TiO_2 which was not removed during the washing. The pH_{zc} of anatase can be taken as 6.4.

Systematic error in surface charge measurement

To examine the possibility of systematic error in the measurement of the surface excess, the pH at which the common point of intersection occurs can be compared with the pH_{ZH} values reported by other workers.

The pH_{ZH} values for TiO_2 reported in the literature are tabulated in Table 6.4. A large variation of pH_{ZH} values is evident from this table. The method of preparation of the oxide appears to be an important factor determining the pH_{ZH} .

The pH_{ZH} for the same oxide as that was used in this experiment (anatase form of TiO_2 , Degussa P-25) was reported as 6.4 (23). The isoelectric point reported for this oxide in an unspecified electrolyte was 6.6 (94). Although the common intersection point in the experimental curve does not coincide with the observed zero surface excess of H^+ , it agrees well with the reported values for pH_{ZH} and the isoelectric point, indicating that the apparent zero surface excess is not the true zero excess.

Table 6.4. Reported values of pH_{ZH} for TiO_2 from surface excess measurements.

Investigator	Type of the oxide	Electrolyte	pH_{ZH}	reference
Parks	pptd. TiO_2	-	6.0	(95)
	(rutile)	-		
	heated TiO_2	-	6.3	
	heated in H_2		7.4	
Ahmed	rutile	0.001 KNO_3	5.3	(20)
		0.1	5.4	
		1 M	5.7	
Berube and de Bruyn	rutile	NaClO_4	5.9	(19)
James et al.	rutile	KNO_3	5.8	(28)
Yates et al.	rutile	KNO_3	5.9	(27)
Schindler	anatase Degussa P-25	NaClO_4	6.4	(23)

A residual acid in the TiO_2 which was not removed during the washing of the suspension is probably responsible for the difference between apparent and true values of surface excess concentrations. The following expressions for surface excess concentrations explain the effect of residual acid.

The apparent surface excess of H^+ is calculated from the apparent value of $(T_A - T_B)$:

$$(\Gamma_{\text{H}^+} - \Gamma_{\text{OH}^-})^{\text{app}} = \{ (T_A - T_B)^{\text{app}} - [\text{H}^+] + [\text{OH}^-] \} / A \quad 6.36$$

The true value of $(T_A - T_B)$ is related to the apparent value by the residual acid in the TiO_2 that is leached into the solution.

$$(T_A - T_B)^{\text{true}} = (T_A - T_B)^{\text{app}} + T_A^0 \quad 6.37$$

Then the true value of the surface excess is greater than the apparent value by T_A^0 / A .

$$(\Gamma_{\text{H}^+} - \Gamma_{\text{OH}^-})^{\text{true}} = (\Gamma_{\text{H}^+} - \Gamma_{\text{OH}^-})^{\text{app}} + T_A^0 / A \quad 6.38$$

The value of T_A^0 calculated from the data in Figure 6.19 for the $1.7 \mu\text{C}/\text{cm}^2$ shift is $8 \times 10^{-5} \text{ M}$.

The titanium dioxide is prepared by hydrolysis of TiCl_4 at high temperature. Therefore, there is a likelihood of residual HCl in TiO_2 . During the preparation of the oxide suspension, the washings of the oxide suspension were analysed for Cl^- . Washing was continued until Cl^- could no longer be detected by the Cl^-

ion-selective electrode. The lowest level of Cl^- that could be detected was approximately 1×10^{-5} M. It is conceivable that additional HCl was leached from the TiO_2 between the time of washing and the time of titration of the oxide.

Determination of K^+ adsorption on oxide surface

As the pH of an oxide suspension is changed, cations or anions can be adsorbed or desorbed depending on whether the pH is increased or decreased. In this experiment, K^+ adsorption on the oxide as a function of pH and ionic strength was measured. The pH of the solution was obtained from the response of the glass electrode. The K^+ adsorption was determined by from the K^+ ISE response as described in Section 6.2.

The percentage gain or loss of K^+ , $\Delta\text{K}\%$ at any point of the titration is given by

$$\Delta\text{K}\% = \frac{T_{\text{K}^+} - [\text{K}^+]}{T_{\text{K}^+}} \quad 6.39$$

Figure 6.20 shows the $\Delta\text{K}\%$ values so calculated from Equation 6.39 for oxide suspensions in 1×10^{-3} and 5×10^{-4} solutions, as a function of solution pH. A sharp increase in K^+ adsorption with increasing pH is evident from this figure.

The response of K^+ electrode was very noisy in the oxide suspensions (1-2 mV), compared with the relatively noise-free response (0.2-0.5 mV) in supporting electrolyte solutions. The increased noise have several sources.

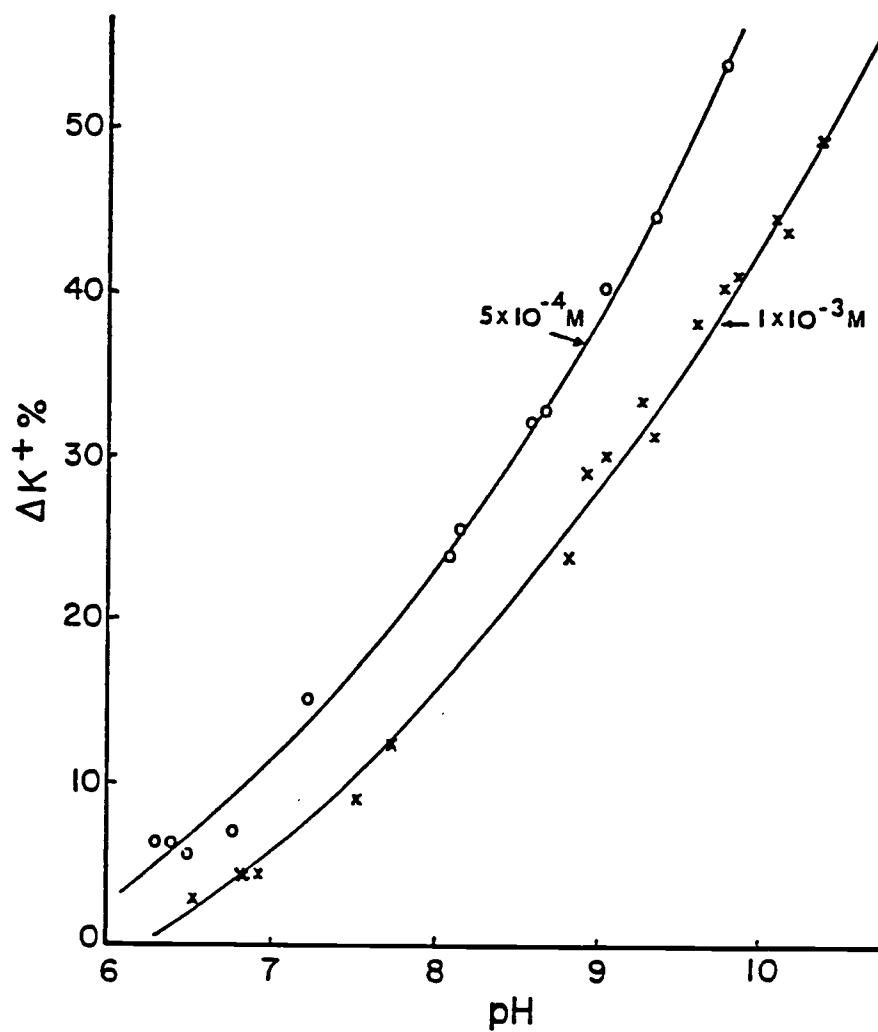


Figure 6.20. Loss of K^+ as a function of pH in TiO_2 suspended in (a) $5 \times 10^{-4} \text{ M}$, (b) $1 \times 10^{-3} \text{ M}$ KNO_3 solutions.

(1) The liquid junction between the suspension and the salt bridge solution becomes more noisy due to the presence of charged oxide particles.

(2) Although the response of the K^+ electrode was not affected due to a film of colloidal oxide on the electrode, presence of larger oxide particles near the K^+ ion-selective membrane may interfere with its response. Since the oxide particles are transported to the electrode surface in a random manner, the electrode response may become noisy.

The uncertainty of 4-8 percent can be estimated in the measured K^+ concentration due to the noise of the electrode response, from Equation 6.13.

The change in response of K^+ ISE during the titrations in the solutions of 0.01 M and 0.1 M KNO_3 could not be distinguished from the noise of the electrode response. Since only a small fraction of K^+ ions are adsorbed in concentrated KNO_3 solutions it is extremely difficult to measure a change in K^+ ion concentration.

The surface excess measurements of H^+ and K^+ can be combined to interpret the properties of the electrical double layer at the TiO_2 /solution interface.

In this analysis, three quantities will be examined as functions of pH

(1) σ_H determined through the measurement of surface excess of H^+ .

(2) σ_K determined through the measurement of surface excess of K^+ .

(3) charge density σ_d of the diffuse layer calculated from Equation 3.13.

The determination of σ_H and σ_K has been discussed previously. The charge density of the diffuse layer σ_d can be calculated from Equation 3.13. C_{bulk} in this equation was set equal to the measured concentration of K^+ ions. ψ_0 was obtained by assuming a Nernstian behavior. This assumption is based on the observed Nernstian behavior of surface potential of TiO_2 electrodes (75,81) found by other methods. From the common intersection point, the pH_{zc} of TiO_2 was determined to be 6.4. For a given pH, the displacement from pH_{zc} (ΔpH) can be obtained and $\Delta\psi_0$ can be calculated by multiplying the displacement by 59.15 mV. Then σ_d can be calculated, since all the parameters in the right hand side of Equation 3.13 are known.

Figures 6.21 (a) and 6.21 (b) show σ_H , σ_K and σ_d as a function of pH in the solutions of 5×10^{-4} M and 1×10^{-3} M solutions.

The data in the figures can be summarized in the following way.

(1) The curves for the two concentrations of electrolyte, 5×10^{-4} M and 1×10^{-3} M are of the same form: Below pH 9,

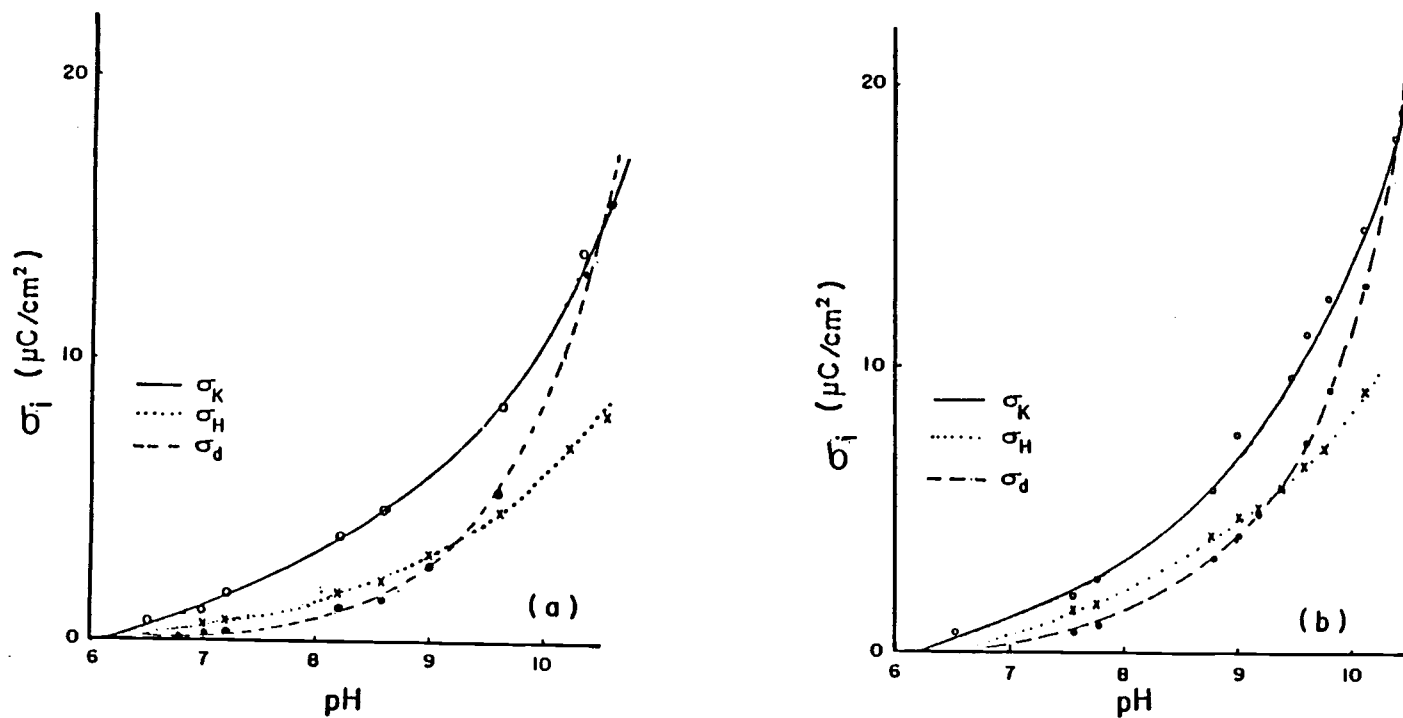


Figure 6.21. Surface excess concentrations converted to $\mu\text{C}/\text{cm}^2$ for H^+ (σ_H), K^+ (σ_K) and calculated charge in the diffused layer (σ_d), assuming Nernstian behavior for surface potential, in (a) $1 \times 10^{-3} \text{ M}$ (b) $5 \times 10^{-4} \text{ M}$ solutions.

$\sigma_K > |\sigma_H| \approx \sigma_d$. Above pH 9, σ_d begins to increase sharply, probably reflecting the invalidity of the simple Gouy-Chapman model at high values of interfacial potentials.

(2) Two features of these curves indicate that K^+ is specifically adsorbed: there is a positive surface excess of K^+ at the pH_{zH} , and the surface excess of K^+ is greater than that of OH^- from pH 6 to pH 10.

The fact that K^+ is specifically adsorbed and that the σ_H vs. pH curves still exhibit a common point of intersection suggest that NO_3^- must also be specifically adsorbed, with approximately the same energy.

Summary

Two important conclusions can be drawn from these data.

(1) specific adsorption of electrolyte ions appears to be significant; and

(2) adsorption of electrolyte ions from oxide suspensions can be quantitated with ion-selective electrodes. Further quantitative interpretation of these data awaits collection of a more complete set of data, including anion and cation concentrations on both sides of the pH_{zc} .

7. Summary and Conclusion

The oxide/electrolyte interface is generally characterized by the interfacial potential and charge. Oxide electrodes can be used to detect the potential change at the oxide/electrolyte interface with change in solution composition. Interfacial charge is determined via the measurement of surface excess concentrations in oxide suspensions.

Since most oxides are insulators, a direct measurement of the interfacial potential changes is not possible, because of the unknown potential drop across the oxide. In practice, the interfacial potential changes are determined indirectly by measuring a property which is dependent on the potential (such as capacitance). In this study, metal/oxide/electrolyte structures were considered for detection of interfacial potential changes through capacitance measurements. Theoretical analysis of these structures, supported by experimental evidence, has shown that the observed capacitance is dominated by the small capacitance of the oxide, so that the potential-dependent capacitance of the double layer cannot be detected. Making an extremely thin oxide layer to obtain a larger oxide capacitance is highly impractical. In order to detect the interfacial potential changes by differential capacitance measurements, another potential dependent capacitor with

capacitance similar to that of the oxide must be incorporated next to the oxide. Semiconductors were prepared for this purpose and used in an

electrolyte/oxide/semiconductor (EOS) structure to determine the potential changes at the oxide/electrolyte interface.

The ac impedance technique was used in the determination of the capacitance of the EOS structures. The instrumentation generally used in the ac impedance measurements has shown phase shifts with entirely resistive circuits at relatively low frequencies. The I/E converter has been identified as being responsible for most of the phase shift, which limits the applicability of the instrumentation to a frequency range below 1000 Hz. In this work, the upper frequency limit of the measurement system has been expanded somewhat by correcting for the capacitive impedance of the feedback loop of the I/E converter.

A circuit model for the electrochemical cell is necessary to interpret the measured in-phase and out-of-phase components of the output of the I/E converter. An equivalent circuit to represent the EOS structures was derived from a rigorous mathematical model of the oxide/electrolyte interface. An equivalent circuit for the electrochemical cell as a whole, was obtained by incorporating the circuit deduced for the EOS structure with other circuit elements generally used in representing the physical structure of the cell. The equivalent circuit proposed for the electrochemical cell was

reduced to a simple series RC circuit, and the measured signals were translated to the capacitance of the EOS structure.

Capacitance-voltage curves obtained for the EOS structure studied showed average shifts of 38.5, 34.5, and 26.7 mV/pH in the pH range of 3-7 in KNO_3 solutions of 0.01, 0.05, and 0.1 M respectively. These results agree with the trends reported in the literature. It is difficult to compare the experimental shifts with those reported in the literature, since the methods of fabrication of the electrodes are different.

A theoretical model to explain the response of the EOS structures to the changes in solution composition was developed. Calculations with this model allowed the analysis of the effects of parameters such as surface dissociation constant K_D , surface site density N_s , electrolyte concentration C_{bulk} and the displacement from the pH_{zc} , ΔpH . From the calculations, it was shown that the response of the EOS structures with

- large K_D
- large N_s
- small C_{bulk}

approaches Nernstian behavior. The response near the pH_{zc} was shown to be a maximum if K_D was large and a minimum if it was small.

The calculated values of $\frac{\Delta\psi_0}{\Delta\text{pH}}$ from the theoretical model were compared with the experimental data. EOS structures described by model parameters of $K_D=0.01$, $N_s=8 \times 10^{14}$ explained the experimental data reasonably well. The agreement between calculated

and experimental values was poor for the cases in which the concentration of the electrolyte in solution was high, especially at pH values away from the pH_{zc} . The diffuse layer model was used in describing the electrical double layer. This model is not suitable to describe the double layer either in concentrated solutions or at high potentials. The Stern model for the double layer might have been more appropriate to explain experimental data in the entire range of solution pH and ionic strength.

The surface excess measurements in oxide suspensions were complicated by the presence of a small amount of a protolytic impurity in KNO_3 solutions used in the experiments. This impurity could not be removed by recrystallization. An empirical method of surface excess determination was used to compensate for the impurity. In this method, two titrations were carried out, one for the supporting electrolyte alone (blank) and one for the suspension; then the curve for the blank was subtracted from the curve for the suspension to obtain the surface excess concentrations of H^+ on the oxide. The cubic spline method, which is generally used for curve smoothing, was found to be useful in the numerical subtraction of the titration curves.

Potentiometry of oxide suspensions in the solutions of low ionic strength showed irreproducibility in the measurement. Dilution of the salt bridge solution in the reference electrode by the sample solution was found to be the cause for this irreproducibility. Use of the supporting electrolyte in the salt

bridge made the potentiometric measurements somewhat more reproducible as long as the solution pH was not too high or too low. It would be worthwhile to investigate the possibility of designing a reference electrode with the ability to renew the salt bridge/sample solution junction continuously without disturbing the equilibria in the sample solution.

The surface excess concentrations of H^+ vs. pH curves obtained for TiO_2 suspensions in solutions of different ionic strengths exhibited a common point of intersection at pH 6.4. This point lies at an apparent negative surface excess of H^+ indicating the presence of residual acid in TiO_2 . The value pH 6.4 agrees well with the isoelectric point and the pH_{zc} value reported for the same oxide (Degussa P-25, anatase).

From the measurement of surface excess concentration of K^+ , it was shown that K^+ ions specifically adsorbed on TiO_2 . Since σ_H vs. pH curves exhibit a common intersection point, it appears that NO_3^- also adsorbs on TiO_2 , although one would expect NO_3^- to be adsorbed less strongly than K^+ .

The error involved in K^+ determination amounts to about 10% because of the noise and the drift associated with the K^+ electrode. The K^+ ISE used in this experiment was a liquid membrane electrode, which is preferable to its solid state counterparts in most applications. However, the possibility of using a solid-state electrode also should be studied.

Measurement of surface excess concentrations of anions as well as cations, on either side of the pH_{zc} will be valuable in furthering our understanding of the oxide/electrolyte interface.

8. REFERENCES

- (1) P. Bergveld, IEEE transactions on Biomedical Engineering, BME-17 (1970) 70
- (2) M.A. Arnold and M.Meyerhoff, Anal.Chem., 56 (1984) 20R
- (3) E.A. Jenne, Adv. Chem. Ser. , 73 (1968) 337
- (4) R.J. Gibbs, Geol. Soc. Am. Bull., 88 (1977) 829
- (5) M.S. Shuman, C.L. Haynie and L.A. Smock, Environ. Sci. Technol., 12 (1978) 1066
- (6) D.P. Kharkar, K.K. Turekian and K.K. Bertine, Geochim. Cosmochim. Acta, 32 (1968) 285
- (7) K.K. Turekian and M.R. Scott, Environ. Sci. Technol., 1 (1967) 940
- (8) P.W. Schindler, Thalassia Jugoslavia, 11 (1975) 101
- (9) M. Anderson and A. Rubin, Eds., Adsorption of Inorganics at the Solid Liquid Interface, Ann Arbor Science, 1981
- (10) M.C. Kavanaugh and J.O. Leckie, Eds., Particulates in water, Advances in C
- (11) G.H. Bolt, J. Phys. Chem, 61 (1957) 1166
- (12) G.A. Parks and P.L de Bruyn, J. Phys. Chem, 66 (1962) 967
- (13) S.M. Ahmed, Can. J Chem., 44 (1966) 1663
- (14) H.C. Li and de Bruyn, Surf.Sci, 5 (1966) 206
- (15) G.Y. Onoda Jr. and P.L. de Bruyn, Surf.Sci, 5 (1966) 48
- (16) R.J. Atkinson, A.M. Posner and J.P. Quirk, J.Phys.chem., 71 (1967) 550
- (17) S.M. Ahmed and D. Maksimov, Can.J.Chem, 46 (1968) 3841

- (18) T.F. Tadros and J. Lyklema, J.Electroanal.Chem., 17 (1968) 267
- (19) Y.G. Berube, P.L. de Bruyn, J. Coll.Interface.Sci, 27 (1968) 305
- (20) S.M. Ahmed and D. Maksimov, J.Coll.Interfac.Sci, 29 (1969) 97
- (21) L. Blok and P.L. de Bruyn, J.Coll.Interfac.Sci., 32 (1970)
- (22) Breeuwsma and Lyklema, J.coll. Interfac.Sci, 43 (1973) 437
- (23) P.W. Schindler and H. Gamsjager, Kolloid - Z.u.Z. Polymere., 250 (1972) 759
- (24) C.P. Huang and W. Stumm, J.Coll.Interfac.Sci., 43 (1973) 409
- (25) H. Hohl and W. Stumm, J.Coll.Interfac.Sci., 55 (1976) 281
- (26) J.A. Davis and J.O. Leckie, J.Coll.Interfac.Sci., 67 (1978) 90
- (27) D.E. Yates and T.W Healy, J.C.S Faraday I, 76 (1980) 9
- (28) James et al. in P.H. Thewari, ed. Adsorption from aqueous solutions Plenum, NY, 1981.p19.
- (29) A.E. Regazzoni, M.A. Blesa and A.J.G. Maroto, J.Coll.Interfac.Sci., 91 (1983) 560
- (30) M.A. Blesa, A.J.G. Maroto and A.E. Regazzoni J.Coll.Interfac.Sci., 99, (1984) 32
- (31) M.R. Houchin and L.J. Warren, J.Coll.Interfac.Sci., 100 (1984) 278
- (32) H.J. Modi and D.W. Fuerstenau, J Phys. Chem, 61 (1957) 640
- (33) Y.G. Berube, P.L. de Bruyn, J. Coll.Interface.Sci, 28 (1968) 92

- (34) J. Lyklema and J.T.G. Overbeek, J.Coll.Interface.Sci, 16 (1961) 595
- (35) R.J. Hunter, H.J.L. Wright, J. Coll. Interfac. Sci., 37 (1981) 364
- (36) H.J.L. Wright, R.J. Hunter, Aust. J. Chem, 26, (1973) 1183
- (37) H.J.L. Wright, R.J. Hunter, Aust. J. Chem., 26 (1973) 1191
- (38) L.H. Little, Infrared spectra of adsorbed species, (London and New York) 1966.
- (39) D.M. Griffiths, C.H. Rochester, J.C.S. Faraday I, 73 (1977) 1510
- (40) S. Levine, A.L. Smith, Disc. Far. Soc., 52, (1971) 290
- (41) D.E. Yates, S. Levine, T.W. Healy, Trans. Far. Soc., 70, (1974) 1807
- (42) W.H. Brattain and C.G.B. Garrett, B.S.T.J., 34, (1955) 129
- (43) W.H. Brattain, P.J. Boddy, J. Electrochem.Soc., 109 (1962) 574
- (44) P.J. Boddy, W.H. Braltain, J. Electrochem.Soc. 110, (1963) 570
- (45) T. Watanabe, A. Fuishima, J. Honda, J.Chem.Lett., (1974) 897
- (46) J. Schenk, J.Coll.Interface.Sci 61, (1977) 569
- (47) H. Abe, M. Esashi and T. Matsuo, IEEE Transactions on Electron Devices, ED-26 (1979) 1939
- (48) W.M. Siu and R.S.C. Cobbold, IEEE Trans. Electron Devices, ED-26, 1870
- (49) P.R. Barabash and R.S.C. Cobbold, IEEE Trans. Electron Devices, ED-29 (1982) 102
- (50) L. Bousse, N.F De Rooij and P. Bergveld, IEEE.Trans.Electron Devices, ED-30 (1983) 1263

- (51) T. Akiyama, Y. Ujihira, Y. Okabe, T. Sugano and E. Niki, IEEE Transactions on Electron Devices, ED-29 (1982) 1936
- (52) Gilles Horowitz, J. Electroanal.Chem, 159, (1983) 421
- (53) K. Kinoshita and M.J Madou, J. Electrochem. Soc, 131, (1984), 1089
- (54) H.L.F Von Helmholtz, Wiss. Abhandl.Physik-tech. Reichsanstalt, 1, 925 (1879) cited in Ref 59, p.286.
- (55) G. Gouy, J. Phy., 9, 457 (1910)
- (56) D.L Chapman, Ph.l.Mag., 25, 475 (1913) cited in Ref 59, p.286.
- (57) O.Stern, Z. Electrochem, 30, 508 (1924).
- (58) D.C. Grahame, Chem. Rev., 41 (1947) 441
- (59) B.E Conway, Theory and principles of electrode processes, Ronald Press, N.Y 1965.
- (60) E.Gileadi, K.Kirowa-Eisner and J. Penciner, Interfacial Chemistry, Addison-Wesley (1975)
- (61) P. Delahay, Double layer and Electrode Kinetics, Interscience, N.Y. (1965)
- (62) A.J. Bard and L.R. Faulkner, Electrochemical methods, Wiley (1980)
- (63) M.A.V. Devanathan and B.V.K.S.R. Tilak, Chem Rev, 65 (1965) 635
- (64) A.S. Grove, Physics and technology of semiconductor Divices, Wiley, N.Y (1967)
- (65) S.M. Sze, Physics of semiconductor devices, Wiley, N.Y (1969)
- (66) J.O'M Bockris and A.K.N. Reddy, Modern Electrochemistry, Plenum, N.Y. (1970)
- (67) K.H. Zaininger and F.P. Heiman, Solid State Technology, 5 (1970) 49
- (68) J.C. Westall, unpublished results.

- (69) M. Kuhn, Solid State Electron., 13 (1970) 873
- (70) D.C. Grahame, J. Am.Chem. Soc., 71, (1949) 2975
- (71) D.C. Grahame, Rev. Phys. Chem., 6 (1955) 337
- (72) J.J McMullen and Norman Hackerman, J. Electrochem. Soc., 106 (1959) 341
- (73) L. Ramaley and C.G. Enke, J. Electrochem. Soc., 112 (1965) 943
- (74) M. Babai, N. Tshernikovski and E. Gileadi, J. Electrochem. Soc., 119, (1972) 1018
- (75) G.P. Power and I. Caldwell, Electrochim. Acta, 26, (1981) 625
- (76) L. Bousse, J.Chem Phys, 76.(1982) 5128
- (77) N.F. de Rooij and P. Bergveld in The Physics of SiO₂ and its surfaces, Ed. S.T. Pantelides, Pergamon Press, N.Y (1978) 433
- (78) D. Marino, Ph.D. Thesis, Oregon State University (1981)
- (79) C.M. Seyfert, J.C. Westall and S.L. Hindagolla, unpublished work.
- (80) F. Mansfeld, Corrosion, 36 (1981)
- (81) F. Mansfeld, M.W Kendig and S. Tsai, Corrosion, 38 (1982) 571
- (82) J. O'M. Bockris and S. D. Argade, J. Chem. Phys. 49, (1968) 5133
- (83) J.E.B. Randles, Trans. Faraday Soc. 52, (1956) 1573
- (84) B. Jakuszewski, J. Chem. Phys. 31, (1959) 846
- (85) P. Bergveld, N.F de Rooij and J.N. Zemel, Nature, 273 (1978) 438
- (86) A.G. Revesz, Thin Solid Films, 4 (1977) L 43
- (87) P.W. Cheung, D.G. Flemming, W.H. Ko, M.R. Neuman, Theory, Design and Biomedical applications of solid state Chemical sensors, CRC Press (1978)

- (88) B.E. Deal, E.L. Mackenna and P.L. Castro, J. Electrochem.Soc., 116 (1969) 997
- (89) F.A. Cotton and G. Wilkinson, Basic Inorganic chemistry, Wiley, N.Y (1976) p.220
- (90) C.F. Gerald and P.O. Wheatley, Applied Numerical Analysis, Addison-Wesley (1984)
- (91) E.A. Guggenheim, J. Am.Chem.Soc., 52 (1930) 1315
- (92) E.A. Guggenheim, J. Phys. Chem., 34 (1930) 1758
- (93) D.P. Brezinski, Analyst, 108 (1983) 425
- (94) H.P. Boehm, Angew. Chem.Internat Ed. Vol.5 (1966) 541
- (95) G.A. Parks, Chem Rev, 65 (1965) 177

9. APPENDICES

APPENDIX A : Program to calculate C-V curves for MOS structures

```
REM Program to find Properties of
REM   MOS Capacitors
REM (uses Newton-Raphson iterative technique)
```

```
60SUB 100:REM DIMENSION
60SUB 200:REM INITIALIZE PHYSICAL CONSTANTS
60SUB 300:REM FABRICATION PROPERTIES
60SUB 400:REM INPUT VOLTAGE RANGE
```

	PRINT* VG	PSI	CS	QS	COBS	C/COX*
	<pre>PRINT FOR I=1 TO NP:60SUB 500:NEXT I STOP</pre>					
100	<pre>REM DIMENSION DIM V(30) DIM CS(30),QS(30),N(30),P(30) DIM C(30),CN(30) RETURN</pre>					
200	<pre>REM INITIALIZE PHYSICAL CONSTANTS T=298 K=1.38866E-23 Q=1.60218E-19 E0=8.85418E-14 B=Q/(K*T) KI=3.9 KS=11.9 ES=E0*KS EI=E0*KI RETURN</pre>					
300	<pre>REM FABRICATION PROPERTIES ND=1E15 NA=1E5 NB=ND PB=NA DOX=550E-8 RETURN</pre>					
400	<pre>REM APPLIED VOLTAGE RANGE INPUT*NO. OF POINTS*;NP FOR I=1 TO NP INPUT V(I) NEXT I RETURN</pre>					

```

500  REM BEGIN ITERATION
      J=0
      VG=V(I)

      REM GUESS PSI
      PSI=0.01*VG

      LIMIT=0.001*VG
      LIMIT=ABS(LIMIT)
      COX=EI/DOX
      LD=SQR(ES/(Q*N0*B))
      MF=ES*K*T*SQR(2)/(Q*LD)
      A=MF/COX

550  REM START WITH NEW VALUE OF PSI
      X=B*PSI
      A1=EXP(X)-1
      A2=(P0/N0)*(1-EXP(-X))
      DF=B*(A1+A2)
      F1=(EXP(X)-X-1)+(P0/N0)*(EXP(-X)+X-1)
      F=SQR(F1)
      IF VG<0 THEN F=-F
      D=(A*DF)/(2*F)+1
      D=-D
      Y=VG-(A*F+PSI)
      IF ABS(Y)<LIMIT THEN GOTO 600
      J=J+1
      IF J>40 THEN GOTO 600
      PSI=PSI-Y/D
      GOTO 550

600  REM PRINT RESULTS
      QS(I)=MF*F
      N(I)=N0*EXP(X)
      P(I)=P0*EXP(-X)
      CS(I)=MF*DF/(2*F)
      C(I)=CS(I)*COX/(CS(I)+COX)
      CN(I)=C(I)/COX
      PRINT VG,PSI,CS(I),QS(I),C(I),CN(I)
      RETURN

```


APPENDIX B: Determination of capacitance of electrochemical cells

The objective of this experiment is to determine the double layer capacitance at the interface between metal oxide electrode and an aqueous solution. The description of the experimental technique is divided into four parts

- (1) Basis principle
- (2) Instrumental : operation of the circuit
- (3) Results
- (4) Limitations

Basic principle

When a triangular potential wave form is applied across a capacitor, the current through the capacitor is a square wave form; the amplitude of which is proportional to the capacitance. The applicability of this principle for the measurement of the interfacial capacitance in electrochemical cells is described in this section.

Consider the circuit for a conventional potentiostat shown in Figure B.1 (a) and the equivalent circuit for a three electrode electrochemical cell shown in Figure B.1 (b). The potential at

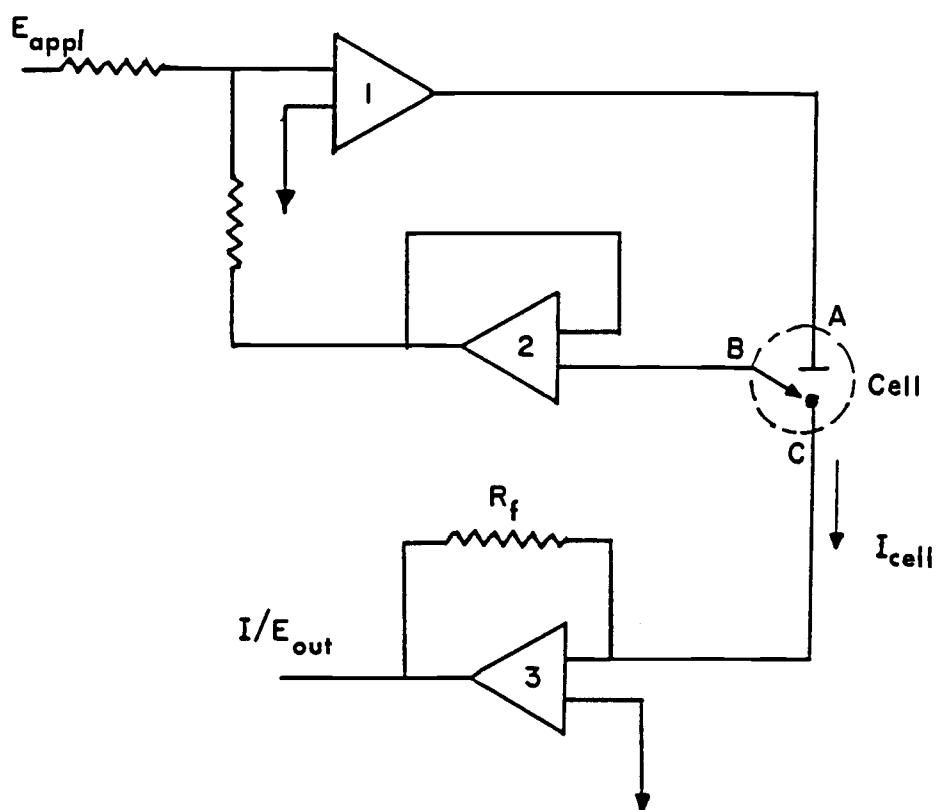


Figure B.1 (a). Schematic diagram of a potentiostat and a three electrode cell

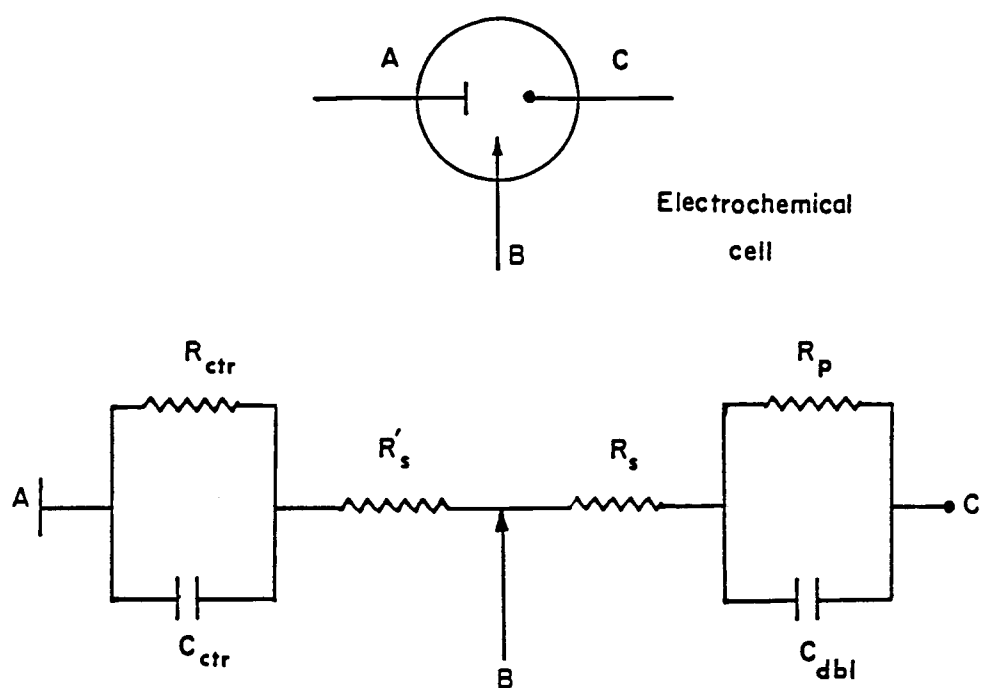


Figure B.1 (b). Equivalent circuit for an electrochemical cell

point B (in either circuit) is always equal in magnitude and opposite in sign to the potential applied to the cell. Therefore, in the actual analysis, it is sufficient to consider the circuit between points B and C.

If the discussion is restricted to a system where the faradaic reactions are absent, R_p can be assumed to be infinite. For the purpose of simplicity, R_s can be ignored initially. The effect of R_s and R_p will be discussed later. The equivalent circuit can now be reduced only to the double layer capacitance. The current through such a totally capacitive electrochemical cell is a square wave, if the applied potential is a triangular wave. The amplitude of this square wave is proportional to the double layer capacitance. In the following section, the measurement of the amplitude of this square wave is discussed.

Instrumentation

Figure B.2 shows a block diagram of the instrumentation used in the experiment. The electrochemical cell was connected to a potentiostat (PAR 173). A triangular wave from a function generator (PAR 175 universal programmer or Tektronix model FG-502) was applied to the potentiostat, and a voltage proportional to the cell current was obtained at the output of the I/E converter (PAR 179).

The measurement of the amplitude of the square wave is accomplished by the part of the circuit enclosed by the dotted line

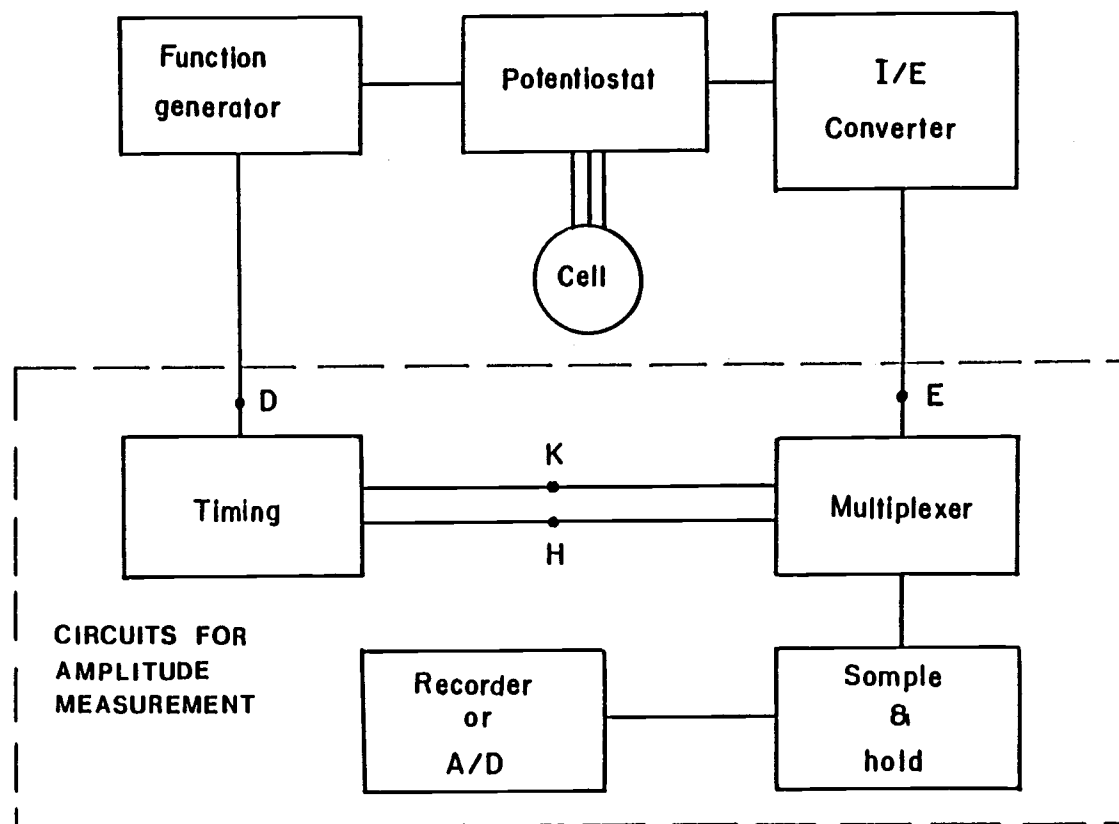


Figure B.2. Block diagram of the instrumentation

of Figure B.2. The actual component circuit diagram for this part is shown in Figure B.3. A master square wave at point D, synchronized with the triangular wave, provides the timing for the measurement circuitry. Figure B.4 shows the timing at various points of the circuit. The voltage at the top and the bottom of the square wave output of PAR 179 is sampled by means of two FET gates (multiplexer) in conjunction with two sample and hold amplifiers. The master square wave at D trigger the monostables 1 and 2. The pulse width of the output of these monostables control the position of sampling pulses E and F with respect to the rising or falling edge of the master square wave.

The duration of the sampling pulse was adjustable with in a range of 50 μ s - 1 ms, using the 10 k potentiometers connected to the monostables. The pulse width was held constant for both sampling pulses at 80 μ s.

The sampled signals are fed to two sample and hold amplifiers. The output of the sample and hold amplifier 4, which is sampling the bottom half of the wave, is inverted by amplifier 6, and the inverted signal is added to the output of the amplifier 5. Thus, the output of the amplifier 7 is the amplitude of the square wave and it can be monitored continuously.

Response of the instrument was calibrated using a circuit representative of an electrochemical cell ($R_p = \infty$, $R_{ctr} = 1 \text{ k}\Omega$, $C_{ctr} = 1 \text{ }\mu\text{F}$). In all measurements, the amplitude of the triangular wave was 20 mV. All measurements were made in a large Faraday cage. Since the cell current depends on the frequency of the

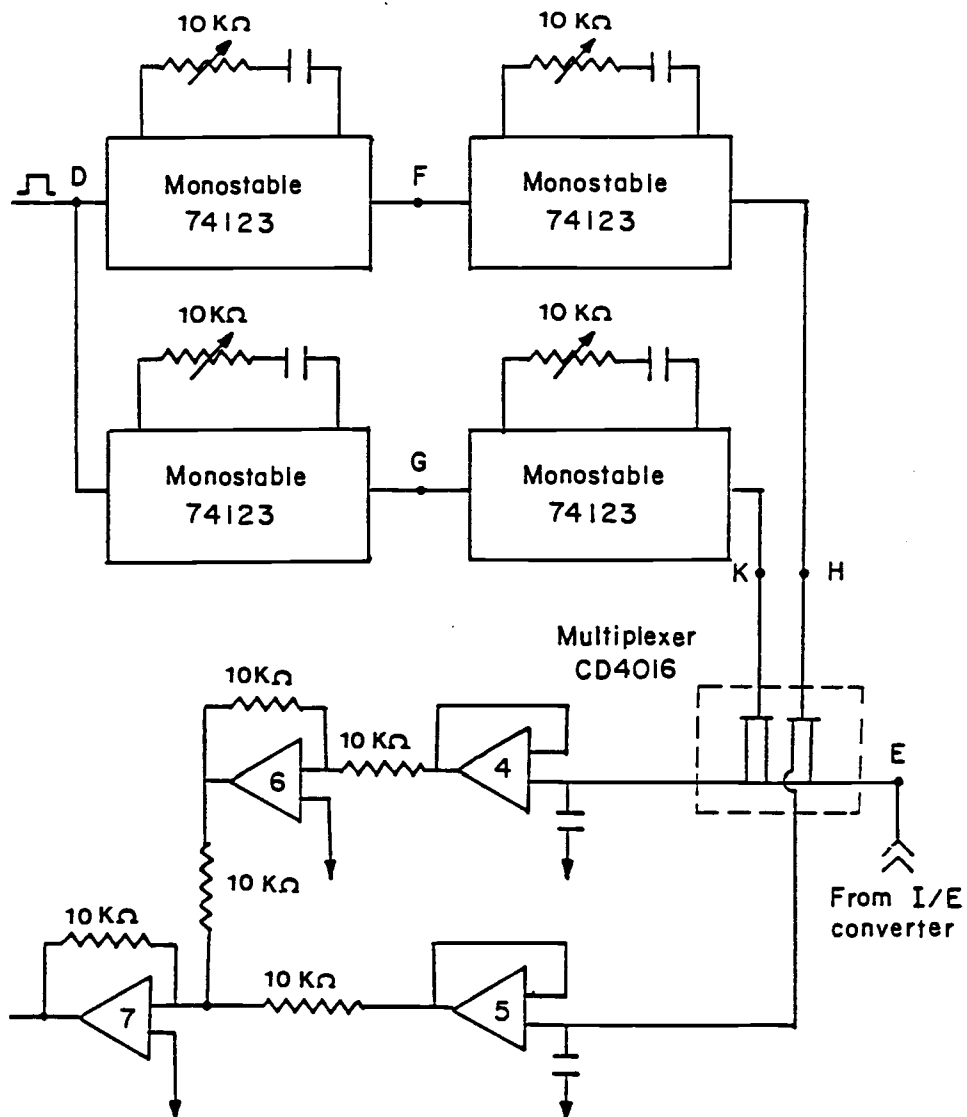


Figure B.3. Actual component circuit diagram for amplitude measurement

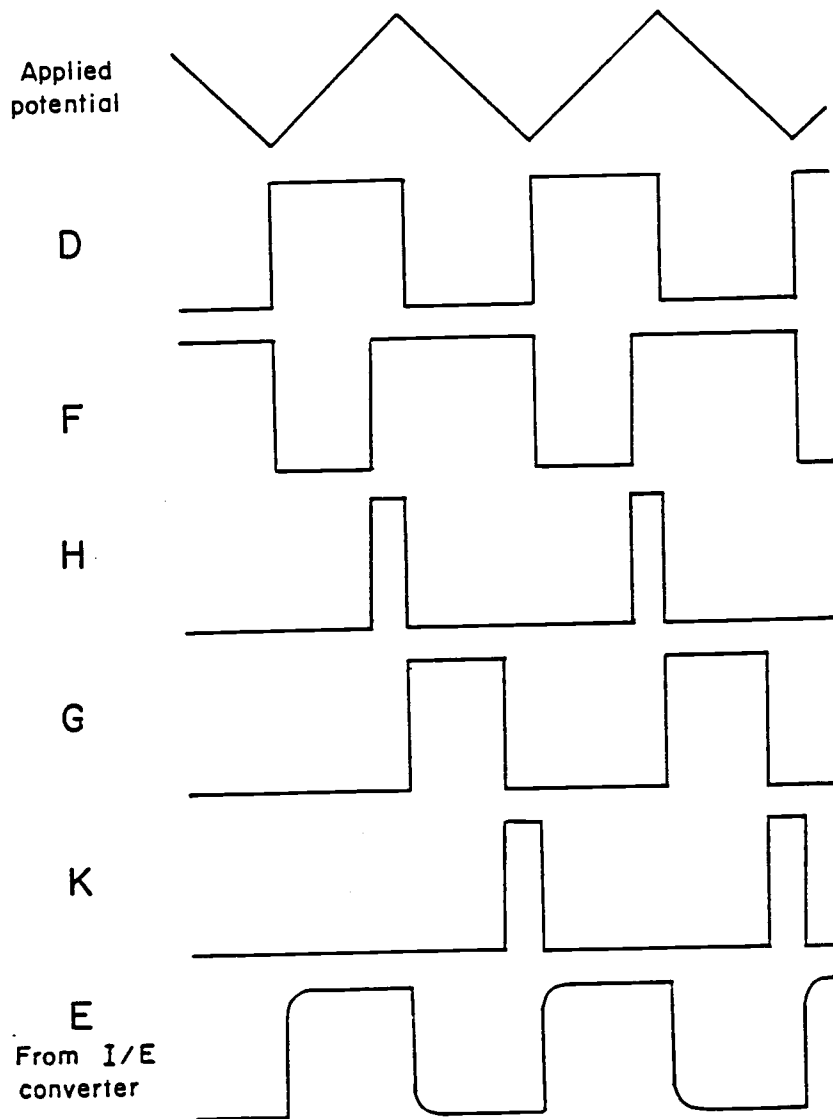


Figure B.4. Timing diagram (waveforms at various points of the circuit)

applied potential, and the capacitance of the cell, the sensitivity of the current-to-voltage conversion step must be selected appropriately so that a signal with a voltage large enough to be measured is obtained.

The performance of the instrument is illustrated in Figure B.5, where a calibration curve for capacitance, a plot of cell current vs capacitance is shown.

Excellent linearity was observed for 4 decades of capacitance. For totally capacitive circuits, the capacitances as low as 3 nF could be measured within a 10% error. The lowest measured capacitance reported by Power and Caldwell is 30 nF, the same range. The reduction of noise achieved by performing the experiments in a Faraday cage can be attributed to the ability of measuring square wave signals of small amplitudes. When the measurements were made in the Faraday cage, only about 1mV p-p noise was observed in the most sensitive I/E conversion scale, whereas outside the cage, approximately ~ 10 mV p-p noise was observed under the same conditions.

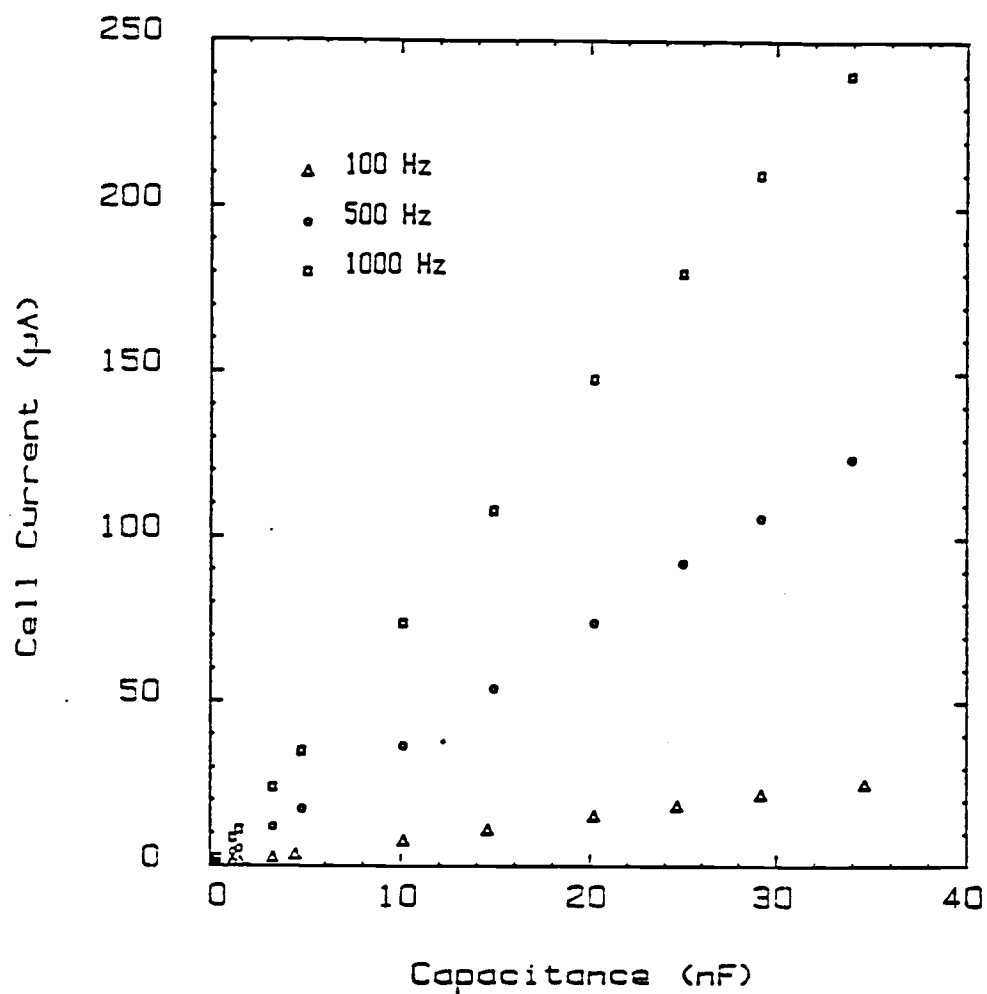


Figure B.5. Calibration curves (cell current vs. capacitance)
at 100, 500 and 1000 Hz

Limitations of the measurement system

As explained previously, a totally capacitive cell would yield a perfect square wave form for current upon the application of a triangular potential perturbation. However, the current observed in many electrochemical cells are not perfect square waves because of the resistive elements in the cells. Series resistance R_s and parallel resistance R_p as shown in Figure B.1 (b), affect the current wave form, and may limit the applicability of the method.

A low value for R_p is equivalent to a leaky capacitor, and the effect of R_p on the current - time response to an applied triangular potential for such a circuit is shown in Figure B.6. This is similar to the observed response for an electrochemical cell where a Faradaic reaction is taking place.

High values for series resistance R_s slows down the rate of charging of the capacitance. Electrochemical cells with very dilute solutions approximate this condition. Small values for R_s leads to a ringing pattern on the square wave. Highly conductive solutions (concentrated electrolyte solutions) have low R_s values. When R_s is small, the circuit resembles an ideal differentiator, in which ringing effects are known to be found. The effect of R_s is shown in Figure B.7. These results are very similar to those which have been published by Power and Caldwell.

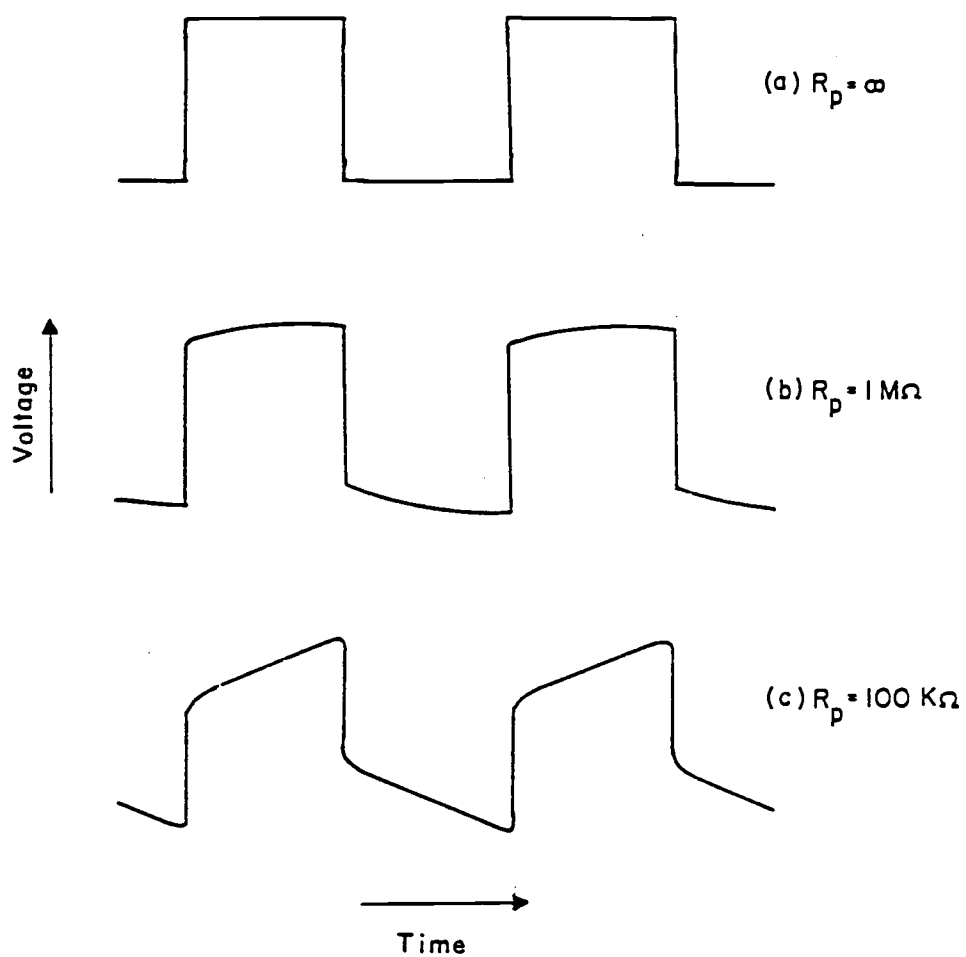


Figure B.6. Effect of R_p on the cell current when the applied potential is a triangular waveform

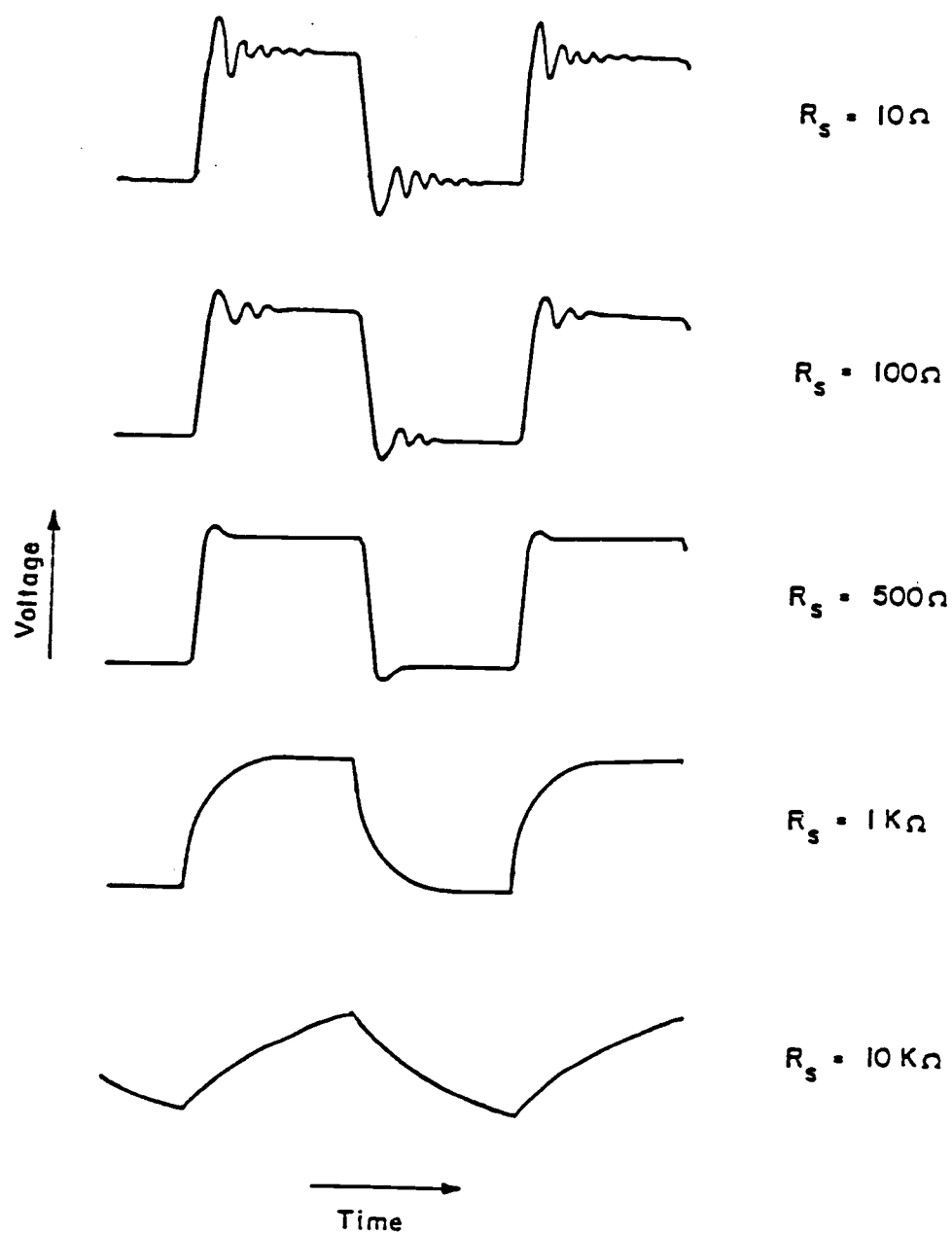


Figure B.7. Effect of R_s on the cell current when the applied potential is a triangular wave

The ringing effect drastically affects the accuracy of the measurement method described herein. When ringing becomes a serious problem in a double layer capacitance measurement, a small resistor can be placed in series with the electrochemical cell to reduce ringing without affecting the amplitude of the square wave.

The range of R_s in which a measurement can be made without error depends on the capacitance of the cell. This is illustrated in Table B.1.

The performance of the capacitance measurement system was evaluated by using hanging mercury drop, titanium and aluminum electrodes. In all cases, the double layer capacitance of the electrode interface was determined in 0.1 M KNO_3 solution. The results are shown in Figure B.8.

The values of capacitance obtained for mercury and the shape of the capacitance-voltage curve agrees well with previous work (73) by other workers. The dissimilarity in the shape of the capacitance - potential curves for mercury and two solid electrodes can be explained by considering the presence of oxide films on the metals.

The observed capacitance for a metal electrode with an oxide layer can be given by

$$\frac{1}{C_{\text{obs}}} = \frac{1}{C_{\text{ox}}} + \frac{1}{C_d}$$

where C_{ox} is the capacitance of the oxide layer and C_d is the capacitance of the double layer.

Table B.1. The Range of R_s in which Capacitance can be measured with in 10% error

frequency	measured capacitance	0.001 μF	0.1 μF	1 μF
100 HZ	lowest R_s	0 Ω	400 Ω	400 Ω
	highest R_s	300k Ω	7 k Ω	1 k Ω
500 HZ	lowest R_s	0 Ω	400 Ω	150 Ω
	highest R_s	100 k Ω	2.5 k Ω	250 Ω

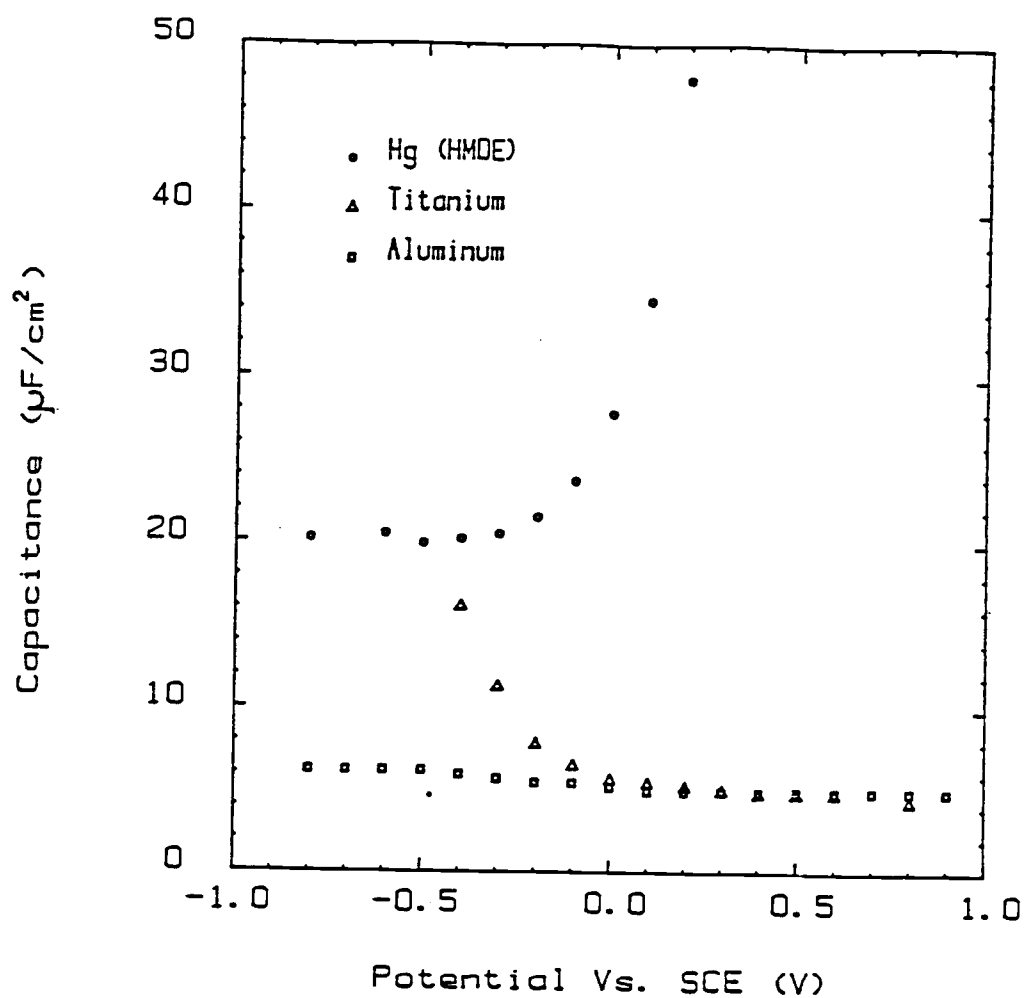


Figure B.8. Double layer capacitance measured at
(a) Hanging mercury drop electrode (HMDE)
(b) Titanium and (c) Aluminum electrodes
in 0.1 M KNO_3 solution.

The oxide capacitance is small compared to the electrical double layer capacitance. Thus, the measured capacitance is primarily that of the oxide film. The oxide film capacitance does not depend on the applied potential, and hence the observed capacitance. The thickness of the oxide on the metal electrodes calculated from the observed capacitance indicate a 20-30 Å oxide on titanium and a 10-15 Å oxide on aluminum electrodes.

Errors less than 10% in capacitance can be obtained only for capacitances above 10 nF. The expected capacitance for the Si/SiO₂/electrolyte interface ranges from 6-20 nF, which is in the same neighborhood as the limit of detection of the measurement method. Therefore, this method was not pursued further.

APPENDIX C : Program to acquire data from impedance measurements

```

10 REM PROGRAM TO OUTPUT A GIVEN VOLTAGE TO DAC
20 REM AND READ TWO CHANNELS OF THE A/D
30 REM
40 REM
50 GOSUB 500:REM DIMENSION
60 GOSUB 600:REM INPUT EXPTL DATA
70 GOSUB 700:REM SET UP DEFAULT VALUES
80 GOSUB 800:REM PROGRAM CONTROL PARAMETERS
90 GOSUB 900:REM POTENTIAL RANGES
500 REM DIMENSION
510 DIM T(150),X(150),Y(150)
520 DIM SX(150),SY(150),X1(50),Y1(50)
590 RETURN
600 REM INPUT EXPTL PARAMETERS
610 INPUT"IONIC STRENGTH";MU
620 INPUT"      PH      ";PH
630 INPUT"  FREQUENCY  ";F
640 INPUT"      DATE   ";D$
650 INPUT"      TIME   ";E$
690 RETURN
700 REM SET THE DEFAULT VALUES
710 VI=2:VF=-2:TM=1000:TI=20:TC=1
720 SD=1:FC=100:CM=400:CL=10
790 RETURN
800 REM PROGRAM CONTROL PARAMETERS
810 L1=248:L2=249:L3=245:L4=246
820 C1=240:C2=241
830 C5=40974
840 DR=10000:D0=-1
850 M1=16:M2=256:M3=4096
860 C4=25
870 POKE 250,C4
890 RETURN
900 REM SET POTENTIAL REGIONS
910 PRINT"ENTER POTENTIAL RANGES R1 THRU R6"
920 PRINT"SUCH THAT R1>R2>.....>R5>R6"
930 PRINT"FORMAT--R1,R2.....,R6"
940 INPUT R1,R2,R3,R4,R5,R6
950 R1=R1*1000:R2=R2*1000:R3=R3*1000
960 R4=R4*1000:R5=R5*1000:R6=R6*1000
990 RETURN
1000 REM CONTROL SUBROUTINES
1020 INPUT"*";A$
1040 IF A$="START" THEN GOTO 2000
1050 IF A$="PCP" THEN GOSUB 1200
1060 IF A$="CCP" THEN GOSUB 1400
1070 IF A$="STOP" THEN GOTO 9999
1080 IF A$="CONT" THEN GOTO 2300
1190 GOTO 1020
1200 REM PRINT CONTROL PARAMETERS
1210 PRINT"INITIAL POTENTIAL      (VI)";VI
1220 PRINT"FINAL POTENTIAL      (VF)";VF

```

```

1230 PRINT"MAX. TIME FOR EXPT          (TM)";TM
1240 PRINT"MAX. WAITING TIME          (TI)";TI
1250 PRINT"5*TIME CONSTANT            (TC)";TC
1260 PRINT"MAX. ALLOWED RSD            (SD)";SD
1270 PRINT"MAX. CHANGE IN POTENTIAL    (CM)";CM
1280 PRINT"MIN. CHANGE IN POTENTIAL    (CL)";CL
1290 PRINT"POTENTIAL REGIONS SET AT"
1300 PRINT R1,R2,R3,R4,R5,R6
1390 RETURN
1400 REM CHANGE CONTROL PARAMETERS
1410 PRINT"TYPE THE VARIABLE TO CHANGE OR (R) TO RETURN"
1420 INPUT A$
1430 IF A$="VI" THEN INPUT"INITIAL POTENTIAL          (VI)";VI
1440 IF A$="VF" THEN INPUT"FINAL POTENTIAL          (VF)";VF
1450 IF A$="TM" THEN INPUT"MAX. TIME FOR EXPT        (TM)";TM
1460 IF A$="TI" THEN INPUT"MAX. WAITING TIME        (TI)";TI
1470 IF A$="TC" THEN INPUT"5*TIME CONSTANT          (TC)";TC
1480 IF A$="FC" THEN INPUT"FIXED CHANGE IN POTENTIAL(FC)";FC
1490 IF A$="CM" THEN INPUT"MAX. CHANGE IN POTENTIAL (CM)";CM
1500 IF A$="CL" THEN INPUT"MIN. CHANGE IN POTENTIAL (CL)";CL
1510 IF A$="SD" THEN INPUT"MAX. ALLOWED RSD          (SD)";SD
1520 IF A$="REGN" THEN GOSUB 900
1530 IF A$="R" THEN RETURN
1590 GOTO 1420
2000 REM EXPERIMENT BEGINS HERE
2005 POKE 4,64;POKE 5,65:Q=USR(0)
2010 CV=VI*1000
2020 GOSUB 3000:REM FIND CORRECT 12-BIT VALUE FOR DAC
2040 GOSUB 3200:REM DAC OUTPUT
2060 INPUT"EXT. SIGNALS ON (Y/N)";A$
2080 IF A$="Y" THEN GOTO 2120
2100 GOTO 2060
2120 INPUT"IS CELL SELECTOR ON EXT. CELL";B$
2140 IF B$="Y" THEN GOTO 2180
2160 GOTO 2120
2180 REM
2200 REM DELAY
2210 FOR I=1 TO 100
2220 G=I
2240 NEXT I
2300 GOSUB 3400:REM START THE CLOCK
2320 PRINT"TIME      X(I)      SX(I)      Y(I)      SY(I)"
2350 GOSUB 3000:REM FIND CORRECT INPUT FOR THE DAC
2400 GOSUB 3200:REM OUTPUT DAC VOLTAGE
2420 REM DELAY
2430 FOR I=1 TO 50:G=I:NEXT I
2500 GOSUB 3800:REM READ TIME
2510 I=I+1:NP=NP+1:T(I)=TR
2600 GOSUB 4000:REM GOSUB ACQUIRE DATA
2650 GOSUB 4200:REM STD. DEVIATION
2660 IF S1<SD AND S2<SD THEN GOTO 2700
2670 I=I-1:NP=NP-1
2680 GOTO 2500
2700 REM

```

```

2700 REM
2710 PRINT T(I),X(I),SX(I),Y(I),SY(I)
2720 GOTO 2350
3000 REM SET THE NEXT BIAS VOLTAGE
3030 IF VI>VF THEN GOTO 3050
3040 IF VI<VF THEN GOTO 3080
3050 GOSUB 4500
3060 CV=CV-DV
3065 IF CV<VF GOTO 9000
3070 GOTO 3100
3080 GOSUB 4600
3090 CV=CV+DV
3095 IF CV>VF GOTO 9000
3100 REM CONVERT VOLTAGE TO A 12-BIT #
3110 NV=(M3/DR)*CV
3120 H=INT(NV/M2)
3130 L=NV-H*M2
3140 POKE L3,H:POKE L4,L
3150 POKE 4,32:POKE 5,65:Q=USR(0)
3190 RETURN
3200 REM OUTPUT DAC VOLTAGE
3210 POKE 4,96:POKE 5,64:Q=USR(0)
3290 RETURN
3400 REM START THE CLOCK
3410 POKE 4,0:POKE 5,64:Q=USR(0)
3490 RETURN
3800 REM READ TIME
3810 POKE C5,64
3820 TR=PEEK(C1)+M1*(PEEK(C2))
3830 POKE C5,192
3840 IF TR-INT(TR/CL)*CL THEN GOTO 3860
3850 GOTO 3800
3860 IF TR=D0 GOTO 3800
3880 D0=TR
3890 RETURN
4000 REM ACQUIRE DATA
4010 POKE 4,144:POKE 5,64:Q=USR(0)
4090 RETURN
4200 REM STD. DEVIATION
4210 B1=18944:B2=19200:B3=19456:B4=19712
4220 FOR J=1 TO N
4230 B1=B1+1:B2=B2+1:B3=B3+1:B4=B4+1
4240 X1(J)=(M1*PEEK(B1)+PEEK(B2)/M1)/409.6
4250 Y1(J)=(M1*PEEK(B3)+PEEK(B4)/M1)/409.6
4260 NEXT J
4270 X2=0:Y2=0
4280 FOR J=1 TO N
4290 X2=X2+X1(J)
4300 Y2=Y2+Y1(J)
4310 XX=X2/N
4320 YY=Y2/N
4330 VX=0:VY=0

```

```

4340 FOR J=1 TO N
4350 VX=VX+(XX-X1(J))*(XX-X1(J))/(N-1)
4360 VY=VY+(YY-Y1(J))*(YY-Y1(J))/(N-1)
4370 NEXT J
4380 X(I)=XX: SX(I)=VX
4390 Y(I)=YY: SY(I)=VY
4490 RETURN
4500 REM POTENTIAL DECREMENT
4520 IF CV<R1 THEN GOTO 4800
4530 IF CV<R2 THEN GOTO 4830
4540 IF CV<R3 THEN GOTO 4860
4550 IF CV<R4 THEN GOTO 4890
4560 IF CV<R5 THEN GOTO 4920
4570 IF CV<R6 THEN GOTO 4950
4580 PRINT"ALL RANGES FAILED":RETURN
4600 REM POTENTIAL INCREMENT
4620 IF CV<R6 THEN GOTO 4950
4630 IF CV<R5 THEN GOTO 4920
4640 IF CV<R4 THEN GOTO 4890
4650 IF CV<R3 THEN GOTO 4860

4660 IF CV<R2 THEN GOTO 4830
4670 IF CV<R2 THEN GOTO 4800
4680 PRINT"ALL RANGES FAILED";RETURN
4800 DV=200
4810 RETURN
4830 DV=100
4840 RETURN
4860 DV=25
4870 RETURN
4890 DV=10
4900 RETURN
4920 DV=50
4930 RETURN
4950 DV=100
4960 RETURN
9000 PRINT"VOLTAGE EXCEEDED THE INTENDED FINAL VALUE"

```

4000 A9 LDA #40
4002 8D STA A00B
4005 A9 LDA #4E
4007 8D STA A004
400A A9 LDA #C3
400C 8D STA A005
400F A9 LDA #00
4011 85 STA F0
4013 85 STA F1
4015 85 STA F2
4017 85 STA F3
4019 A9 LDA #14
401B 85 STA F4
401D A9 LDA #30
401F 8D STA A400
4022 A9 LDA #40
4024 8D STA A401
4027 A9 LDA #C0
4029 8D STA A00E
402C 58 CLI
402D 60 RTS

4030 48 PHA
4031 AD LDA A004
4034 C6 DEC F4
4036 D0 BNE 404A
4038 A9 LDA #14
403A 85 STA F4
403C E6 INC F0
403E D0 BNE 404A
4040 E6 INC F1
4042 D0 BNE 404A
4044 E6 INC F2
4046 D0 BNE 404A
4048 E6 INC F3
404A 68 PLA
404B 40 RTI

4060 A9 LDA #CA
4062 8D STA A00C
4065 A9 LDA #FF
4067 8D STA A002
406A 8D STA A003
406D A5 LDA F8
406F 8D STA A000
4072 A5 LDA F9
4074 8D STA A001
4077 A2 LDX #FF
4079 CA DEX
407A D0 BNE 4079
407C 60 RTS

```
4090 A9 LDA #00
4092 8D STA A002
4095 A9 LDA #FF
4097 8D STA A003
409A A2 LDX #E4
409C 8E STX A00C
409F EA NOP
40A0 A2 LDX #00
40A2 86 STX E0
40A4 86 STX E2
40A6 86 STX E4
40A8 86 STX E6
40AA EA NOP
40AB EA NOP
40AC EA NOP
40AD A2 LDX #4A
40AF 86 STX E1
40B1 E8 INX
40B2 86 STX E3
40B4 E8 INX
40B5 86 STX E5
40B7 E8 INX
40B8 86 STX E7
40BA A4 LDY FA
40BC A2 LDX #01
40BE 8E STX A001
40C1 A2 LDX #50
40C3 CA DEX
40C4 D0 BNE 40C3
40C6 EA NOP
40C7 20 JSR 4100
40CA EA NOP
40CB A2 LDX #09
40CD AD LDA A000
40D0 91 STA (E0),Y
40D2 8E STX A001
40D5 AD LDA A000
40D8 91 STA (E2),Y
40DA EA NOP
40DB EA NOP
40DC A2 LDX #03
40DE 8E STX A001
40E1 A2 LDX #50
40E3 CA DEX
40E4 D0 BNE 40E3
40E6 EA NOP
```

```

40E7 20 JSR 4100
40EA EA NOP
40EB A2 LDX #0B
40ED AD LDA A000
40F0 91 STA (E4),Y
40F2 8E STX A001
40F5 AD LDA A000
40F8 91 STA (E6),Y
40FA 88 DEY
40FB D0 BNE 40BC
40FD 60 RTS
40FE 00 BRK
40FF EA NOP
4100 A2 LDX #E4
4102 8E STX A00C
4105 A2 LDX #C4
4107 8E STX A00C
410A A2 LDX #E4
410C 8E STX A00C
410F A9 LDA #10
4111 2C BIT A00D
4114 F0 BEQ 4111
4116 60 RTS

```

```

4120 A5 LDA F5
4122 0A ASL .A
4123 0A ASL .A
4124 0A ASL .A
4125 0A ASL .A
4126 85 STA F7
4128 A5 LDA F6
412A 4A LSR .A
412B 4A LSR .A
412C 4A LSR .A
412D 4A LSR .A
412E 45 EOR F7
4130 85 STA F8
4132 A5 LDA F6
4134 0A ASL .A
4135 0A ASL .A
4136 0A ASL .A
4137 0A ASL .A
4138 85 STA F9
413A 60 RTS

```

```

4140 A2 LDX #4A
4142 86 STX FF
4144 A0 LDY #00
4146 84 STY FE
4148 A9 LDA #00
414A 91 STA (FE),Y
414C C8 INY
414D D0 BNE 414A
414F E8 INX
4150 E0 CPX #4E
4152 D0 BNE 4142
4154 60 RTS

```


**APPENDIX D : Serial inter-computer data transfer via 20 mA
current loop**

Figure D.1 illustrates the circuit required for inter-computer serial data communication via 20 mA current loop. In this procedure, the interfacing circuit simulates a situation where each computer is communicating with a terminal. When computer 1 sends data, the logic state at point U1 becomes HIGH or LO depending on the bit pattern of the data, causing transistor Q1 to turn ON or OFF accordingly. Accordingly, point S1 becomes LO or HIGH. Since S1 is connected to the point T2 of computer 2, the transistor Q2 becomes OFF or ON causing a LO or HIGH logic level at the PB6 input of the 6522 in computer 2. Table D.1 summarizes the logic levels at different key points in the circuit.

**TABLE D.1: Logic States at different points of the
20 mA current loop serial communication
interface**

PB2(1)	U1	S1	T2	PB6(2)
HI	LO	HI	HI	HI
LO	HI	LO	LO	LO

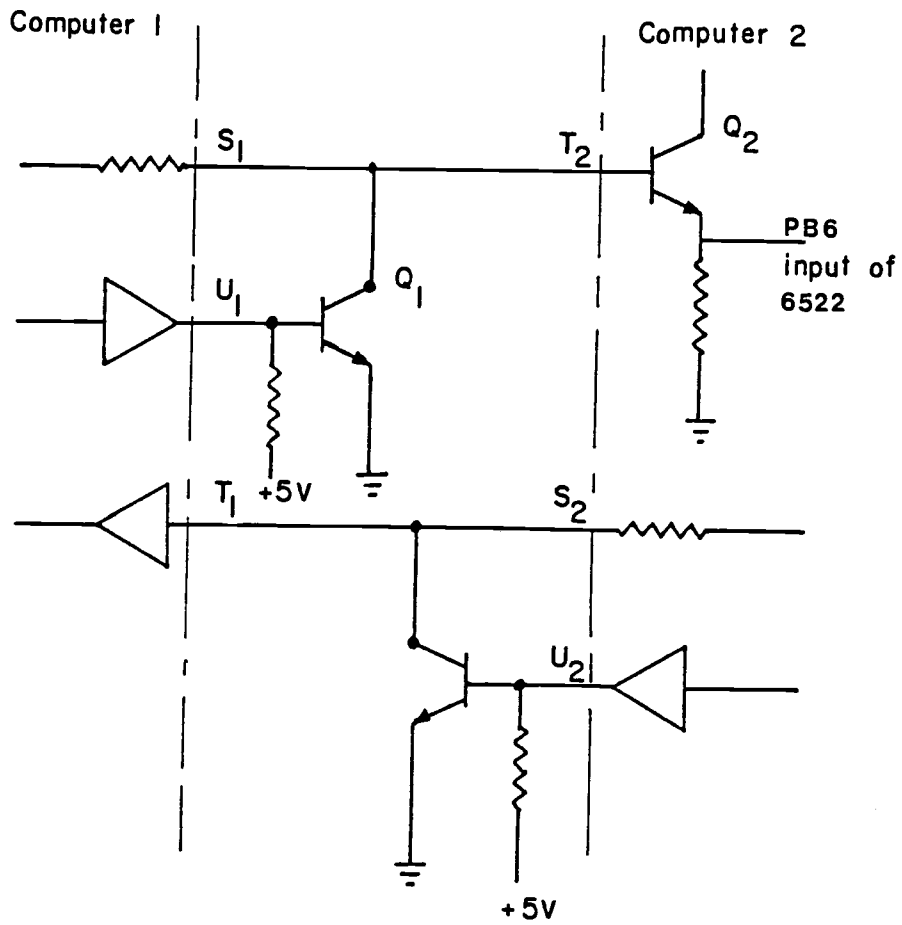


Figure D.1. Circuit for inter-computer serial data communication

**APPENDIX E : Program to compute resistance and capacitance from
in-phase and out-of-phase components of the cell current**

```

      REM AC IMPEDANCE analysis of EOS systems

      REM From in-phase and out-of phase component
      REM of the cell current R & C of the cell is
      REM is calculated using either SERIES or PARALLEL
      REM circuit model.
      REM Also calculate Mott-Schottky plots

10      REM Main Program
      PI=3.141592654

      GOSUB 100:REM DIMENSION
20      GOSUB 200:REM READ DATA
      GOSUB 300:REM CORRECT UNITS
      GOSUB 400:REM CALCULATE 1/ZF
      GOSUB 500:REM CALCULATE Z(CELL)
      GOSUB 600:REM SERIES CIRCUIT
      GOSUB 700:REM PARALLEL CIRCUIT
      GOSUB 800:REM OTHER USEFUL QUANTITIES
      GOSUB 900:REM BUILD 2-D DATA ARRAY
      PRINT:PRINT
      INPUT"NEED C-V TYPE PLOTS";A$
      IF A$="N" THEN GOTO 40
      PRINT"CREATE X-Y FILES FOR C-V TYPE PLOTS"
      GOSUB 1000:REM CREATE X-Y FILES
      PRINT:PRINT
40      INPUT"NEED MOTT-SCHOTTKY PLOTS";A$
      IF A$="N" THEN GOTO 80
      GOSUB 2000:REM MOTT-SCHOTTKY PLOTS
80      INPUT"NEED ANOTHER SET OF DATA";A$
      IF A$="Y" THEN GOTO 20
      STOP

100     REM DIMENSION
      DIM RZ(50),IZ(50),EB(50),X(50),Y(50)
      DIM RY(50),IY(50),SR(50),SC(50),PR(50),PC(50)
      DIM XS(50),XP(50),QS(50),QP(50)
      DIM RZC(50),IZC(50),AD(50,15)
      RETURN

200     REM READ DATA
      INPUT"FILE NAME";NAME$
      FILE NAME$
      IF END1 THEN GOTO 250
      READ#1;EIN
      READ#1;F
      READ#1;RF
      READ#1;CS
      READ#1;CF
      READ#1;M
      FOR I=1 TO M
      READ#1;EB(I),X(I),Y(I)
      NEXT I
      PRINT"DATA READ IN"
250     PRINT"END OF FILE"
      CLOSE 1
      RETURN

```

```

300      REM CONVERSION OF UNITS
        E0=EIN*10000/10600
        CS=CS*1E-9:CF=CF*1E-9
        W=2*PI*F
        RETURN

400      REM CALCULATE 1/ZF
        I=4:K=6:RZ(I)=RF:IZ(I)=0
        GOSUB 9350:REM INVERSE
        I=5:K=7:RZ(I)=0:IZ(I)=-1/(W*CF)
        GOSUB 9350:REM INVERSE
        I=6:J=I+1:K=J+1:GOSUB 9000:REM ADD
        RZF=RZ(K):IZF=IZ(K)
        RETURN

500      REM CALCULATE Z(CELL)
        FOR N=1 TO M
          I=N:J=N+1:K=J+1
          RZ(I)=RZF:IZ(I)=IZF
          RZ(J)=X(N):IZ(J)=Y(N)
          GOSUB 9100:REM MULTIPLY E(OUT)*1/ZF
          RA=RZ(K)/E0
          IA=IZ(K)/E0

550      REM 1/Z(CELL) = 1/ZA - 1/Z(STRAY)
          RZ(I)=0:IZ(I)=-1/(W*CS)
          GOSUB 9350:REM INVERSE
          RSTINV=RZ(K):ISTINV=IZ(K)
          RZ(I)=RA:IZ(I)=IA
          RZ(J)=RSTINV:IZ(J)=ISTINV
          GOSUB 9050:REM SUBTRACT
          RY(N)=RZ(K)
          IY(N)=IZ(K)
          REM CELL IMPEDANCE
          RZ(I)=RY(N):IZ(I)=IY(N)
          GOSUB 9350:REM INVERSE
          RZC(N)=RZ(K)
          IZC(N)=IZ(K)
        NEXT N
        RETURN

600      REM SERIES CIRCUIT
        FOR N=1 TO M
          RZ(I)=RY(N):IZ(I)=IY(N)
          GOSUB 9350:REM INVERSE
          SR(N)=RZ(K)
          SC(N)=-1/(W*IZ(K))
        NEXT N
        RETURN

```

```

700      REM PARALLEL CIRCUIT
      FOR N=1 TO M
      PR(N)=1/RX(N)
      PC(N)=IY(N)/W
      NEXT N
      RETURN

800      REM CALCULATE OTHER QUANTITIES
      FOR N=1 TO M
      XS(N)=1/(W*SC(N))
      XP(N)=1/(W*PC(N))
      QS(N)=XS(N)/SR(N)
      QP(N)=XP(N)/PR(N)
      NEXT N
      RETURN

900      REM BUILD UP THE 2-D ARRAY
      FOR I=1 TO M
      AD(I,1)=EB(I):AD(I,2)=SC(I):AD(I,3)=PC(I)
      AD(I,4)=SR(I):AD(I,5)=PR(I):AD(I,6)=XS(I)
      AD(I,7)=XP(I):AD(I,8)=QS(I):AD(I,9)=QP(I)
      AD(I,10)=RY(I):AD(I,11)=IY(I)/W
      AD(I,12)=RZC(I):AD(I,13)=IZC(I)
      NEXT I
      RETURN

9000     REM ADD SUBROUTINE
      RZ(K)=RZ(I)+RZ(J)
      IZ(K)=IZ(I)+IZ(J)
      RETURN

9050     REM SUBTRACT SUBROUTINE
      RZ(K)=RZ(I)-RZ(J)
      IZ(K)=IZ(I)-IZ(J)
      RETURN

9100     REM MULTIPLY SUBROUTINE
      RZ(K)=(RZ(I)*RZ(J)-IZ(I)*IZ(J))
      IZ(K)=(RZ(I)*IZ(J)+RZ(J)*IZ(I))
      RETURN

9200     REM DIVIDE SUBROUTINE
      D=(RZ(J)*RZ(J)+IZ(J)*IZ(J))
      RZ(K)=(RZ(I)*RZ(J)+IZ(I)*IZ(J))/D
      IZ(K)=(IZ(I)*RZ(J)-RZ(I)*IZ(J))/D
      RETURN

9350     REM INVERSE SUBROUTINE
      D=RZ(I)*RZ(I)+IZ(I)*IZ(I)
      RZ(K)=RZ(I)/D
      IZ(K)=-IZ(I)/D
      RETURN

```

```

1000    REM SUBROUTINE TO CREATE AN X-Y ARRAY

1150    GOSUB 1200:REM SELECT X & Y
        GOSUB 1300:REM BUILD XY ARRAY
        GOSUB 1400:REM STORE XY ARRAY
        INPUT"NEED MORE XY FILES FROM SAME DATA-(Y/N)";C$
        IF C$="Y" THEN GOTO 1150
        RETURN

1200    REM SELECT X & Y
        PRINT"DEFINE THE X-Y VARIABLES"
        PRINT:INPUT"X-AXIS VARIABLE";A$
        INPUT"Y AXIS VARIABLE";B$

1250    REM SELECT X
        IF A$="EB" THEN J=1
        IF A$="SC" THEN J=2
        IF A$="PC" THEN J=3
        IF A$="SR" THEN J=4
        IF A$="PR" THEN J=5
        IF A$="XS" THEN J=6
        IF A$="XP" THEN J=7
        IF A$="QS" THEN J=8
        IF A$="QP" THEN J=9
        IF A$="RY" THEN J=10
        IF A$="IY" THEN J=11
        IF A$="RZC" THEN J=12
        IF A$="IZC" THEN J=13

1275    REM SELECT Y
        IF B$="SC" THEN K=2
        IF B$="PC" THEN K=3
        IF B$="SR" THEN K=4
        IF B$="PR" THEN K=5
        IF B$="XS" THEN K=6
        IF B$="XP" THEN K=7
        IF B$="QS" THEN K=8
        IF B$="QP" THEN K=9
        IF B$="RY" THEN K=10
        IF B$="IY" THEN K=11
        IF B$="RZC" THEN K=12
        IF B$="IZC" THEN K=13
        RETURN

1300    REM BUILD XY ARRAY
        FOR I=1 TO M
            X(I)=AD(I,J)
            Y(I)=AD(I,K)
        NEXT I
        RETURN

```

```

1400  REM STORE XY ARRAY
      INPUT "TITLE OF THE PLOT-LINE1";TITL1$
      INPUT "TITLE OF THE PLOT-LINE2";TITL2$
      XV$="EB VS. SCE (V)"
      YV$="C (F)"
      PRINT
      PRINT "FILE NAMING FORMAT"
      PRINT
      PRINT "(XVAR)(YVAR)(P#)(CHIP#)"
      PRINT:INPUT "NAME OF THE XY FILE";NAM$
      FILE NAM$
      PRINT#1;TITL1$
      PRINT#1;TITL2$
      PRINT#1;XV$
      PRINT#1;YV$
      FOR I=1 TO M
      PRINT#1:X(I),Y(I)
      NEXT I
      PRINT "XY DATA STORED IN  ";:PRINT NAM$
      CLOSE 1
      RETURN

2000  REM MOTT-SCHOTTKY PLOTS
      REM CALCULATE V(FB) AND DOPING DENSITY
      INPUT "OXIDE CAPACITANCE";CO
      REM MAIN PROGRAM
      GOSUB 3000:REM BUILD X-Y ARRAY
      GOSUB 4000:REM LINEAR REGRESSION ROUTINE
      GOSUB 5000:REM CREATE NEW FILES
      RETURN

3000  REM BUILD X-Y ARRAY
      PRINT "WHAT CAPACITANCE DO YOU WANT TO PLOT"
      PRINT "THE CHOICES ARE THE FOLLOWING"
      PRINT "1. IY   2. SC   3. PC"
      INPUT A$
      IF A$="IY" THEN GOTO 3200
      IF A$="SC" THEN GOTO 3400
      IF A$="PC" THEN GOTO 3600
      INPUT "TYPE 1 TO TRY AGAIN OR ELSE 0";B$
      IF B$="1" THEN GOTO 3000
      IF B$="0" THEN GOTO 3800

3200  REM IMAGINARY ADMITTANCE
      FOR I=1 TO M
      YI=AD(I,11)
      YI=CO/YI
      Y(I)=YI*YI
      NEXT I
      GOTO 3800

```

```

3400  REM SERIES CAPACITANCE
      FOR I=1 TO M
      CS=AD(I,2)
      Y(I)=CO/CS
      Y(I)=Y(I)*Y(I)
      NEXT I
      GOTO 3300

3500  REM PARALLEL CAPACITANCE
      FOR I=1 TO M
      CP=AD(I,3)
      Y(I)=CO/CP
      Y(I)=Y(I)*Y(I)
      NEXT I

3600  FOR I=1 TO M
      EB(I)=AD(I,1)
      X(I)=EB(I)
      NEXT I
      RETURN

4000  REM LINEAR REGRESSION
      PRINT"SELECT THE SPAN OF POINTS TO BE FITTED"
      INPUT"FIRST POINT";K
      INPUT"LAST POINT ";L
      SS=0:YS=0: SX=0:SY=0:SP=0
      M1=L-K+1
      FOR I=K TO L
      SX=SX+X(I):SY=SY+Y(I)
      SS=SS+X(I)*X(I):YS=YS+Y(I)*Y(I)
      SP=SP+X(I)*Y(I)
      NEXT I
      YA=SY/M1
      A=((SX*SP)-(SS*SY))/(SX*SX-M1*SS)
      B=((SX*SY)-M1*SP)/(SX*SX-M1*SS)
      D=YS-A*SY-B*SP
      SE=SQR(D/(M-2))
      REM CORRELATION COEFF
      SD=0:DA=0
      FOR I=K TO L
      SD=SD+(Y(I)-(A+B*X(I)))*(Y(I)-(A+B*X(I)))
      DA=DA+(Y(I)-AY)*(Y(I)-AY)
      NEXT I
      A1=-A/B
      R2=1-(SD/DA)
      PRINT"SLOPE= ";B;:PRINT TAB(30);:PRINT"INTERCEPT= ";A
      PRINT"CORRELATION COEFFICIENT= ";R2
      PRINT
      PRINT"      X-INTERCEPT = ";A1
      INPUT"NEED TO EXAMINE ANOTHER SPAN(Y/N)";B$
      IF B$="Y" THEN GOTO 4000
      RETURN

```



```
5000 REM CREATE NEW FILES
PRINT "SPAN OF POINTS WHICH M-S PLOT IS LINEAR"
INPUT "FIRST POINT";K
INPUT "LAST POINT ";L
INPUT "FILE NAME FOR M-S PLOT";N$
FILE N$
INPUT "FIRST TITLE LINE";TIT1$
INPUT "SECOND TITLE LINE";TIT2$
XV$="EB VS. SCE (V)"
YV$="(CO/C)**2"
PRINT#1;TIT1$
PRINT#1;TIT2$
PRINT#1;XV$
PRINT#1;YV$
FOR I=K TO L
PRINT#1;X(I),Y(I)
NEXT I
CLOSE 1
PRINT "NEW FILE STORED"
INPUT "NEED TO STORE ANOTHER SPAN OF POINTS";C$
IF C$="Y" THEN GOTO 5000
RETURN
```

APPENDIX F : Calculation of titration curves

Titration curves are simulated for the following three cases of possible contaminants.

- (1) Strong acid
- (2) weak acid (monoprotic)
- (3) weak acid (diprotic)

The procedure of simulation is the same for all three cases. First, the H^+ concentration is calculated and then the electrode response is calculated from the Nernst equation. The calculation of H^+ is different for three cases.

The following variables are common for all three cases.

C_o	= concentration of the residual acid.
V_o	= initial volume of the electrolyte solution
V_A, V_B	= volume of the titrant acid or base.
C_A, C_B	= concentration of the titrant acid or base
T_H, T_{OH}	= total concentration of H^+ and OH^-
V_T	= total volume = $(V_o + V_A + V_B)$
T_A	= $C_o V_o / V_T$

Strong acid

$$T_H = (C_A V_A + C_O V_O - C_B V_B) / V_T$$

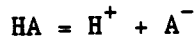
If $T_H > 0$ then $[H^+] = T_H$

If $T_H < 0$ then $T_{OH} = -T_H$

and $[H^+] = K_W / T_{OH}$

Monoprotic acid

Equilibrium reaction for dissociation of the acid can be written as follows.



Law of mass action yields:

$$[H^+] [A^-] = K_1 [HA] \quad F.1$$

Material balance gives:

$$[A^-] + [HA] = T_A \quad F.2$$

From charge neutrality in solution:

$$[H^+] + C_B V_B / V_T - [A^-] - [OH^-] - C_A V_A / V_T = 0 \quad F.3$$

By considering ionization of water one can write

$$[H^+] [OH^-] = K_W \quad F.4$$

Unknowns in Equations F.1 through F.4 are $[H^+]$, $[OH^-]$, $[HA]$ and $[A^-]$. Therefore, these equations can be solved for $[H^+]$.

These equations can be reduced to the following form.

$$A [H^+]^3 + B [H^+]^2 + C [H^+] + D = 0 \quad F.5$$

Where $A = 1$

$$B = (C_B V_B / V_T + K_1 - C_A V_A / V_T)$$

$$C = (K_1 C_B V_B / V_T - K_1 T_A - K_w - K_1 C_A V_A / V_T)$$

$$D = -K_w K_1$$

The cubic equation is solved using Newton's method for approximate solution of numerical equations as given at the end of this appendix.

Diprotic weak acid

The following equilibrium reactions can be written for the dissociation of the diprotic acid.



From the law of mass action:

$$[H^+][HA^-] = K_1[H_2A] \quad F.8$$

$$[H^+][A^{2-}] = K_2[HA^-] \quad F.9$$

Material balance requires:

$$[H_2A] + [HA^-] + [A^{2-}] = T_A \quad F.10$$

Charge balance in the solution yields:

$$[H^+] + C_B V_B / V_T - [OH^-] - [HA^-] - 2[A^{2-}] - C_A V_A / V_T = 0 \quad F.11$$

The unknown in Equations F.8-F.11 and D.4 above are $[H^+]$, $[OH^-]$, $[A^{2-}]$, $[HA^-]$, and $[H_2A]$. These five equations can be reduced to the form

$$A[H^+]^4 + B[H^+]^3 + C[H^+]^2 + D[H^+] + E = 0 \quad F.12$$

where $A = 1$

$$B = K_1 + C_B V_B / V_T - C_A V_A / V_T$$

$$C = (K_1 K_2 + K_1 C_B V_B / V_T - K_w - K_1 T_A - K_1 C_A V_A / V_T)$$

$$D = K_1 K_2 C_B V_B / V_T - K_w K_1 - 2K_1 K_2 T_A - K_1 K_2 C_A V_A / V_T$$

$$E = -K_w K_1 K_2$$

Newton's method for the iterative solution of numerical equations

Consider an equation of the form

$$y = f(x) = Ax^n + Bx^{n-1} + Cx^{n-2} + \dots = 0 \quad F.12$$

These are n roots to this equation. Let r be the desired root of the equation.

$$\text{i.e., } Ar^n + Br^{n-1} + Cr^{n-2} + \dots = 0 \quad F.13$$

Guess a value v near r such that

$$r = v + h \quad F.14$$

From Taylor's theorem

$$f(v+h) = f(v) + hf'(v) + h^2 f''(v)/2! + \dots \quad F.15$$

Since $f(v+h) = f(r) = 0$, neglecting higher powers of h ,

$$h = -f(v)/f'(v) \quad F.16$$

After guessing the value v , $f(v)$ and $f'(v)$ and hence h can be calculated. A new value for v can be guessed as

$$v_{\text{new}} = v_{\text{old}} + h \quad F.17$$

Using a computer program, this process can be continued until h becomes very small.

The equations for chemical equilibrium have one real positive root. Therefore if a provision is made in the iteration scheme for avoiding convergence to a negative root, the one physically meaningful root is easily found.

**APPENDIX G : Program to subtract titration curves by cubic spline
smoothing method**

```

REM UPDATED ON 06/30/85
REM PROGRAM CHASPL
REM CUBIC SPLINES ON BLANK
REM CALCULATE DELTA U FOR A GIVEN E VALUE
REM SELECTED FROM SAMPLE CURVE
F=96487
GOSUB 100:REM DIMENSION
GOSUB 200:REM READ INPUT INFO
NPTS=N:NF=N
GOSUB 4000:REM CORRECT E FOR EJ
GOSUB 300:REM FORMAT DATA
GOSUB 500:REM CALCULATE SPLINES
GOSUB 1500:REM CALCULATE A,B,C,D
GOSUB 200:REM READ FILE FOR INTERPOLATION
NPTS=N
GOSUB 4000:REM CORRECT FOR EJ
GOSUB 2100:REM FORMAT
GOSUB 2200:REM INTERPOLATE
GOSUB 3000:REM CALCULATE TH AND REH
GOSUB 3500:REM STORE RESULTS
INPUT"NEED TO CHECK THE CUBIC FIT";A$
IF A$="N" THEN GOTO 99
GOSUB 7000:REM CALCULATE CUBIC POLYNOMIAL FOR CHECKING
99  STOP

100  REM DIMENSION
    DIM A(100,4),X(100),Y(100),S(100)
    DIM A1(100),B1(100),C1(100),D1(100)
    DIM XX(100),YY(100)
    DIM U(100),DU(100)
    DIM PH(100),E(100),TH(100),REH(100)
    DIM XE(100),FUNC(100),H(100)
    DIM REOH(100),TOH(100),SS(100)
    DIM KW(100),GAMH(100)
    RETURN
200  REM INPUT DATA
    INPUT"FILE NAME";NAME$
    FILE NAME$
    READ#1;DATE$
    READ#1;TIME$
    READ#1;ACID$
    READ#1;BASE$
    READ#1;MED$
    READ#1;FLAG
    READ#1;CONC
    READ#1;VOL
    READ#1;V0
    READ#1;TITL1$
    READ#1;TITL2$
    READ#1;XV$
    READ#1;YV$
    N=0

```

```

      FOR I=1 TO 100
      READ#1;TT,U(I),E(I),EK
      N=N+1
      IF END #1 THEN 250
      NEXT I
250   CLOSE 1
      RETURN

300   REM FORMAT DATA
      FOR I=1 TO NP
      X(I)=U(I)
      Y(I)=E(I)
      NEXT I
      RETURN

500   REM CALCULATE
      NM2=N-2
      NM1=N-1
      DX1=X(2)-X(1)
      DY1=(Y(2)-Y(1))*6/DX1
      FOR I=1 TO NM2
      DX2=X(I+2)-X(I+1)
      DY2=(Y(I+2)-Y(I+1))*6/DX2
      A(I,1)=DX1
      A(I,2)=2*(DX1+DX2)
      A(I,3)=DX2
      A(I,4)=DY2-DY1
      DX1=DX2
      DY1=DY2
      NEXT I
      IEND=1

600   FOR I=1 TO NM2
      A(I,2)=A(I,2)-(A(I,1)*A(I-1,3))/A(I-1,2)
      A(I,4)=A(I,4)-(A(I,1)*A(I-1,4))/A(I-1,2)
      NEXT I
      A(NM2,4)=A(NM2,4)/A(NM2,2)

      FOR I=2 TO NM2
      J=NM1-I
      A(J,4)=(A(J,4)-A(J,3)*A(J+1,4))/A(J,2)
      NEXT I

      FOR I=1 TO NM2
      S(I+1)=A(I,4)
      NEXT I

700   REM TYPE 1
      S(1)=0
      S(N)=0
      RETURN

```



```

1500  REM CALC. A,B,C,D
      FOR I=1 TO N
      H(I)=X(I+1)-X(I)
      A1(I)=(S(I+1)-S(I))/(6*H(I))
      B1(I)=S(I)/2
      C1(I)=(Y(I+1)-Y(I))/H(I)-(2*H(I)*S(I)+H(I)*S(I+1))/6
      D1(I)=Y(I)
      NEXT I
      RETURN

2100  REM FORMAT DATA
      FOR J=1 TO NPTS
      XX(J)=V(J)
      NEXT J
      RETURN

2200  REM SELECT RANGE OF DATA
      YMIN=Y(1):YMAX=Y(N)
      FOR J=1 TO NP
      IF Y(J)<YMIN THEN YMIN=Y(J)
      IF Y(J)>YMAX THEN YMAX=Y(J)
      NEXT J
      K=1:L=N
      FOR J=1 TO N
      IF E(J)<YMIN THEN K=K+1
      IF E(J)>YMAX THEN L=L-1
      NEXT J
      I=1
      FOR J=K TO L
2300  I=I+1
      IF I>N-1 THEN GOTO 2350
      IF FLAG=0 THEN GOTO 2325
      IF E(J)=Y(I) THEN GOTO 2300
      GOTO 2350
2325  IF E(J)<=Y(I) THEN GOTO 2300
2350  I=I-1
      GOSUB 5000:REM SOLVE
      V(J)=XXNEW
      DV(J)=XX(J)-V(J)
      GOSUB 5600:REM FIND ERROR IN SIGMA

      I=1
      NEXT J
      RETURN

3000  REM CALCULATE CHARGE
      PRINT
      INPUT"SLOPE AND E0 OF GLASS ELECTRODE";SL,E0
      INPUT"OFFSET";OFFSET
      PRINT
PRINT"  PH          TOT. H+          H+          EXCESS"
      PRINT

```

```

FOR J=K TO L
PH(J)=(E0-E(J))/SL
REH(J)=10^(-PH(J))
REH(J)=REH(J)/GAMH(J)
REOH(J)=KW(J)/REH(J)
EXCESS=DV(J)*CONC/(ABS(V(J))+V0+VOL)
EXCESS=EXCESS-OFFSET
TH(J)=REH(J)-REOH(J)-EXCESS
PRINT PH(J),TH(J),REH(J),-EXCESS
NEXT J
RETURN
3500 REM STORE FILE
INPUT"FILE NAME FOR PCE FILES";NA$
FILE NA$
PRINT#1;TITL1$
PRINT#1;TITL2$
PRINT#1;XV$
PRINT#1;YV$
FOR J=K TO L
PRINT#1;PH(J),TH(J),REH(J),-(REH(J)-REOH(J)-TH(J))
NEXT J
CLOSE 1
RETURN

4000 REM SUBROUTINE FOR JNC.POTENTIAL CALCULATION
REM SET PARAMETERS
R=8.314:F=96487:T=298
KW0=1.01E-14
REM DEBYE-HUCKEL
AA=0.5115:B=0.3291
ANA=4:AK=3:ANO=3:AH=9:AOH=3
UK=7.319E-4:UNA=5.193E-4
UNO=7.404E-4:UH=3.625E-3:UOH=2.05E-3
REM INITIALIZE PARAMETERS
CK0=0:CNA0=0:CNO0=0
CKADD=0:CNADD=0:CNOADD=0
VTOT=0

REM INPUT INFORMATION
INPUT"(N)OH or (K)OH";TITR$
4005 PRINT:INPUT"Electrolyte (N)OH or (K)OH";ELEC$
PRINT:INPUT"Concentration of Electrolyte";CELEC
PRINT:PRINT
INPUT"Ref. Electrode solution (N)OH or (K)OH";REF$
INPUT"Cons. of Reference solution";CREF
REM SET EXPTL CONSTANTS
IF ELEC$="N" THEN CNA0=CELEC
IF ELEC$="K" THEN CK0=CELEC

```

```

      REM BEGINING OF CALCULATIONS

      KW(1)=KW0
      PRINT
      FOR I=1 TO NPTS
      GOSUB 4100:REM CALCULATES C(I)
      GOSUB 4200:REM CALCULATE MU(I)
      GOSUB 4300:REM CALCULATE ACTIVITIES AC(I)
      GOSUB 4400:REM RECALCULATE
      GOSUB 4500:REM CALCULATE JNK.POTENTIAL EJ(I)
      NEXT I
      RETURN
4100  REM CALCULATE CONCENTRATIONS

      CNOADD=0
      CKADD=0:CNADD=0
      IF V(I)<0 THEN GOTO 4105
      IF TITR$="K" THEN CKADD=CONC
      IF TITR$="N" THEN CNADD=CONC
      GOTO 4110
4105  CNOADD=CONC
4110  REM
      VTOT=V0+VOL+ABS(V(I))
      CK=(CK0*V0+CKADD*ABS(V(I)))/VTOT
      CNA=(CNA0*V0+CNADD*ABS(V(I)))/VTOT
      CNO=(CELEC*V0+CNOADD*ABS(V(I)))/VTOT
      IF V(I)<0 THEN GOTO 4125
      IF ABS(V(I))=0 THEN V(I)=1E-3
      COH=CONC*ABS(V(I))/VTOT
      CH=KW(I)/COH
      GOTO 4150
4125  IF ABS(V(I))=0 THEN V(I)=1E-3
      CH=CONC*ABS(V(I))/VTOT
      COH=KW(I)/CH

4150  RETURN
4200  REM CALCULATE MU
      MU=(CH+COH+CK+CNA+CNO)/2
      RETURN
4300  REM CALCULATE ACTIVITY COEFF
      NUM=-AA*SQR(MU)
      GMOH=NUM/(1+B*AOH*SQR(MU))
      GMH=NUM/(1+B*AH*SQR(MU))
      GMNA=NUM/(1+B*ANA*SQR(MU))
      GMK=NUM/(1+B*AK*SQR(MU))
      GMNO=NUM/(1+B*ANO*SQR(MU))
      GMH=10^GMH:GMOH=10^GMOH:GMNA=10^GMNA
      GMK=10^GMK:GMNO=10^GMNO
      ACH=CH*GMH:ACOH=COH*GMOH:ACNO=CNO*GMNO
      ACK=CK*GMK:ACNA=CNA*GMNA
      GAMH(I)=GMH
      RETURN

```

```

4400 REM RECALCULATE
      KW1=KW0/(GMH*GMOH)
      DIFF=(KW(I)-KW1)/KW1
      DIFF=ABS(DIFF)
      IF (DIFF*100)<1 THEN GOTO 4450
      KW(I)=KW1
      GOSUB 4100
      GOSUB 4200
      GOSUB 4300
      GOTO 4400
4450 KW(I)=KW1
      RETURN
4500 REM CALCULATE JUNCTION POTENTIALS

      NUM=-AA*SQR(CREF)
      GMNA=NUM/(1+B*ANA*SQR(CREF))
      GMK=NUM/(1+B*AK*SQR(CREF))
      GMNO=NUM/(1+B*ANO*SQR(CREF))
      GMNA=10^GMNA:GMK=10^GMK:GMNO=10^GMNO
      ANAALP=CREF*GMNA:AKALP=CREF*GMK:ANOALP=CREF*GMNO
      AHALP=0:AOHALP=0
      IF REF$="K" THEN ANAALP=0
      IF REF$="N" THEN AKALP=0
      ASUM1=UNA*(ACNA-ANAALP)+UK*(ACK-AKALP)
      ASUM1=ASUM1+UH*(ACH-AHALP)
      ASUM2=ASUM1+UNO*(ACNO-ANOALP)+UOH*(ACOH-AOHALP)
      ASUM1=ASUM1-UNO*(ACNO-ANOALP)-UOH*(ACOH-AOHALP)
      ASUM3=UK*AKALP+UNA*ANAALP+UNO*ANOALP
      ASUM4=UK*ACK+UNA*ACNA+UNO*ACNO
      ASUM4=ASUM4+UH*ACH+UOH*ACOH

      R1=ASUM1/ASUM2:R2=(R*T)/F
      R3=ASUM3/ASUM4
      R4=LOG(R3)
      EJ=R1*R2*R4*1000
      E(I)=E(I)-EJ
      RETURN
5000 REM SOLVE
      XOLD=(X(I+1)+X(I))/2
      FOR J1=1 TO 20
        DER=3*A1(I)*XOLD*XOLD+2*B1(I)*XOLD+C1(I)
        FUN=A1(I)*XOLD*XOLD*XOLD+B1(I)*XOLD*XOLD
        FUN=FUN+C1(I)*XOLD+D1(I)
        FUN=FUN-E(J)
        HH=-FUN/DER
5100 XNEW=XOLD+HH
        IF XNEW=0 THEN GOTO 5200
        HH=HH/10
        GOTO 5100
5200 DIFF=ABS(XNEW-XOLD)
        ABNEW=ABS(XNEW)
        IF (DIFF/ABNEW)<0.0001 THEN GOTO 5300
        XOLD=XNEW
      NEXT J1
5300 XXNEW=XNEW+X(I)
      RETURN

```

```

5600  REM CALCULATE ERROR IN CHARGE
      RETURN
7000  REM EVALUATE THE POLYNOMIAL
      INPUT "NO. OF DIVISIONS IN EACH INTERVAL";ND
      K=0
      PRINT "VOLUME      CALC.FUNC"
      FOR I=1 TO NP-1
        J=0
        INTV=(X(I+1)-X(I))/ND
6100  J=J+1
        K=K+1
        IF K=100 THEN GOTO 6200
        XE(K)=X(I)+INTV*J
        HH=XE(K)-X(I)
        FUNC(K)=A1(I)*HH*HH*HH+B1(I)*HH*HH
        FUNC(K)=FUNC(K)+C1(I)*HH+D1(I)
        PRINT XE(K),FUNC(K)
        IF J<ND-1 THEN GOTO 6100
      NEXT I
6200  PRINT "TOTAL NO OF POINTS";K
      INPUT "FILE NAME TO STORE THE FUNCTIONS";NA$
      FILE NA$
      PRINT #1;TITL1$
      PRINT #1;TITL2$
      PRINT #1;XV$
      PRINT #1;YV$
      FOR I=1 TO K
        PRINT #1;XE(I),FUNC(I),I
      NEXT I
      CLOSE 1
      RETURN

```

APPENDIX H : Table of symbols and their definitions

Symbol	Definition	Units
A	area of the suspension	$\text{m}^2 \text{L}^{-1}$
A'	constant in the Debye-Huckel equation equals 0.5111 at 25 °C	-
A ⁻ (x)	concentration of ionized acceptors	cm^{-3}
a	size factor	-
a _i	activity of an ion i	mol L^{-1}
B'	a constant in the Debye-Huckel equation equals 0.3291 at 25 °C	
C _{bulk}	concentration of the bulk solution	mol m^{-3}
C _{ctr}	capacitance of the counter electrode	F m^{-2}
C _d	capacitance of the diffuse layer	F m^{-2}
C _H	capacitance of the Helmholtz layer	F m^{-2}
C _{K⁺}	initial concentration of K ⁺	mol L^{-1}
C _{K⁺}	concentration of K ⁺ in the titrant	mol L^{-1}
C _{obs}	observed capacitance	F m^{-2}
C _{ox}	capacitance of the oxide	F m^{-2}
C _{rxn}	capacitance due to the reactions at the oxide/electrolyte interface defined as	F m^{-2}
C _{sc}	capacitance of the space charge layer of the semiconductor	F m^{-2}
C _{ss}	capacitance of the surface states	F m^{-2}
C _i	concentration of the titrant	mol L^{-1}
C _T	total capacitance in the electrochemical cell	F m^{-2}
CF	conversion factor used in resistivity determination by the four point probe	-
C _{sol}	capacitance of the solution side of the oxide/electrolyte interface	F m^{-2}

C_{elec}	capacitance of the Si/SiO ₂ electrode	F m ⁻²
d	thickness of the Helmholtz layer	m
d_{ox}	thickness of the oxide layer	m
$D^+(x)$	concentration of the ionized donors	m ⁻³
E_A	energy of the acceptor levels	J
E_C	energy of the conduction band	J
E_D	energy of the donor levels	J
E_F	energy of the Fermi level	J
E_H	response of the glass electrode relative to a reference electrode	mV
E_K	response of the K ⁺ ISE relative to relative to a reference electrode	mV
E_i	general representation of the electrode response of a sensing electrode relative to a reference electrode	mV
E_V	energy of the valence band	J
E_{out}	output of the current-to-voltage converter	mV
E_{in}	input voltage to the electrochemical cell	mV
E^0	thermodynamic constant specific to a given potentiometric cell	mV
E_j	junction potential	mV
E_{ref}	potential of the reference electrode relative to the NHE	mV
E_{chem}	electrostatic potential due to reactions at the oxide/electrolyte interface	mV
F	Faraday constant	C mol ⁻¹
f	frequency	Hz
g	degeneracy factor	-
$[H^+]$	concentration of H ⁺ in the bulk	mol m ⁻³
$[H^+]_{zc}$	concentration of H ⁺ in the bulk at zero surface charge on the oxide	mol m ⁻³
I	current	A
K'_1	intrinsic constant for protonation of XOH groups	mol m ⁻²

K'_2	intrinsic constant for de-protonation of XOH groups	mol m^{-2}
K_+	equilibrium constant for protonation of XOH groups	$\text{m}^3 \text{mol}^{-1}$
K_-	equilibrium constant for de-protonation of XOH groups	mol m^{-3}
K_D	surface dissociation constant of the oxide	-
K^+	concentration of K^+ ions "lost"	mol L^{-1}
k	Boltzman constant	J K^{-1}
b_H	intercept of the calibration curve for the glass electrode	mV
b_K	intercept of the calibration curve for the K^+ ISE	mV
L_D	Debye length of the semiconductor	m
n	concentration of electrons in the space charge layer of the semiconductor	m^{-3}
n^0	concentration of electrons in the bulk of the semiconductor	m^{-3}
n_{XOH}	surface concentration of XOH groups	mol m^{-2}
n_{XOH^+}	surface concentration of XOH_2^+ groups	mol m^{-2}
n_{XO^-}	surface concentration of XO^- groups	mol m^{-2}
N_A	concentration of acceptors	m^{-3}
N_D	concentration of the donors	m^{-3}
N_{ss}	surface state density	$\text{cm}^{-2} \text{eV}^{-1}$
p	concentration of holes in the space charge layer	m^{-3}
p^0	concentration of holes in the bulk of the semiconductor	m^{-3}
q	elementary charge	C
R_{sc}	resistance of the semiconductor	Ω
R_{ox}	resistance of the oxide layer	Ω
R_{sol}	resistance of the solution between the counter electrode and reference electrode	Ω

R'_s	resistance between the counter electrode and the working electrode	Ω
R_{ctr}	resistance of the counter electrode	Ω
R_{ref}	resistance of the reference electrode	Ω
s_H	slope of the glass electrode	mV/log $[H^+]$
s_K	slope of the K^+ ISE	mV/log $[K^+]$
T	absolute temperature	K
T_A	total analytical concentration of H^+	mol L^{-1}
T_B	total analytical concentration of OH^-	mol L^{-1}
T_{K^+}	total analytical concentration of K^+	mol L^{-1}
T	total charge density across an interface	$C\ m^{-2}$
V	voltage across the two inner probes when a current I is passed through the four point probe	V
V_{appl}	applied potential to an electrochemical cell or an MOS structure	V
V_{CT}	cumulative volume of the solution during a titration	L
V_{FB}	flat band potential	V
V_T	volume of the titrant added	L
ΔV	volume of titrant that should be added to the oxide suspension to bring the electrode response to the same as that of the blank	L
X	in-phase component of the output of the current-to-voltage converter	V
x	distance from the electrode surface	m
x_d	width of the depletion layer	m
Y	out-of-phase component of the output of the current-to-voltage converter	V
Z_{total}	total impedance of an electrochemical cell	Ω
Z_{te}	impedance of the test cell	Ω
Z_m	impedance of the feed back loop of the current-to-voltage converter	
z	charge of an ion	-

Greek Symbols

δ	phase angle	deg
β	defined as (q/kT)	V^{-1}
ϵ_0	permittivity in free space	$F\ m^{-1}$
ϵ_w	dielectric constant of water in the bulk	-
ϵ'_w	dielectric constant of water in the Helmholtz layer	-
ϵ_{ox}	dielectric constant of the oxide	-
ϵ_s	dielectric constant of the semiconductor	-
γ	activity coefficient	-
μ	chemical potential	J
μ'	ionic strength of the solution	$mol\ L^{-1}$
μ_n	electron mobility in silicon lattice	
ψ	potential at a distance x from the Helmholtz layer relative to the bulk	V
ϕ	potential at a distance x from the surface of the semiconductor	
ψ_d	potential at the Helmholtz plane	V
ϕ_s	potential at the surface of the semiconductor	
ψ_o	potential at the oxide surface relative to the bulk of the solution	V
ψ_m	potential of the metal in the MOE structure relative to the bulk of the solution	V
ϕ_d	charge density in the diffuse layer	$C\ m^{-3}$
α	resistivity of the semiconductor	m^{-1}
σ_d	surface charge density of the diffuse layer	$C\ m^{-2}$
σ_f	fixed charge in the oxide	$C\ m^{-2}$
σ_{sc}	surface charge density of the space charge layer	$C\ m^{-2}$
σ_o	surface charge density of the oxide	$C\ m^{-2}$
Γ_i	surface excess concentrations	$mol\ m^{-2}$